

*The use of ATR-FTIR to probe the release mechanism from hydrophilic matrices.*

JABLONSKA, Wioletta

Available from the Sheffield Hallam University Research Archive (SHURA) at:

<http://shura.shu.ac.uk/7283/>

## A Sheffield Hallam University thesis

This thesis is protected by copyright which belongs to the author.

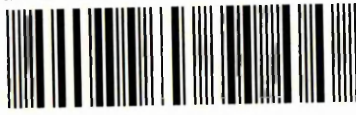
The content must not be changed in any way or sold commercially in any format or medium without the formal permission of the author.

When referring to this work, full bibliographic details including the author, title, awarding institution and date of the thesis must be given.

Please visit <http://shura.shu.ac.uk/7283/> and <http://shura.shu.ac.uk/information.html> for further details about copyright and re-use permissions.

Learning and Information Services  
Adsetts Centre, City Campus  
Sheffield S1 1WD

102 100 357 3



Sheffield Hallam University  
Learning and Information Services  
Adsetts Centre, City Campus  
Sheffield S1 1WD

**REFERENCE**

ProQuest Number: 10697168

All rights reserved

INFORMATION TO ALL USERS

The quality of this reproduction is dependent upon the quality of the copy submitted.

In the unlikely event that the author did not send a complete manuscript and there are missing pages, these will be noted. Also, if material had to be removed, a note will indicate the deletion.



ProQuest 10697168

Published by ProQuest LLC (2017). Copyright of the Dissertation is held by the Author.

All rights reserved.

This work is protected against unauthorized copying under Title 17, United States Code  
Microform Edition © ProQuest LLC.

ProQuest LLC.  
789 East Eisenhower Parkway  
P.O. Box 1346  
Ann Arbor, MI 48106 – 1346

**The use of ATR-FTIR to probe the release  
mechanism from hydrophilic matrices.**

**Wioletta Jablonska**

A thesis submitted in part fulfillment of the requirements of  
Sheffield Hallam University  
for the degree of Doctor of Philosophy

June 2011



## **Acknowledgements:**

I would like give my sincere thanks to my academic supervisor Dr Chris Sammon for his invaluable advice and general support throughout this project. These thanks are also extended to my industrial supervisor Dr Graham Clarke of Bristol-Myers Squibb whose enthusiasm and support was greatly appreciated.

This thesis was made possible by collaborations with many experts and to this end, I would like to thank Dr Thomas Dearing of the University of Hull for introducing me to the chemometric data analysis, John Gamble of Bristol-Myers Squibb for his help and support with work on NIR Imaging data as well as Lisa Carter for her technical assistance with the dissolution testing and Dr Sarah Nicholson of Bristol-Myers Squibb for her invaluable help and support during the whole project.

Thanks to Bristol-Myers Squibb for funding this research.

Thanks also go to the members of the Polymers, Composites and Spectroscopy Group at Sheffield Hallam University for the general support and technical assistance.

Special thanks to my Mum, Stanislawa and Dad, Michal, sister Elzbieta and Piotr Mirek for their support throughout all of my studies.

# **Content of thesis:**

Abstract.....	i
List of Abbreviations.....	ii
<b>1. Introduction.....</b>	<b>1</b>
1.1 Properties of HPMC.....	2
1.1.1 Solubility.....	4
1.1.2 Thermal gelation.....	4
1.1.3 Viscosity.....	5
1.1.4 Surface activity.....	6
1.1.5 Influence of polymer on the drug release.....	6
1.1.6 Applications of cellulose ethers.....	8
1.2 Influence of active substance on the drug release from hydrophilic matrices.....	9
1.2.1 Chemical properties of 6-hydroxy Bupirone hydrochloride.....	11
1.2.2 Pharmacological influence of 6-OH bupirone.....	15
1.3 pH modifiers.....	16
1.4 Drug release from hydrophilic matrices.....	21
1.5 Drug release kinetics.....	26
1.6 Aims of the thesis.....	30
<b>2. Materials, methods and techniques.....</b>	<b>31</b>
2.1 Materials.....	31
2.2 Methods and techniques.....	32
2.2.1 Infrared spectroscopy.....	32
2.2.1.1 Principles of infrared spectroscopy.....	32

2.2.1.2	Instrumentation.....	36
2.2.1.3	Advantages and limitations of FTIR spectroscopy.....	38
2.2.1.4	Sampling techniques.....	41
2.2.1.4.1	Transmission.....	42
2.2.1.4.2	Attenuated total reflectance spectroscopy (ATR).....	42
2.2.2	NIR Imaging.....	50
2.2.2.1	Fundamentals of NIR-CI.....	50
2.2.2.2	Instrumentation.....	52
2.2.2.3	Data processing.....	54
2.2.2.4	Applications of NIR Imaging.....	58
2.2.3	Chemometric data analysis.....	59
2.2.4.1	Partial least squares (PLS).....	59
2.2.4.2	Multivariate curve analysis.....	62
2.2.5	UV/Visible spectroscopy.....	64
2.2.5.1	Principles of the UV/visible spectroscopy.....	64
2.2.5.2	Instrumentation.....	64
2.2.5.3	Applications.....	65
2.2.6	Dissolution testing.....	66
2.2.6.1	Instrumentation.....	67
<b>3.</b>	<b>Optimization of the compaction process.....</b>	<b>69</b>
3.1	Aims.....	70
3.2	Materials and methods.....	71
3.2.1	Materials.....	71

3.2.2 Preparation of the mixtures.....	71
3.2.2.1 Mixtures with unmatched particle size of the powders.....	71
3.2.2.2 Mixtures with particle size less than 106 microns.....	71
3.2.3 Mixing procedures used to prepare formulations.....	72
3.2.3.1 Manual shaking.....	72
3.2.3.2 Tumble blending.....	72
3.2.3.3 Grinding.....	72
3.2.4 Compaction process.....	73
3.2.4.1 Design of compaction cell.....	73
3.2.4.2 Creating tablets in situ on ATR crystal.....	74
3.2.4.3 Parameters for the tablet compaction.....	75
3.2.5 PLS analysis.....	75
3.2.6 NIR analysis.....	76
3.3 Results and discussion.....	77
3.3.1 Effect of different mixing procedures and particle size on the reproducibility of the samples.....	77
3.3.1.1 Mixtures with unmatched particle size of the powders.....	77
3.3.1.2 Mixtures with particle size less than 106 microns.....	79
3.3.2 Effect of different mixing procedures and particle size on the prediction of concentration values.....	80
3.3.2.1 Mixtures with unmatched particle size of the powders.....	80
3.3.2.2 Mixtures with particle size less than 106 microns.....	84

3.3.3. Effect of particle size on the distribution of the components in the tablet.....	86
3.3.3.1 Mixtures with an unmatched particle size.....	87
3.3.2.2 Mixtures with particle size less than 106 microns.....	91
3.4 Conclusions.....	94
<b>4. Investigations of solid dosage form: binary formulations.....</b>	<b>96</b>
4.1 Aims.....	97
4.2 Materials and methods.....	98
4.2.1 Materials.....	98
4.2.2 Preparation of the mixtures.....	98
4.2.3 Compaction process.....	98
4.2.4 PLS analysis.....	99
4.2.5 NIR Imaging.....	99
4.3 Results and discussion.....	100
4.3.1 Investigations of possible interactions of the powders in the compacted tablet.....	100
4.3.1.1 Formulation: HPMC and citric acid.....	100
4.3.1.2 Formulation HPMC and active substance.....	103
4.3.2 Prediction of the concentration values of the formulation ingredients...	105
4.3.2.1 Mixtures of HPMC and citric acid.....	105
4.3.2.2 Mixtures of HPMC and active substance.....	108
4.3.3 Distribution of the components in a binary formulation tablets.....	112
4.3.3.1 Formulation: HPMC and citric acid.....	112

4.3.3.2 Formulation active substance and HPMC.....	117
4.4 Conclusions.....	124
<b>5. Investigations of binary formulations in a dissolution media.....</b>	<b>125</b>
5.1 Aims.....	126
5.2 Materials and methods.....	127
5.2.1 Materials.....	127
5.2.2 The analyzed formulation.....	127
5.2.3 Dissolution testing.....	127
5.2.4 Preparation of the solutions.....	130
5.2.4.1 Preparation of the HPMC solutions.....	130
5.2.4.2 Preparation of API solutions.....	130
5.2.4.3 Preparation of Citric acid solutions.....	130
5.2.5 Hydration and Hyphenation experiments.....	131
5.2.5.1 Preparation of the dissolution media.....	132
5.2.6 MCR data analysis.....	133
5.3 Results and discussion.....	134
5.3.1 Effect of pH dissolution media on the drug release from binary formulation.....	134
5.3.1.1Dissolution of the binary formulation in distilled water.....	134
5.3.1.2 Dissolution testing of the binary formulations in pH 6.8 and 0.1 N HCl.....	136
5.3.2 Investigations of possible interactions of the binary formulation in the hydrated state.....	139

5.3.2.1 Aqueous solutions of formulation's excipients.....	139
5.3.2.2 Hydration experiments.....	146
5.3.2.2.1 Formulation HPMC and active substance.....	146
5.3.2.2.2 Formulation HPMC and citric acid.....	152
5.3.2.3. Hyphenation experiments of API and HPMC.....	157
5.3.2.3.1 Hyphenation experiments in the pH 6.8.....	157
5.3.2.3.2 Hyphenation experiments in the 0.1N HCl.....	160
5.3.3 Prediction of the possible components existing in the hyphenated samples using MCR data analysis.....	166
5.4 Conclusions.....	176
<b>6. Investigations of tertiary formulations in the solid state.....</b>	<b>178</b>
6.1 Aims.....	179
6.2 Materials and methods.....	180
6.2.1 Materials.....	180
6.2.2 Preparation of the mixtures.....	180
6.2.3 Compaction process.....	180
6.2.4 PLS analysis.....	180
6.2.5 NIR Imaging.....	180
6.3 Results and discussion.....	182
6.3.1 Investigations of possible interactions of the powders in the compacted tablet.....	182
6.3.2 PLS data analysis.....	187
6.3.3 NIR Imaging.....	191

6.3.3.1 The tertiary formulations of HPMC, active substance and citric acid.....	192
6.3.3.2 The RGB results of tertiary formulation of HPMC, active substance and citric acid bottom side.....	199
6.4 Conclusions.....	207
<b>7. Investigations of the tertiary formulations in a dissolution media.....</b>	<b>208</b>
7.1 Aims.....	209
7.2 Materials and methods.....	210
7.2.1 Materials.....	210
7.2.2 The analyzed formulation.....	210
7.2.3 Dissolution testing.....	210
7.2.4 Hydration and Hyphenation experiments.....	210
7.2.5 MCR data analysis.....	210
7.3 Results and discussion.....	211
7.3.1 Hydration experiments.....	211
7.3.2 Effect of different pH dissolution media on the drug release from tertiary formulation.....	217
7.3.3 Hyphenation experiments.....	218
7.3.3 MCR data analysis.....	226
7.4 Conclusions.....	231
<b>8.Conclusions.....</b>	<b>232</b>
8.2 Further work.....	234
8.2.1 Reconstruction of the compaction cell.....	234



8.2.2 ATR-FTIR Imaging as a main technique of further investigation.....	235
8.2.3 Future experiments.....	236
Word count.....	238
References.....	239

## **Abstract**

Hydrophilic matrices are widely used in the pharmaceutical industry as control release agents in solid oral dosage formulations. One of the key parameters that controls release in such systems is the distribution of excipients within the formulation, which in turn is governed by the processing and manufacturing procedures. This thesis explores the effect of processing on the distribution of excipients in binary and tertiary formulations obtained using different mixing procedures, (manual shaking, tumble blending and grinding) with a range of particle size distributions. Samples were prepared by compacting processed powder mixtures directly onto a diamond attenuated total reflectance (ATR) crystal using an in-house built compaction cell which proved to be a successful tool for small scale tablet manufacturing. For this study the following excipients were used; the hydrophilic matrix HPMC grade K4M, the drug 6-hydroxy buspirone hydrochloride and citric acid. The homogeneity of the formulations were determined by the reproducibility of the spectra obtained from the tablets after compaction and the concentration of excipients within the samples was successfully predicted using Partial Least Squares (PLS) data analysis. The distribution of the components was confirmed using Near Infrared imaging with principal components analysis (PCA). Standard dissolution tests of the binary and tertiary systems gave an indication about the release behaviour of the formulations in different dissolution media. Total dissolution of the drug was observed in 0.1N HCl for binary mixtures and in both pH 6.8 buffer and 0.1 N HCl for tertiary formulations highlighting the impact of citric acid on the dissolution results and confirming the pH dependence of the system. The release of drug was also studied using the complementary technique of ATR-FTIR by performing hydration experiments on the compacted tablets. Both standard data analysis approaches, such as peak area changes, and multivariate curve resolution (MCR) were applied to these datasets. The MCR studies showed some promise, but also highlighted a need for further development. The standard data analysis showed that the rate of release of the API and citric acid was higher than the rate of solvation of HPMC, indicating a diffusion controlled release mechanism. Standard dissolution experiments and infrared spectroscopy measurements were combined, by developing a hyphenated system, whereby dissolution media was circulated through the ATR compaction cell and out through a UV/VIS flow detector in a closed loop. These results were in good agreement with the data from both the standard dissolution tests and the ATR-FTIR hydration studies.

## List of Abbreviations:

ATR	attenuated total reflectance
API	active pharmaceutical ingredient
BMS	Bristol Myers-Squibb
BP	buspirone hydrochloride
6OHBP	6-hydroxy buspirone hydrochloride
CA	citric acid
cm <sup>-1</sup>	wavenumber
DS	degree of substitution
EHEC	ethylhydroxyethylcellulose
FCC USP	food chemical codex U.S. Pharmacopeia
FTIR	Fourier transformed infrared
HEC	hydroxyethylcellulose
HEMC	hydroxyethylmethylcellulose
HPC	hydroxypropylcellulose
HPMC	hydroxypropylmethylcellulose
MC	methylcellulose
MCR	multivariate curve resolution
MS	molar substitution
NaCMC	sodium carboxymethylcellulose
nm	nanometer
PCA	principal component analysis
PLS	partial least squares

RMSECV     root-mean-square error of cross-validation

USP H VISC     US Pharmacopeia high viscosity

UV             ultraviolet

w/w             weight in weight

μm             micrometer

# 1. Introduction

Compressed powder mixtures of one or more hydrophilic polymers with water swelling properties, drug and excipients are called hydrophilic matrices. The ability of hydrophilic polymer matrix systems to provide a desirable drug release profile, cost effectiveness and also broad acceptance of U.S. Food and Drug Administration (FDA) makes them one of the most widely used type of matrices in a controlled release formulation [1, 2]. One of the most commonly used hydrophilic polymers for pharmaceutical formulations is hydroxypropyl methylcellulose (HPMC). This polymer, due to its non toxic nature, non pH dependence and ability to accommodate a large percentage of the drug, fulfills the requirements proposed by the Pifferi and Restani of the modern pharmaceutical excipient [3]. Moreover the ability to hydrate rapidly when in contact with liquid water to form a protective gel around the tablet matrix is an essential HPMC property for drug release [4, 5].

In this introduction the drug release mechanism from hydrophilic matrices along with the properties of hydroxypropyl methylcellulose (HPMC), one of the cellulose derivatives, are discussed, focusing on the use of HPMC as an extended release polymer. Also the factors influencing the drug release and possible modifications of this process by incorporating pH modifiers into the formulation are included.

Finally, the aims of the thesis will be addressed.

## 1.1 Properties of HPMC

Cellulose is a linear polymer consisting of anhydroglucose units joined by  $\beta$  1-4 glycosidic linkages. The substance is insoluble in water due to the presence of inter- and intramolecular hydrogen bonding between hydroxyl groups and the glucose ring oxygen, which influences the high degree of crystallinity. Cellulose contains three reactive hydroxyl groups, two secondary and one primary at the position C-2, C-3 and C-6 atoms on each AGU unit [6, 7].

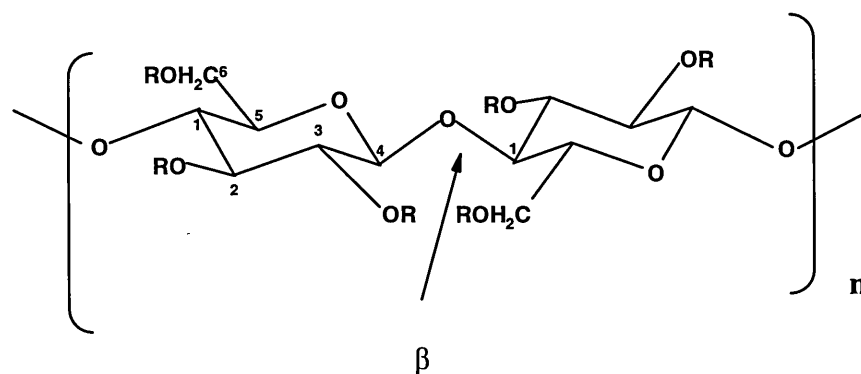


Fig.1-1 Structure of hydroxypropylmethylcellulose

Hydroxypropyl methylcellulose (also called hypromellose) is mixed cellulose ether, containing hydroxypropyl and methoxyl groups in anhydroglucose unit (AGU), which is the basic repeating structure of cellulose. Production of HPMC involves heating cellulose fibres with sodium hydroxide solution to break inter- and intra-molecular hydrogen bonding (mercerisation process). The disrupted polymer has the ability to swell in water which allows reactants to penetrate and later to start the substitution process. Adding methyl chloride and propylene oxide to the alkali cellulose created in the mercerisation

process, leads to the hydroxypropyl and methyl substitution of anhydroglucose units. The hydroxypropyl and methyl substitution can be controlled by the weight ratio and concentration of added reagents during the production process [8, 9]. The ratios of those two substituents give the hypromellose different characteristics. The average number of hydroxyl groups per AGU unit where hydrogen atom is replaced by methyl is defined as degree of substitution (DS), whilst the term molar substitution (MS) is used to describe the average number of moles of propylene oxide per anhydroglucose unit [10, 11]. Viscosity is typically given as a mean, or as a range due to viscometer acceptable ranges of error and the results of various test methods and viscometers which do not necessarily correspond to each other. The pharmaceutically important grades of HPMC are classified in United States Pharmacopeia (USP) according to the hydroxypropyl and methoxy group content.

#### **Dow HPMC grades (Methocel™) use in pharmaceuticals**

<b>Methocel™ grade</b>	<b>USP type</b>	<b>Methoxy [%]</b>	<b>Methoxy (DS)</b>	<b>Hydroxypropyl [%]</b>	<b>Hydroxypropyl (MS)</b>	<b>Viscosity [cps]</b>
<b>J</b>	1828	16.5 - 20	0.93 – 1.15	23 – 32	0.61 – 0.91	5000 - 75000
<b>E</b>	2910	28 - 30	1.65 – 1.9	7 – 12	0.2 – 0.3	5 – 4000
<b>F</b>	2906	27 – 30	1.6 – 1.8	4 – 7.5	0.1 - 0.2	50 – 4000
<b>K</b>	2208	19 - 24	1.1 – 1.4	4 - 12	0.1 – 0.3	35 - 100000

Table1-1. Grades of HPMC [12, 13]

### 1.1.1. Solubility

The physical properties of cellulose ethers depend on the uniformity, amount and type of the substituent groups. The methylcellulose dissolves readily in the cold water at 1.3-2.6 DS, whilst in polar organic solvents from about 2 DS. The presence of hydroxypropyl substitution gives the solubility in cold water at 1.5 DS, in the case of hydroxyalkyl cellulose derivatives the minimum starts at 0.65 for HEC. The rates of aqueous medium absorption by cellulose tablet matrix may affect the drug release profile. The water soluble cellulose derivatives depending on the substitution shows varied hydrophilicity. Depending on DS and MS values the derivatives shows increasing hygroscopicity in order:



### 1.1.2 Thermal gelation

Solutions of most nonionic cellulose ethers show ‘‘reversible thermal gelation’’, that is the ability to form the structured gel upon heating (due to dehydration of polymer) and gelation is reversible upon cooling. Gelation of HPMC is thought to arise from hydrophobic interactions between the methoxyl substitutions of the polymer. Sakar has defined HPMC gel as an intermediate, non-equilibrium metastable state where this three dimensional network structure is formed due to the secondary valence forces [16]. The inverse solubility-temperature behaviour of HPMC was observed in the case within the narrow temperature range and as a result the cross-linking by covalent bonding is unlikely. Cross-links may be formed as a result of hydrogen or hydrophobic bonds as the solvent power of



the medium decreases [16]. The gelation temperature indicates the hydrophilicity of the cellulose ether and depends on the substitution type and amounts of substituents groups and their distribution. The presence of hydroxyalkyl groups leads to the higher gel point temperatures as these derivatives are more soluble in water, whilst highly substituted molecules have lower gel point temperatures. The gel temperature depends also on the concentration of the substance in a solution, presence of other materials in the solution, for e.g inorganic salts or particular organic additives (sorbitol, glycerol) which can depress the gel point. In addition substances that are good solvents for the polymer (propyleneglycol) are able to increase the gel point [14, 16-18].

### 1.1.3.Viscosity

The viscosity of HPMC solutions increases as the concentration of the polymer increases. Viscosity values for cellulose ether solutions are quoted for 2% w/w concentrations at 20 ° C. The Philipoff's equation describes the relationship between viscosity and concentration of the cellulose ethers, where the eighth root of the apparent viscosity is linearly related to the concentration:

$$\frac{\eta}{\eta_0} = \left( 1 + \frac{[\eta]c}{8} \right)^8 \quad (\text{eq.1.1})$$

Where:  $\eta$  – the apparent viscosity,  $\eta_0$  – the solvent viscosity,  $[\eta]$  – intrinsic viscosity, c- the concentration of the polymer.

The viscosity of the solution depends on the molecular weight grade and on the type and amount of substituent groups. The apparent viscosity of the polymeric solutions can also be affected by the additives and temperature. The viscosity of the cellulose ethers solutions decreases with the increasing temperature. Presence of some electrolytes in the solution reduces the viscosity below the gelation temperature [14, 19, 20].

#### 1.1.4.Surface activity

The active surface of the HPMC polymer is the result of the ability of solute molecules to alter the attractive interactions between two dissimilar molecules (air-water or oil-water) at the interface. This property can be attributed to the presence of alkyl (hydrophobic) and hydroxyl (hydrophilic) groups along the cellulose backbone. Surfactant molecules are able to reduce the surface/interfacial tension as their hydrophilic and lipophilic ends of each molecule are oriented into each phase. The maximized interactions of water and oil molecules at the interface result in the lowered interfacial tension. Surface activity is increased with the raise of the temperature until the gelation temperature is reached. The concentration of HPMC in such solution was found to have little effect on surface activity [21-23].

#### 1.1.5 Influence of polymer on the drug release.

Since diffusion plays a prominent role in controlling drug release, the release kinetics constantly changes because of the changing diffusional path length. Escudero studied the possibility of modulation of theophylline release by mixing HPMC of different viscosity

grades and a new generation of copolymers [24]. It was found that the degree of substitution of HPMC used may also influence drug release characteristics.

Another factor that has an influence on the rate of drug release is the particle size of the polymer in the formulation. There is a lot of work published concerning the impact of HPMC particle size in formulation of release rates. In the case of water-soluble drugs, the effect of particle size on the release rate was visible with a low dose of HPMC in a tablet and large particle size of the drug [25-29].

It has been proposed that the drug:polymer concentration ratio (increasing drug concentration) is the most influential variable controlling the drug release. The reduction of the drug release rate from the tablets has been attributed to the reduced erosion of the gel layer and the increase of the drug diffusion pathlength and tortuosity [27, 28, 30].

The degree and ratio of the methoxyl and hydroxypropyl substitution determines the physico-chemical characteristics of different HPMC types. The hydrophobic methoxy groups decrease the capability of the polymer chains to form hydrogen bonding, influencing the interactions with water. The HPMC type effects the tensile strength of matrices, hydration rates of the polymer and drug release. However, when a certain polymer content has been reached (30-40%) the HPMC substitution degree has less significance and similar drug profiles can be obtained.

The infrared spectrum of HPMC (Fig. 1-2) shows the presence of a strong characteristic vibration band at  $\sim 1100\text{ cm}^{-1}$   $\nu(\text{CO})$ . In the region  $\sim 3570\text{--}3200\text{ cm}^{-1}$   $\nu(\text{OH})$ , the bands are associated with the presence of hydroxyl groups from the polymer and also the band  $\nu(\text{CH})$   $2800\text{--}3000\text{ cm}^{-1}$  is present [31, 32].

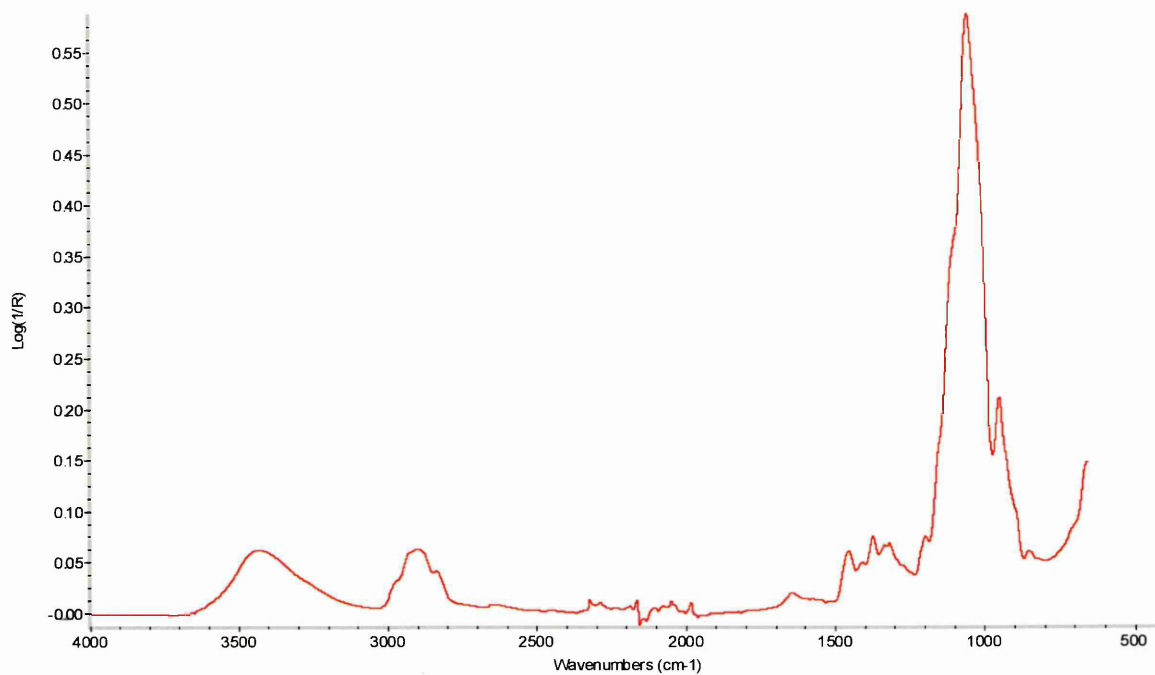


Fig 1-2. FTIR spectrum of pure HPMC.

#### 1.1.6 Applications of cellulose ethers

Cellulose compounds are widely used in the pharmaceutical industry as tablet binders, thickeners, suspending agents, emulsifiers, film builders, bioadhesive materials and tablet matrices for controlled release applications [14, 33]. Cellulose ethers are also employed in many different industries with many applications owing mainly to their solution properties. Some examples include: adhesives, agricultural applications, ceramics, constructions and cosmetics [11, 29].

Wollenweber noted that the emulsion stabilizing activity of HPMC, leads to the extended use of this polymer in food, cosmetics and pharmaceutical industry as the result of its surface active nature [20].

## **1.2 Influence of active substance on the drug release from hydrophilic matrices.**

The physicochemical properties of the active substance in a formulation have substantial effect on the nature of drug release. Aqueous solubility of the active substance is an important factor which influences release, transport and absorption of the drug in the body. In general, the drug release mechanism of soluble active pharmaceutical ingredient (API) from HPMC matrices is considered to follow a Fickian diffusion process. In the case of poorly soluble drugs the release by gel layer erosion is generally observed. Eyjolfsson (1999) investigated release kinetics of a practically water insoluble model drug incorporated in two types of HPMC (K4M and K100LV). The non-Fickian behavior of drug release was reported [34, 35].

Subsequently, a range of drug release rates and release mechanism changes have been characterized after incorporation in hydrophilic matrices (HPMC and HPC), for APIs with varying drug solubility. Freely soluble diclofenac sodium showed the highest and fastest release in pH 6.5 phosphate buffer followed by ibuprofen and naproxen with medium solubility and practically insoluble indomethacin which gave the slowest release [36].

During studies on the release mechanism of API's with different solubility from swelling matrices (HPMC), Colombo (2001) [66] showed that the rate and amount of drug released was dependent on the active substance dissolution and diffusion rates, and but also from the "drug particle translocation" process. In the case of low solubility drugs the solid particles of active substance were transported from the swelling front of the matrices to the eroding front of the gel layer. The particle displacement process was explained as a result of the spring-like action of macromolecular chains upon transition from glassy to rubbery state of

the polymer. The expansion of the polymer chains by relaxation led to movement of dissolved drug. The release mechanism continued to be a diffusion-controlled after the glassy core of the hydrated tablet disappeared, as the dissolved drug was already in the system.

Significantly increasing rates of poorly soluble drugs release after a complete hydration of the matrix core were reported. It was proposed that drug particles were reducing the entanglement of the polymer chains and increasing the erosion rate of the gel layer [37, 38].

There is a lot of work published concerning the impact of drug particle size in formulation of release rates. It was observed that release rates decreased with increasing particle size of insoluble drug as a result of slower dissolution of large dry particles, the surface area to volume ratio decreased [26, 27, 30].

On the other hand, Velasco (1999) found no dependence between the particle size of diclofenac Na on the release rate at low concentration of HPMC in a formulation, whilst at larger concentration of HPMC, as the particle size increased, the release rate increased as well. No reasonable explanation was given for these findings, but it is possible that the HPMC particle size effected the increase of dissolution rates [39].

### 1.2.1 Chemical properties of 6-hydroxy Buspirone Hydrochloride

The 6-hydroxy buspirone (6OH BP) is a hydroxylated derivative of buspirone. The substance is produced by the hydroxylation of buspirone, which leads to the final product, racemic mixture of alcohols [40, 41]. Pharmaceutically acceptable acid salt can be made by the reaction of 6-hydroxy buspirone with organic or inorganic acid. However, the anion of the added acid should not contribute in a significant way to the pharmacologic or toxicity of the base form of 6-hydroxy buspirone. Acids commonly used for this process are carboxylic acids, tartaric acid, succinic acid, fumaric acid, acetic acid, HCl, HBr, HI, and sulfuric acid. 6-hydroxy buspirone was found in forms: racemate, R-enantiomer and S-enantiomer. It is interesting to note that neither the racemate nor the enantiomers have been described in the literature properly from a chemical point of view and commercially these substances are not available. This project involves the use of the racemic form of 6-hydroxy buspirone hydrochloride BMS-528215 as an active substance in tested pharmaceutical formulations [42-45].

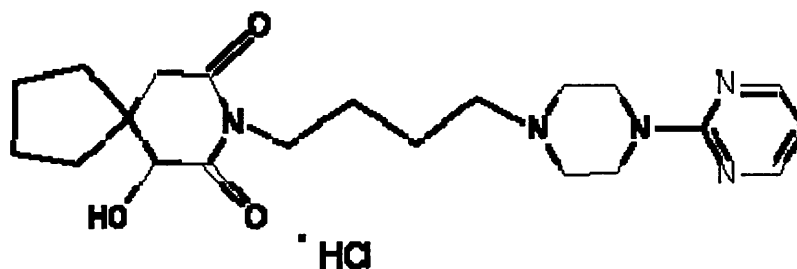


Fig. 1-3. Chemical structure of 6-hydroxy buspirone hydrochloride

6OH BP is a white crystalline powder, freely soluble in water, methylene chloride and methanol, soluble in ethanol and acetonitrile, slightly soluble in ethyl acetate, and practically insoluble in hexane [46].

Sheikhzadeh and co-workers studied the qualitative and quantitative characterization of buspirone hydrochloride and its polymorphs. Qualitative characterization involved  $^{13}\text{C}$  and  $^1\text{H}$  NMR analysis and single crystal X-ray studies. Quantitative analysis of buspirone hydrochloride involved usage of various techniques such as; Differential Scanning Calorimetry (DSC), Thermogravimetric analysis (TGA), X-ray powder diffraction (XRPD), laser Raman spectroscopy and FTIR. The polymorphs were distinguished on the basis of their melting points, XRPD and vibrational peaks, also various chemometric methods such as partial least squares (PLS) and principal component regression (PCR) were used in order to develop calibration curves for quantitative analysis of the collected data [47, 48].

FTIR spectroscopy of solid state 6-OH BP hydrochloride (Fig.1-4) showed the presence of characteristic bands for buspirone hydrochloride. The spectrum showed a relatively strong absorbance band in the region  $1650\text{-}1700\text{ cm}^{-1}$  associated with  $\text{C}=\text{O}$  stretching mode,  $\text{C}=\text{C}$  skeletal benzene ring breathing modes in the region  $1500\text{-}1600\text{ cm}^{-1}$ , presence of the bands associated with  $\text{C-H}$  in aromatic ring at  $3000\text{-}3100\text{ cm}^{-1}$ , as well as  $\text{OH}$  stretching vibration absorbance band at  $3100\text{-}3500\text{ cm}^{-1}$  which appeared as a result of buspirone hydroxylation process. Also the band in the region  $1130\text{-}1270\text{ cm}^{-1}$  associated with  $\text{C-N}$  stretch was reported [49, 50].



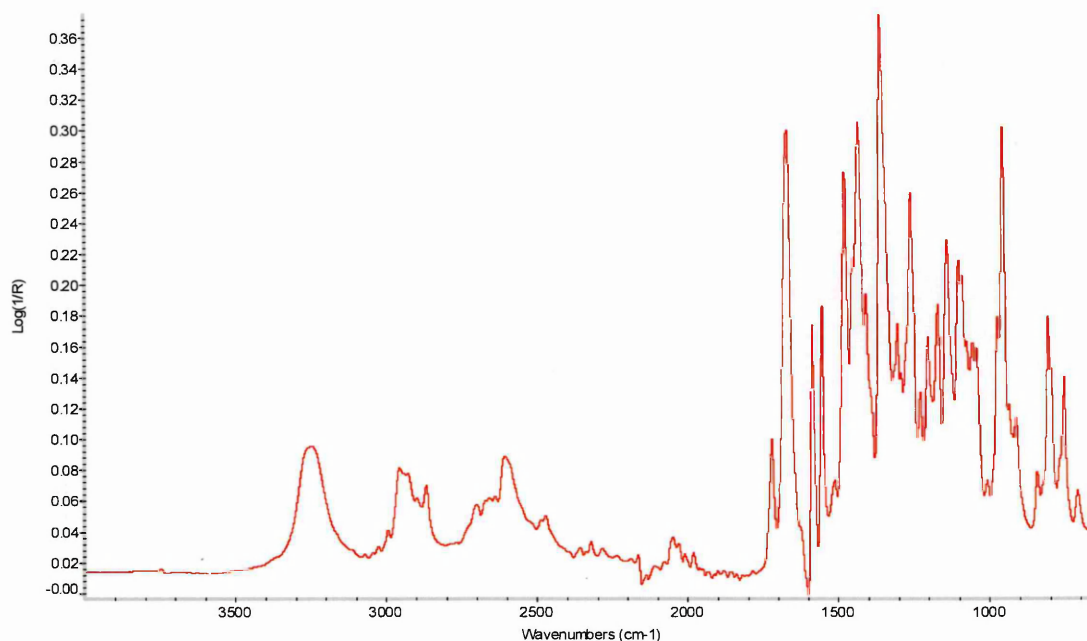


Fig1-4. Spectrum of 6-hydroxy buspirone hydrochloride.

Additionally single crystal studies and molecular modelling analysis performed on buspirone hydrochloride by Sheikhzadeh and co-workers [47,48] revealed that between the oxygen and nitrogen atoms in the structure the main source to accept the hydrogen atom from HCl molecule is N17, as nitrogen atom in this position presented the highest negative charge.

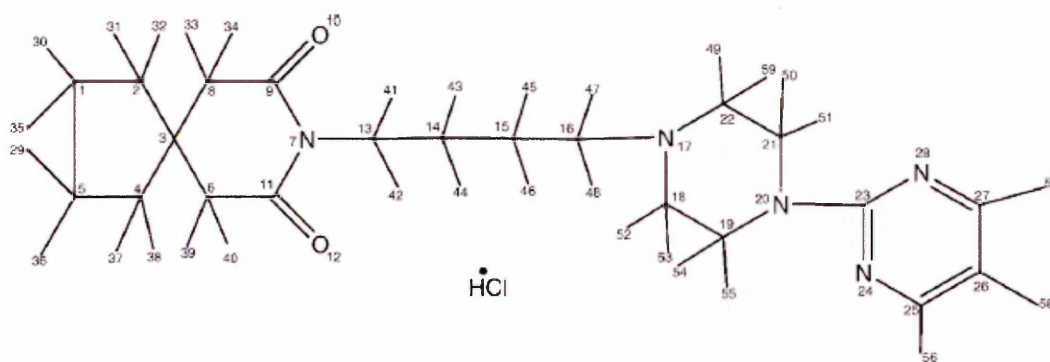


Fig1-5. Chemical structure of buspirone hydrochloride [47].

The hydrogen atom connected with N17 also showed the ability to form intermolecular and intramolecular hydrogen bonding with the chloride ion [47].

The buspirone hydrochloride was found to make complexes with ion exchange polymers in tested controlled release formulations. The complex was usually formed with anionic exchange resins or with easily dispersible, hydrophilic polymers with an average molecular weight of less than 500,000. First of all, the substances were admixed and the formation of the complex started after exposure to water either during preparation of the liquid dosage form or in situ (the solid dosage form comes into contact with the aqueous or gastrointestinal tract environment) [51]. There is no information available about the activity of the 6-hydroxy buspirone hydrochloride in complex formation, nor any data published about the stability of this substance. The kinetic studies made on the rate of decomposition of the solid state buspirone hydrochloride in bulk and in a tablet under the trade name BUSPAR, proved better stability of the drug in bulk than in the solid dosage form both in humid and dry conditions [52].

### 1.2.2 Pharmacological influence of 6OH BP

Buspirone hydrochloride is an anxiolytic drug from azapirones approved for the treatment of anxiety disorders and depression by the US Food and Drug Administration.

It does not exert anticonvulsant or muscle effects and lacks the prominent sedative effect associated with more typical anxiolytics [53-56]. However, some adverse effects like dizziness, nausea, headache, nervousness, light headedness as well as symptoms of restlessness were reported. It became desirable to find a drug with more robust anxiolytic potency but with a lack of the adverse effects. Over the years, studies indicated that buspirone is extensively metabolized in the body. The 6OH BP is believed to be its major active metabolite circulating in human plasma. It has been found to be effective in the treatment of anxiety disorders and depression, has partial agonist activity at the 5-HT<sub>1A</sub> receptors and could be used as an effective anxiolytic agent alternative to the “parent compound” [57-59]. The clinical studies performed on all three forms of 6OH BP: racemate, R-enantiomer and S-enantiomer did not show any advantages of one form of the other regarding pharmacokinetics nor the tolerability. For future clinical trials and development the racemate was chosen as its form is fairly easy to synthesize [43-45].

### **1.3 pH modifiers**

Drug release is influenced not only by the properties of polymer matrices or active substances but also by those of drug release modifiers. These can be soluble and insoluble components. It was reported that replacing HPMC (reduced to 50 %) with an insoluble component resulted in an increased drug dissolution rate being observed. Also the presence of surfactants can enhance the drug release rate by controlling wettability [33]. The addition of other polymers showed some influence for drug release (depending on active substances and the kind of polymer used). Hypromellose showed pH independence in the range 3-11. However pH changes may affect the ability of the polymer to swell. That applies to the external environment surrounding the tablet and gel as well as the microenvironment within the gel matrix. If an acidic drug is buffered to a pH above its pKa and then dissociated, the drug may have a better solubility which results in a faster drug-release process. Acidification of the matrix core stabilizes the gel pH microenvironment such that the particular pH is maintained within the matrix core. It should potentially stabilize the drug release profile of a pH dependent drug [33]. Addition of organic acids to the hydrophilic matrices allows the maintenance of low pH values within the tablets during drug release in phosphate buffer (pH 6, 8 or 7). The most common organic acids are: citric, tartaric, fumaric, maleic and succinic acid.

Organic acids are used as pH-stabilizers within the core. Without organic acids, once the pKa value of the weakly basic drug or the pH value at which drug precipitation occurs is exceeded by the pH of intestinal fluids, precipitation of the weakly water-soluble free base takes place within the dosage form. The precipitated drug is no longer capable of diffusing through the film coating and is not released. By adding organic acids, the pH

value within the core is maintained and a constant drug release can be achieved over the wide pH range (depending on the type and amount of organic acids)

Depending on strength of the organic acid we can observe different dissolution rates followed by controlled release of the tablet. The strength of an acid in water i.e. the extent to which it is dissociated, may be determined by the equilibrium [30]:



Then the equilibrium constant in water is given by:

$$K_a = \frac{[\text{H}_3\text{O}^+][\text{A}^-]}{[\text{HA}]} \quad (\text{eq1.3})$$

$K_a$  is a specific type of equilibrium constant that indicates the extent of dissociation of hydrogen ions from an acid. The equilibrium is that of a proton transfer from an acid, HA, to water,  $\text{H}_2\text{O}$ .

Because this constant differs for each acid and varies over many degrees of magnitude, the acidity constant is often represented by the additive inverse of its common logarithm, represented by the symbol  $\text{p}K_a$  (using the same mathematical relationship as  $[\text{H}^+]$  is to pH).

$$\text{p}K_a = -\log_{10} K_a \quad (\text{e.q1.4})$$

In general, a larger value of  $K_a$  (or a smaller value of  $\text{p}K_a$ ) indicates a stronger acid, since the extent of dissociation is larger at the same concentration.

The acid dissociation constant  $K_a$  is determined by the difference in free energies  $\Delta G^\circ$  between the reactants and products, specifically, between the associated (AH) and dissociated ( $A^-$ ) states. Molecular interactions that favour the dissociated ( $A^-$ ) state over the associated (AH) state will increase  $K_a$  (because the ratio  $[A^-]/[AH]$  increases) or, equivalently, decrease  $pK_a$ . Conversely, molecular interactions that favour the associated (AH) state over the dissociated ( $A^-$ ) state will decrease  $K_a$  (because the ratio  $[A^-]/[AH]$  is lower) or, equivalently, increase  $pK_a$ .

The magnitude of the  $pK_a$  shift can even be determined from the change in  $\Delta G^\circ$  using the equation

$$K_a = e^{-\frac{\Delta G^\circ}{RT}} \quad (\text{eq1.5})$$

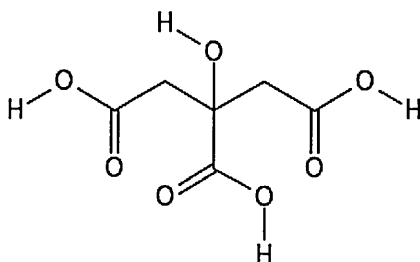


Fig1-6 Structure of citric acid

The  $pK_a$  value(s) of a compound influence many characteristics of the compound such as its reactivity, solubility and spectral properties (colour). Very weak acids ( with  $pK_a$  greater than 16 ) will not deprotonate in water at all, but if acids are sufficiently strong ( low enough  $pK_a$  ) they will be essentially fully ionised in water and will thus all appear to be of the same strength - which is known as the levelling effect of water.

Fumaric and citric acid have similar values of  $pK_a$  and they are stronger acids than succinic acid. As a consequence these two former acids when in a water environment would dissolve faster than the succinic acid, and so in a HPMC matrix tablet the addition of fumaric or citric acid will allow the active substance to diffuse out from the tablet quicker.

Addition of citric acid to the HPMC matrices produces greater dissolution rates (depending on the amount). This effect is considered to be mainly due to a loosening of the matrix after dissolution and release of its citric acid content. The effect of adding an acid is especially marked if the acid is in the tablet matrix. The effect is weaker if the acid is in granule cores. Formulations can be optimized by adding varying amounts of acid.

The advantage of using organic acids during formulations is that the local pH of the environment of our tablet can be controlled, which is very important because it can change the speed of drug release [60-62].

The infrared spectrum of citric acid (Fig 1-7) showed in the region  $\sim 3570-3200\text{ cm}^{-1}$   $\nu(\text{OH})$  the bands associated with the presence of hydroxyl groups from the chemical structure of the acid.

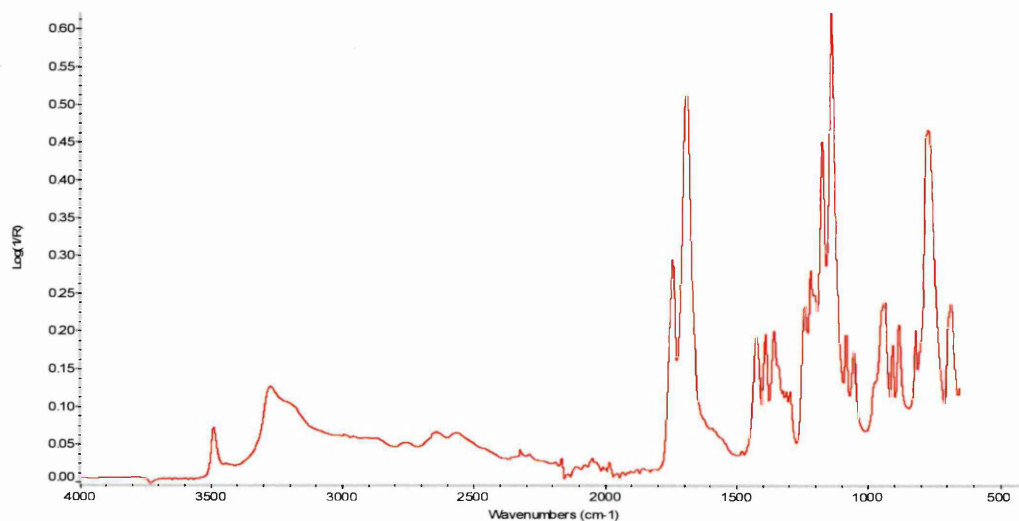


Fig1-7 The infrared spectrum of pure citric acid.

In the region  $\sim 3570\text{-}3200\text{ cm}^{-1}$   $\nu(\text{OH})$  the band is associated with the presence of hydroxyl group in the chemical structure of the citric acid. The shape of it is modified by the presence of  $\nu(\text{OH})$  band associated with citric acid where non hydrogen bonded hydroxyl group forms narrow sub-maximum peak  $\sim 3500\text{ cm}^{-1}$  as well as OH bonded stretching absorption at lower wavenumber within the discussed region. The secondary absorption for  $\nu(\text{OH})$  near the  $\sim 2600\text{ cm}^{-1}$  region is observed as the effect of overlap of the CH stretching region. The citric acid bands are also observed at  $\sim 1750\text{-}1680\text{ cm}^{-1}$  region associated with the characteristic carbonyl group  $\text{C}=\text{O}$  stretching frequency, and with presence of  $\sim 1175\text{-}1045\text{ cm}^{-1}$  strong absorption  $\nu(\text{CO})$  and  $\sim 955\text{-}890\text{ cm}^{-1}$  region associated with OH deformation vibration of carboxyl group [31, 32].



## **1.4 Drug release from hydrophilic matrices**

Matrices containing HPMC prolong drug release by rapidly forming a protective layer around the tablet surface when exposed to aqueous liquids. This hydrated viscous layer controls water penetration into the central dry core of the tablet and prevents disintegration. During the exposure of the polymer to an aqueous medium, HPMC undergoes rapid hydration and chain relaxation to form a viscous layer which is commonly termed the “gel layer”, at the surface of the tablet [37, 39]. If the uniform gel layer is not formed it may cause immediate drug release as the gel layer controls water uptake and modifies the mechanism of drug release from the matrix. The gel layer growth is observed as water permeates through it to hydrate the polymer particles. In the same time outer layers become fully hydrated and dissolve.

Water continues to penetrate towards the core of the tablet until the tablet has fully dissolved. Considering that during water uptake and drug release, the gel layer will contain polymer, drug and excipients experiencing different degrees of hydration or solution, it is generally assumed that water soluble drugs are released primarily through diffusion through the gel layer (Fig 1-8) and that poorly water soluble drugs are primarily released through erosion process [26, 27].

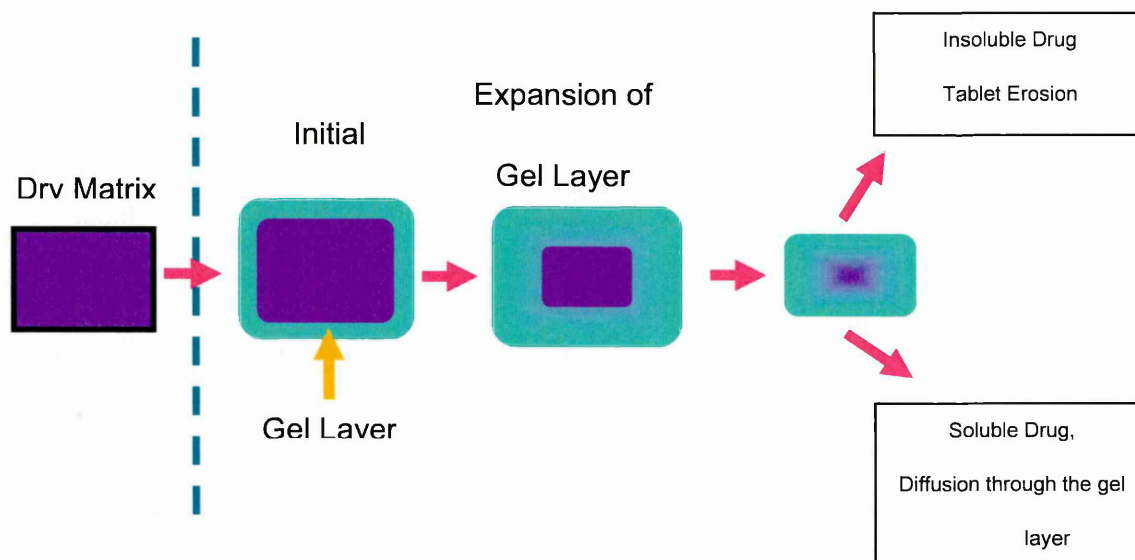


Fig.1-8 Schematic representation of the formation of the gel layer upon hydration of HPMC matrix tablet and the mechanism by which drugs are released.

Drug release at the molecular level is determined by polymer swelling, polymer front movement, drug dissolution, diffusion and matrix erosion. During the hydration of the HPMC one could select stages: liquid penetration, uncoiled and extended chains of the polymer and broken polymer hydrogen bonds which makes sites for hydrogen bonding with water molecules and leads to polymer mass entanglement with increasing content of water layer formation of gel layer by retardation of water uptake by the rest of tablet ingredients.

When the gel layer is formed the rate of drugs release is often reduced and dependent on the rate which: the drug molecules diffuse through the gel and the barrier layer is mechanically removed by attrition and disentanglement. Diffusion and erosion in most cases can occur simultaneously.

Colombo [66] suggested identification of three different distinct moving fronts (Fig. 1-9):

- *swelling front*: boundary between still glassy polymer (water has yet to fully penetrate the matrix) and its rubbery state (gel layer), the mobility of macromolecules is very low which leads to low diffusion rates of drug
- *erosion front*: boundary between the matrix and dissolution medium, mobility of polymer chains is increased – higher rates of active substance diffusion process
- *diffusion front*: boundary in the gel layer itself between solid and dissolved drug – here occurs drug dissolution.

The thickness of the dissolved drug-gel layer is the main controller for drug release.

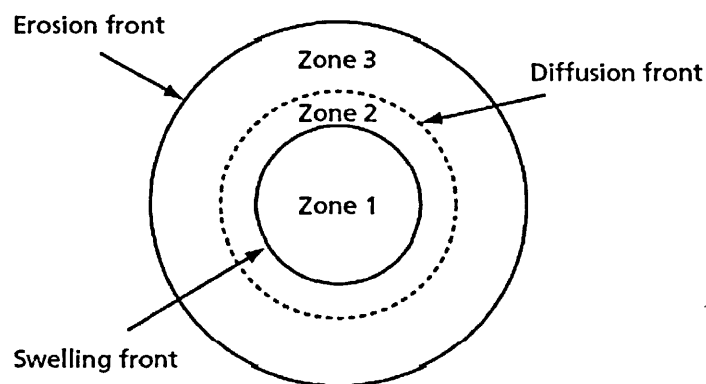


Fig 1-9 Schematic illustration of a swell able hypromellose-based matrix during drug release [33].

Movement of the erosion front determines drug release kinetics.

In the case if the polymer in the diffusion front is diluted so that the gel has no structural integrity it dissolves and erodes [33, 36]

Siepmann (Fig. 1-10) suggested that as the polymer concentration in the gel layer decreases towards the outer edge of the gel layer the polymer molecules entangle and disentangle without restriction. As the concentration decreases the rate of disentanglement exceeds re-entanglement and the gel layer erodes. The outer region of the gel layer represents polymer hydrated to the point where it no longer has structural integrity and may dissolve or erode away [63].

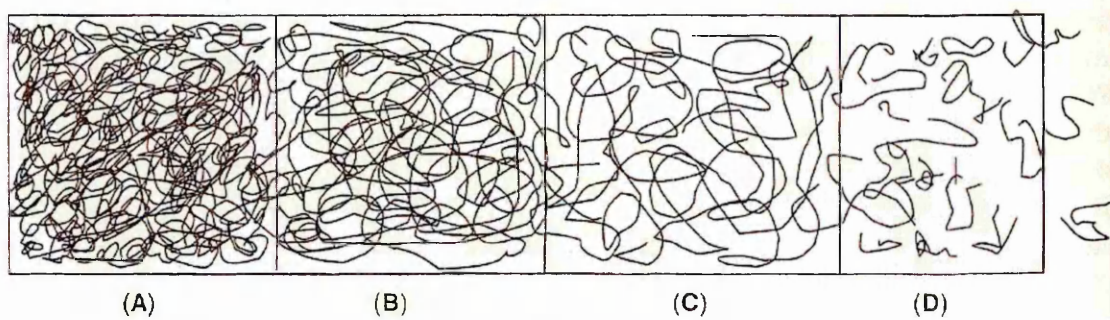


Fig. 1- 10 Process involved in polymer dissolution, (A) non-swollen polymer, (B) swelling polymer with water concentration gradient, (C) disentangling polymer molecules (D) unstirred layer with the polymer –concentration gradient [14].

## **1.5 Drug release kinetics**

Drug release in general is not purely swelling controlled, since it occurs mostly as the result of a combination of polymer relaxation and Fickian diffusion. The equation was proposed to describe drug release kinetics from drug delivery systems controlled by swelling [64]. The equation is based on power law dependence

$$\frac{M_t}{M_\infty} = kt^n \quad (\text{eq.1.6})$$

Where

$M_t$  is the amount of drug released at time  $t$ ,

$M_\infty$  the amount of drug released at infinite time,

$k$  a kinetic constant

$n$  is the diffusional exponent.

Based on the value of the diffusional exponent the drug transport in slab geometry is classified either as Fickian diffusion ( $n = 0.5$ ), non-Fickian or anomalous transport ( $0.5 < n < 1$ ), or Case II transport ( $n = 1$ ), where the dominant mechanism for drug transport is due to polymer relaxation during gel swelling. Anomalous transport occurs due to a coupling of Fickian diffusion and polymer relaxation.

The mechanism of drug release from HPMC matrices depends on many parameters including drug solubility, geometry of the dosage form and the conditions under which the drug is released. Siepmann et al [64] proposed that the overall mechanism of drug release is subject to many influences

- 1) An initial steep water concentration gradient at the matrix surface leading to inhibition of water into the matrix. The process is affected by the geometry of the system and in the case of cylindrical tablets the mass transport of water in axial and radial direction should be considered
- 2) Swelling of HPMC leading to changes in polymer and drug concentrations and increasing the dimensions of the tablet
- 3) Dissolution and diffusion of the drug in the hydrated medium out of the matrix as a result of the concentration gradient
- 4) Changes in the diffusion of the drug in the hydrated medium out of the matrix as a result of concentration gradient
- 5) The drug type as poorly soluble drugs may exist in the gel as either dissolved drug able to diffuse out of the matrix and non-dissolved drug particles released by the erosion
- 6) Drug loading as for high drug loadings the gel layer structure may change significantly during release resulting in more porous and erodible gel layer as drug is released
- 7) The type and molecular weight of HPMC used and its associated dissolution rate [13, 63, 64].

Higuchi [65, 66] derived the equation designed to predict the release of medicaments from ointments and creams

$$\frac{M_t}{M_\infty} = k\sqrt{t} \quad (\text{eq1.7})$$

Where

K and t is a constant related to the geometry of the system

Mt/M<sub>∞</sub> is the fraction of drug released at time t

This equation is the most often used to describe the release rate of drugs from matrix system as a result of simplicity.

The Higuchi model assumes:

- 1) The suspended particles are smaller in diameter than the thickness of the system
- 2) The initial drug concentration in the matrix exceeds the solubility of the drug
- 3) Mathematical analysis of diffusion is one-dimensional and as a result the effects of water penetration in axial and radial directions at the edge of tablets are considered negligible
- 4) Swelling or dissolution of HPMC is considered negligible and therefore the drug release occurs mainly by diffusion
- 5) Diffusivity of the drug is constant
- 6) Perfect sink conditions (conditions referring to the excess solubilizing capacity of the dissolution medium assuring the complete dissolution of the drug) should be maintained [65, 66].



There is no universal drug release mechanism valid for all HPMC based systems.

Different mathematical models may be applied for describing the kinetics of the drug-release process from matrix tablets, the most suited being the one which best fits the experimental results.

## **1.6 Aims of the thesis:**

- To optimize the preparation process of proposed pharmaceutical formulations ensuring the content uniformity of the mixtures
- To manufacture the reproducible tablets *in-situ* on the ATR crystal and build a PLS model to predict the concentration values for the particular excipients of analyzed formulation
- To confirm the distribution of the components in the tablets using imaging techniques.
- To investigate the drug release from binary and tertiary formulation in different media
- To conduct the analysis of interactions of the components in an aqueous environment
- To monitor the hydration and hyphenation experiments (by coupling the FTIR, UV spectrophotometer and HPLC pump) and develop information about the formulation behaviour in static and dynamic conditions
- To validate MCR as a tool to study such systems and conduct the analysis of the analyzed systems

## 2. Materials, methods and techniques

### 2.1 Materials

The materials used to make the model pharmaceutical formulations involved the amphiphilic polymer HPMC as the controlled release matrix tablet, citric acid to potentially modify microenvironmental pH, and the active substance. Further information about investigated formulation excipients are available in Chapter 1 (Section 1.1, 1.2, 1.3).

**Materials used in the project**

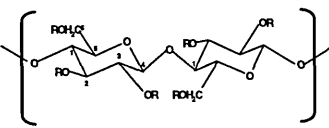
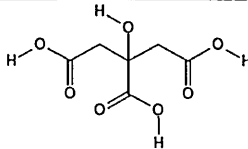
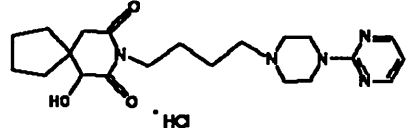
Substance	Structure of the substance	Material no.	Batch no.
Hydroxypropyl methylcellulose HPMC USP H VISC		1020278	4K83846
Citric acid anhydrous FCC USP		1020402	4D84505
BMS 528215-02 6-OH Buspirone HCL salt		1136941	4K85703

Table 2-1 The substances used for the project.

Hydroxypropyl methylcellulose (HPMC type 2208) grade K4M, 6-hydroxy buspirone hydrochloride and citric acid were a gift from Bristol-Myers Squibb and used as received without further purification.

#### Compounds used for dissolution testing and hyphenation experiments:

Hydrochloric acid, ACS reagent 37%, sodium hydroxide, solid, potassium dihydrogen orthophosphate were obtained from Sigma- Aldrich Co. Ltd Dorset UK

## **2.2 Methods and techniques**

### **2.2.1 Infrared Spectroscopy**

Infrared spectroscopy has been widely used for materials analysis in the laboratory for over seventy years. This useful technique can be used to provide qualitative and quantitative information of investigated materials. An infrared spectrum represents a fingerprint of a sample with absorption peaks which correspond to the frequencies of vibrations between the covalent bonds of the atoms making up the material.

Infrared radiation is electromagnetic radiation combining all the wavelengths between the visible and microwave region of the electromagnetic spectrum.

The IR region can be divided into three main sub regions: near IR ranging from 13,000 to 4,000  $\text{cm}^{-1}$ , mid IR ranging from 4000 to 400  $\text{cm}^{-1}$  and far IR ranging from 400 to 10  $\text{cm}^{-1}$

IR spectroscopy is a rapid method, which can be useful in kinetic studies of dynamic experiments.

#### **2.2.1.1 Principles of infrared spectroscopy**

In molecules, bonds vibrate in a variety of ways, and the vibrational energies of molecules may be assigned to quantum levels in the same manner as their electronic states.

A molecule consisting of two atoms is supposed to keep the balance between the attractive and repulsive forces and maintain the energy of the system at minimum. However all attempts to squeeze or pull apart the atoms would require an input of energy as the

repulsive/attractive forces will rise rapidly. The bond would likely behave like a spring and follow Hooke's law:

$$f = -k(r - r_{eq}) \quad (\text{eq. 2.1})$$

$f$  – restoring force,

$k$  - force constant

$r$  - intermolecular distance

$r_{eq}$  - intermolecular distance at equilibrium

The potential energy curve of such a system is parabolic and is given by:

$$E = \frac{1}{2}k(r - r_{eq})^2 \quad (\text{eq.2.2})$$

$k$ - force constant of the bond

A diatomic vibrating molecule system, as described above, is known as the simple harmonic oscillator model (SHO). As the vibrational energies are quantized, it is possible to calculate the allowed vibrational energies using the Schrodinger equation:

$$E_v = \left(v + \frac{1}{2}\right)h\omega_{osc} \quad (v = 0, 1, 2, 3, \dots) \quad (\text{eq.2.3})$$

$v$ - vibrational quantum number

$h$ - Planck's constant

$\omega_{osc}$  – oscillating frequency

Further use of the Schrodinger equation will lead to the simple selection rule for undergoing vibrational changes in harmonic oscillator where

$$\Delta v = \pm 1 \quad (\text{eq.2.4})$$

Real molecules however don't harmonically oscillate therefore the bonds don't obey Hooke's law. Although the bonds are elastic, larger amplitudes of vibration can lead to

bonds breaking, which lead to the dissociation of the atoms. The Morse function is an empirical approximation for the potential energy in a real diatomic system and is given in the eq 2.5:

$$E = D[1 - \exp\{a(r_{eq} - r)\}]^2 \quad (\text{eq.2.5})$$

D – depth of the potential minimum

a – constant

The dissociation energy of the molecule can be found by substituting energy levels from Morse function into the Schrodinger equation and has a form:

$$\varepsilon_v = \omega_e \left\{ 1 - x_e \left( v + \frac{1}{2} \right) \right\} \left( v + \frac{1}{2} \right) \quad (\text{eq.2.6})$$

$x_e$  - anharmonicity constant

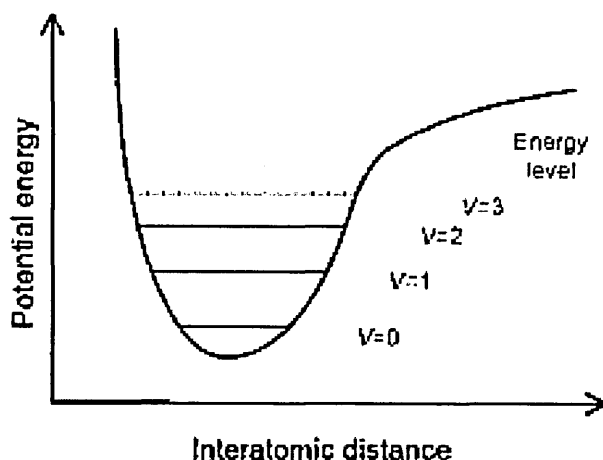


Figure 2-1. Energy diagram of the anharmonic diatomic oscillator [67]

The general observed transitions are:  $v = 1 \leftarrow 0$  represents fundamental,  $v = 2 \leftarrow 0$  represents 1<sup>st</sup> overtone,  $v=3 \leftarrow 0$  2<sup>nd</sup> represents overtone. The energy at  $v=0$  is termed as zero point energy however the real amount can be calculated from equation 2.6

Although most molecules are examples of polyatomic systems, the theory from diatomic molecules is useful to understand their spectra after modification [68].

A polyatomic molecule with  $n$  atoms has  $3n$  degrees of freedom which corresponds  $x$ ;  $y$  and  $z$  coordinate axes. To describe translational motion and rotational motion of the molecule additional 3 degrees are required. For nonlinear molecules  $3n-6$  degrees of motion are true fundamental vibrations, for linear ones  $3n-5$  degrees of freedom.

Usually polar bonds yield strong IR absorption. Modes which produce a change in the net dipole moment of the molecule are determined IR active while those which produce a net polarisability change are Raman active. The resultant band in IR spectroscopy is a fundamental vibrational band with intensity proportional to the square of the change in dipole moment. If the band arises from the combination of two or more different frequencies it's called a combination band. Also particular frequencies may give multiple bands belonging to a single band and they are referred to overtones. The frequency of the overtone is an integer multiple of the fundamental frequency, although the intensity is much lower.

The intensity of the band in an infrared spectrum can be modified by the amount of sample in the beam, vibrational level population and selection rules, for example, symmetry.

The Boltzmann distribution can be used to calculate the initial vibrational state at thermal equilibrium, which has an impact on the intensity of the spectral line. At room temperature the ground state is the most populated. [68-73]

Quantitative measurement of concentration can be obtained from infrared spectroscopy using the Beer-Lambert law:

$$I = I_0 \exp(-\epsilon cl) \quad (\text{eq.2.7})$$

or in the logarithmic form

$$\log\left(\frac{I_0}{I}\right) = \epsilon cl \quad (\text{eq.2.8})$$

Where:

$I$ - transmitted intensity

$I_o$ = incident radiation

$l$  - path length

$\varepsilon$  = frequency dependent extinction coefficient

$c$  – concentration

### **2.2.1.2 Instrumentation**

IR radiation can be measured by a dispersive spectrometer (in high-precision work) but more commonly using Fourier Transform Infrared spectroscopy (FTIR). Fourier transform involves the conversion of the time domain instrument response into the frequency domain spectrum. Modern FTIR instruments are based upon the Michelson interferometer, which is an optical device that splits a beam of radiation into two paths and recombines them; the intensity of variations of the exit beam can be measured by a detector as a function of path difference. The interferometer consists of four arms (Fig. 2-2). The first arm contains a source of infrared light (A) such as a mercury lamp or a silicon (Globar) rod, the second and third arm contain two mutually perpendicular planed mirrors - fixed mirror (C) and movable mirror (D) and the fourth arm is open. The movable mirror is moved at a constant velocity over the fixed distance and is also responsible for the quality of interferogram. A parallel, polychromatic beam of radiation from source is directed to the beamsplitter (B), a piece of semi-reflective material, such as thin Ge coating sandwiched between two pieces of KBr, where a beam of radiation from the source is split with approximately half of the light going to the fixed mirror which reflects the light back to the beamsplitter. KBr acts as a transmitter of radiation, and protects the beamsplitter coating from the environment. The rest of the light passes through to the moving mirror; and this



beam is also reflected back to the beamsplitter. The combined portion of the light which has travelled to both mirrors reaches the sample (E) and is transmitted towards to the detector (F) and the result is an interferogram. The major detectors used in mid-infrared systems are deuterated triglycine sulfate (DTGS) or liquid nitrogen cooled mercury cadmium telluride (HgCdTe), the so called “MCT” detector [67, 74, 75].

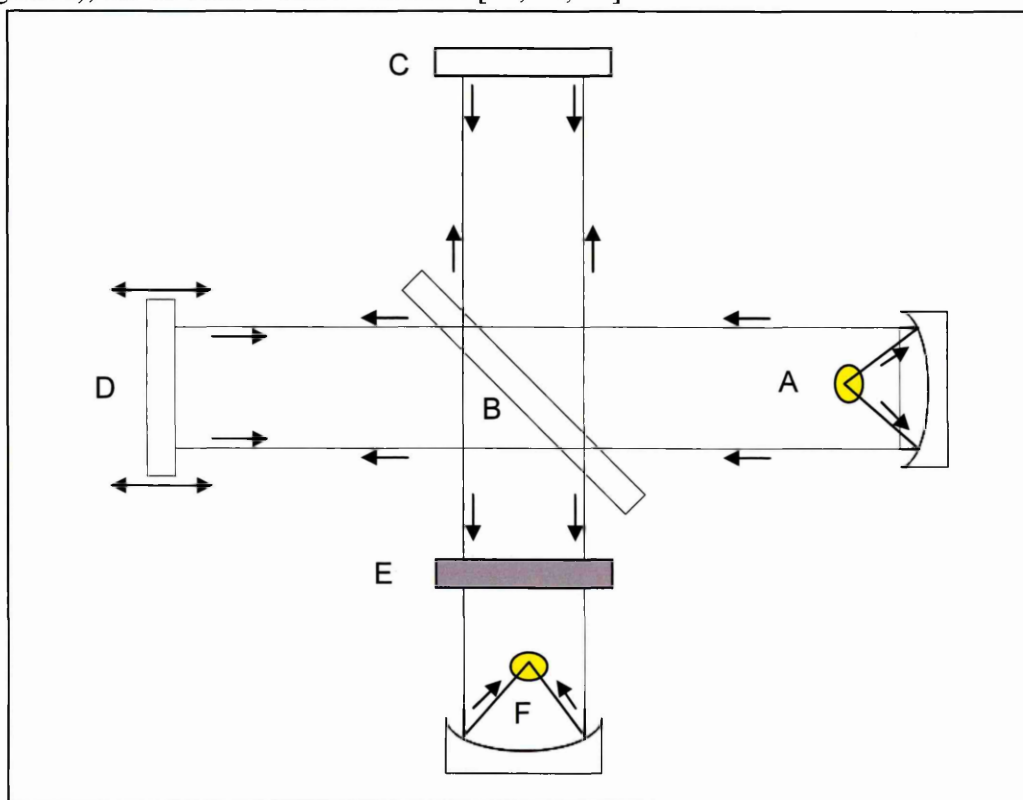


Fig. 2-2. Scheme of a FTIR instrument.

Depending on the path distance the light would travel between mirrors and beamsplitter, there will be constructive (radiation in phase) and destructive (light beams out of phase) interference present. As the moving mirror changes the position against the beamsplitter, depending on the rate the distance the mirror moves and frequency of the light beam, different wavelengths of the radiation will be in phase and out of phase at the frequency. The pattern of overlaying sinusoidal waves which is in the time domain is defined as an

interferogram. The interferogram is converted by means of Fourier transform and the result is a spectrum [75-78].

### 2.2.1.3 Advantages and limitations of FTIR spectroscopy

There are various advantages of the FTIR technique over conventional dispersive spectrometers. A few of the advantages of FTIR spectroscopy approach are outlined below.

#### 1) The throughput (Jaquinot) advantage:

In FTIR instruments there are no slits restricting the wavenumber range and therefore no reduction of the radiation intensity unlike the traditional dispersive approach. This results in increased light energy passing through the sample, thus improving the signal to noise ratio when compared to the dispersive systems.

The spectral optical conductance of a dispersive instrument is given by:

$$G_v^G = \frac{hH}{f\nu} R_0 \quad (\text{eq.2.9})$$

Where  $G_v^G$  is the optical conductance per wavenumber of grating,

$H$  is the height of the grating,

$h$  is the length of the entrance slit,

$f$  is the focal length of the collimator,

$R_0$  is the theoretical resolving power.

The interferometer optical conductance is expressed by:

$$G_{\bar{\nu}}^1 = \frac{2\pi H^2}{\bar{\nu}} \quad (\text{eq.2.10})$$

The ratio of these two optical conductances (eq.2.11) equates to throughput around 100 times more in an FTIR system than in dispersive instrument.

$$\frac{G_{\bar{\nu}}^1}{G_{\bar{\nu}}^G} \approx \frac{2\pi f}{h} \quad (\text{eq.2.11})$$

$\pi$  – constant

$f$  – focal length of the collimator

## 2) **The multiplex ( Fellgett) advantage:**

The FTIR instrument can detect all the frequencies at the same time whilst the dispersive systems are able to measure only a small wavenumber range at a time. If the spectrum is considered to be made up by M individual measurements at equal frequency and resolution then with increasing amount of spectral details the increase of M would be observed. In the case of a dispersive instrument, increasing the number of spectral elements will result in an increase in the length of time ( $\tau$ ) needed to conduct a particular experiment. The signal to noise ratio is influenced by this advantage and for the dispersive system is given by:

$$S / N_D \propto \frac{\tau^{\frac{1}{2}}}{M^{\frac{1}{2}}} \quad (\text{eq.2.12})$$

For FTIR spectrometers the signal to noise ratio is proportional to the square root of the total number of measurements (eq.2.13)

$$S / N_{FT} \propto \tau^{\frac{1}{2}} \quad (\text{eq.2.13})$$

The complete spectrum can be acquired much faster by FTIR spectrometers it allows an increasing signal to noise ratio to be achieved on the order of  $\sqrt{M}$ .

### 3) **The Connes advantage:**

In FTIR systems, the spectral wavelength is determined very accurately by sampling at known time intervals given by the output of highly monochromatic laser (usually at wavelength of 632.8 nm). As the time intervals of measurement are accurately known, the process of conversing time domain spectrum to the frequency domain spectrum is also highly accurate. This advantage provides the analyst an absolute control of the spectral wavelength and enables the application of manipulative techniques like spectral subtraction. Signal to noise ratio can also be further improved during the analysis of the many collected and averaged spectra. Such a high level of accuracy means as well that spectral calibration is not necessary.

There are some limitations with FTIR spectrometers connected with the technique itself. First of all the FTIR instrument doesn't produce a spectrum, but an interferogram which is difficult for people to deduce information about the analyzed sample. The computational power (cheap and fast CPUs) to perform a Fourier transform is required; the frequency domain spectrum can be produced in a short time. Another problem is that if light from the source is "noisy" (the Fellgett disadvantage) at a certain frequency range the detector still detects noise at all frequencies. Next important issue for the analyst from the practical point of view is presence of the CO<sub>2</sub> and water vapour bands in the spectrum. These unwanted bands can be eliminated by purging the sample compartment with infrared inactive dry gas like nitrogen during the measurement or subtraction process. Another disadvantage which is the cost of FTIR instrument becomes less important nowadays in comparison with similar price of single frequency dispersive system [75].

#### 2.2.1.4 Sampling techniques

Infrared spectroscopy gives a choice of sampling technique depending on the specific type of samples one would like to study. Each approach has its own strengths and weaknesses. This section will discuss only the sampling techniques relevant to the project.

##### 2.2.1.4.1 Transmission

Transmission (Fig. 2-3) is the most basic technique where infrared irradiation is passed through the sample and the transmitted radiation is measured. The spectrum obtained represents the whole sampled area i.e. the bulk sample. This method is useful for thin samples ( $<10\text{ }\mu\text{m}$ ), or during the investigation of weak bands like overtones in thicker samples [79]. Solid samples may require preparation before the measurement for example preparing KBr pellets or dispersions in Nujol mull, which is a time consuming process and difficult to reproduce.

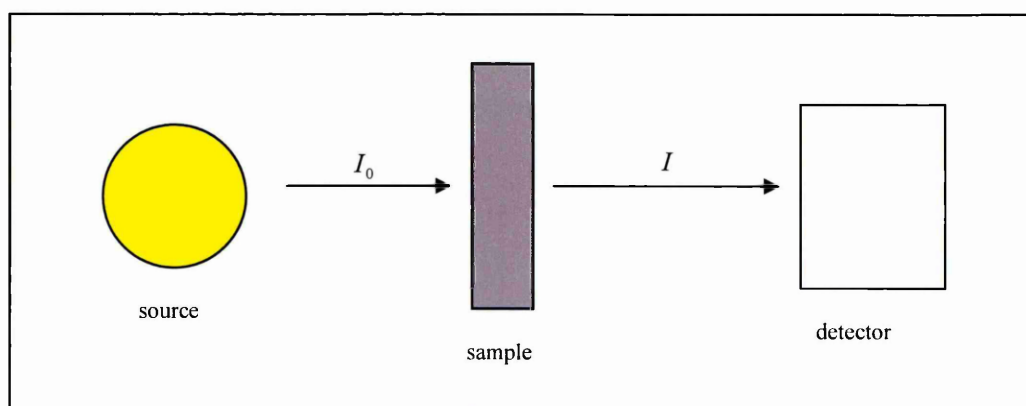


Fig. 2-3. The transmission experiment.

The transmittance is given by:

$$T = \frac{I}{I_0} = \exp(-\alpha l) \quad (\text{eq.2.14})$$

$I$  – transmitted intensity

$I_0$  – incident intensity

$\alpha$  – molar extinction coefficient

$l$  - sample thickness

#### 2.2.1.3.2. Attenuated total reflectance spectroscopy (ATR)

Attenuated total reflectance is also known as internal reflectance spectroscopy and is where the sample is placed in contact with an internal reflection element (IRE) of higher refractive index (Fig. 2-4). The technique is used to obtain spectra of thick solids, strongly absorbing liquids, semisolids, thin films, fibres, pastes and samples difficult to analyze using transmission (Fig. 2-3) as a sampling method [79, 80].

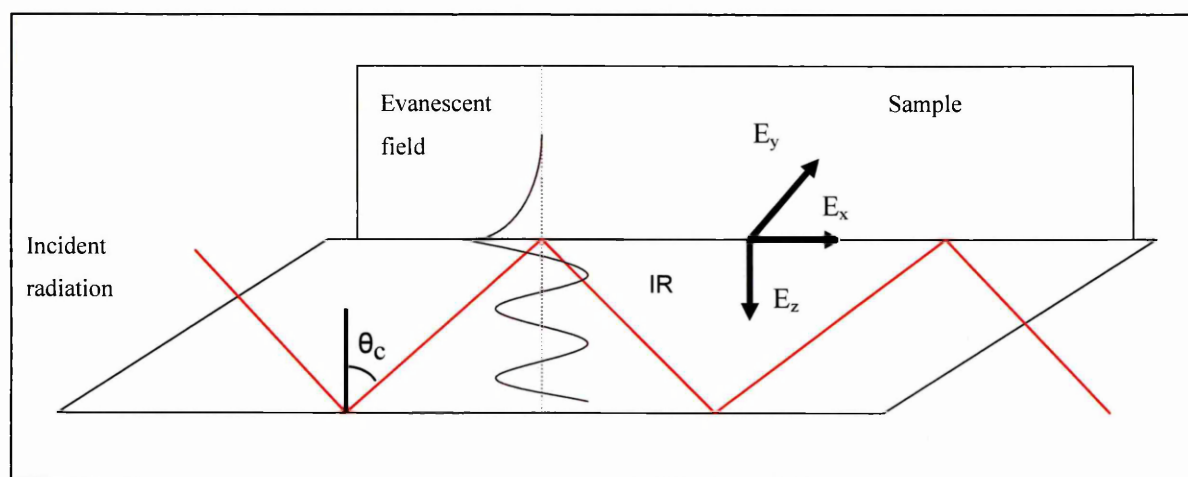


Fig.2-4 Schematic of ATR experiment

The presence of the evanescent field created at the surface of the ATR crystal is one of the most important theoretical aspects of ATR spectroscopy. Infrared light passes through the optical denser, medium with high refractive index (ATR crystal) at an angle of incidence greater than the critical angle ( $\theta_c$ ) and reflects at the interface of rarer medium, the material with lower refractive index (sample). The propagating light passes through the ATR crystal but an electric field penetrates into the sample and the intensity of the electric field decays exponentially with increasing distance from the interface. This non-transverse wave is known as an evanescent field and its rate of decay depends on angle of incidence and wavelength of the light, as well as on the refractive indices of the denser and rare media.

If the sample absorbs radiation, the reflection is said to be attenuated; in the case of a none absorbing medium the reflected rays will show the same intensity as the incident ones. Total internal reflection occurs when the incident angle is greater than the critical angle. During the reflection there should be no radiation lost in an ideal system unless it is absorbed by propagating medium, practically the ATR material should have a high refractive index and be infrared transparent. Commonly used materials for ATR crystals are shown in a Table 2-2.

<b>Material</b>	<b>Refractive index</b>	<b>Spectral range (cm<sup>-1</sup>)</b>
ZnSe	2.4	20,000 - 650
KRS-5 (TlI <sub>2</sub> /TlBr <sub>2</sub> )	2.4	20,000 - 350
Ge	4.0	5,500 - 870
Si	3.4	8,300 - 1100

Table 2-2. Common materials used for ATR crystal and some their properties.

The most important properties of the evanescent field are as follow:

- 1) There is no loss of energy between the rarer and denser media and propagating radiation in the ATR crystal is totally internally reflected.

- 2) The evanescent field is confined to the surface of the sample and decreases in intensity with the distance to the interface along z-axis.
- 3) The evanescent field is a non-transverse wave which has components in all spatial directions.
- 4) There is non-zero energy flow along the x-axis, parallel to the surface which results in a so called Goos-Hanchen shift; displacement of the incident and reflected waves.

The decrease in intensity of the evanescent field at the surface of the rarer medium is expressed by:

$$E = E_0 \exp - \frac{2\pi}{\lambda_1} (\sin^2 \theta - n_{21}^2)^{\frac{1}{2}} z \quad (\text{eq.2.15})$$

Where E is the value of the electric field at distance Z into the sample

$E_0$  is the electric field amplitude at the surface of the sample

$\theta$  is angle of incidence

$\lambda_1$  is wavelength of the radiation in the ATR crystal ( $\lambda_1 = \lambda/n_1$ )

Exponential constant is replaced by the electric field amplitude decay coefficient  $\gamma$  giving:

$$E = E_0 \exp[-\gamma Z] \quad (\text{eq.2.16})$$

$$\gamma = \frac{2\pi (\sin^2 \theta - n_{21}^2)^{\frac{1}{2}}}{\lambda_1} \quad (\text{eq.2.17})$$

In the rarer medium the depth of penetration ( $d_p$ ) of the evanescent field is defined as the depth (Z) at which the value E equals to  $E_0 \exp[-1]$

$$Z = d_p = \frac{1}{\gamma} \quad (\text{eq.2.18})$$

However the real sampling depth of penetration ( $d_e$ ) is approximately three times  $d_p$ . The thickness of the sample which gives the same absorbance for the transmission experiment



at normal incidence is known as effective thickness ( $d_e$ ). The dependence between reflectivity and the effective thickness in the realistic case of rarer medium is given by:

$$R = \frac{I_R}{I_0} = \exp(-\alpha d_e) \approx (1 - a) \quad (\text{eq.2.19})$$

$$a = \alpha d_e \quad (\text{eq.2.20})$$

Where R is reflectivity

a is the absorption parameter for single reflection

$\alpha$  is absorption coefficient the same as for transmission

If one would like to calculate the effective thickness ( $d_e$ ) the electric field components needs to be determined.

Electromagnetic wave has two polarizations; the transverse magnetic (TM) which is parallel to the plane of incidence and the transverse electric (TE) perpendicular to the plane of incidence. The TM has components in the x and z planes whilst the TE wave have components in the y plane.

$$TE = E_{\perp} = E_y \quad (\text{eq.2.21})$$

$$TM = E_{\parallel} = \sqrt{|E_x|^2 + |E_z|^2} \quad (\text{eq.2.22})$$

The properties of the evanescent field depend on thickness of the rarer medium. Two cases can be determined; the semi-infinite bulk where the electric field amplitude falls to the very low value within the thickness of the sample ( $t \gg 1/\gamma$ ) and the thin film case where the electric field amplitude value remains constant over the thickness of the film ( $t \ll 1/\gamma$ ).

The semi-infinite bulk case:

TE wave,

$$E_y = \frac{2 \cos \theta}{\sqrt{(1 - n_{21}^2)}} \quad (\text{eq.2.23})$$

TM wave,

$$E_x = \frac{2 \cos \theta \sqrt{(\sin^2 \theta - n_{21}^2)}}{\sqrt{(1 - n_{21}^2)} \sqrt{[(1 + n_{21}^2) \sin^2 \theta - n_{21}^2]}} \quad (\text{eq.2.24})$$

$$E_z = \frac{2 \sin \theta \cos \theta}{\sqrt{(1 - n_{21}^2)} \sqrt{[(1 + n_{21}^2) \sin^2 \theta - n_{21}^2]}} \quad (\text{eq.2.25})$$

Where  $n_{21} = \frac{n_2}{n_1}$

The thin film case:

TE wave,

$$E_y = \frac{2 \cos \theta}{\sqrt{(1 - n_{31}^2)}} \quad (\text{eq.2.26})$$

TM wave,

$$E_x = \frac{2 \cos \theta \sqrt{(\sin^2 \theta - n_{31}^2)}}{\sqrt{(1 - n_{31}^2)} \sqrt{[(1 + n_{31}^2) \sin^2 \theta - n_{31}^2]}} \quad (\text{eq.2.27})$$

$$E_z = \frac{2 \sin \theta \cos \theta}{\sqrt{(1 - n_{31}^2)} \sqrt{[(1 + n_{31}^2) \sin^2 \theta - n_{31}^2]}} \quad (\text{eq.2.28})$$

$n_{31} = \frac{n_3}{n_1}$ ,  $n_{32} = \frac{n_3}{n_2}$

Plotted values of electric field amplitudes for different angles of incidence (Fig 2-5) showed that  $E_y$  and  $E_z$  reach maxima at the critical angle,  $E_x$  is equal zero. At the point  $90^\circ$  the electric field amplitude is zero for all directions.

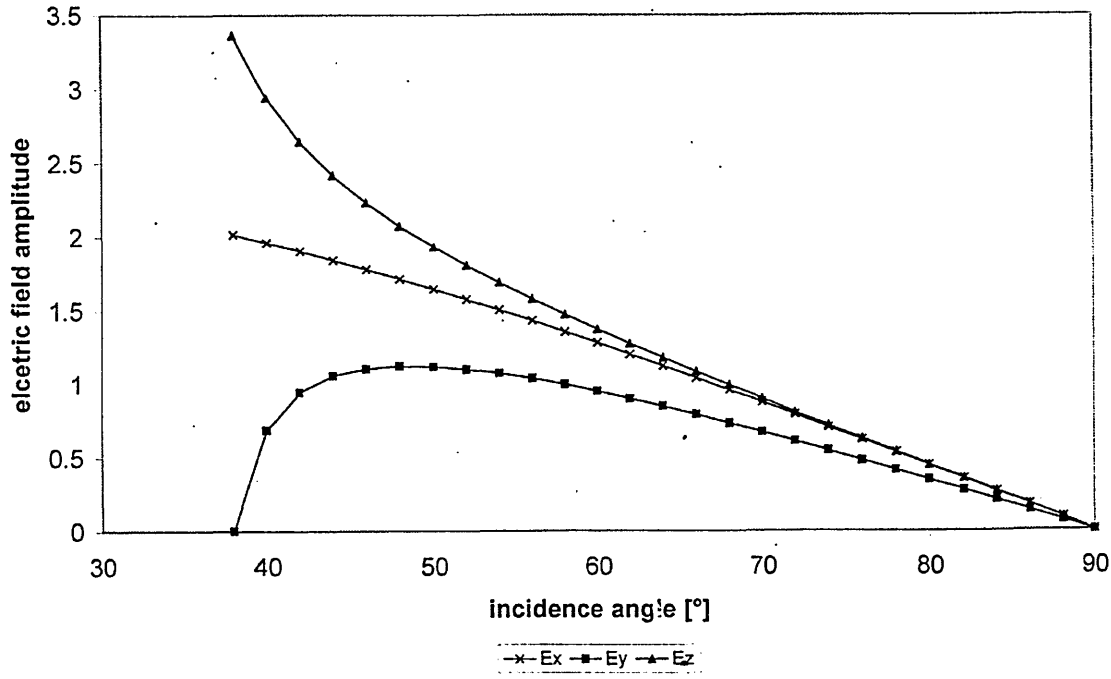


Fig. 2-5. The variations of calculated electric field amplitudes with angle of incidence for polarized radiation.

The relation between the electric field E and the absorption parameter a, is given by:

The thin film case:

$$a = \frac{n_{21}\alpha}{\cos\theta} \int_0^{\infty} E^2 dZ \quad (\text{eq.2.29})$$

The semi-infinite bulk case:

$$a = \frac{A}{N} = \frac{n_{21}\alpha C}{\cos\theta} \int_0^{\infty} E^2 dZ \quad (\text{eq.2.30})$$

Where A is absorbance

C is the concentration

N is the number of reflections

$\alpha$  is the molar absorption coefficient

Giving:

$$a = \frac{n_{21} \alpha E_0^2}{2\gamma \cos \theta} \quad (\text{eq.2.31})$$

And for the thin film case where (t=d):

$$a = \frac{n_{21} \alpha d E_0^2}{\cos \theta} \quad (\text{eq.2.32})$$

Where d is a film thickness

By the substitution of the equations 2.32 into 2.21 for thin film case and 2.17 and 2.23-2.25 for semi-infinite bulk case one gets

The semi-infinite bulk case

TE wave,

$$d_{e\perp} = \frac{n_{21} \lambda_1 \cos \theta}{\pi(1 - n_{21}^2) \sqrt{(\sin^2 \theta - n_{21}^2)}} \quad (\text{eq.2.33})$$

TM wave.

$$d_{e\parallel} = \frac{n_{21} \lambda_1 (2 \sin^2 \theta - n_{21}^2) \cos \theta}{\pi(1 - n_{21}^2) [(1 + n_{21}^2) \sin^2 \theta - n_{21}^2] \sqrt{(\sin^2 \theta - n_{21}^2)}} \quad (\text{eq.2.34})$$

The thin film case

TE wave,

$$d_{e\perp} = \frac{4n_{21} d \cos \theta}{(1 - n_{31}^2)} \quad (\text{eq.2.35})$$

TM wave,

$$d_{e\parallel} = \frac{4n_{21} d \cos \theta [(1 + n_{32}^4) \sin^2 \theta - n_{31}^2]}{(1 - n_{31}^2) [(1 + n_{31}^2) \sin^2 \theta - n_{31}^2]} \quad (\text{eq.2.36})$$

The total effective thickness is given by:

$$d_{e_{\text{u}}} = \frac{d_{e_{\parallel}} + d_{e_{\perp}}}{2} \quad (\text{eq.2.37})$$

The effective sampling thickness ( $d_{\text{eu}}$ ) depends on parameters like the electric field decay constant ( $\gamma$ ), the wavelength of radiation ( $\lambda$ ), the angle of incidence ( $\theta$ ), the electric field at the surface ( $E_0^2$ ), the sampling area and refractive indices of rarer and dense medium [79-83].

The analyzed samples have different refractive indexes based on the type of formulation and whether the sample is a solid dosage or hydrated form. Considering the dependence of depth penetration and wavelength of the incoming radiation; the depth of penetration will be greater at higher wavelengths using the FTIR-ATR technique whilst the NIR shows the reverse phenomena the longer the wavelengths the less penetration into the sample.

The ability to control the sampling depth has allowed for concentration-depth profiling of absorbing species, however in order to achieve good quality, reproducible data, pressure needs to be applied to the sample to ensure good contact between the sample and ATR crystal.

### 2.2.2 NIR Imaging

NIR chemical imaging (NIR-CI) is a rapidly emerging analytical methodology that combines the strengths of both digital imaging and near infrared (NIR) spectroscopy. The technique provides qualitative and quantitative insight into chemically heterogeneous samples in the form of high resolution chemical maps showing the visual location of components within the analyzed samples [34].

In this project, the NIR Chemical Imaging approach was used to determine the distribution of components in the investigated tablets, which will have a significant impact on release properties of the formulation.

#### **2.2.2.1 Fundamentals of NIR-CI**

Hyperspectral or Chemical Imaging is a technique which allows spatially resolved collection of sample spectra. The spectra are obtained at each data point in the spatial image. Spectral images are visualized as a three-dimensional block and termed a hypercube (Fig. 2-6). One of the three dimensions is wavelength ( $\lambda$ ) and the other two are the spatial dimensions (x and y).

The hypercube can be visualized as channels or pixels. Pixel is spatially resolved spectrum so called as one detector element. Selections of the particular pixels will yield spectra at the particular spatial point. Channels or the Image planes are spectrally resolved images, which yield the spatial image information at a particular wavelength point [84].

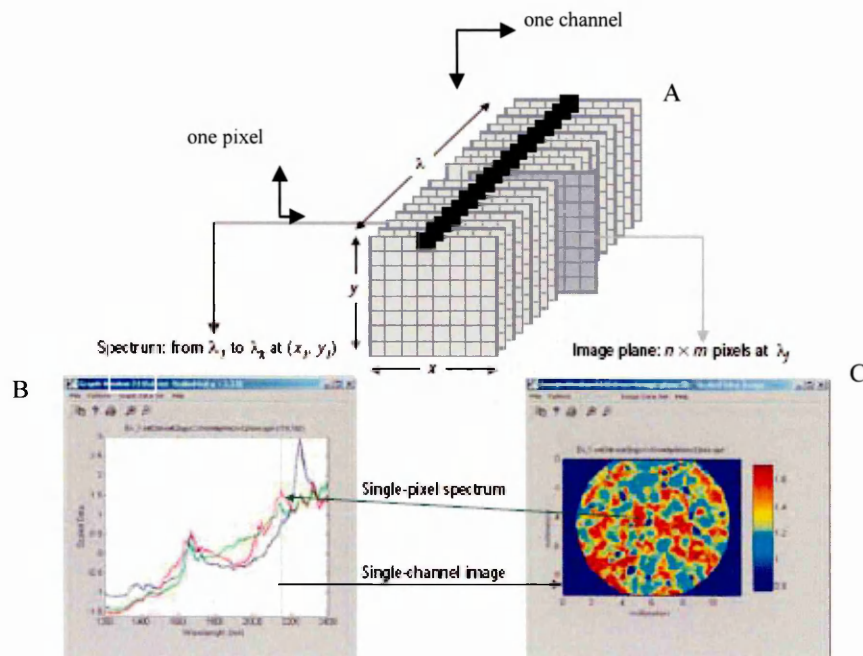


Fig.2-6 Scheme of spectral imaging hypercube representing the spectral and spatial dimensions [85].

The 3-dimensional cube shown in Figure 2-6 consists of both spatially resolved spectra and wavelength-dependent images. The X and Y axes represent spatial information, and the  $\lambda$  axis represents reflectance at the selected NIR wavelengths. The image cube can be seen as a series of wavelength-resolved images (i.e. the image plane in Fig. 2-6C) or as a series of spatially resolved spectra (i.e. the spectra in Fig. 2-6B), one for each point on the pixel. The complete integration of spatial and spectral information adds a new dimension to data analysis. The ability to explore the interdependency of spectral and spatial information is the basis for its unique capabilities which is different qualitatively from simple point-by-point spectroscopy [85, 86].

NIR Chemical Imaging also combines the benefits of NIR spectroscopic measurements.

The near infrared region of the electromagnetic spectrum extends along the range 780–2526 nm ( $12800 - 4000 \text{ cm}^{-1}$ ). The technique is based on molecular overtone and combination bands from stretching and bending vibrations, of predominantly O-H, C-H and N-H

functional groups, since the absorption bands in the near infrared region are typically quite weak, NIR can be used to analyze much thicker samples due to the size of the wavelength, it penetrates much further into a sample than mid infrared radiation [84, 87, 88]. Near infrared spectroscopy is therefore not a particularly sensitive technique, but it can be very useful in probing bulk material with little or no sample preparation. The molecular overtone and combination bands seen in NIR spectrum are typically very broad, often overlapping, leading to complex spectra; one can find it difficult to assign specific features to specific chemical components. Careful development of a set of calibration samples and application of multivariate calibration techniques is helpful for near infrared analytical methods [89].

#### **2.2.2.2 Instrumentation**

Chemical Imaging (general specification) radiation sources are usually quartz-tungsten halogen lamps with adapters for polarization and filtering connected to an integral computer system to control sample illumination. The sample is placed on a precise XYZ stage which can be operated manually or programmed for automated measurements of multiple samples (Fig 2-7). Typical scan times of the sample area are ~2 minutes, after the background and dark-field images are measured. The radiation interacts with the surface of the sample and it is diffusely reflected to the imaging optics. The camera allows the flexibility of directing it at fields of different areas, by the use of interchangeable refractive objectives. The refractive objective lenses are able to provide sample magnification. The Field of View (FOV) 12x10 mm (FOV's of 3x2.5 mm to 25x20 mm are available with optional objectives) and resolution 9  $\mu\text{m}/\text{pixel}$  at 2x2 mm; 39.7  $\mu\text{m}/\text{pixel}$  at 12x10 mm; 50  $\mu\text{m}/\text{pixel}$  at 13x10 cm. The diffuse reflectance image of the sample passes through the liquid crystal tunable filter LCTF. The tunable filter uses electrically controlled liquid crystal elements to select a specific wavelength of light for transmission through the filter at



the exclusion of all others. The LCTF in this NIR Chemical Imaging system covers a spectral range of 1200-2450 nm.

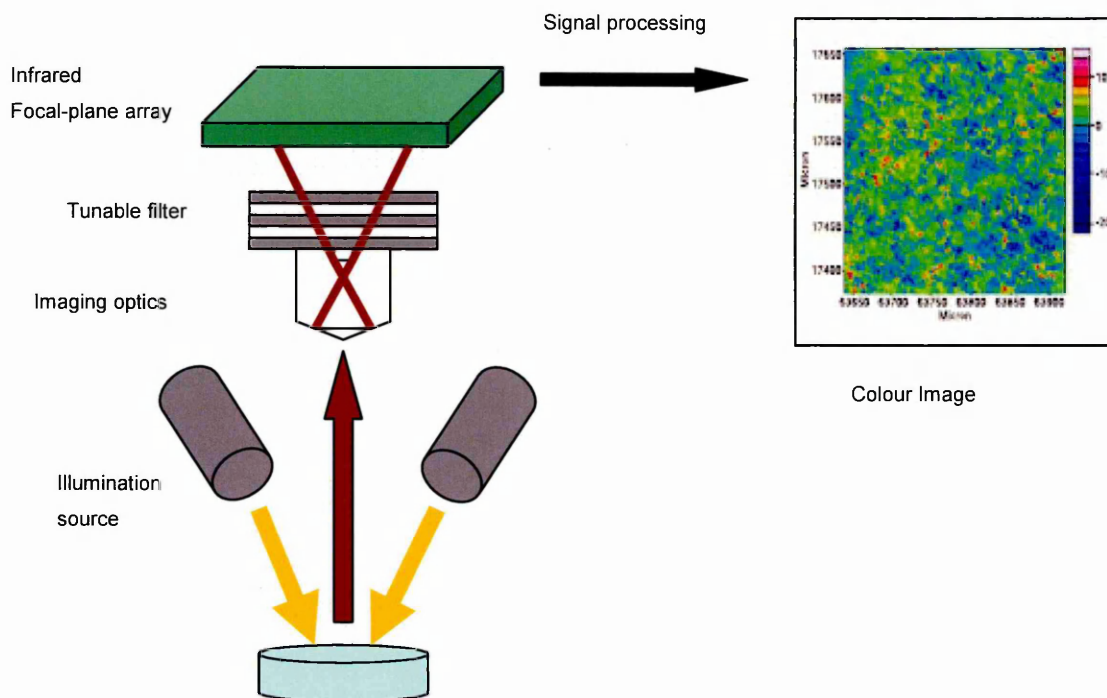


Fig 2-7. Schematic diagram of the NIR Chemical Imaging system used in this study.

A series of images of the investigated sample are captured by the NIR sensitive Stirling-cooled InSb Focal Plane Array (FPA) detector. The array contains 320x256 pixels or 81,920 equivalent spectra. The camera can be directed at different fields of view varying the sampling area by the interchangeable refractive objectives. The vibrational spectra collected for each pixel on the array detector creates a third dimension, the obtained data sets are referred to as the hyperspectral image cubes or hypercube [86, 87, 90, 91].

The system is supplied with a versatile chemical imaging analysis software package, ISys. ISys provides all the usual multivariate routines available in a NIR spectral software package and is compliant to 21 Code of Federal Regulations (CFR) part 11 [92, 93].

### 2.2.2.3 Data processing

In order to generate the chemical maps of the excipients distribution, the appropriate data analysis following the selection of the wavelength and spectral pre-processing is required. Data pre-processing removes the interfering parameters such as light scattering and possible path length variations caused by the physical properties of the sample. The pre-treatment methods include:

- 1) Mean centring: this calculates the average spectrum from all the spectra in a data set. The calculated value is subtracted from each vector (spectrum) in the data set. Also the mean concentration value of constituents (components) present in the analysed sample is calculated and subtracted from the individual excipient concentration. Mean centring removes the common variations (intensity of the peaks, etc.) from the data and is applied before calculating any model from the analysed data set [94].
- 2) First and second derivative: this corrects the baseline effects in spectra removing variations in baseline offset and baseline slopes. The first derivative measures the slope of the spectral curve at each point and removes any baseline offset. The second derivative measures the changes in the slope of the analysed curve and removes baseline offset and slope from a spectrum. It also takes away the offset of the first derivative.
- 3) Smoothing and filtering: this improves the signal-to-noise ratio of the recorded signal. The most commonly applied type is Savitzky-Golay polynomial smoothing. The polynomial smoothing function is fitted by least squares to the data using a specified number of data points before and after the derivative point. The Savitzky-Golay method gives control over the smoothing parameters during derivative

processing and avoids derivative noise enhancement which can appear while removing offsets [95-97].

- 4) Normalization: this corrects the spectra for indefinite path length or isolates the band of the constant concentration component. The spectra are normalised taking into consideration the area under the curve of the entire spectrum. It is important to avoid the interference of offsets and concentration variations between analysed samples and standards.
- 5) Standard Normal Variate transform (SNV) and Multiplicative Scatter Correction (MSC): these methods correct differences in the path length and baseline offsets in particle size distribution reflectance spectra. The advantage of MSC over SNV is that the processed spectra retain the original magnitude of the Y scale whereas the SNV transformation requires a mean subtraction, which results in spectra centred about the zero axis. Both methods can be used to process transmission spectra [94-96].

The hyperspectral image cubes can be processed using univariate or multivariate data analysis. Depending on the chemical and physical properties of the investigated sample different data modelling approaches can be used as authors have reported analysing data from pure substances and binary mixtures using either the intensity of single wavelength [86, 98-101], correlation coefficients or peak-height ratios [99, 102]. Univariate methods use one measurement per sample (either peak height or peak area). Reference spectra and calibration sets are required to perform qualitative or quantitative data analysis such as identifying an isolated peak in the spectra. The created univariate model is optimised by Least Squares Regression techniques [95, 103].

Another approach in data modelling is spectral matching (compare correlation). This method produces an image with values ranging from 1 to 0, where the value 1 means perfect correlation. Each region of the chemical map is assigned to a sequence of colours e.g. blue, light blue, green, yellow, red. The colours represent the level of correlation of the investigated image sample with the reference material. This type of image is presented as a false coloured image. Good correlations values have a range from 0.99 to 0.80 (assigned as red on the image colour bar) and indicate the regions in the image belonging to certain reference material in the spectral library to which it's compared. Consequently, the blue areas on the image correspond to very low correlation values for a particular material and indicate its absence in the area of the investigated material [96, 104, 105].

Reduction of variables by Principal Component Analysis (PCA) is another approach to the modelling of imaging data. PCA is a mathematical procedure which reduces the spectral data into scores (scaling constants for spectral variations for example concentration of constituents) and loadings (number independent variations occurring in the spectral data like constituents of the sample, detector noise, possible inter-constituents interactions, etc). The number of principal components of the sample can be calculated. The reduced data can be used further for calibration modelling [96, 106]. Quantitative analysis of the data can be achieved by using a multivariate calibration approach on the set of samples. Addition calibration standards, which are representative of the analysed samples must be selected to determine the reference values and are related to spectral variations of the analysed analytical target. The model can be validated by cross validation or using an independent validation set [94, 96].

In the case of complex mixtures, multivariate approaches have generally proved to be more beneficial since more information is extracted about analysed samples than with univariate methodology. Published work includes data analysis methods like: principal component analysis (PCA) [102, 107-110], classical least squares (CLS) [100, 111], partial least squares (PLS-1 for linear methods, PLS-2 for non-linear methods) [107, 109, 111-114] and multivariate curve resolution (MCR) [115, 116]. Processing the data using different data analysis methods can provide different chemical information from analyzed sample images [117].

In this study NIR Imaging was used to determine the distribution of the components in the solid dosage form, the collected data was pre-processed and a PLS-2 model built.

#### **2.2.2.4 Applications of NIR imaging**

NIR spectral imaging provides a rapid approach for acquiring high-resolution spatial and spectral information on pharmaceuticals. It is a technology capable of providing an in-sight into the structure and function of modern solid dosage forms. It combines the capability of spectroscopy for molecular analysis with the power of visualization affording precise characterization of the chemical composition, domain structure, and chemical architecture. A NIR Chemical Imaging spectrometer is a solid state system without movable parts so often no calibration of the system is required, the presence of filters allow for specific wavelength image acquisition. There is no need for liquid nitrogen to cool down the system as focal plane array detectors can use electronic cooling to reach the conditions of liquid nitrogen operating temperature. The system allows for imaging of a wide range of samples without previous preparation including samples with uneven or shiny surfaces since the specular glare is removed by polarizers [91, 92]. The technique is useful in the investigation of blend uniformity, raw material and impurity detection and identification [84, 91], pharmaceutical solid dosage form analysis, tablet deconstruction, the content of moisture in excipients or wet granulation mixture as well as in determination of different fabric types and animal feed studies [84, 91, 114, 118, 119].

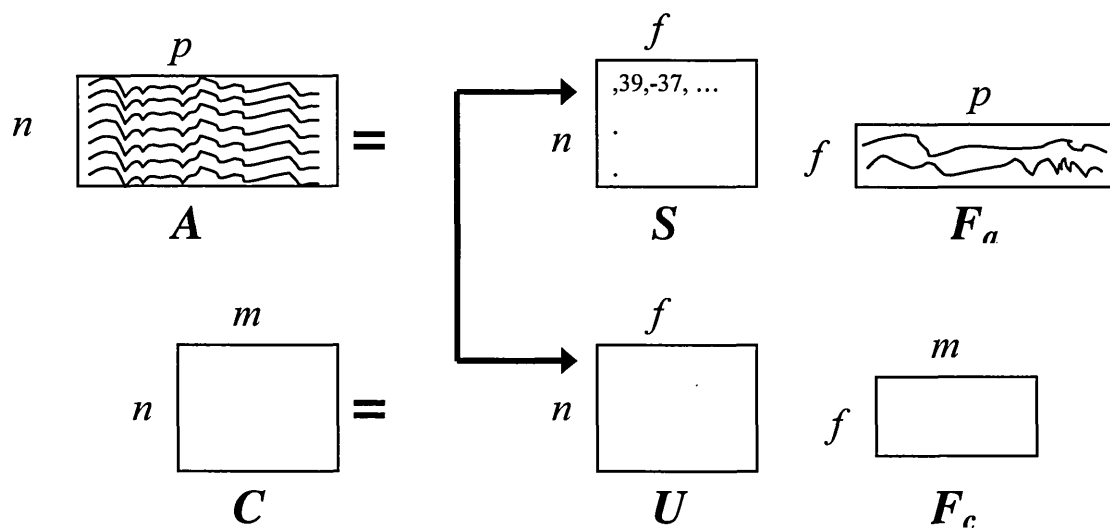
#### 2.2.4 Chemometric data analysis

The interdisciplinary field which involves using analytical chemistry, multivariate statistics, computer science and mathematical modelling is called chemometrics. Application of this data analysis provides a possibility to extract from the analytical data; maximum chemical information, optimization of experimental procedures and chemical measurements and also significance testing as well as calibration and validation of the analyzed data sets [94, 95, 97].

In this project PLS and MCR analysis was used to extract additional information from the spectroscopic data.

##### **2.2.4.1 Partial least squares (PLS)**

Partial Least Squares data analysis is a quantitative spectral decomposition technique for multivariate data. PLS is a regression method for constructing predictive models. It takes into account errors in both the concentration estimates and the spectra. The technique decomposes spectral and concentration data at the same time (Fig 2-8). In effect this generates two sets of vectors and two sets of corresponding scores; one set for spectral data, and the other for the constituent concentration. As every new factor calculated for the scores is “exchanged” the contributing factor is removed from the data. The reduced matrices are then used when calculating the next factor. The process repeats until the appropriate number of factors is calculated [94, 96].



$A$  = Spectral Data

$C$  = Constituent Concentration Data

$S, U$  = Spectral, Conc. Scores

$F_a, F_c$  = Spectral, Conc. Scores Factors

$n$  = Number of spectra

$p$  = Number of data points

$m$  = Number of constituents

$f$  = number of principal components

Fig. 2-8 Scheme of the PLS decomposition process [96].

There are two versions of the PLS algorithm; PLS-1 and PLS-2. The PLS-2 algorithm calibrates for all the constituents simultaneously, which means that the results of spectral decomposition give one set of scores and one set of eigenvectors for the calibration. However the calculated vectors are not optimized for each individual constituent. On the other hand the PLS-1 algorithm calculates a separate set of scores and loading vectors for each constituent of interest which should give more accurate predictions, but the time taken for the data analysis is increased [96, 103].

One of the most difficult tasks is determining the right number of loading vectors (factors) to use to model the data. If too few vectors are used to construct the model there will be a lack of prediction accuracy for unknown samples, this is known as under-fitting. If the number of factors gets too large, which will include noise from the data, the model will fit the sampled data perfectly but will fail to predict new data well, this is called over fitting.



Therefore it is important to define a model that contains enough vectors to properly model the components of interest without adding too much contribution from the noise.

One of the most effective methods to calculate the number of factors is PRESS ( Prediction Residual Error Sum of Squares). PRESS is calculated by building the calibration model with the number of factors, then predicting some samples of known concentration against the model.

$$PRESS = \sum_{i=1}^n \sum_{j=1}^m (Cp_{i,j} - C_{i,j})^2$$

n- number of samples, m- number of constituents, Cp- matrix of predicted sample concentration, C-matrix of known concentrations.

The smaller the value of PRESS, the better the prediction for a random effect model with a value of 0 indicating perfect prediction [120]. However, during the selection of number of factors (apart from the PRESS value) the number of components in the sample needs to be considered. There are a variety of methods which can be used to validate the model, like self –prediction, leverage or cross validation [96, 97, 121].

There are several advantages of the PLS methodology compared to PCA:

- 1) the eigenvectors are directly related to the constituents of interest rather than largest common variations
- 2) calibrations are usually more robust providing that the calibration set accurately reflects the range of variability expected in unknown samples
- 3) the technique can be used for very complex mixtures when knowledge about constituents of interest is required
- 4) sometimes it can be used to predict samples with constituents (contaminants) by modifications of the SIMPLS algorithm [122].

There are also PLS disadvantages, which involve longer calculations than in other classical methods, generally a large number of samples are required for accurate calibration and the samples for the calibration set must avoid co-linear constituent concentrations [96, 123].

#### **2.2.4.2 Multivariate curve resolution analysis (MCR)**

Multivariate Curve Resolution – Alternating Least Squares (MCR-ALS) - this iterative method finds the matrices of concentration profiles and instrumental responses. Multivariate curve analysis works by considering that the response matrix  $D$  containing raw measurements of all the components present in a data set can be separated into two matrices, one containing the pure normalised spectra (factors) and the other containing intensity information (scores). All the real spectra can then be considered as a linear combination of the factors and their scores. This is usually achieved by using methods like constrained least squares optimisation process [94].

Both matrices  $S$  (factors) and  $C$  (scores) (Fig. 2-9) are optimized at each cycle, none of them has a priority, The general operating procedure includes: determining the number of compounds in matrix  $D$ , calculating initial estimates, using the estimate  $C$  to calculate matrix  $S$ , using the estimate  $S$  to calculate matrix  $C$ , and from the product of  $C$  and  $S$  calculate and estimate the original data matrix  $D$  [94, 124].

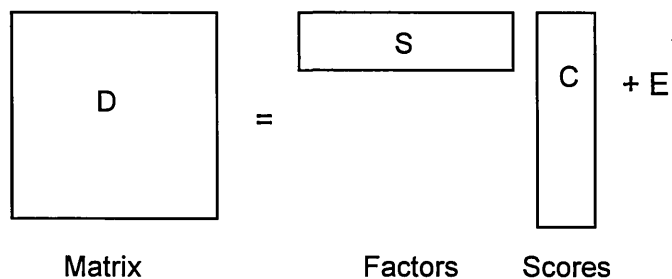


Fig 2-9 Scheme of MCR

During analysis it is often necessary to impose some defined limits such as forced zero to eliminate negative bands which have no physical meaning and an equality constraint to force all the variance into the scores matrix.

Although rotational ambiguity and noise are the two main sources of uncertainty in the multivariate curve resolution data analysis, the degree of selectivity of components from complex mixtures depends on the amount of band overlap in the region of interest from certain components with other constituents and from the distribution of the different components in the data set [125, 126]. Additional spectra of standards to data matrices are one way to avoid influence of rotational ambiguity.

MCR is widely reported as a desirable method of data analysis in biochemical processes like protein folding or protonation, environmental data analysis and complexation of nucleic acids [94].

### 2.2.5 UV/visible spectroscopy

Ultraviolet spectroscopy can provide quantitative information about investigated materials for monitoring kinetic reactions. A UV spectrum is often used as an identity check for the standard materials. UV/visible radiation is electromagnetic radiation combining all the wavelengths from the ultraviolet and visible region of the electromagnetic spectrum wavelength from 200 to 700 nm [127].

#### **2.2.5.1 Principles of UV/visible spectroscopy**

Radiation in the UV/visible is absorbed through the excitation of electrons involved in bonds between particular atoms of the molecule. If in the molecule the double bonds are present in the conjugated form; two or more double bonds separated by a single bond, so called chromophore system, the UV absorption will take place at the longer wavelength and with higher intensity.

UV/visible spectroscopy follows the Beer-Lambert law discussed in details in the section 2.2.1.4.1

#### **2.2.5.2 Instrumentation**

UV/visible spectrophotometer include a light source, which is usually a deuterium lamp for UV region from 190-350 nm, and quartz halogen or tungsten lamp for the visible region from 350-900 nm. The radiation passes through slits to reach a monochromator, which disperses the light to the constituent wavelengths further selected by a slit. The monochromator can be rotated so the full range of wavelengths is passed through the sample in the quartz cell whilst the instrument scans across the spectrum. The absorbed

radiation is reflected to the detector. A blank solution can also be used to correct for the background reading in the sample spectrum.

### **2.2.5.3 Applications**

UV/VIS spectroscopy is a robust and commonly used method for the quantification and characterization of materials, it can also be used indirectly to determine the pKa values for drugs and the solubilities of substances. UV-vis spectroscopy is widely used in dissolution apparatus to detect drug release from formulations and to monitor degradation products of the drug in the solution. It is a relatively cheap and easy-to-use method for making quantitative measurements and routine analysis.

The technique cannot be used easily in the case of complex mixtures and its selectivity depends on the chromophore of the material [127, 128].

### 2.2.6 Dissolution testing

Drug release in the human body can be measured 'in-vivo' by measuring plasma or urine concentrations in the subject concerned. However, there are certain obvious impracticalities involved in employing such techniques on a routine basis. These difficulties have led to the 'in-vitro' tests which are now the basic type of dissolution testing. Tablet dissolution is a standardised method for measuring the rate of drug release from a dosage form. The principal function of the dissolution test may be as follows:

- Optimisation of therapeutic effectiveness during product development and stability assessment.
- Routine assessment of production quality to ensure uniformity between production batches.
- Assessment of 'bioequivalence', that is, production of the same biological availability from discrete batches of products from one or different manufacturers.
- Prediction of 'in-vivo' availability [27, 129].

### 2.2.6.1 Instrumentation

Many different types of equipment have been developed for measuring dissolution rates. The solid state properties (e.g. morphology of the material) play a crucial role on the dissolution behaviour of a solid system. Also the dissolution media (most often phosphate buffer) may have an impact on the behaviour of the solid material, and these changes may alter the dissolution behaviour of the drug formulation/substance. Typical examples of these changes are alterations at the molecular level (polymorphic changes), re-crystallization or formation of hydrates/ solvates. A result of dissolution measurement is the concentration of the drug in the dissolution medium. With conventional dissolution apparatus (Fig 2-10) the liquid medium is pumped out of the vessel and measured with a UV-Vis spectrophotometer every 3 min. In case of sensitive measurements other specialized techniques like fibre optics can be used.

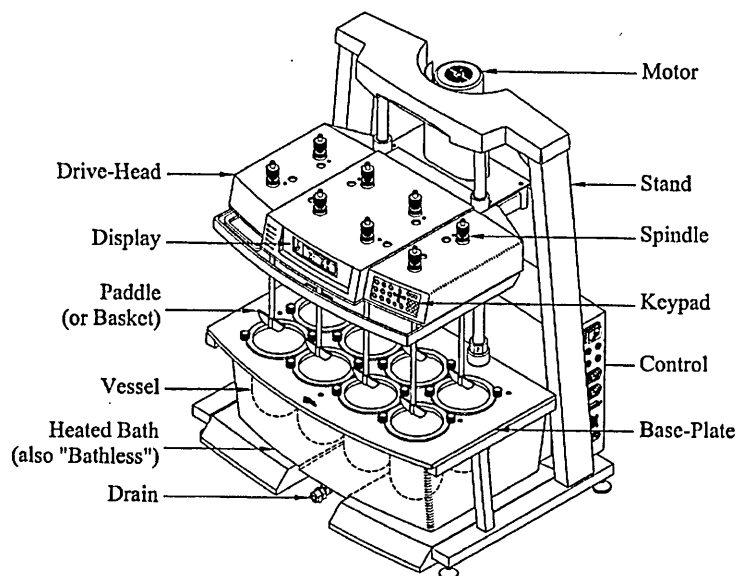


Fig 2-10 Schematic of the dissolution system apparatus [130]

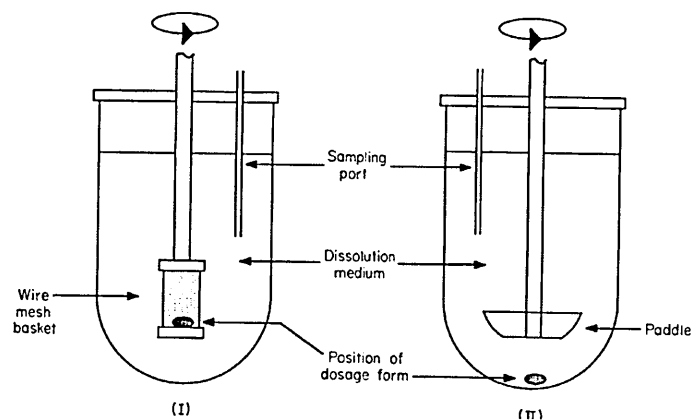


Fig 2-11 The dissolution vessels with mixing apparatus, I) baskets, II) paddles [130]

The basket (USP apparatus 1) as shown in Fig 2-11, consists of a stainless steel wire basket (approximately 25 mm diameter x 37 mm high 40-mesh) rotated at constant speed. The tablet is placed in the closed basket and all the samples at the same time are placed into the media in the vessels with at a constant temperature 37°C. The measurements are collected during the experiment in real time.

In this project the Dissolution testing method was used in order to determine drug release from the analyzed formulation [87, 130].



### 3. Optimization of the compaction process

Pharmaceutical formulations are multicomponent systems consisting of the active substance and a number of functional excipients like binder, disintegrant, lubricant, filler and glidant. During the early stage of method development it is critical to ensure the content uniformity of the investigated mixture. Apart from the chemical purity of the active substance and other ingredients, the physical properties of raw materials such as crystal form, particle size, moisture content and density need to be considered as these factors affect the mixing efficiency, determine the selection of the mixing method and influence the kinetics of drug release. The homogeneity of distributed components in the pharmaceutical formulation are important to ensure the final tablet quality [46, 131, 132]. The compressibility characteristics of powders and their tableting process require further exploration of the compaction force range suitable for certain formulation and appropriate tooling for the compression equipment.

A significant body of literature has been written about the subject of optimization parameters for pharmaceutical method development of solid dosage forms containing hydrophilic matrices [25, 101, 133-139]. Nokhodchi (1995) investigated the influence of different viscosity grades of HPMC, particle size and compression force on the HPMC compaction process [29, 140], whilst Velasco (1999) discussed the significance of particle size and compression force of the selected drug and HPMC formulation in dissolution studies [28]. Over the years, research has also concentrated on more complex mixtures, where the optimization of formulation development and its compaction process is more challenging [129, 141, 142].

The first experimental part of this project concentrated on optimizing the preparation, process and parameters for the proposed content of the formulation and is discussed in this chapter.

### **3.1 Aims:**

- To optimize the preparation process of proposed pharmaceutical formulations ensuring the content uniformity of the mixtures
- To manufacture reproducible tablets *in situ* on the ATR crystal and build a PLS model to predict the concentrations of particular excipients of the analyzed formulation
- To confirm the distribution of the components in the tablets using imaging techniques

## **3.2 Materials and methods:**

### **3.2.1 Materials**

Materials used in this Chapter are detailed in Chapter 2, section 2.1

### **3.2.2 Preparation of the mixtures**

Formulations were prepared according to proposed concentration values listed in Table 3-1.

**Formulation of HPMC and citric acid**

HPMC	Citric acid
95	5
90	10
80	20
50	50

Table 3-1. Composition of binary formulations derived from HPMC and citric acid mixtures

#### **3.2.2.1 Mixtures of powders with unmatched particle sizes**

Every formulation was mixed in three different ways; manual shaking (1 min), tumble blending (5 hrs) and grinding (2 mins) to optimize the mixing conditions for the formulation. The total mass of each mixture tested was 33.3 g.

#### **3.2.2.2 Mixtures with particle sizes less than 106 microns**

Citric acid was ground and sieved manually (the size of the sieve <106 microns) to produce a particle size range comparable to that of sieved HPMC (sieve <106 microns). The sample was placed on the 20 cm diameter, stainless steel sieve.

Four formulations with the composition shown in Table 3-1 were prepared using tumble blending for 15 min as a mixing method. The total mass of every mixture was 5 g.

### 3.2.3 Mixing procedures used to prepare formulations

#### **3.2.3.1 Manual shaking**

The mechanical stress caused by the shaking process is one of the methods that one could use to mix two or more substances. However, the effect of manual shaking depends on the materials used in a formulation, what may result in forming aggregates (conjunction of the particles into the mass) in the mixtures could have significant influence on the release of drug from the formulation (decreasing rates or more rapid release at different time points during the experiment) [143].

#### **3.2.3.2 Tumble blending**

The most common approach in industry is the use of tumble blending to homogeneously mix substances. Possible problems may occur with potential over- or under-blending of the mixture. Over-blending can affect the hardness of the tablet or retard the dissolution rates whilst the under-blending can cause compaction difficulties including reducing the compression rate or the tablet sticking to the punch [131, 144]. In this project a Stuart Rotordrive STR4 homogenizer was used to blend the samples. A hollow container with a mixture was attached horizontally to the rotating shaft for the required amount of time.

#### **3.2.3.3 Grinding**

This technique of mixing reduces the particle size of the components, it can lead to changes in the crystalline structure of the substances, improve the molecular interactions in the mixtures and enhance the solubility along with dissolution rates as required [145, 146].

The analyzed formulations were manually ground using a pestle and mortar for the predetermined time.

#### 3.2.4 Compaction process

The tablets were manufactured using the direct compression approach. The dry mixture of powders was compacted directly *in situ* on the ATR crystal, using an appropriate compaction cell.

##### **3.2.4.1 Design of compaction cell**

The design of the compaction cell for this project was based on Kazarian's published studies and reproduced with permission [147, 148].

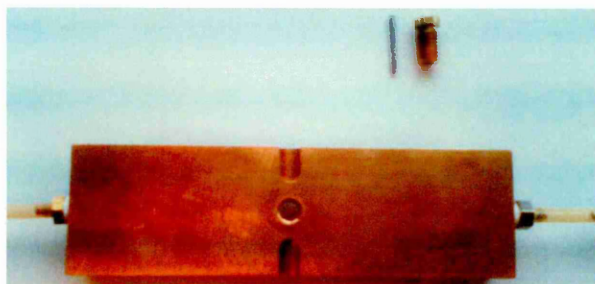


Photo 3-1. Top view of the compaction cell used for the hydration studies.

The compaction cell consists of three parts: brass base plate – diameters 36 x 32 x 12 mm (l x w x h), sleeve and stainless steel punch. The plate contains a 10 mm threaded internal hole, positioned slightly off-centre (1.5 mm). A 3 mm hole is drilled into the centre of the sleeve and forms the die for the tablet. The predetermined mass of powder is pressed using the ~3 mm diameter stainless steel punch. To generate the controlled force on the sample the torque screw is applied.

### 3.2.4.2 Creating tablets in situ on ATR crystal

#### The compaction cell experimental setup

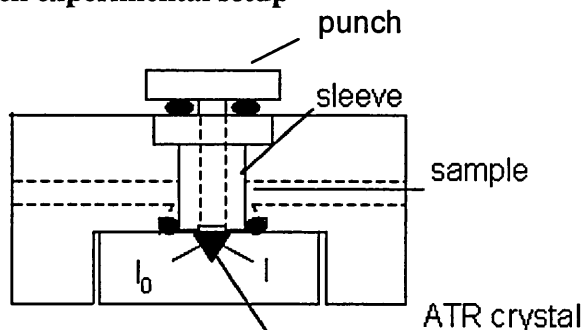


Fig. 3-1. Scheme of experimental setup: compaction cell, sample and ATR accessory.

The compaction cell is positioned at the center of the ATR unit, so that the created tablet covers the whole surface of the ATR crystal. Measurement is made at 37 °C. The system is settled by the lower “o”-ring being compressed by the sleeve. The spectrum of the sample is recorded at spectral resolution 8 cm<sup>-1</sup>, with 100 scans.

The pressed sample was kept in position and spectra were collected after 5 and 10 minutes. Whilst the tablet is still under compression by the punch, the ring is lifted, and a spectrum of the tablet is recorded again.

All spectra were collected and analyzed by a Thermo Nicolet Nexus FTIR spectrometer controlled by Omnic 6.1 software. The data were collected at resolution 8 cm<sup>-1</sup>, and were the result of the average of 100 scans over the spectral range 4000-750 cm<sup>-1</sup>.

### **3.2.4.3 Parameters for the tablet compaction**

Mixtures of components with unmatched particle size - the powders were compacted on the ATR crystal and the results from the 90 and 120 [cN.m] torques were compared to investigate possible variations on the compaction pressure and determine any final properties of the investigated tablets. The total compaction time for each tablet was 10 min, the weight of each compact 20 mg. From each compositional mixture prepared with three different mixing procedures 6 tablets with force 90 [cNm] and another 6 tablets with force 120 [cNm] were created

Mixtures with particle size less than 106 microns - samples were compacted on the ATR crystal with a controlled force of 90 [cN.m] torque. The total compaction time per tablet was 10 min, and the weight of each compact 10 mg. From each blended mixture 6 tablets were manufactured.

The results of the experiments will be described using the example of the 80% HPMC and 20% citric acid composition (HC80/20) as all other mixtures showed similar tendencies in results obtained.

### **3.2.5 PLS analysis**

The sample spectra in a spectral range  $4000\text{--}750\text{ cm}^{-1}$  generated in the compacting process (after raising the ring walls) were divided randomly into two sets. The calibration set contained 4/6 of the total amount of the spectra; the validation set 2/6. The calibration set was created in order to establish the PLS model whilst the remaining data were used to test the model. The data were preprocessed as discussed in Chapter 2 section 2.2.3, to create the PLS model.

### 3.2.6 NIR analysis

The NIR Chemical images were acquired using the Spectral Dimensions Sapphire 2450 Imaging System. Spectra were collected from 1400-2400 nm in steps of 10 nm with 16 co-added scans at each wavelength range. Six tablets selected randomly from each batch were placed on a mirrored slide during data collection to eliminate background when processing the data. A background and “camera dark image” were collected using the same parameters as the images.

Data were analyzed using ISys <sup>TM</sup> 3.1 (Spectral Dimensions, Inc.) chemical imaging software. To determine reflectance in the data preprocessing stage the camera dark cube (image of the dark background) (D) was ratioed against the subtracted sample image (S) and the white background (B) image was ratioed against the subtraction the camera dark cube (D). The next stage of data preprocessing was the conversion of reflectance  $R$  to  $\log(1/R)$ .

$$A = \log\left(\frac{1}{R}\right) \quad \text{where} \quad R = \frac{(S - D)}{(B - D)} \quad \text{eq(3.1)}$$

The applied spatial mask eliminated pixels coming from outside tablet area. The multiplicative scatter correction (MSC) of spectra was achieved by mean centring and normalization to correct for path length and thickness differences at each pixel. In the next step a second derivative was applied. The standard substances image cubes were processed and data were saved in the library [108].

The preprocessed data were used to build a PLS-2 model. The amount of possible principal components (PC's) in the sample was selected and the appropriate separation of components was applied. The classification (concentration) images for analyzed principal components were created.



### **3.3 Results and discussion**

#### **3.3.1 Effect of different mixing procedures and particle size on the reproducibility of the samples**

The homogeneity of the mixtures is one of the critical conditions to ensure reproducibility of the manufactured tablets. There are many factors that influence the content uniformity of compacts, the most important of which are the particle size of the components and the preparation of the formulation. In this project different mixing methods and particle size matched versus unmatched particles were compared.

##### **3.3.1.1 Mixtures with unmatched particle size of the powders**

FTIR spectra of the compacted tablets from composition HC80/20 (Fig. 3-2) showed a variation of intensity between individual spectra in each set of samples, as well as variation of the shape of the bands. The highest level of agreement between samples from the same set was observed in the case of tablets created with torque 90 [cN.m] from previously tumble blended samples, however this result still didn't provide the required level of reproducibility. From the six spectra generated from this formulation, two showed significant differences to the other four. This would significantly influence the quality of any further data analysis carried out (e.g. PLS).

Spectra collected from the composition 80% HPMC 20% citric acid (Fig 3-2) from all investigated methods of mixing showed a disproportionally strong intensity of bands associated with citric acid. In fact if one would consider the comparison of the pure citric acid spectrum and the generated mixture spectra the resulting similarity between them

could suggest that in the formulation spectra the main component with the highest concentration value present would be citric acid.

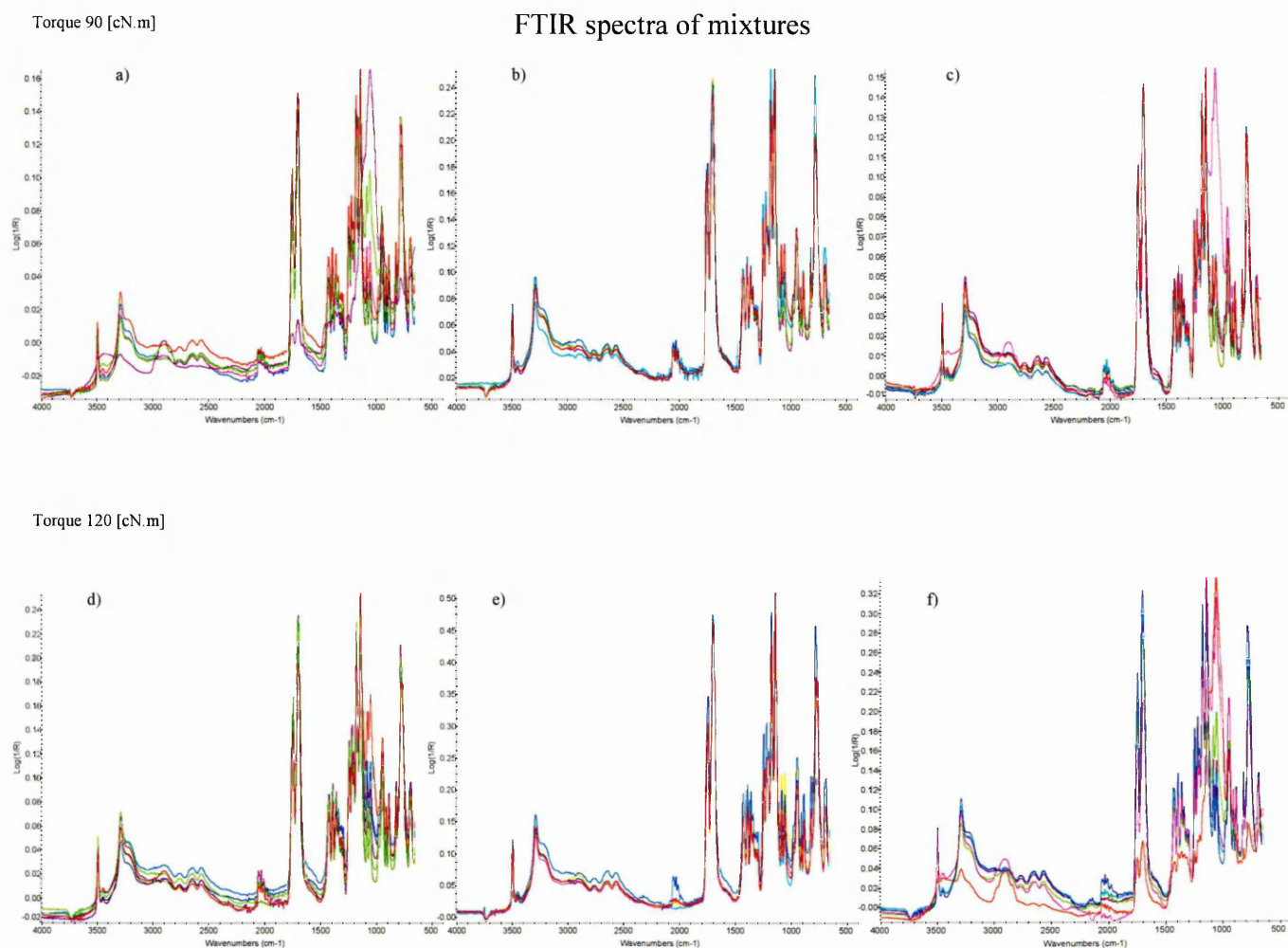


Fig. 3-2. FTIR spectra of the formulation containing 80% HPMC and 20% Citric acid (HC80/20) spectra a), d) represent tablets obtained from manually shaken mixtures, b), e) samples from tumble blended mixtures, c), f) spectra of tablets from ground mixtures.

The citric acid was present in its crystalline form in the formulation HC80/20. It is known that citric acid in its crystalline form is a substance with a low level of compressibility in contrast to the highly compressing HPMC powder. The variability was caused in the non-uniformity of the mixture due to the particle size of that component being significantly larger in comparison to the polymer. This difference also had an influence for the efficiency of formulation mixing and as a result for the compaction process. The obtained results obviously suggest the presence of heterogeneity in the analysed mixtures.

### 3.3.1.2 Mixtures with particle size less than 106 microns

The raw FTIR spectra for each compaction tablet from the formulation HC80/20 composition are shown in Fig. 3-3.

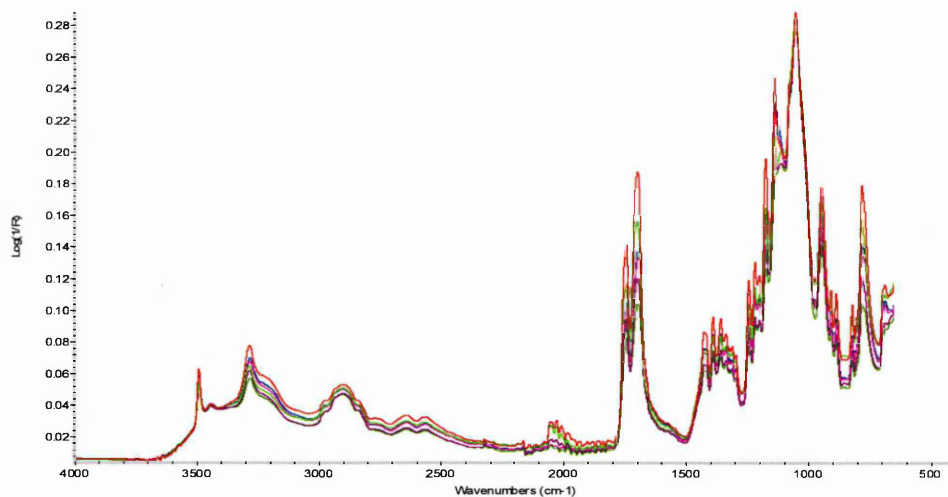


Fig. 3-3. FTIR spectra from blended mixture of HC80/20 with controlled particle size.

The infrared spectra recorded showed a highly level of similarity in shape, intensity and position of bands. The spectra of tablets can be overlaid and all components can be readily discerned. The characteristic band  $\sim 1100\text{ cm}^{-1}$   $\gamma(\text{CO})$  due to the presence of HPMC is observable as are the characteristic bands associated with  $\gamma(\text{OH}) \sim 3000\text{-}3100\text{ cm}^{-1}$  of the

citric acid. The matching of particle size within the composition had significantly improved the reproducibility of infrared spectra.

### 3.3.2 Effect of different mixing procedures and particle size on the prediction of concentration values.

The quantitative analysis of samples very often involves the modeling of the data in order to predict concentrations. There are numerous examples in the literature published about the use of partial least squares (PLS) data analysis to predict the concentration of components in the analyzed sample.

PLS-2 has extensively been used in this project to determine homogeneity and reproducibility of the compaction process.

#### **3.3.2.1 Mixtures with unmatched particle size of the powders**

The application of PLS to the FTIR data, has been used to quantify excipients within the compacts. The PLS model selection criterion involved the cross-validation method. The samples were divided into two sets; calibration set (12 samples) and prediction set (8 samples). The data were preprocessed using path length correction, mean centering, and the NIPALS algorithm was used for optimization. The independent sample was included in the data to test the model.

## Results for tablets made from shaken mixtures

a) 90 [cN.m]

b) 120 [cN.m]

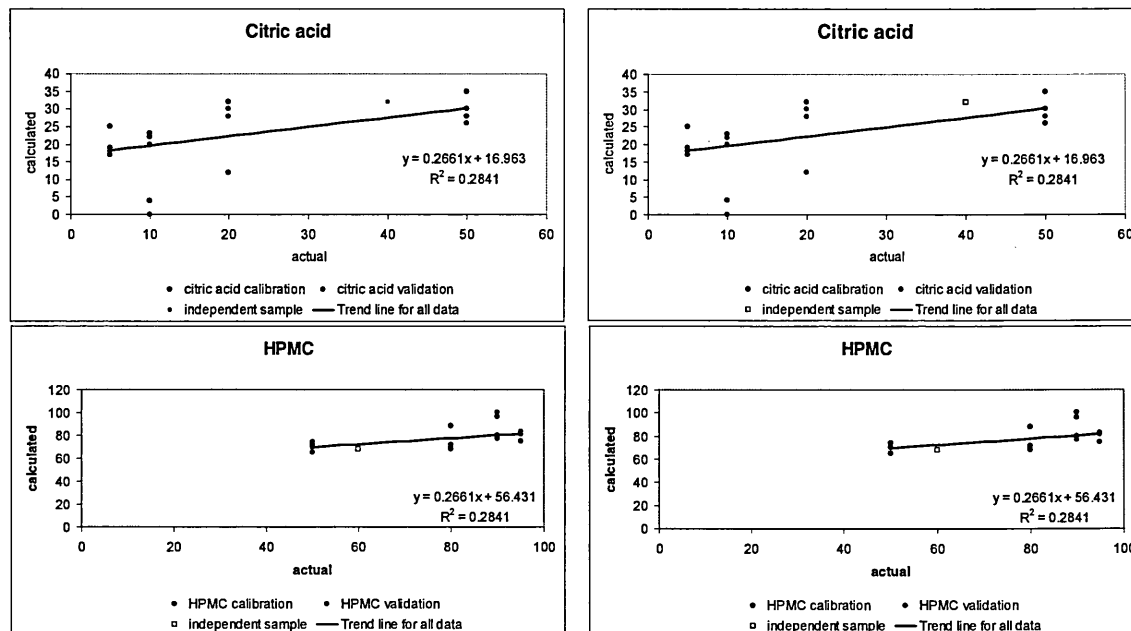


Fig 3-4. Plot of calculated (from PLS model) versus actual concentration levels.

Mean and standard deviation for two components used in shaken samples for certain actual concentration values.

a)

concentration of HPMC [%]	mean HPMC [%]	concentration of citric [%]	mean citric [%]	st dev
50	71.0	50	29.0	3.74
80	74.0	20	26.0	8.00
90	86.2	10	13.8	10.92
95	79.2	5	20.8	3.89

b)

concentration of HPMC [%]	mean HPMC [%]	concentration of citric [%]	mean citric [%]	st dev
50	71	50	29	3.74
80	74	20	26	8.00
90	86.2	10	13.8	10.91
95	79.2	5	20.8	3.89

Table 3-2(a,b) Comparison of the mean and standard deviation calculated concentration with the actual concentration for the manual shaken samples.

## Results for tablets made from blended mixtures

a) 90 [cN.m]

b) 120 [cN.m]

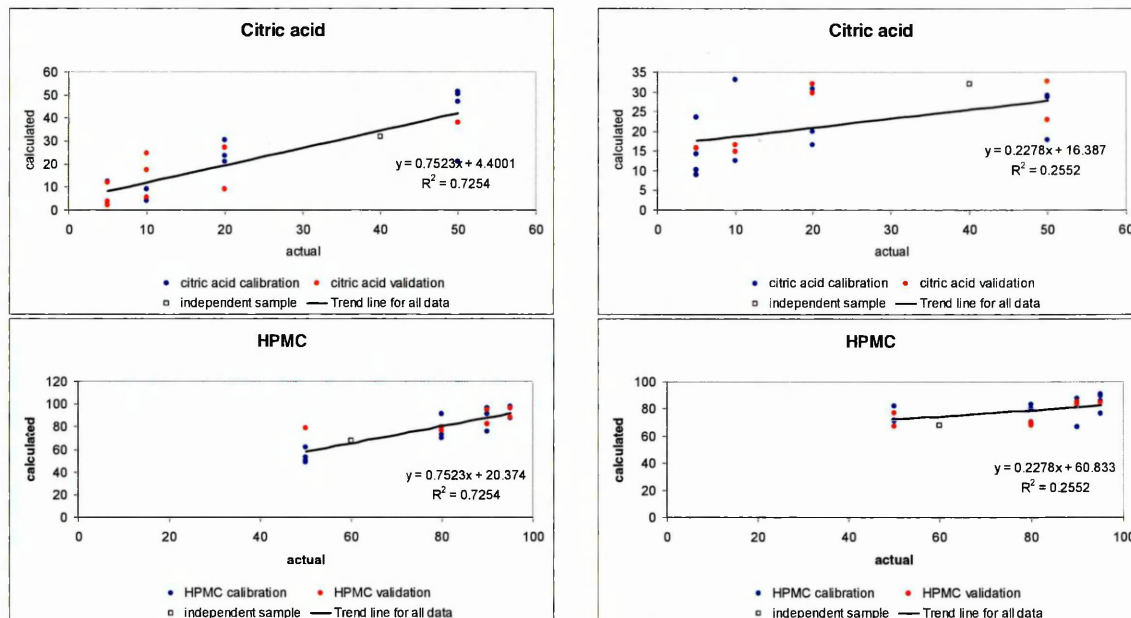


Fig 3-5. Plot of calculated (from PLS model) versus actual concentration levels.

## Mean and standard deviation for two components used in blended samples

a)

concentration of HPMC [%]	mean HPMC [%]	concentration of citric [%]	mean citric [%]	st dev.
50	58.50	50	41.50	12.61
80	77.87	20	22.13	8.13
90	87.97	10	12.03	8.73
95	93.61	5	6.39	5.25

concentration of HPMC [%]	mean HPMC [%]	concentration of citric [%]	mean citric [%]	st dev
50	73.81	50	26.18	5.89
80	74.18	20	25.81	7.03
90	81.61	10	18.39	8.34
95	85.47	5	14.52	5.70

b)

Table 3-3(a,b) Comparison of the mean and standard deviation calculated concentration with the actual concentration for the blended samples.

## Results for tablets made from ground mixtures

a) 90 [cN.m]

b) 120 [cN.m]

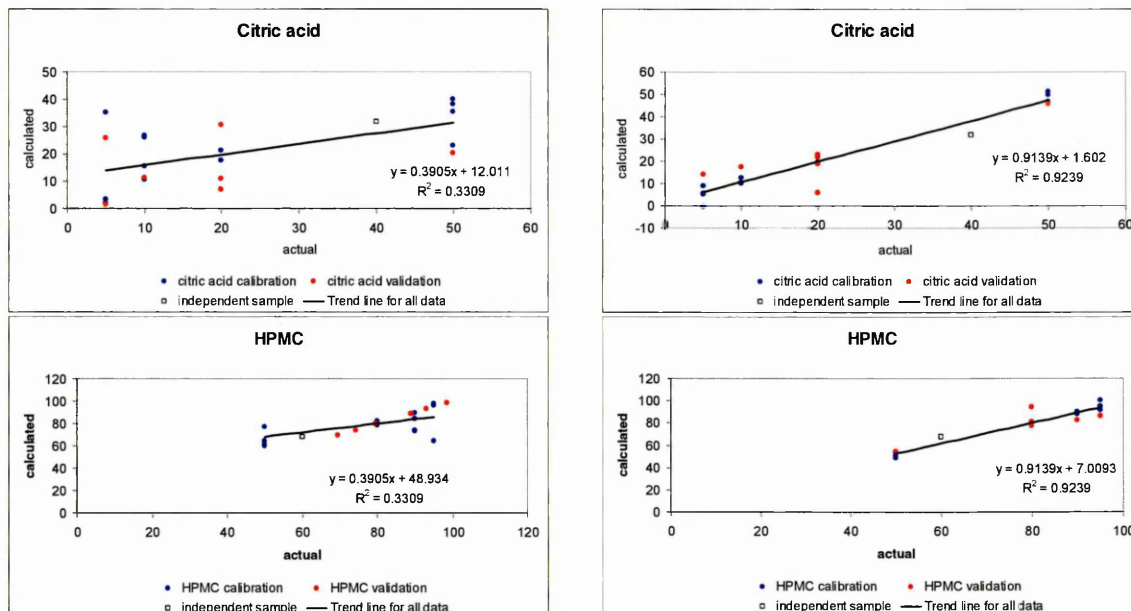


Fig 3-6. Plot of calculated (from PLS model) versus actual concentration levels.

## Mean and standard deviation for two components used in grinded samples

a)

concentration of HPMC [%]	mean HPMC [%]	concentration of citric [%]	mean citric [%]	st dev
50	68.55	50	31.45	9.07
80	82.59	20	17.41	9.20
90	82.09	10	17.91	7.90
95	86.39	5	13.61	15.78

b)

concentration of HPMC [%]	mean HPMC [%]	concentration of citric [%]	mean citric [%]	st dev
50	51.20	50	48.79	2.60
80	82.16	20	17.83	6.79
90	87.92	10	12.08	3.21
95	93.38	5	6.62	5.20

Table 3-4 (a,b) Comparison of the mean and standard deviation calculated concentration with the actual concentration for the ground samples.

From PLS analysis Fig 3-4, 3-5, and 3-6 showing the calculated concentration values versus the actual concentration for different types of mixing procedures. The PLS models

indicated a high standard deviation in the compositions of the tablet surface. Changing the number of factors (the used one was two) didn't improve results. Low  $R^2$  values for analyzed samples, confirm that the data do not fit well with the developed model. The application of different mixing types didn't provide a uniformity of the mixtures. Manual shaking mixtures provided the most variability of the predicted values, probably because the samples were mixed manually for only a short time leading to an ineffective method of mixing. Tumble blending showed better predicted values of the components however the length of time which the sample was mixed and influence of particle size still potentially lowered the chance of getting reproducible tablets. One of the most reproducible results was generated from the ground samples which were compacted with 120 [cNm] torque value. The slightly better reproducibility is explainable considering the fact that during the grinding of the mixture the particle size of citric acid was modified to that approaching the HPMC one. The high value of torque applied also ensured better compaction of the samples.

### 3.3.2.2 Mixtures with particle size less than 106 microns

To try to improve the PLS model samples were prepared by reducing the particle size of the components within the mixture prior to blending.

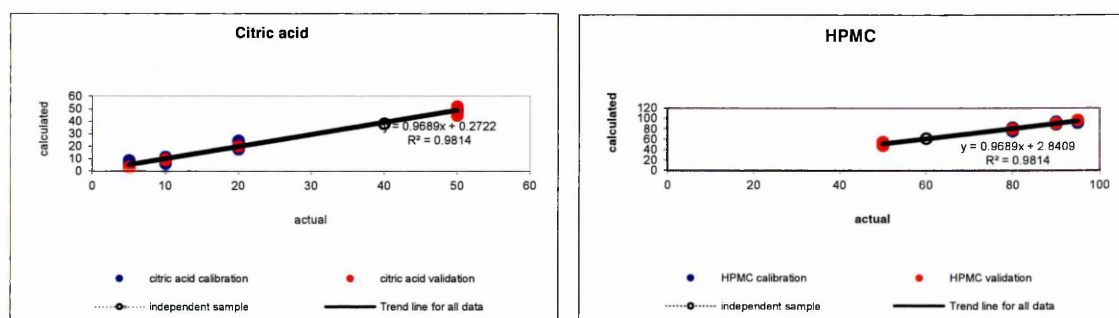


Fig 3-7 Plot of calculated (from PLS model) versus actual concentration levels for citric acid and HPMC.



The samples selected for PLS modelling were divided into two sets; for the calibration set 12 samples and for the validation set 8 samples. The preprocessing of the data undertaken included path length correction and mean centering, which is same for all sets of data in the project. Before constructing the model optimal calculation of the number of principal components present in the sample is crucial, as selection of the incorrect number of factors can lead to over fitting or under fitting. If the number of factors is more than the number required for the sample, more noise will be added to the model. If the number retained was less than required, there is a risk of ignoring meaningful data for the calibration [149, 150].

#### Mean and standard deviation for two components used in blended samples

concentration of citric [%]	mean citric [%]	concentration of HPMC [%]	mean HPMC [%]	st dev.
50	48.48	50	51.52	2.55
20	21.21	80	78.79	2.73
10	8.67	90	91.33	1.91
5	5.26	95	94.73	2.34

Table 3-5 Comparison of the mean and standard deviation calculated concentration with the actual concentration for the samples.

The data (Fig 3-6) fitted well into a PLS linear model, using two factors for the analysis, showing good resemblance of generated pure component spectra with real ones and obtaining high  $R^2$  values. As indicated previously the plots show the predicted versus the actual concentration, within the individual data points having an excellent grouping and similarity to the actual concentration values. The results for the HPMC model show the slightly better fit than citric acid, as there is less variability in the predicted values of concentrations. The analysis confirmed significant improvement in terms of reproducibility compared to the previous models.

The predicted concentrations values of the sample components were compared with the actual concentrations and used to calculate the Root-Mean-Square Error of Cross-

Validation (RMSECV). The RMSECV indicates the precision and accuracy of predictions[94].

$$RMSECV = \sqrt{\sum_{i=1}^n \frac{(y_i - y_{-i,k})^2}{n}} \quad \text{eq(3.1)}$$

where n – number of calibration samples

$y_i$  – predicted value

$y_{i,k}$  – actual value

The further detailed data analysis is discussed in Chapter 4.

### 3.3.3. Effect of particle size on the distribution of the components in the tablet

The evolution of the tablet structure during the compaction of the components is controlled by the compression mechanics of the particles, their dimensions and also the fracture toughness and tensile strength. It has been reported that the distribution of the particle size is an important factor for the processing behavior of a powder during pharmaceutical manufacturing. It also has an effect on the tablet forming ability of a powder. Also the distribution of the particles in the pharmaceutical tablet has a significant influence on the drug release profile [101, 107, 151, 152].

Therefore in this section the distribution of components in the analyzed tablets will be discussed.

#### **3.3.3.1 Mixtures with an unmatched particle size**

During the optimization process and the development stage it is crucial to achieve an understanding of the formulation and the possible physical and chemical interactions

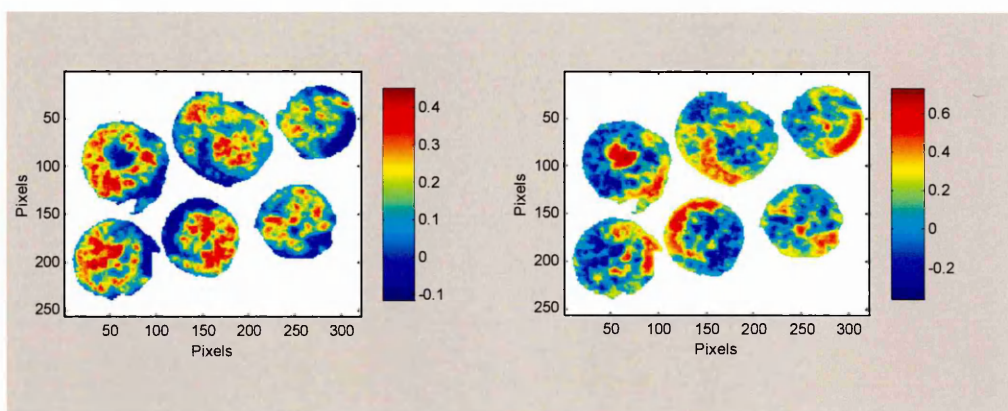
within. The analysis of the tablets made from unmatched particle sizes was conducted in order to check the homogeneity of the formulations and observe any possible changes in chemistry on the surface of the tablet.

The analysis was performed according to parameters described in a Chapter 3 Section 3.2.6, with the weight of tablet being 20 mg.

Results showing the set of six images collected from manufactured tablets using powders manually shaken.

a) Citric acid distribution

HPMC distribution



b)

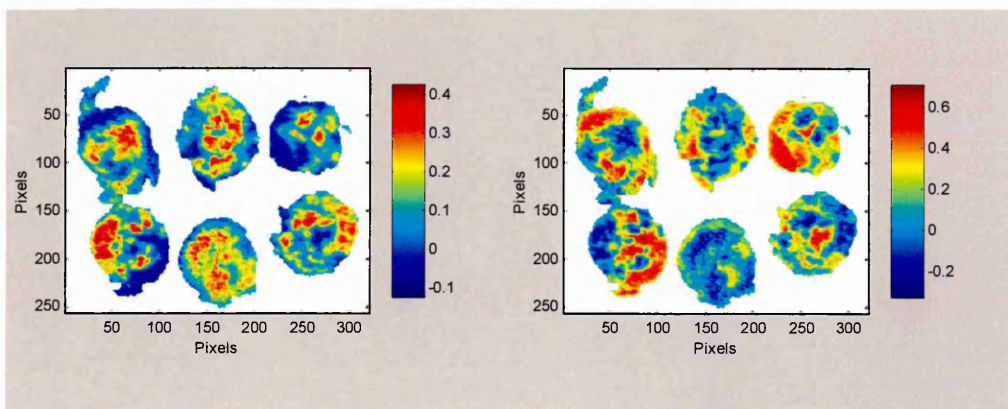
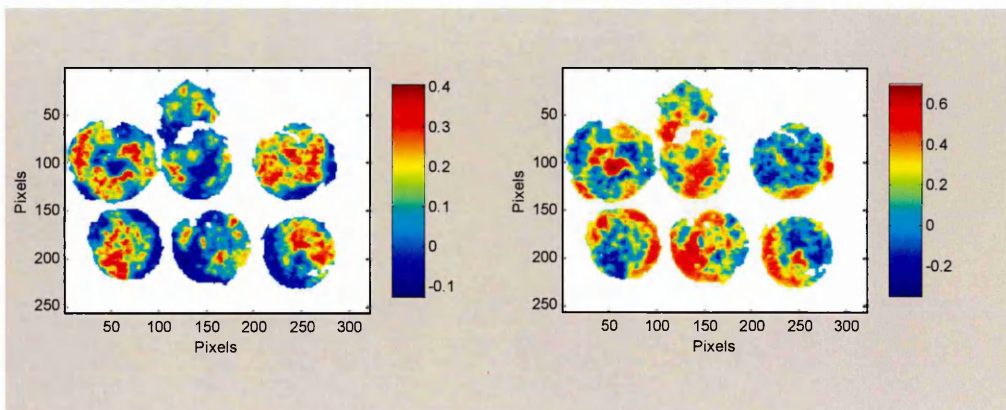


Fig. 3-7. NIR images of tablets prepared by manually shaking binary mixture HC80/20 of citric acid and HPMC using, a) torque 90 [cN.m], b) torque 120 [cN.m] applied pressure.

Results showing the set of six images collected from manufactured tablets using powders blended.

a) Citric acid distribution

HPMC distribution



b)

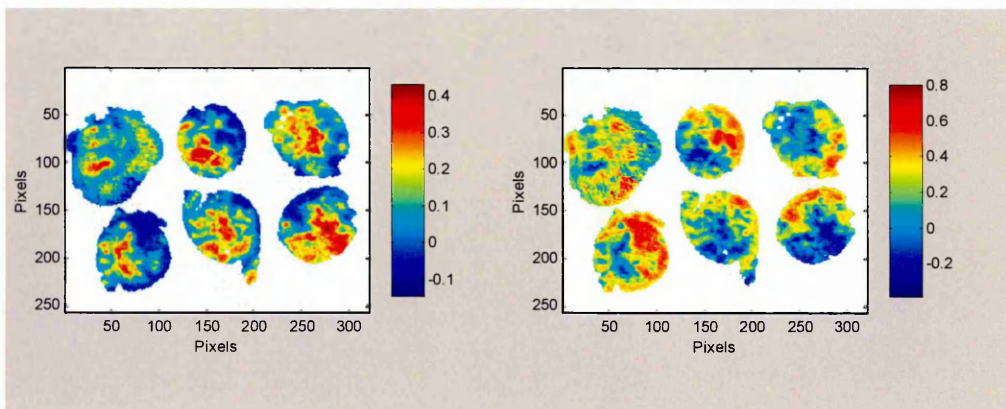
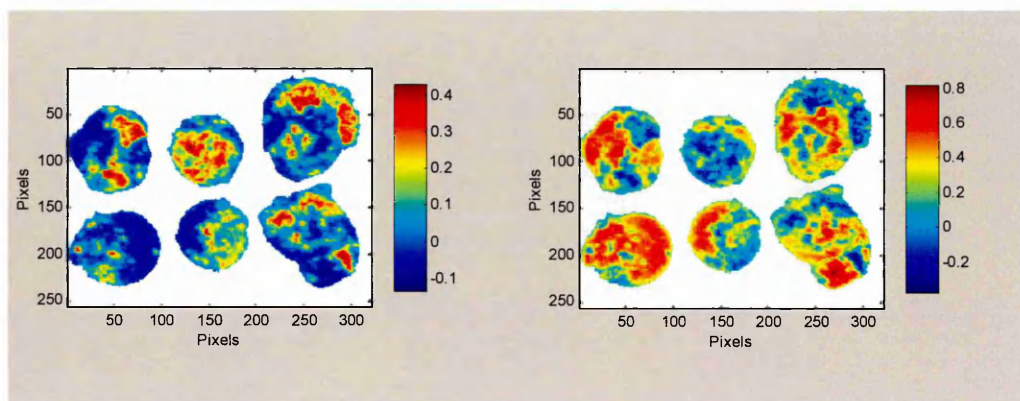


Fig. 3-8. NIR images of the tablets prepared by blending binary mixture HC80/20 of citric acid and HPMC using, a) torque 90 [cN.m], b) torque 120 [cN.m] applied pressure.

Results showing the set of six images collected from manufactured tablets using powders ground.

a) Citric acid distribution

HPMC distribution



b)

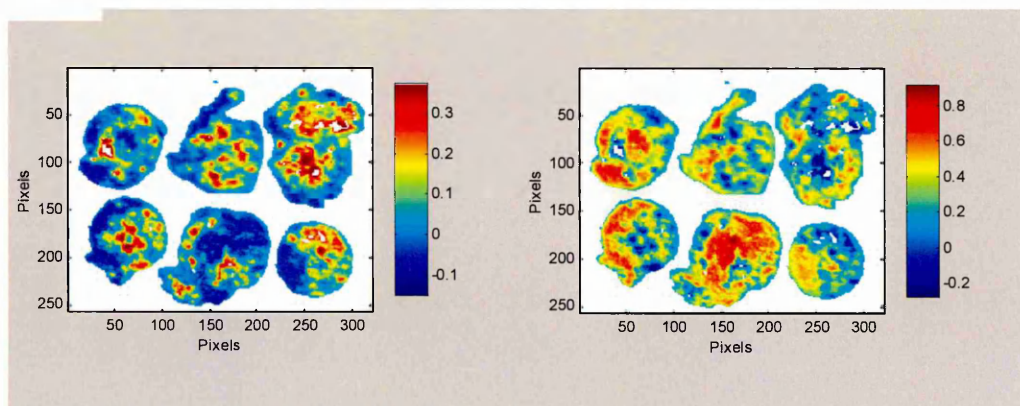


Fig. 3-9. NIR images of the tablets prepared by grinding binary mixture HC80/20 of citric acid and HPMC using, a) torque 90 [cN.m], b) torque 120 [cN.m] applied pressure.

NIR images of the tablets are chemical maps of the surface with a spatial resolution of 25 $\mu$ m. The colour bar on a right side of the image shows the concentration of the substance; red represents the highest concentration and blue shows the lowest concentration of the substance. The results of the NIR images collected from manually shaken citric acid and HPMC (Fig 3-7) indicate a somewhat heterogeneous surface with large aggregates of both

components. The components are not mixed well enough to ensure the reproducibility of the results within the same batch.

The classification scores collected from the tumble blender formulation (Fig 3-8) also are following the “heterogeneous path” of the poorly distributed components on the surfaces of the tablet. Critically, in the case of these images is visible defragmentation of the samples which is affected by the particle size but also poor compressibility of the citric acid. For the ground samples (Fig 3-9) the NIR images of the surface structure shows a range of aggregate sizes for the components. It confirms the heterogeneous distribution of the excipients. This could suggest that grinding has changed the particle size of the components and also the compressibility of powders independently of the pressure applied.

Most of the NIR images show a higher proportion of HPMC than would be expected. As this excipient has a visibly smaller particle size than the citric acid, and as the images were acquired from the lower face of the compaction, it seemed likely that the results were affected due to segregation of the HPMC to the bottom of the compaction cell. This however was not supported by the FTIR data where citric acid gave a much stronger response in the mixtures.

There were a few possible explanations of the formulation behaviour;

1. Citric acid was being lost at the point of sampling - small flat faced spatula was used to sample the bulk blend, which could increase the likelihood of the loss of larger crystalline particles during the sampling process.
2. Due to the longtime of tumble blending segregation may be occurring within the bulk blend maybe occurring immediately after blending was stopped. This could result in the heterogeneous mixture being sampled for the compaction and the disproportionate presence of HPMC measurements compared to citric acid.

3. The powder at the end of the ATR compaction process can easily spread around the ATR crystal (changing the surface of the tablet) during the dismantling of the equipment, probably due to the relaxation of the HPMC particles once the metal punch is no longer applying pressure.

4. During the compression process the segregated mixture may cause the bigger size particles of citric acid to fall to the bottom of the sampled powder in the die, this theory the resulting ATR spectra from the compaction experiments seem to confirm.

The problems which occurred during the experiments with discussed formulations could be resolved by changing parameters of mixing procedure, particle size of the excipients providing better compressibility of the samples and the components distribution.

#### **3.3.2.2 Mixtures with particle size less than 106 microns**

The strong presence of aggregates in the tablets with unmatched particle size suggested that changing the particle size of the components used will make it possible to identify the best methods to mix formulations. The applied parameters with reduced amount of tumble blending time on the formulation allow the generation of more homogeneous tablets.



Results showing the set of six images collected from manufactured tablets using powders with matching particle size blended.

Citric acid distribution

HPMC distribution

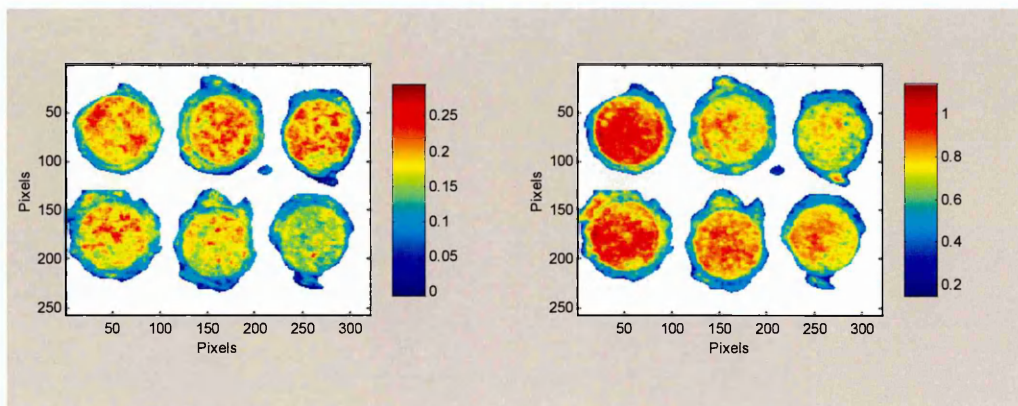


Fig. 3-10. NIR images of the tablets prepared by blending binary mixture HC80/20 of citric acid and HPMC using torque 90 [cN.m] applied pressure, the mixed powders matching the particle size.

The NIR images (Fig 3-10) show the two principal components present in the tablet within a formulation. A significantly more homogeneous surface confirms that the preparation of pharmaceutical formulation with an uncontrolled particle size of the components can be challenging. The uniform distribution of the citric acid compared with the previously discussed results (Fig 3-8 and 3-9) indicates that the modification of the particle size and the blending time allowed us to obtain samples with an acceptable level of reproducibility and content uniformity. This result was supported by the PLS analysis and ATR spectra.

The NIR images show also presence blue circles what suggest the edge effect, what could influence the spectral data collection. However to investigate further presence of edge effect the Infinity Focus Microscope technique which could provide the topographical information would need to be applied.



The generated results during the optimization process provided valuable information about the physical solid state behaviour of the investigated powders. The chemical properties of the excipients and possible interactions within the formulation will be discussed in the next section of this work.

### **3.4 Conclusions**

In the early stage of new drug method development, the optimization of the parameters for a reproducible manufacturing process of the formulation is the most critical issue. In this chapter experiments were conducted testing the effect of different mixing procedures, (manual shaking, tumble blending and grinding) and variability of particle size on the uniformity of the formulations determined by FTIR-ATR with PLS data analysis and NIR imaging. The prepared formulations of HPMC and Citric acid showed that the samples without matching particle size and mixing procedure had a high degree of heterogeneity. The presence of component aggregates on the surfaces of analyzed samples determined by NIR confirmed the low level of uniformity of the tablet images generated by NIR chemical imaging and also explained the within-batch differences observed for spectra obtained from the same composition using the diamond ATR crystal and compaction cell. The PLS data analysis showed a large degree of variability between the predicted values of concentration when compared with the actual ones used for the preparation of the formulations.

It was observed that the particle size dimensions and the degree of variability had a significant impact on experimental data in terms of reproducibility and heterogeneity of the samples. The differences in the results obtained using three different mixing procedures suggested that the appropriate time and technique used to mix powders can provide significant improvement of the uniformity of the pharmaceutical formulation.

The optimal tablet reproducibility and homogeneity of components has been achieved by controlling the particle size of the substances used for mixture preparation. The samples were compacted *in situ* on the ATR crystal in a compaction cell which proved to be a successful tool in a small scale tablet manufacturing process. The variation in the intensity

of FTIR-ATR spectra, PLS analysis and NIR Imaging confirmed homogeneity of the manufactured samples as well as possibility of creating lab scale reproducible tablets.

## **4. Investigations of solid dosage form: binary formulations.**

Solid state reactions in formulations and drug substances may include chemical reactions, solid state phase transformations, dehydration and desolvation. Particular interest is usually directed to the drug-substance which can react with other excipients of the formulation. The main aim of understanding the solid pharmaceutical system is to prevent possible unnecessary reaction of the active substance and at the same time improve the stability of drug substances and the medicinal products. However if the drug substance does react in a certain formulation in the solid state then the process needs to be analyzed and corrected. In the first step possible water absorption and increased molecular mobility needs to be considered following the possible molecular changes in the chemical bonds of the reactant, solid solution formation and final separation of the product. The most common solid state reactions of the drug substances include the deamidation, hydrolysis, cyclization and oxidation. The reactions of the active substance with the excipients of the formulation have influence on the stability of the product. Mechanical stress during the compaction process is one of the factors which can have impact on the solid state reactions as creating surface area, increasing the number of defects and the presence of amorphous material in the result of compaction of the tablet could accelerate the interactions [151, 153].

In this chapter the solid tablets compacted from the binary formulation are analyzed and the possible interaction within the samples are discussed.

## **4.1 Aims:**

- To manufacture the reproducible tablets *in situ* on the ATR crystal from binary formulations and investigate possible interactions of the components of the mixtures
- To build a PLS model and predict the concentration values for the excipients of analyzed formulation
- To conduct the analysis of the components distribution in the tablets

## **4.2 Materials and methods:**

### **4.2.1 Materials**

Materials used in this chapter are listed in Chapter 2, Table 2.1

### **4.2.2 Preparation of the mixtures**

Formulations were prepared according to proposed concentration values (Table 4-1).

#### **Formulation of:**

<b>HPMC and citric acid</b>		<b>HPMC and active substance</b>	
<b>HPMC [%]</b>	<b>Citric acid [%]</b>	<b>HPMC [%]</b>	<b>Active substance [%]</b>
95	5	90	10
90	10	80	20
80	20	70	30
50	50	60	40
		50	50

Table 4-1. Concentrations of binary formulations

The binary formulations were prepared by the method described in Section 3.2.2.2.

The active substance was ground and passed through the sieve (the size of the sieve <106 microns) to match the particle size of other excipients. The formulations were tumble blended for 15min.

### **4.2.3 Compaction process**

The compression of the tablets followed the procedure described in Section 3.2.4.2 and the parameters for the mixtures with particle size less than 106 microns detailed in Section 3.2.4.3

#### 4.2.4 PLS analysis

The predicted values of excipients concentration of the formulations were obtained as a result of the data analysis described in Section 3.2.5.

#### 4.2.5 NIR Imaging

Distribution of the components and image data analysis was conducted according to parameters listed in Section 3.2.6.

## **4.3 Results and discussion**

### **4.3.1 Investigations of possible interactions of the powders in the compacted tablet**

Various structural features in the samples may be revealed by the analysis of infrared spectra which provides information on a molecular level. The absorption bands of a particular group may be shifted by possible interactions between excipients. Conjugation, van der Waals forces, hydrogen bonding or electron withdrawal by a neighbouring substituent are few examples of interactions which one could recognize in the spectrum of analyzed mixtures [69, 70, 154].

In this study the spectra from tablets were analyzed in order to confirm if any solid state interactions between the substances took place during the mixing and compaction process.

#### **4.3.1.1 Formulation: HPMC and citric acid**

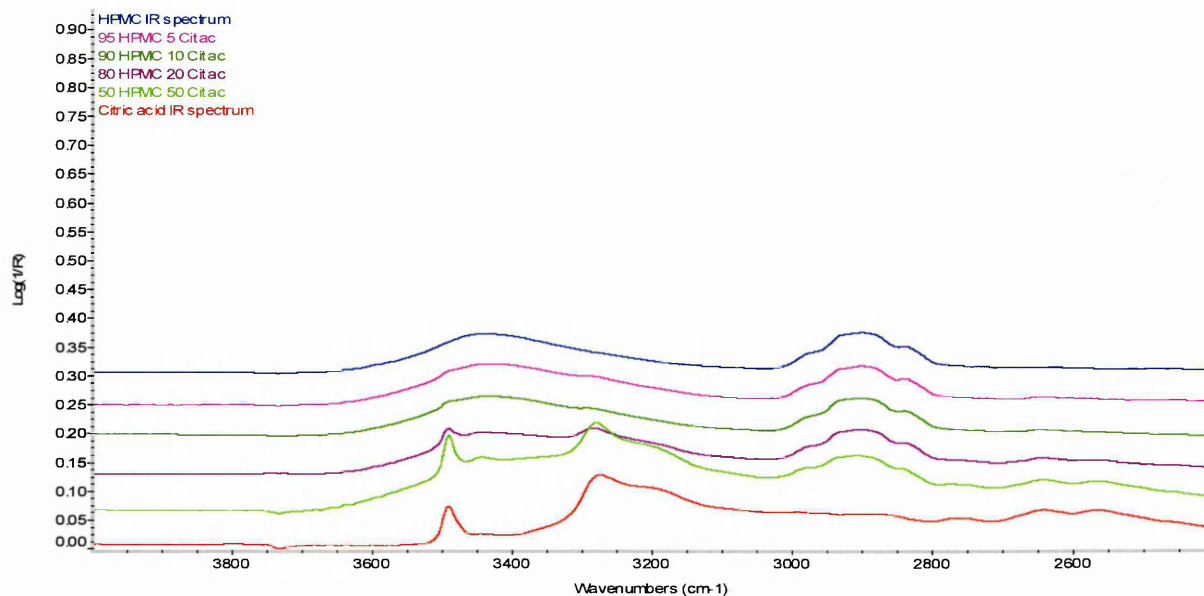
Spectra from the formulation HPMC citric acid (Fig 4-1) showed the strong characteristic band  $\sim 1100\text{ cm}^{-1}$   $\nu(\text{CO})$  associated with the presence of HPMC in the samples along with with the increasing concentration of the citric acid. The shape of the bands change proportionally to the increasing amount of citric acid in the sample however the peak positions remained the same. In the region  $\sim 3570\text{--}3200\text{ cm}^{-1}$   $\nu(\text{OH})$  the overlapping bands associated with the presence of hydroxyl groups in the polymer and citric acid result in a wide band. The shape is contributed to the presence of  $\nu(\text{OH})$  band associated with citric acid where non hydrogen bonded hydroxyl groups forms a narrow sub-maximum peak  $\sim 3500\text{ cm}^{-1}$  as well as OH bonded stretching absorption at lower wavenumber within the discussed region. The secondary absorption for  $\nu(\text{OH})$  near the  $\sim 2600\text{ cm}^{-1}$  region is



observed as the effect of overlap of the CH stretching region. Increasing intensity of the citric acid bands proportionally to its concentration in the formulation is also observed in mixtures spectra between  $\sim 1750\text{-}1680\text{ cm}^{-1}$  associated with the characteristic carbonyl group (C=O) stretching frequency, and with presence of  $\sim 1175\text{-}1045\text{ cm}^{-1}$  strong absorption  $\nu(\text{CO})$  and  $\sim 955\text{-}890\text{ cm}^{-1}$  region associated with OH deformation vibration of carboxyl group. However the solid mixtures spectra have no indication of bands shifts which could suggest any solid state interactions between the ingredients of the sample [31, 32].

## Formulation of HPMC and Citric acid

a)



b)

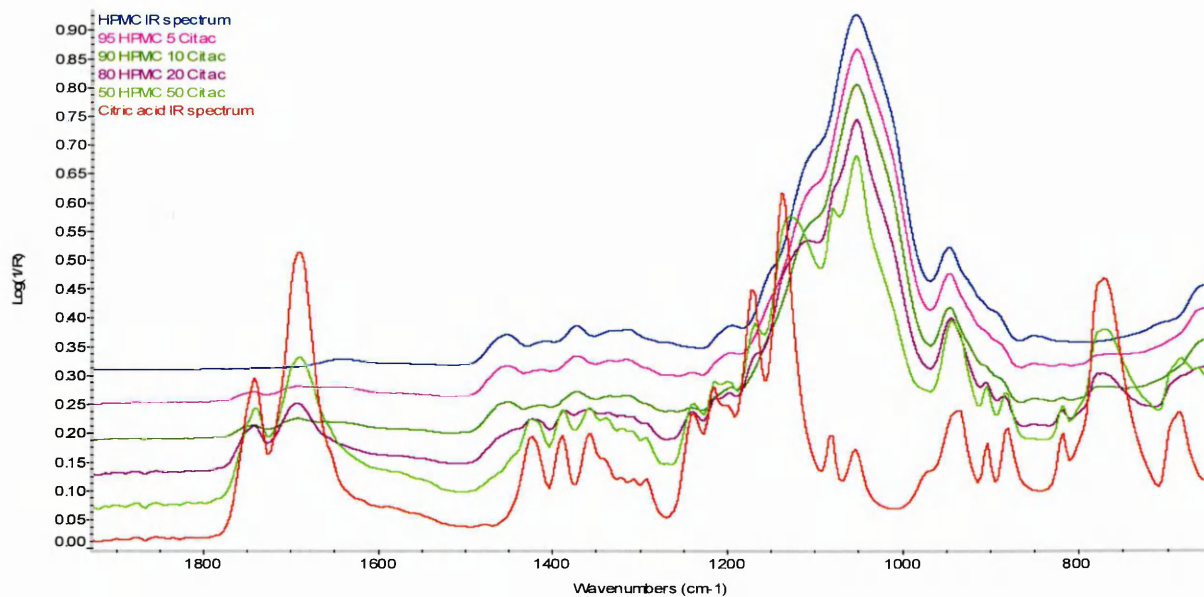
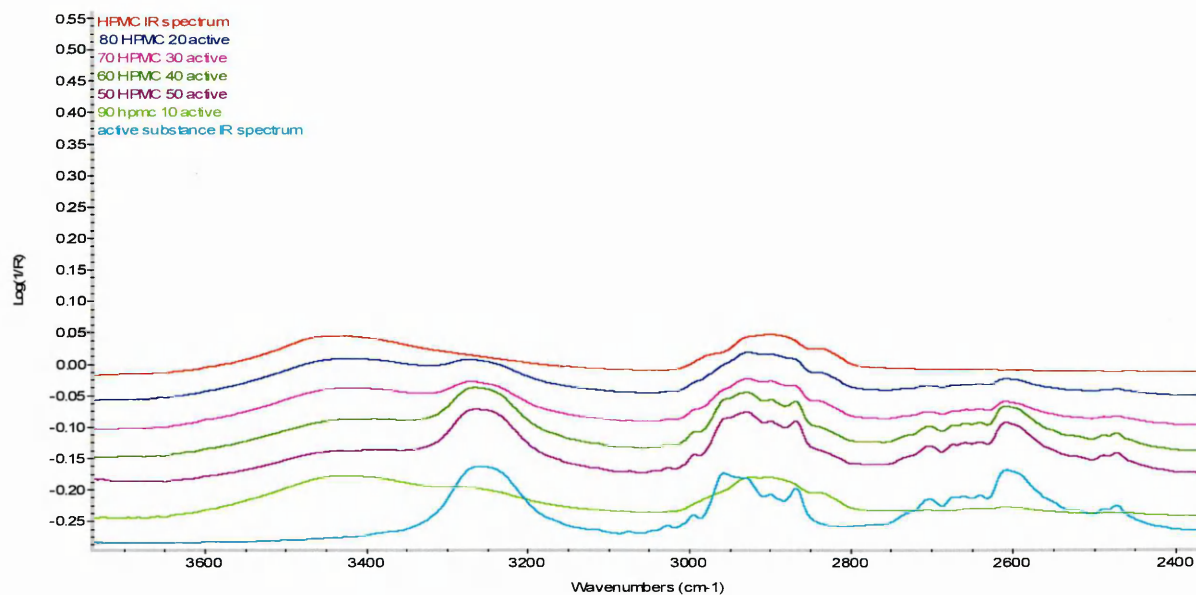


Fig 4-1. Infrared spectra of: pure HPMC, the mixtures of HPMC and citric acid with proposed concentrations and pure citric acid, a) region 3700-2400  $\text{cm}^{-1}$ , b) region 1900-700  $\text{cm}^{-1}$ .

### 4.3.1.2 Formulation HPMC and active substance

Spectra collected from formulations of HPMC and active substance (Fig 4-2) showed increasing impact of active substance in the mixture spectrum proportional to increasing concentration of API in the mixtures. The spectra of the formulations showed a relatively strong absorbance band in the region  $1700\text{-}1650\text{cm}^{-1}$  which is associated with the C=O stretching mode and C=C skeletal benzene ring breathing modes in the region  $1600\text{-}1500\text{cm}^{-1}$ , which increased in intensity with the amount of active substance in the mixture. In the range  $3500\text{-}3100\text{ cm}^{-1}$ , the OH stretching band is associated with the presence of hydroxyl groups in HPMC as well as 6OH BP. The strong band in the region  $\sim 1100\text{ cm}^{-1}$  is associated with the CO stretch of the HPMC [49, 50].

The prepared mixtures spectra showed the presence of overlapping peaks at certain wavenumbers however there are no shifts in the positions of the bands which suggest that during the admixing of powders and compaction process no chemical interactions between the excipients took place.



b)

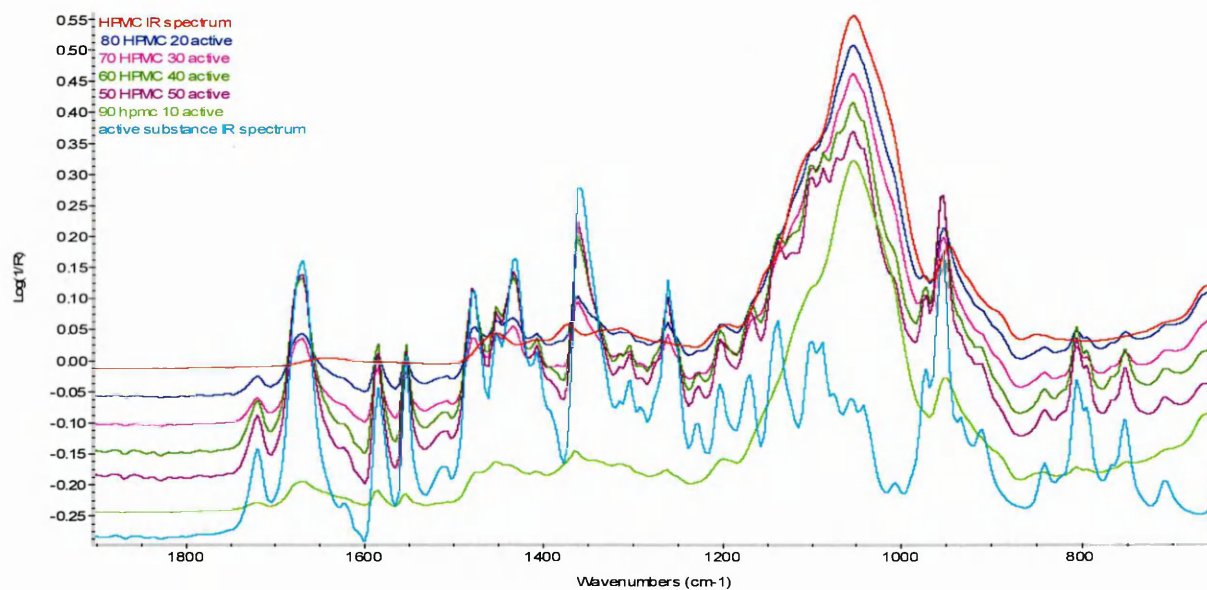


Fig. 4-2 Infrared spectra of: pure HPMC, mixtures of HPMC and API, pure active substance a) spectral region 3700-2400  $\text{cm}^{-1}$ , b) region 1900-700  $\text{cm}^{-1}$ .

### 4.3.2 Prediction of the concentration values of the formulation ingredients

The concentration values of the excipients in the analyzed tablets were predicted using PLS data analysis on the previously collected sample spectra from binary formulations [94].

#### 4.3.2.1 Mixtures of HPMC and citric acid

The samples selected for PLS data analysis were divided into two sets: the calibration set which consisted of 12 samples and the prediction set which consisted of 8 samples. Preprocessing of all the data was conducted and included path length correction and mean-centering.

#### Formulation HPMC and Citric acid

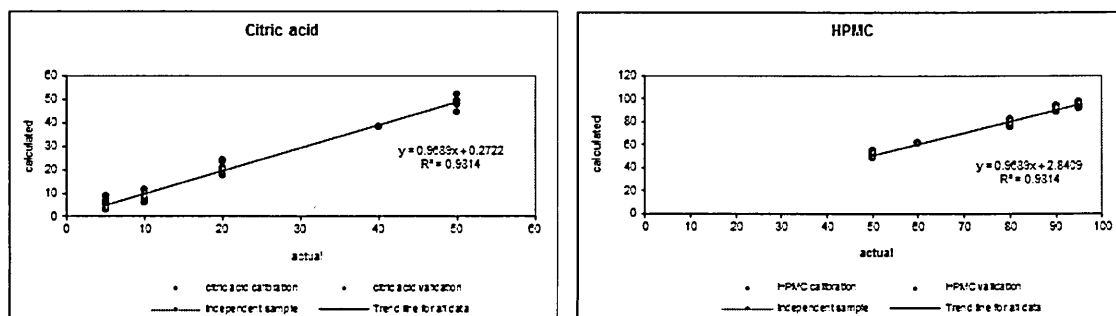


Fig 4-3 Output of the PLS analysis showing the predicted versus calculated values for various binary mixtures of formulation HPMC and citric acid.

#### Mean and standard deviation for two components used in blended samples

concentration of citric [%]	mean citric [%]	concentration of HPMC [%]	mean HPMC [%]	st dev.
50	48.48	50	51.52	2.55
20	21.21	80	78.79	2.73
10	8.67	90	91.33	1.91
5	5.26	95	94.73	2.34

Table 4-2 Comparison of the mean and standard deviation calculated concentration with the actual concentration for the samples.

The plots (Fig 4-3), show the predicted versus the actual concentrations from the PLS data analysis. The data fitted into the PLS linear model obtaining values of  $R^2$  coefficient around 0.9814. The collected spectra from samples of the same formulation show some variability

in the intensity values for some bands, these differences in the data as well as possible measurement error will influence the final  $R^2$  coefficient value.

The predicted concentration values show a high level of similarity when compared to the actual concentrations values. The calculated mean and standard deviation values for both components and the independent sample which fitted into the model confirmed the high level of reproducibility of the analyzed samples.

In the next step of the PLS analysis, the predicted spectra of pure components were compared with the IR spectra collected from pure standard substances (Fig 4-4).

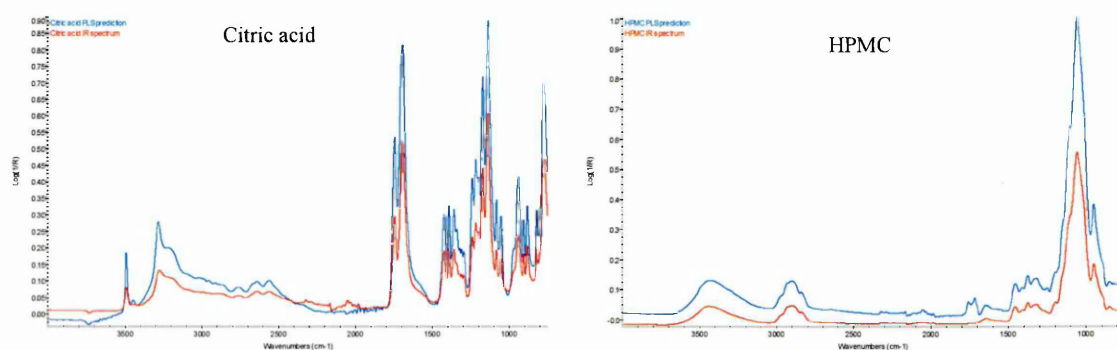


Fig. 4-4 Predicted pure component spectra from PLS analysis compared with the IR spectra of pure substances: red colour -IR spectra, blue colour-the predicted PLS spectra.

The presence of any noise and the wide variety of the bands intensity according to used concentrations will affect the final intensity of the estimated spectra. Analyzing the position and shape of the particular bands, characteristic for the substances with full confidence one could recognize and justify the presence of citric acid spectrum and HPMC. There are no band shifts present in the predicted spectra.

Also the principal components spectra (Fig 4-5) indicated the presence of characteristic bands for citric acid (principal component1) and for HPMC (principal component2).

Principal components (eigenvectors) represent the changes in spectral data common to all calibration spectra. Multiplying the PC1 & PC2 by the set of scores and summing the results with the mean spectrum one should be able to recreate the calibration data set.

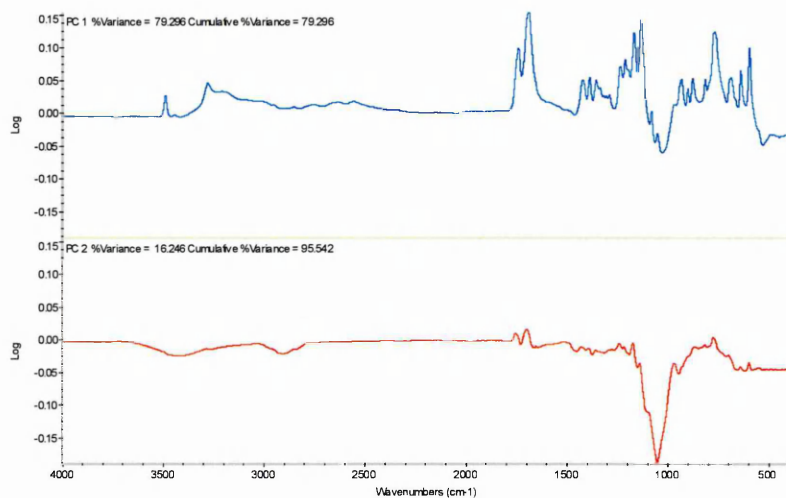


Fig 4-5 Principal components predicted by the PLS analysis HPMC and citric acid formulation.

The press plot (Fig 4-6) indicates that 2 factors are required to describe the variance in this data set. Therefore this number was used for the PLS analysis.

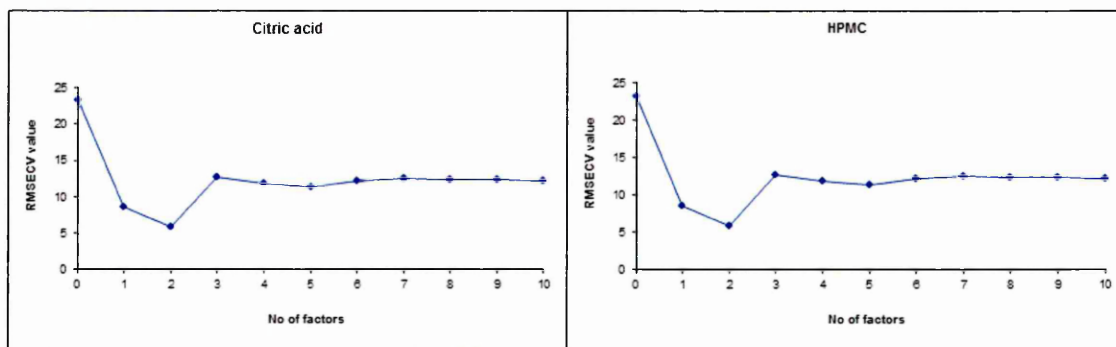


Fig 4-6 Press plots showing the number of factors required for the PLS analysis of the citric acid and HPMC formulations.

The RMSECV values calculated for both substances showed high level of similarity, consequently the press plots for the analyzed substances indicated the same amount of factors [155, 156].

#### 4.3.2.2 Mixtures of HPMC and active substance

The samples selected for PLS data analysis for this formulation included 30 sample spectra from 5 formulations, 6 spectra each; plus independent sample spectra. The data set was divided into two groups: calibration set 19 samples and prediction set 11 samples.

##### Formulation HPMC and active substance

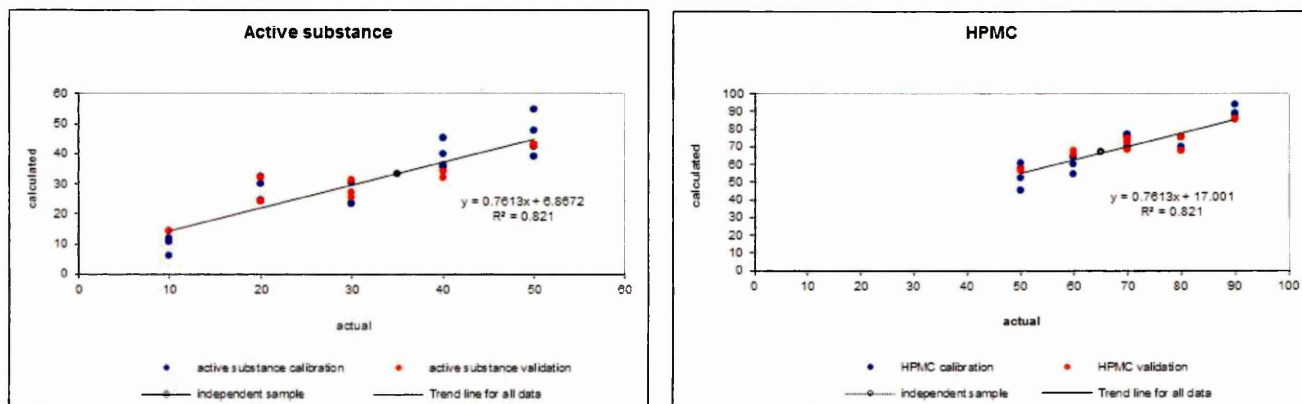


Fig 4-7 Output of the PLS analysis showing the predicted versus calculated values for various binary mixtures of formulation HPMC and active substance.

#### Mean and standard deviation for two components used in blended samples

Concentration of HPMC [%]	mean HPMC [%]	Concentration of active [%]	mean active [%]	st dev
50	54.97	50	45.02	5.49
60	62.79	40	37.20	4.83
70	73.16	30	26.83	3.41
80	72.04	20	27.95	4.02
90	88.43	10	11.57	3.07

Table 4-3 Comparison of the mean and standard deviation calculated concentration with the actual concentration for the samples.



The data generated from formulation HPMC and active substance (Fig. 4-7) are showing the predicted concentration versus the actual one, using stated calibration samples and validation set. The values obtained for HPMC and active substance fitted into the model with visible variability. The obtained values of  $R^2$  coefficient are  $<0.9$  which is connected with the variance between the collected data values. The mean and standard deviation values (Table 4-4) are confirming slightly bigger variability between analyzed samples than in case of formulation HPMC and citric acid.

The results suggest higher level of heterogeneity of the tablets in the formulation HPMC and API compared with the mixtures made from citric acid and HPMC. The active substance showed different compressibility properties than citric acid, also one could assume the segregation process occurring within the tablet based on lower level of reproducibility of the analyzed samples.

The PLS predicted spectra of pure components compared with the IR spectra collected from pure standard substances (Fig 4-8) indicated the presence of active substance characteristic bands and the HPMC strong absorption band  $\sim 1100\text{ cm}^{-1}$  associated with  $\nu(\text{CO})$ . The negative peak associated with the presence of HPMC in the active substance spectrum was observed, as well as the pure component spectrum (HPMC) contains the bands associated with the active substance, suggesting that the PLS method could not exactly predict the pure components for this data set

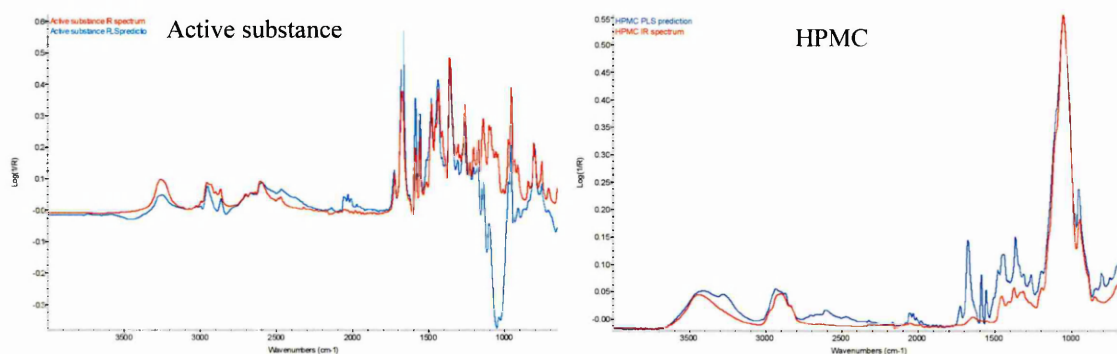


Fig 4-8 Comparison of IR spectra of pure substances (red colour) with the predicted pure components spectra (blue colour).

The principal components analysis (Fig 4-9) showed presence of three principal components (PC's). The PC1 and PC2 contain a mixture of bands characteristic for both substances, although PC2 shows the significantly increased intensity of the bands associated with the presence of HPMC and few negative peaks of active substance. PC3 spectrum is a negative spectrum of the pure API.

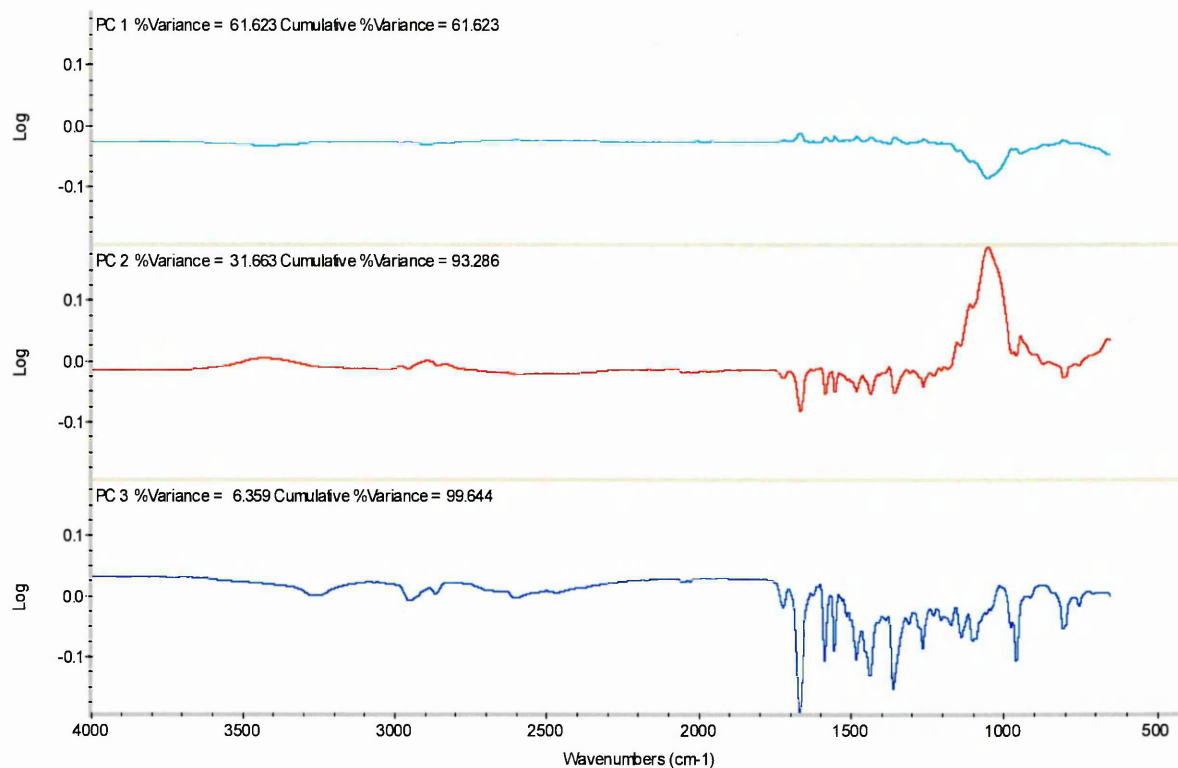


Fig 4-9 Principal components spectra generated in the PLS analysis of the formulation HPMC and active substance.

The press plots (Fig 4-10) generated for both components of the formulation showed the calculation of the factor numbers. The software application suggested using the one factor.

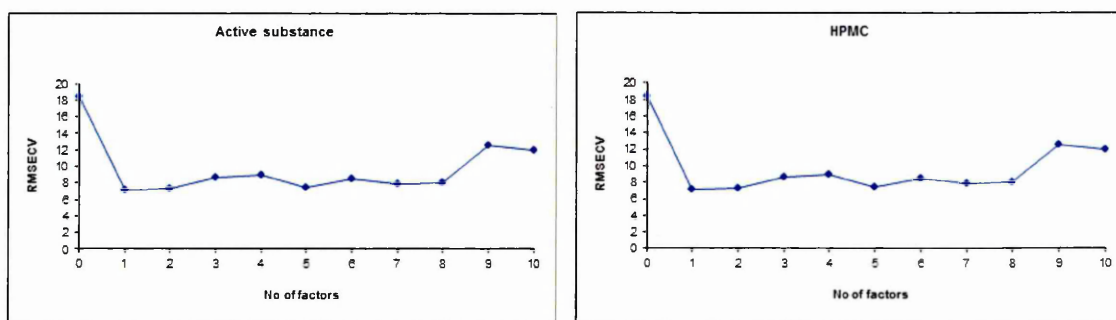


Fig. 4-10 Press plots showing the number of factors required for the PLS analysis of the active substance and HPMC formulations.

In order to avoid under-fitting of the model 2 factors were used for the analysis. The values of RMSECV showed similar amounts for both substances. Changing the number of factors didn't bring an improvement in this data analysis [150, 157, 158].

#### 4.3.3 Distribution of the components in a binary formulation tablets

The most significant factor determining the quality of the formulated product is the structure of the matrix. It is critical to eliminate any potential manufacturing defects which may influence the solid dosage form and its release. The content uniformity; homogeneously distributed components in the product are one of the most desirable achievements in the early stage of method development [88, 159].

The distribution of components in the binary formulations was analyzed in order to compare the effect of admixing citric acid or active substance separately into the polymer matrix.

#### 4.3.3.1 Formulation: HPMC and citric acid

Results showing the set of six images top and bottom side collected from manufactured tablets using powders predominantly blended.

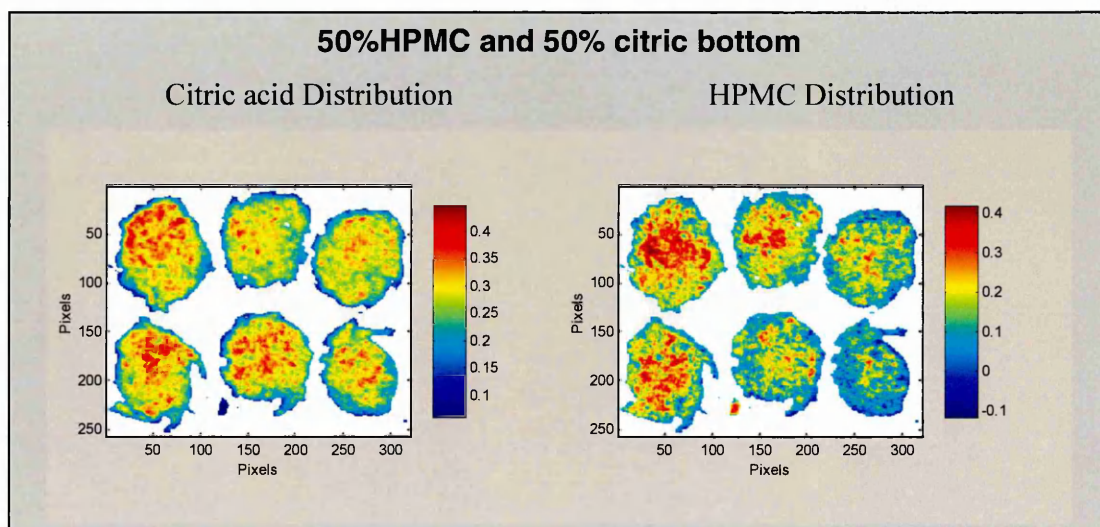


Fig 4-11a. NIR images bottom side of the tablets prepared by blending binary mixture HC50/50 of citric acid and HPMC using torque 90 [cN.m] applied pressure.

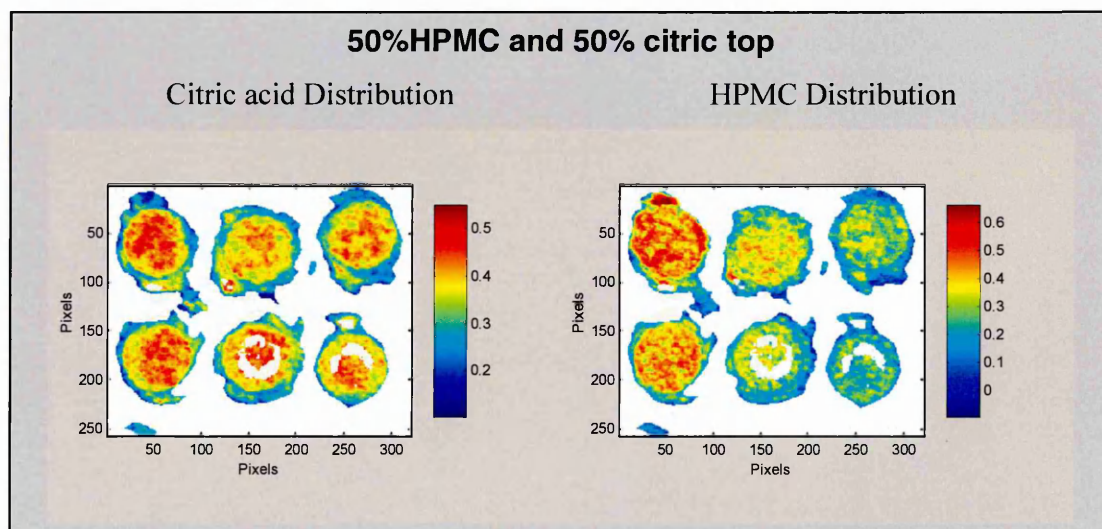


Fig 4-11b. NIR images top side of the tablets prepared by blending binary mixture HC50/50 of citric acid and HPMC using torque 90 [cN.m] applied pressure.

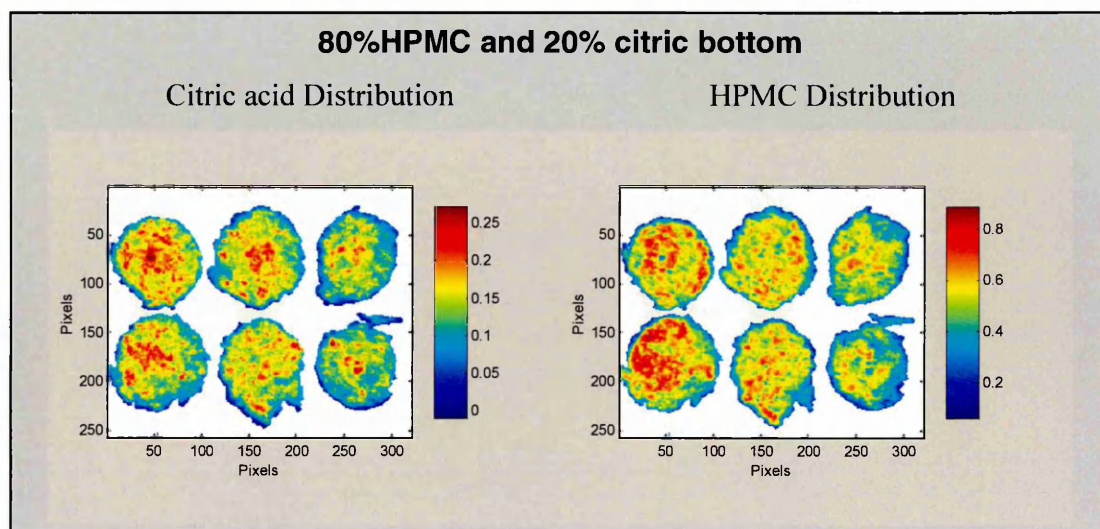


Fig 4-11c. NIR images bottom side of the tablets prepared by blending binary mixture HC80/20 of citric acid and HPMC using torque 90 [cN.m] applied pressure.

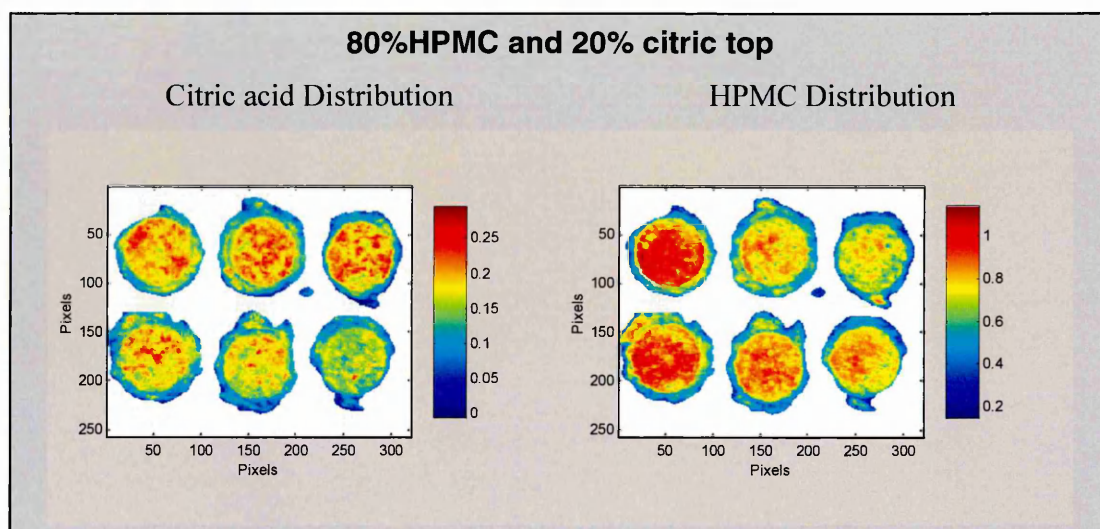


Fig 4-11d. NIR images top side of the tablets prepared by blending binary mixture HC80/20 of citric acid and HPMC using torque 90 [cN.m] applied pressure.



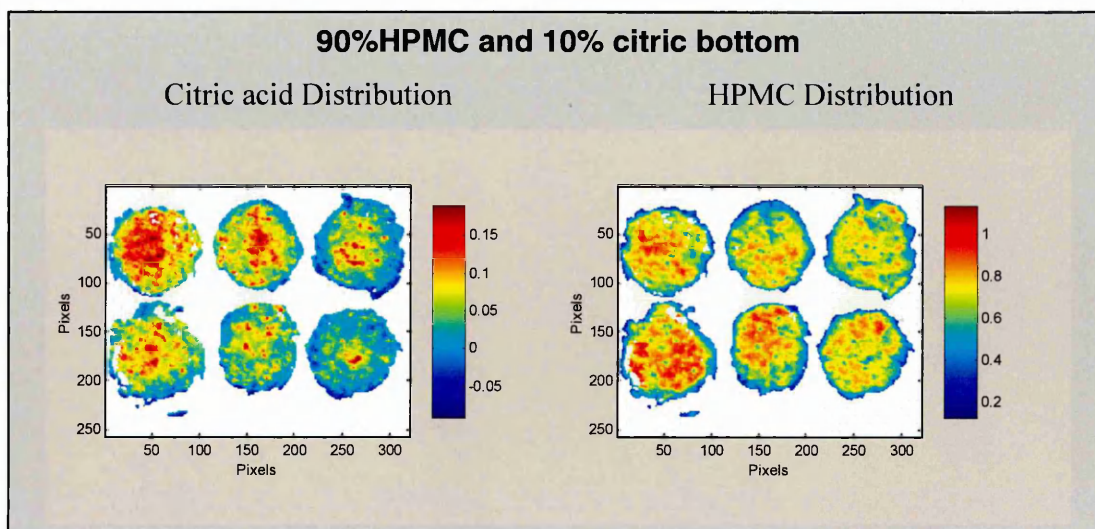


Fig 4-11e. NIR images bottom side of the tablets prepared by blending binary mixture HC90/10 of citric acid and HPMC using torque 90 [cN.m] applied pressure.

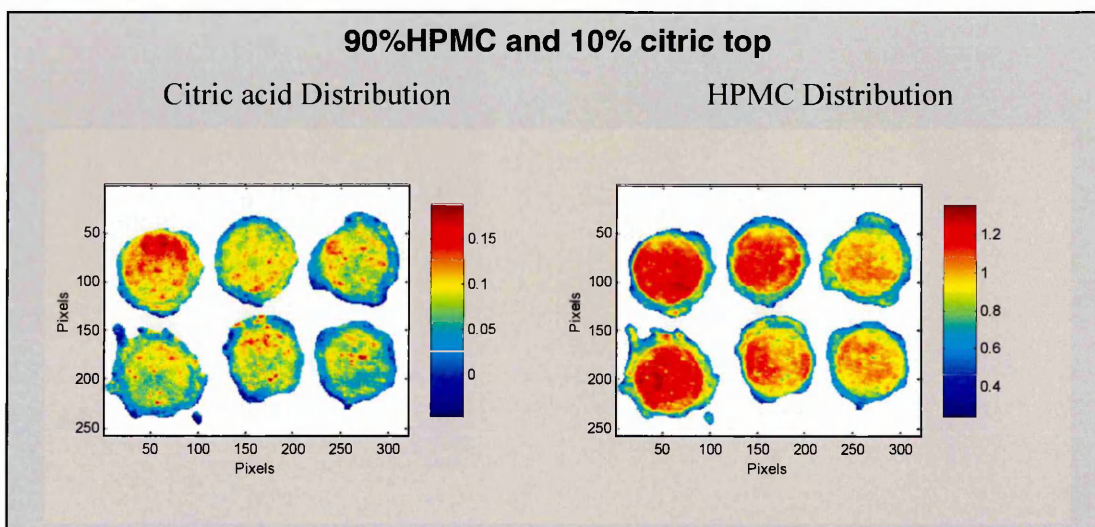


Fig 4-11f. NIR images top side of the tablets prepared by blending binary mixture HC90/10 of citric acid and HPMC using torque 90 [cN.m] applied pressure.

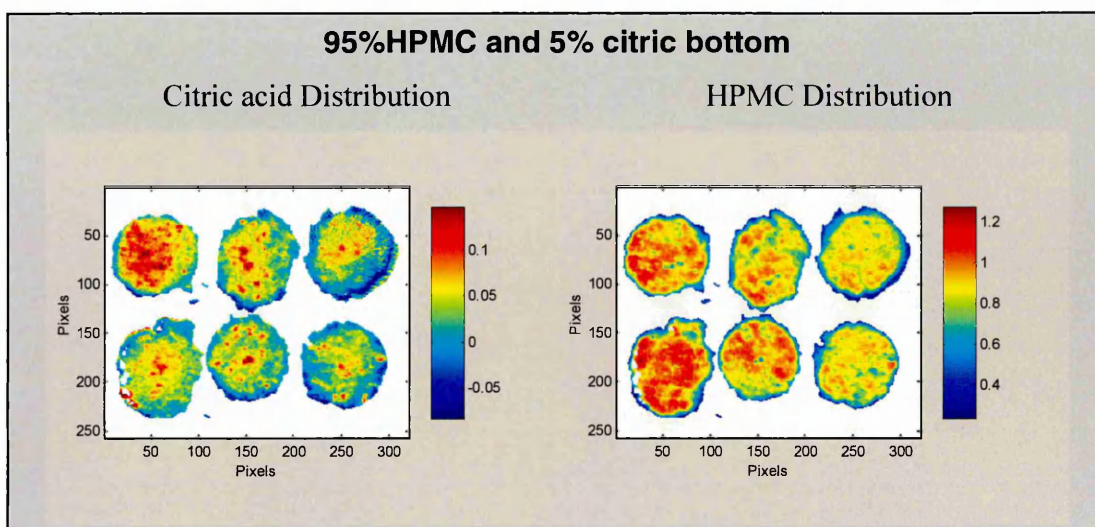


Fig 4-11g. NIR images bottom side of the tablets prepared by blending binary mixture HC95/5 of citric acid and HPMC using torque 90 [cN.m] applied pressure.

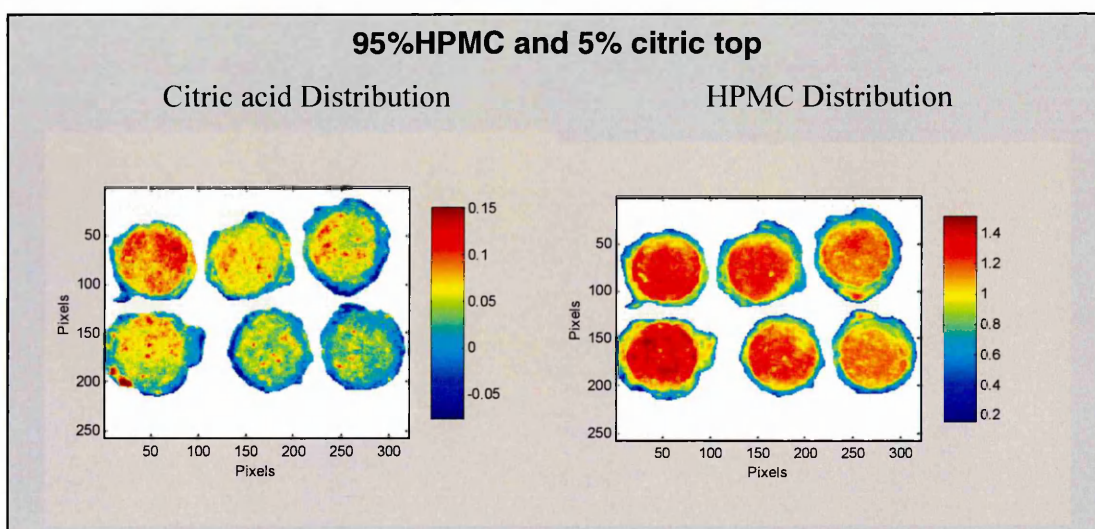


Fig 4-11h. NIR images top side of the tablets prepared by blending binary mixture HC95/5 of citric acid and HPMC using torque 90 [cN.m] applied pressure.



The generated NIR images of the formulations of HPMC and Citric acid (Fig 4-11a-h) showed the distribution of the two excipients present in the analyzed tablets. These chemical maps of the samples provided information about the level of intensity of the particular component on the tablet surface. The red colour is associated with strong intensity value and therefore high concentrations of the component, whilst dark blue colour is an indication of low concentration of the substance in the particular region of the sample. There is a significant difference in the intensity observed between the samples images collected from the top and bottom side of the tablet. The tablet images from the top surface show a more uniform distribution within components of the tablet. There are no aggregates visible or any clusters visible although they can still be found on the images of the bottom side (Fig4-11g-h). Also the tablets from the top side images have recognizable regular shape whilst the bottom side of the tablet is deformed by the relaxation of the polymer during the tablet manufacturing process. The further analysis of the samples with different concentrations shows the general trend of segregation of the compacted powders within the tablet. The increasing concentration of HPMC - red colour on the chemical map is mainly observed on the top side of the tablets whilst on the bottom side the presence of both components is visible. Also the roughness of the sample surface has an influence on the quality of the generated images, as smoother surface of the sample from the top side of the tablet improves the quality image compared to the bottom part. The presence of blue circles around the edges of the tablets is associated with the lack of integrity of the tablet at the edge.

Although the distribution and uniformity of the citric acid and HPMC compared with previously discussed results (Chapter 3) is significantly improved through the modification of particle size and blending time, there are still visible differences within a set of 6 tablets from the same concentration of the components. The HPMC is heterogeneous with respect to its particle size and therefore more challenging in terms of obtaining appropriate sized particles. The possible improvement of the mixture preparation could be obtained by first granulation of the excipients, then blending the mixture followed by compaction of samples.

#### 4.3.3.2 Formulation active substance and HPMC

Results showing the set of six images top and bottom side collected from manufactured tablets using powders predominantly blended.

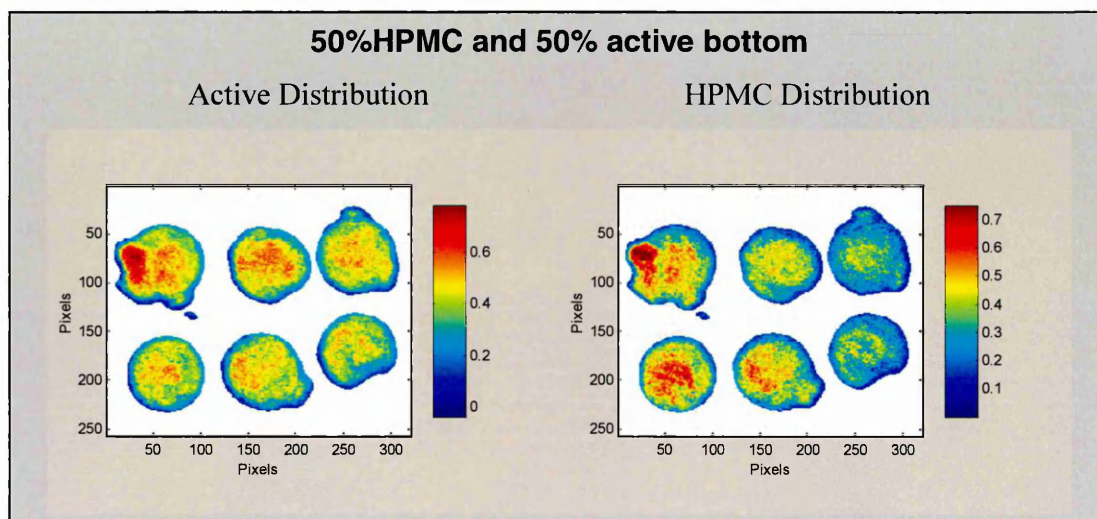


Fig 4-12a. NIR images bottom side of the tablets prepared by blending binary mixture HA50/50 of active substance and HPMC using torque 90 [cN.m] applied pressure.

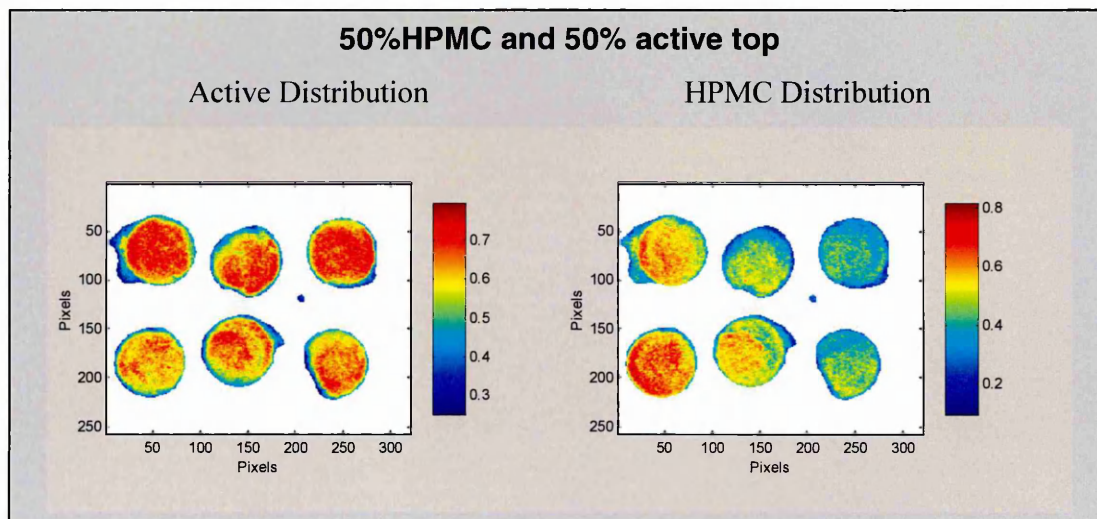


Fig 4-12b. NIR images top side of the tablets prepared by blending binary mixture HA50/50 of active substance and HPMC using torque 90 [cN.m] applied pressure.

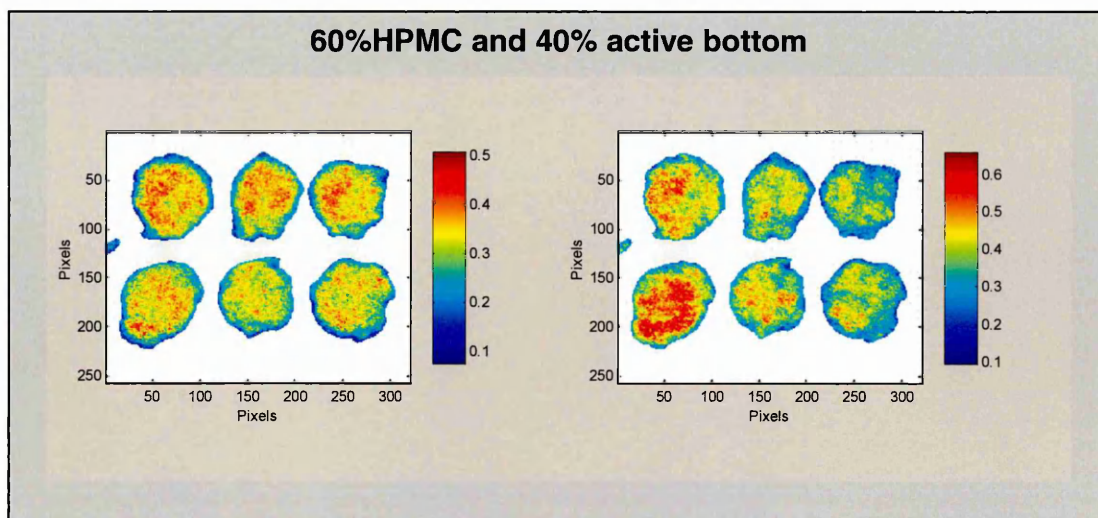


Fig 4-12c. NIR images bottom side of the tablets prepared by blending binary mixture HA60/40 of active substance and HPMC using torque 90 [cN.m] applied pressure.

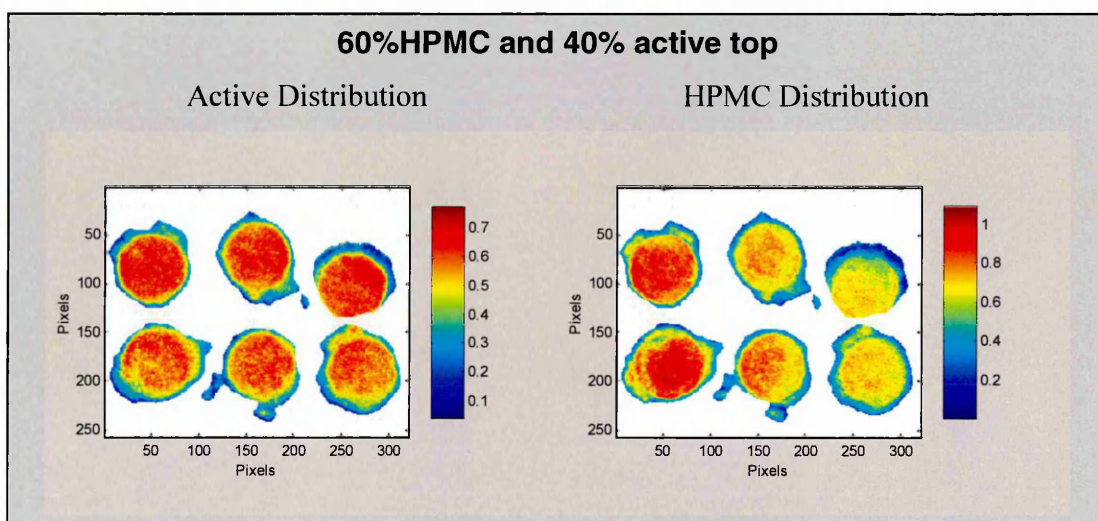


Fig 4-12d. NIR images top side of the tablets prepared by blending binary mixture HA60/40 of active substance and HPMC using torque 90 [cN.m] applied pressure.



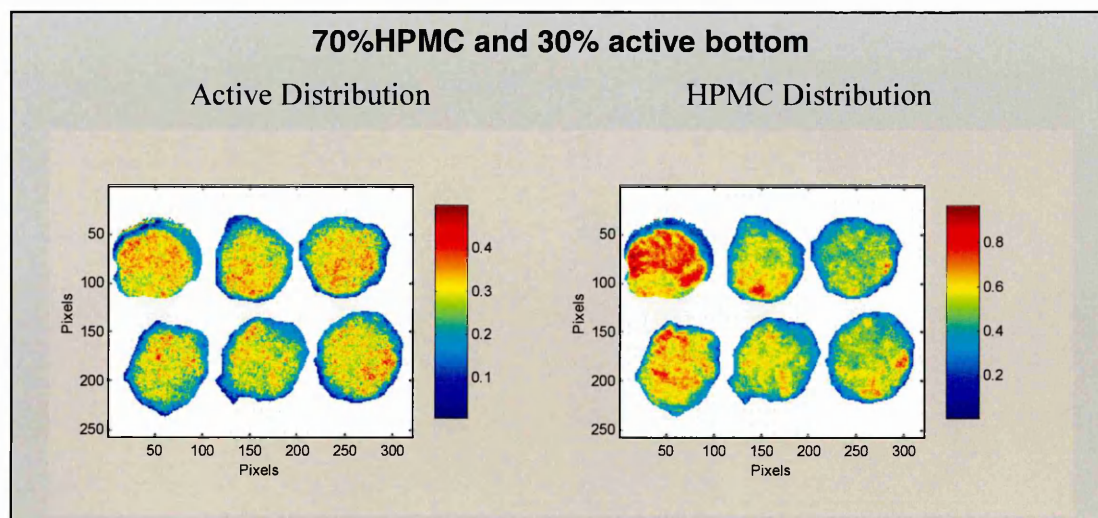


Fig 4-12e. NIR images bottom side of the tablets prepared by blending binary mixture HA70/30 of active substance and HPMC using torque 90 [cN.m] applied pressure.

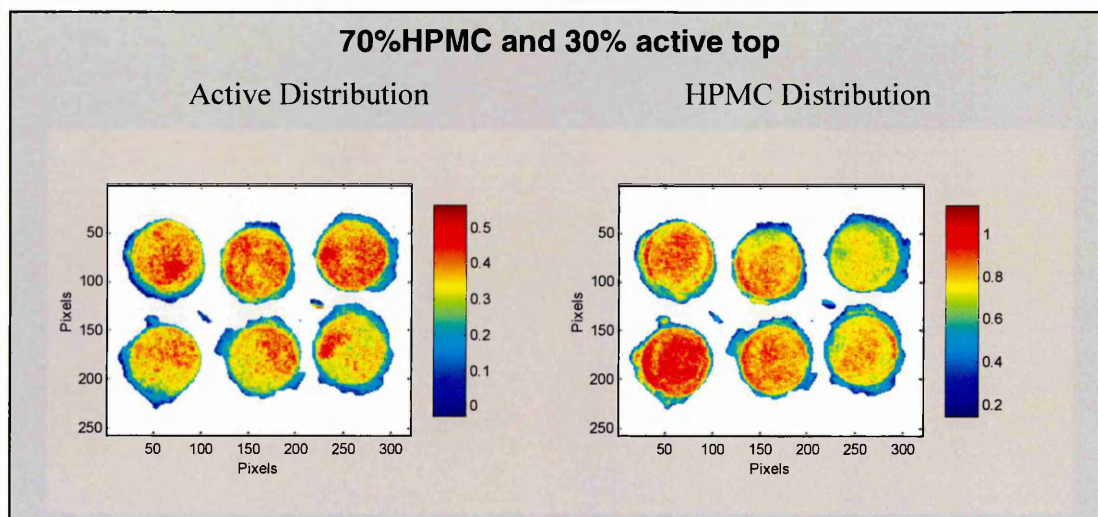


Fig 4-12f. NIR images top side of the tablets prepared by blending binary mixture HA70/30 of active substance and HPMC using torque 90 [cN.m] applied pressure.

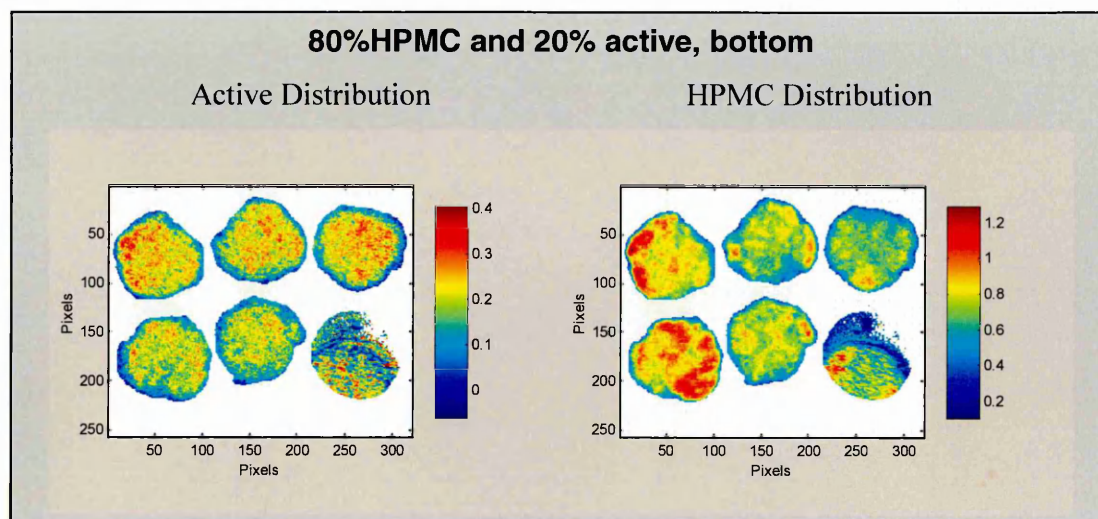


Fig 4-12g. NIR images bottom side of the tablets prepared by blending binary mixture HA80/20 of active substance and HPMC using torque 90 [cN.m] applied pressure.

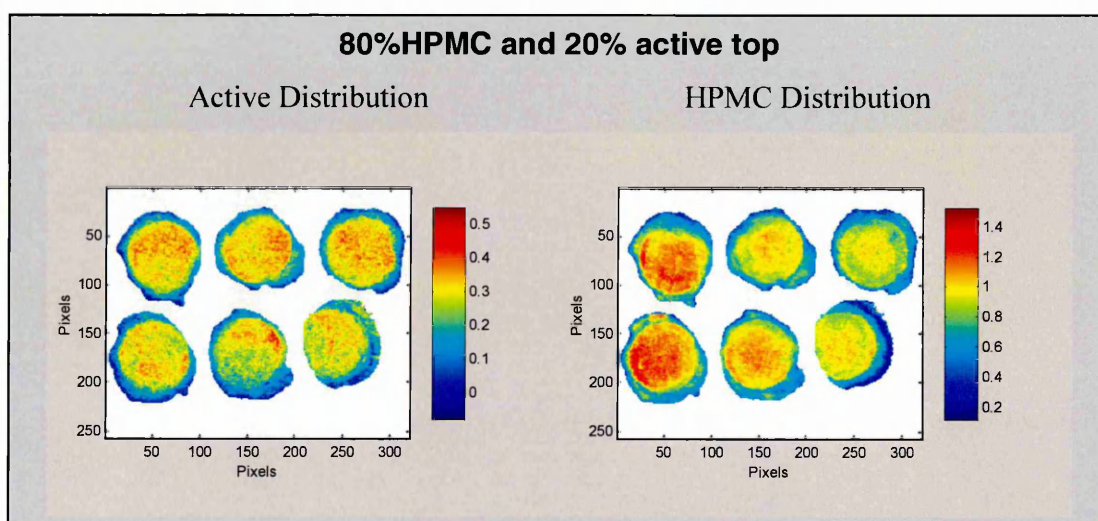


Fig 4-12h. NIR images top side of the tablets prepared by blending binary mixture HA80/20 of active substance and HPMC using torque 90 [cN.m] applied pressure.

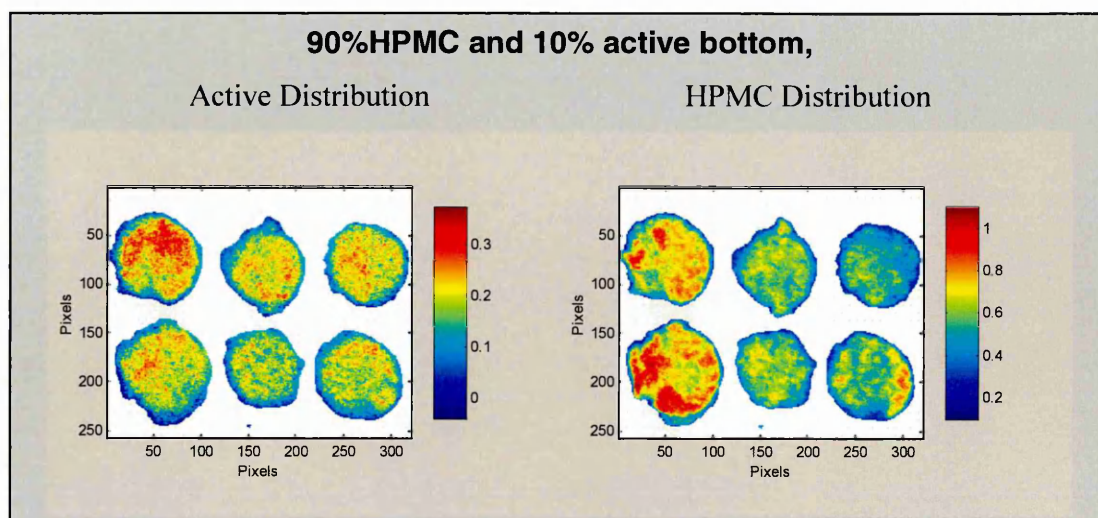


Fig 4-12i. NIR images bottom side of the tablets prepared by blending binary mixture HA90/10 of active substance and HPMC using torque 90 [cN.m] applied pressure.

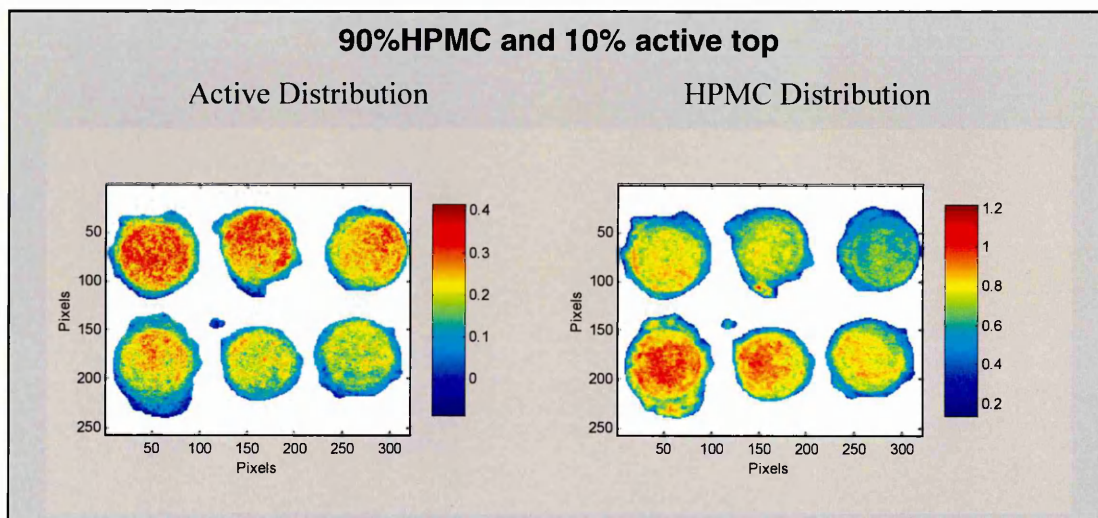


Fig 4-12j. NIR images bottom side of the tablets prepared by blending binary mixture HA90/10 of active substance and HPMC using torque 90 [cN.m] applied pressure.



The analysis of the NIR images (Fig 4-12a-j) from the top and bottom sides clearly indicated an increased regularity of distributed components on the top of the tablet together with higher intensity values. The images from the top samples indicated possible segregation of the components within the tablet since more of the active substance particles seemed to be present on the top side than the bottom side and also showed higher intensity values. In addition the general distribution of API within each set of six tablets was more uniform on the top rather than on the bottom side. However it is known that active substances tend to be distributed in the form of clumps or small particles rather than be evenly dispersed, this could be observed in the bottom NIR images from the samples showing the drug distribution [159, 160].

In the case of HPMC chemical maps a more uniform distribution of particles were observed on the top side of the tablet however the intensities obtained for the top and bottom sides of the tablet were similar. There was definitely more variety observed for the bottom sides within the set of six tablets for each concentration. Each set shows the selection of six tablets with the range of high level absorption (dark red colour) to the very low values of the intensity (blue colour) on the surface. The differences between the tablets within one set of respective concentrations could be explained by the fact that HPMC itself is a heterogeneous substance (i.e. with respect to particle size). Although the optimization of the mixing conditions of the formulation improved the distribution of the HPMC within the tablet, as almost no more clusters or aggregates were found in the samples, this component still showed more heterogeneous distribution on the tablet surface than the active substance. Also the irregular shape of the tablets images bottom side is connected with the stress relaxation of the HPMC after the tablet manufacturing process, which also has an influence on the analyzed results. Finally the image of the sample 80% HPMC and 20% of active substance bottom side (Fig 4-12g) shows clearly the impact of mechanical



defect occurred after manufacturing process [159, 161, 162]. The dark blue region on the images of both components shows the lack of substances in that particular place. As the compressed tablets in-situ on the ATR crystal used to sometimes stick to the crystal, the spatula was required in order to remove them. The blue region is caused by the necessity of using spatula which generated the changes on the surface removing the outer layer of the powder from the bottom side of the tablet.

## **4.4 Conclusions**

The analysis of solid dosage forms from binary systems provided information about the chemical and physical properties of the mixed and compressed formulations. The FTIR analysis of the prepared mixtures showed the presence of the characteristic bands for the analysed substances however no changes in the position of the bands were observed indicating there was no hydrogen bonding between the mixed excipients in the analyzed spectra. The peaks of the mixed substances overlapped with each other indicating the necessity of using more advanced methods of data analysis in order to adequately analyze the data which will be generated in the presence of dissolution media.

The conducted PLS data analysis confirmed a good level of reproducibility of the samples in case of HPMC and citric acid formulations, which were also compatible with the chemical imaging data. However in case of HPMC and API formulation the results obtained from PLS showed higher levels of variance of the HPMC component in the tablets. Chemical maps of the HPMC distribution confirmed the more heterogeneous surface for this component in comparison with API distribution.

Also the analysis of the images of the top side of the tablets showed the general tendency of API to segregate on that part of the tablet as all analyzed samples indicated higher intensity for the API particles than on the bottom side. Both substances presented more uniform distributed particles on the top side of the tablet than on the bottom.

## **5. Investigations of binary formulations in a dissolution media.**

Drug dissolution involves many interactions in formulations with drug substances including chemical reactions, hydration of the sample, protonation/deprotonation, the emergence of new species, hydrogen bonding and solvation. Particular interest is usually directed at the drug-substance which can react with other excipients of the formulation during its release from the polymer matrix. The main aim of investigating controlled drug release is to prevent possible unnecessary reactions of the active substance in the dissolution media and also improving and modifying the drug release behaviour so the final mechanism of the formulation will be understood.

In the first step any new possible chemical species or molecular changes in the chemical bonds of the reactants should be monitored, to provide information about the properties of the investigated formulation. Standard dissolution testing provides the percentage of the dissolved drug released over a specified duration of time. However, this technique is not able to provide any information about the formulation at the molecular level [151, 153].

In this chapter the solid tablets compacted on the diamond ATR were introduced to the dissolution media, possible molecular interactions in the experiments are a subject of discussion.

## **5.1 Aims:**

- To investigate drug release from binary formulation in different media
- To conduct the analysis of interactions of the components in an aqueous environment
- To monitor the hydration and hyphenation experiments and develop information about the formulation behaviour in static and dynamic conditions
- To validate MCR as a tool to study such systems

## **5.2 Materials and methods:**

### **5.2.1 Materials**

Materials used in this chapter are listed in Chapter2, Table 2.1

### **5.2.2 The analyzed formulation**

#### **Formulation of:**

#### **HPMC and citric acid                  HPMC and active substance**

HPMC [%]	Citric acid [%]	HPMC [%]	Active substance [%]
95	5	90	10
90	10	80	20
80	20	70	30
50	50	60	40
		50	50

Table 5-1. Concentrations of binary formulations

The binary formulations were prepared by the method described in Section 3.2.2.2.

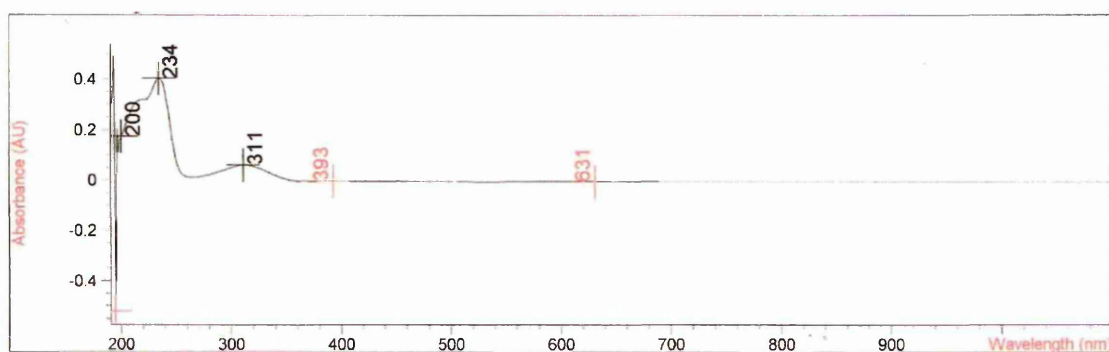
The active substance was passed through a sieve to match the particle size of API with the other excipients.

### **5.2.3 Dissolution testing**

The experiments were carried out for 12 h at  $37.0 \pm 0.5$  ° C, basket rotational speed was  $100 \text{ rpm} \pm 4 \text{ rpm}$  and during the last 30 min an infinite spin was used which increased speed of basket rotation to 200 rpm. The types of media used were distilled water, 0.1N HCL, pH 6.8 phosphate buffer. The volume of medium was  $1000 \text{ ml} \pm 10 \text{ ml}$ . For

dissolution testing the USP apparatus I (baskets); QE Distek bath DT1/UV20 and PD Distek bath PT13/UV19 were used. The spectrophotometer Agilent 8453 UV automated dissolution system was set with a wavelength of 238 nm for distilled water and phosphate buffer and 234nm for 0.1N HCl. The wavelength appropriate for the active substance in different media was chosen based on the UV response for the standard solutions (API dissolved in the media) as shown at the Fig 5-2.

a)



b)

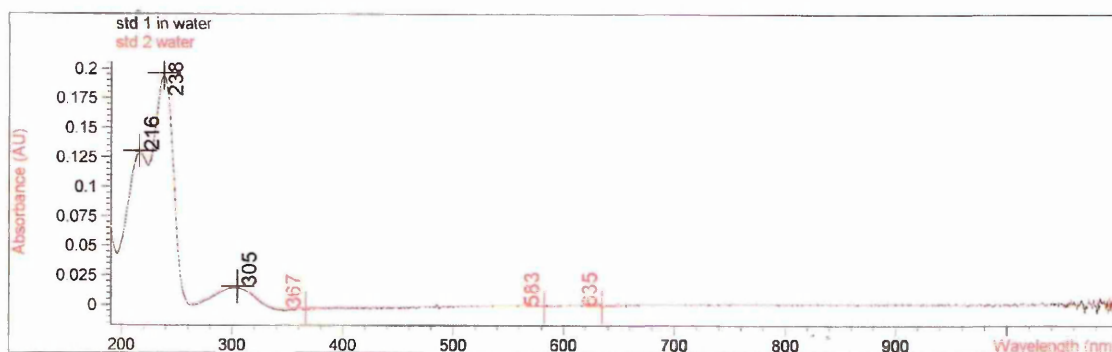


Fig 5-2 The example of UV spectra showing the wavelength values for two standards made from the active substance dissolved in 0.1 N HCl (a) and API dissolved in distilled water (b).

The total weight of the tablet tested was 200 mg. The tablets were compacted using the Stylcam 100R compression simulator with the compression force 850-950 daN. The choice of compression force used was based on the comparison between different forces and measured thickness, weight of the sample and hardness of the tested tablets from two chosen formulations.

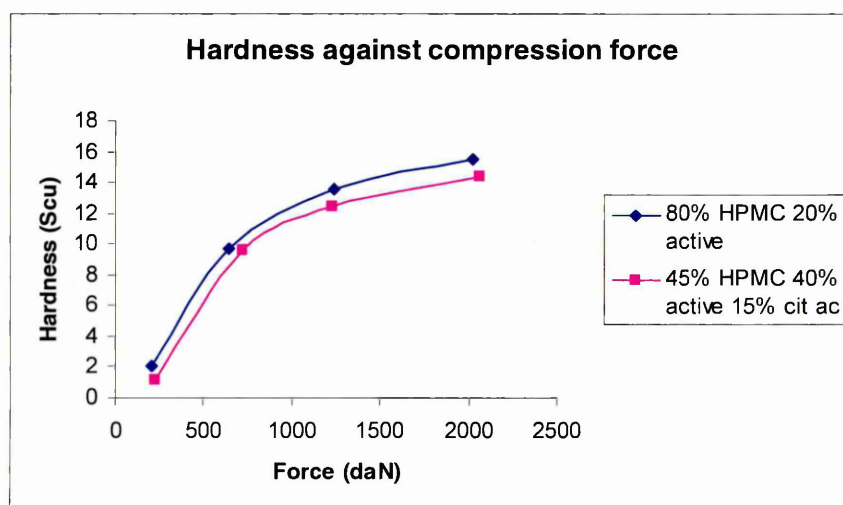


Fig5-3. Hardness of tested tablets against compression force. Each data point represents the average value of three tablets.

The hardness of the tablets was tested using a Schleuniger Pharmatron Tablet Hardness Tester, model 6D. Preferable hardness for tablets with weight of 200 mg is between 9-10 Scu\* [163].

\*1 Scu = 7N

\* 1 N = 0.1 daN

#### 5.2.4 Preparation of the solutions

The HPMC, API and Citric acid solutions were prepared independently and FTIR spectra were collected with the spectral parameters described in a chapter 3, section 3.2.4.2.

##### **5.2.4.1 Preparation of the HPMC solutions**

The required weight of polymer was mixed with water in a mortar and pestle. When the powder appeared evenly distributed in the water, the solution was transferred to a sealed glass container. The solutions were stored at 4 °C for one week to allow the polymer to fully hydrate. Eleven solutions were prepared using 10 ml of water and the required polymer weight to obtain aqueous solutions in the range from the 45%-95% (every 5%).

##### **5.2.4.2 Preparation of API solutions**

The active substance is freely soluble in water so the solutions were prepared by incorporating the required weight of API powder to the appropriate mass of water. The percentage of prepared solutions w/v was 1%, 2%, 5% and 10% in 10 ml of distilled water.

The solutions of API exceeding 10% were saturated such that the active substance powder was visible in the solution.

##### **5.2.4.3 Preparation of Citric acid solutions**

The citric acid solutions were prepared by incorporating the required weight of the acid powder to the appropriate mass of water. The percentage of prepared solutions was 5%, 10%, 15%, 20% and 50% in 10 ml of distilled water.



#### 5.2.5 Hydration and Hyphenation experiments

Static hydration experiments were conducted *in situ* on the diamond ATR. The dissolution media was introduced through the channels of the compaction cell to the compacted tablet. The experiment was monitored for a duration of 12 h, and the spectra were recorded every 3 mins. The parameters for spectral collection were kept the same as those used for the solid dosage form.

The hyphenation experiments were conducted by coupling the compaction cell on the FTIR-ATR equipment to a UV detector and HPLC pump to make a closed circulation system for dissolution media. The HPLC pump was connected to the compaction cell with PE tubing, the dissolution media with a flow rate of ~0.5 ml/min was introduced to the compacted sample; the temperature was set to 37 °C on the ATR crystal.

The outlet from the compaction unit was directed to the UV detector where the signal from the sample was measured. The liquid from the UV detector was directed back into the reservoir beaker, and the total volume of the dissolution media was 450 ml. The liquid in the beaker was constantly mixed throughout the duration of the experiment, and pumped through the compaction cell. Values measured from the UV detector were recorded by the voltagemeter Ut60a software.

A calibration of the UV absorbance was made using different concentrations of active substance in water and the output was recorded, using the wavelength of 238 nm. The data is shown in Fig 5-4.

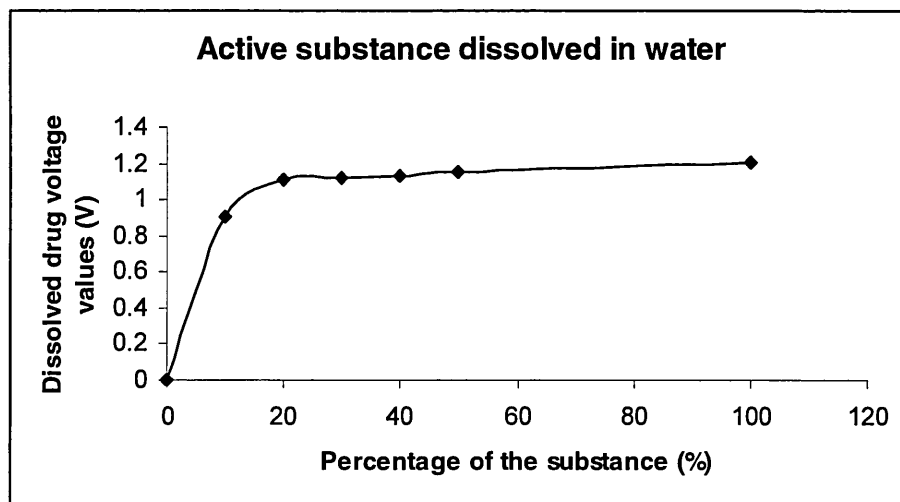


Fig. 5-4 Output of the signal from voltagemeter connected to the UV detector using active substance dissolved in distilled water

API is a freely soluble in water substance. Based on the values obtained during the calibration experiment the UV output from the mixtures of different formulations will be analyzed for the appropriate values of API in the samples.

#### 5.2.5.1 Preparation of the dissolution media

##### *6.8 pH phosphate buffer*

Sodium hydroxide (0.83g) and potassium dihydrogen orthophosphate (6.48g) were dissolved in 1 liter of distilled water.

##### *0.1n HCl solution*

1 liter solution: 100 ml of concentrated HCl was added to distilled water 900 ml.

The pH of the prepared dissolution media was measured by a PHM220 pH Meter 657R056NO11.

#### 5.2.6 MCR data analysis

The MCR analysis was conducted using the three different applications (Tauler, Hancewicz and PLS toolbox) to allow an independent comparison of the calculated results [164, 165]. The predicted number of components for binary system was set as 5 considering the number of components i.e. pure active substance, pure HPMC, medium, hydrated API and hydrated HPMC. Apart from pure substances one would assume the presence of the hydrated species in the samples. ALS optimization was used to optimize the MCR results. The MCR-ALS method is very flexible and applicable to many samples. [94].

## **5.3 Results and discussion**

### **5.3.1 Effect of pH dissolution media on the drug release from binary formulation.**

Despite the solubility of the active substance, drug/polymer load in the formulation and manufacturing conditions (for example compression force, hardness of the tablet), the drug release is also influenced by the surrounding conditions for example pH of dissolution media especially when the drug has pH dependent solubility [27, 30].

The dissolution experiments for HPMC and active substance formulation were conducted in distilled water, pH 6.8 phosphate buffer and 0.1 N HCl; pH 1.5.

#### **5.3.1.1 Dissolution of the binary formulation in distilled water using gelatin capsules.**

The appropriate amount of powder of formulations HPMC and active substance was placed in the gelatine capsules and the dissolution testing was conducted. The possible interference coming from gelatine capsule was removed from the obtained results by running the dissolution analysis of the empty capsule in the dissolution vessel and extracting the capsule values from the formulation results.

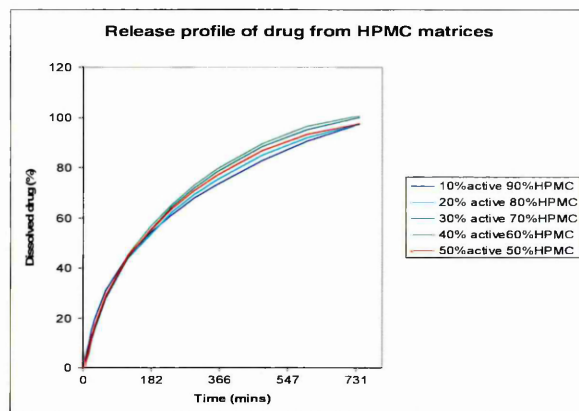


Fig 5-3 Mean dissolution profiles for formulations of HPMC and active substance. The 300 mg gelatin capsules were dissolved in distilled water.

The dissolution profiles of the binary formulation (Fig 5-3) obtained from the experiment in distilled water as a medium, showed variability between 97-100 % drug release values over the course of the experiment. Also the curve of the obtained profiles suggests that the drug from the capsule is released gradually during the test and dissolution rate is determined in such a case by dissolution and diffusion process [130]. Alternatively one would expect sudden changes in dissolution drug percentage resulting from the tablet erosion.

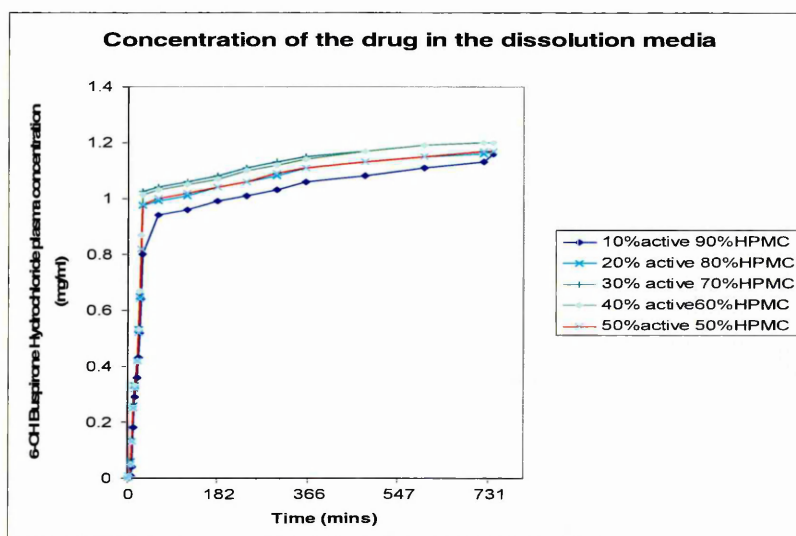


Fig. 5-4 Dissolution rates, mean concentration profiles of active substance versus time.

The concentration versus time profiles (Fig 5-4) for active substance showed very similar dissolution rates for all analyzed concentrations of the formulations. The rate of release for 90% HPMC and 10% of active substance formulation is reduced in comparison with 50% of HPMC and API in the mixture [166].

According to Ford *et al* (1985) the most important factor affecting the drug release from HPMC matrices is the drug/HPMC ratio as the increased polymer concentration causes an increase of the viscosity of the gel layer and as a consequence the longer diffusional paths decrease drug release rates [26, 27].

#### 5.3.1.2 Dissolution testing of the tablets from binary formulations in pH 6.8 and 0.1N HCl.

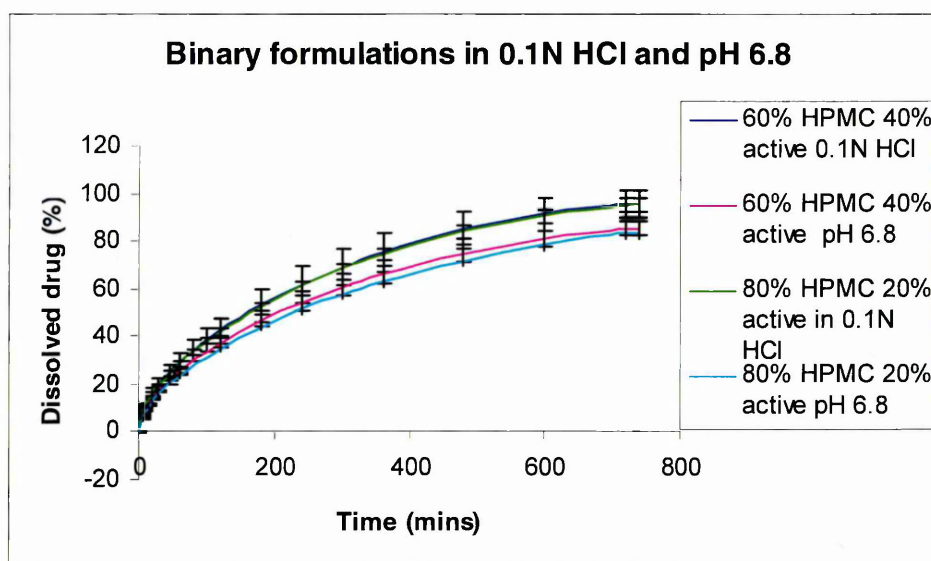


Fig 5-5 Mean dissolution profiles for formulations of HPMC and active substance, the 200 mg tablets were placed in pH 6.8 phosphate buffer or 0.1N HCl as the dissolution media.

The dissolution profiles of binary mixtures (Fig 5-5) showed a significant difference between the samples tested in pH 6.8 and 0.1N HCl. Quicker release and higher percentages of dissolved active substance was observed in case of 0.1N HCl medium as expected. The profiles of dissolved tablets in the same medium obtained similar values of released drug over time independently from the amount of active assayed in tested formulations.

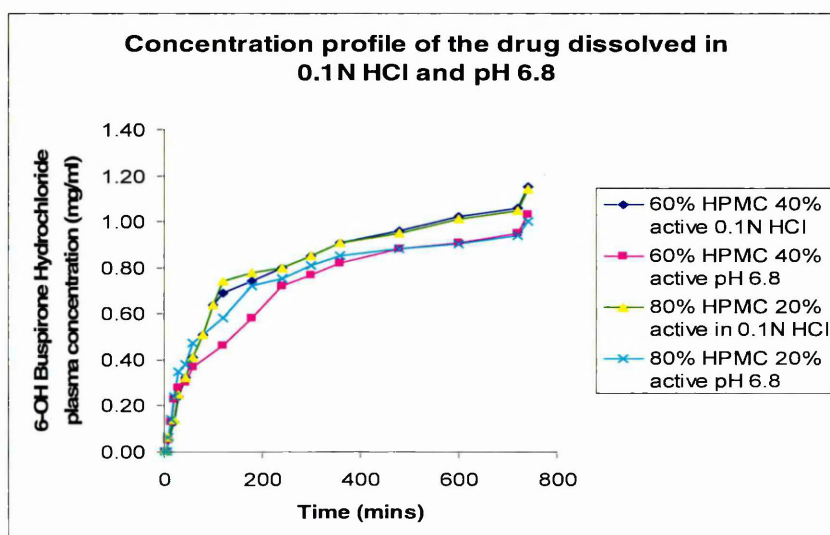


Fig 5-6 Dissolution profiles for HPMC and active substance formulation within pH 6.8 phosphate buffer and 0.1 N HCl as a dissolution media.

The concentration profiles analysis confirmed the higher amount of released drug in shorter time in the case of samples tested in 0.1 N HCl compared to those in the pH 6.8 media. The binary mixtures tested in different pH's had a larger variability of the final percentage dissolved drug of 84% (samples tested in pH 6.8 medium) to 97% for samples tested in 0.1N HCl. Such a difference can be visually confirmed by the amounts of remaining residues of active substance in the HPMC gel after the 12 h dissolution experiment finished

The presence of high numbers of air bubbles in the gel (Fig 5-7b, 5-8b) confirm the high percentage of the drug release from the polymer matrix in 0.1 N HCl during the 12h experiment compared to the pH 6.8 media which gave slower release and lower percentage released values for dissolved drug.

The results from pH 6.8 and distilled water showed similar dissolution rates.

### 5.3.2 Investigations of possible interactions of the binary formulation in the hydrated state

The analysis of the infrared spectra of hydrated samples provides information on a molecular level which is not possible to obtain directly from standard dissolution testing methods. The absorption bands of the characteristic groups may reveal the possible interactions between the excipients of the formulation and the dissolution medium. Also the presence of any new products in the sample could be justified as a result of the chemical interactions like protonation/deprotonation processes, van der Waals force or hydrogen bonding effecting the bands position in the spectra [69, 70, 154].

In this study the hydrated tablets spectra were analyzed in order to confirm the presence of possible interactions between the substances.

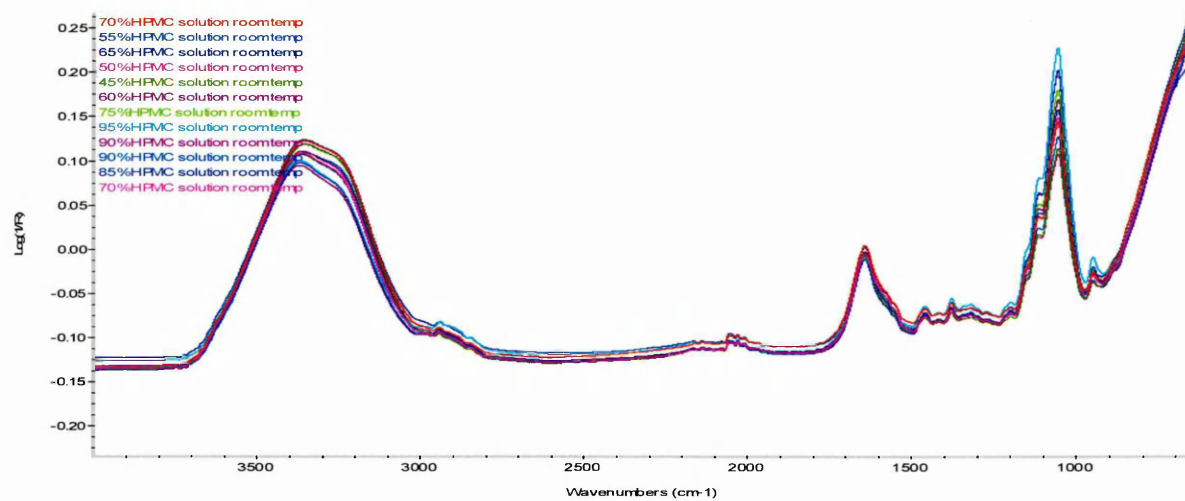
#### 5.3.2.1 Aqueous solutions of excipients

Aqueous solutions of HPMC, active substance and citric acid were prepared independently and their spectra were collected using FTIR-ATR instrument as described previously in the Chapter 3.

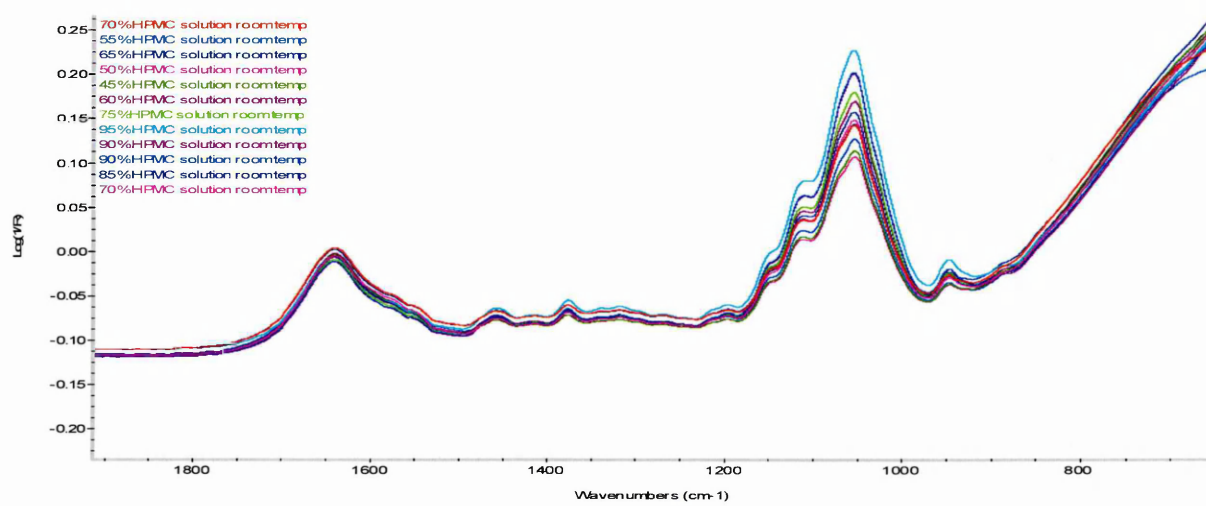


## Aqueous solution of HPMC

a)



b)



c)

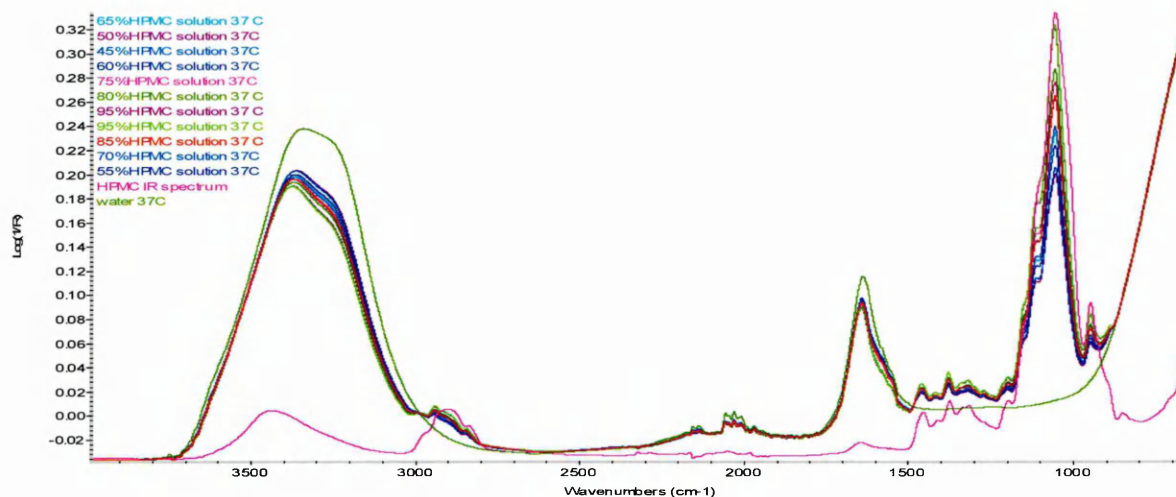


Fig 5-13. a) Spectra of different HPMC concentrations as aqueous solutions, b) Spectra of same HPMC aqueous solutions region in  $1900\text{--}700\text{ cm}^{-1}$ , c) Comparison of HPMC solutions spectra with solid polymer and water spectra.

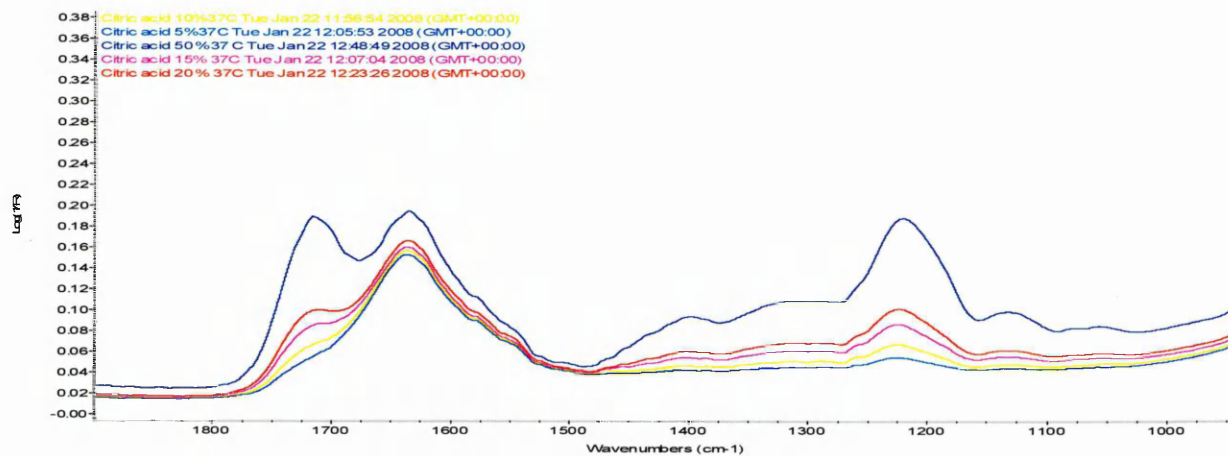
Increasing concentration of HPMC has significant impact on the changes in the intensity of the bands between  $1000\text{--}1200\text{ cm}^{-1}$  ( $\nu\text{ C-O}$ ), and  $2800\text{--}3000\text{ cm}^{-1}$  ( $\nu\text{ (CH)}$ ). Comparing the spectrum of solid HPMC with solutions spectra, the complex band  $1250\text{--}950\text{ cm}^{-1}$  is wider than in the solutions spectra. These changes are a result of polymer hydration process with the dominance of inter-molecular H bonding over the intra-molecular H-bonding [167].

The change in the shape of the  $\nu(\text{OH})$  band and its shift to the wavenumber  $3600\text{--}3000\text{ cm}^{-1}$   $\nu(\text{OH})$  was observed as well. It is the indication of weakening of the water H-bond network as the effect of inclusion HPMC in water solution. Also the visible shift to the higher wavenumber suggests the presence of the component referred to as weakly hydrogen bonded water. The OH bending mode of liquid water is less sensitive to changes in the

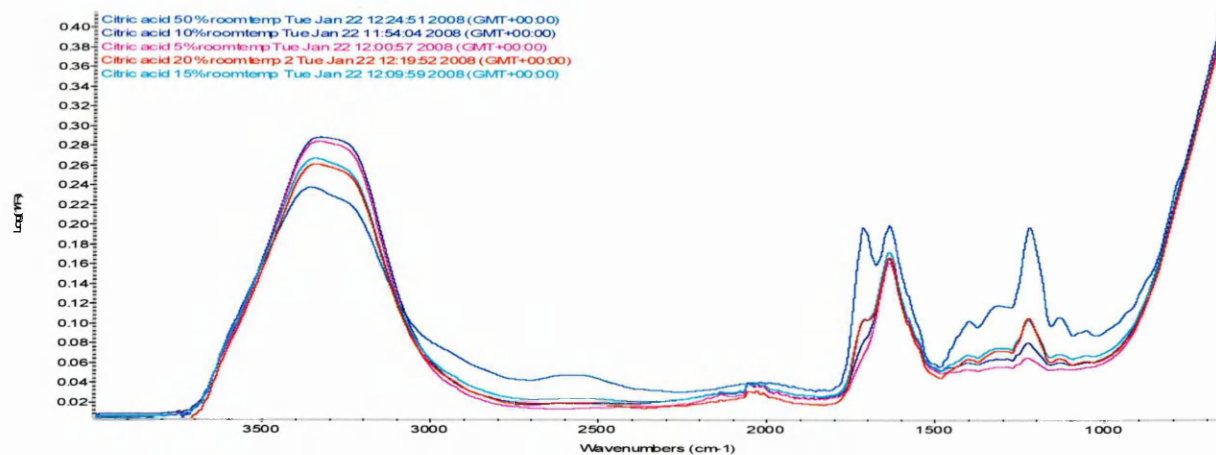
hydrogen bonded network decreases in the intensity with the increasing polymer concentration, as one would expect.

### Aqueous solutions of Citric acid

a)



b)



c)

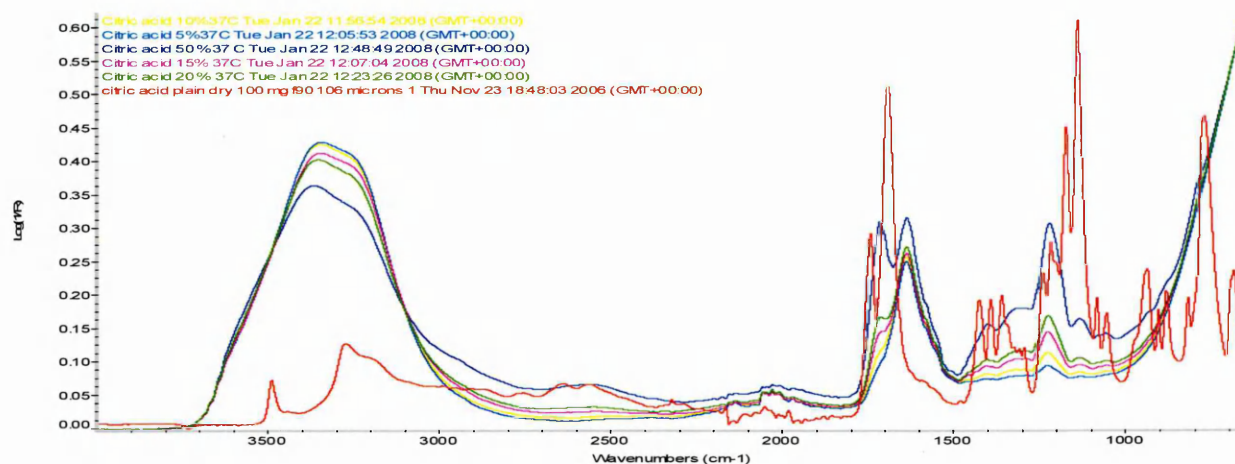
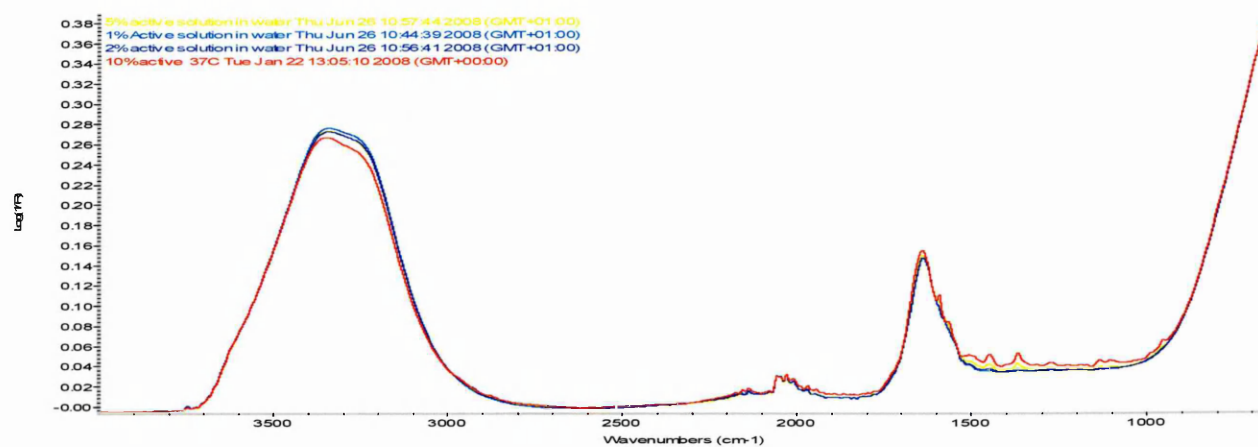


Fig 5-14 a). Citric acid aqueous solution spectra, b) Citric acid solutions spectra in region  $1000\text{-}1400\text{cm}^{-1}$  and  $1500\text{-}1700\text{cm}^{-1}$ , c) Comparison of aqueous citric acid solutions spectra with solid substance spectrum

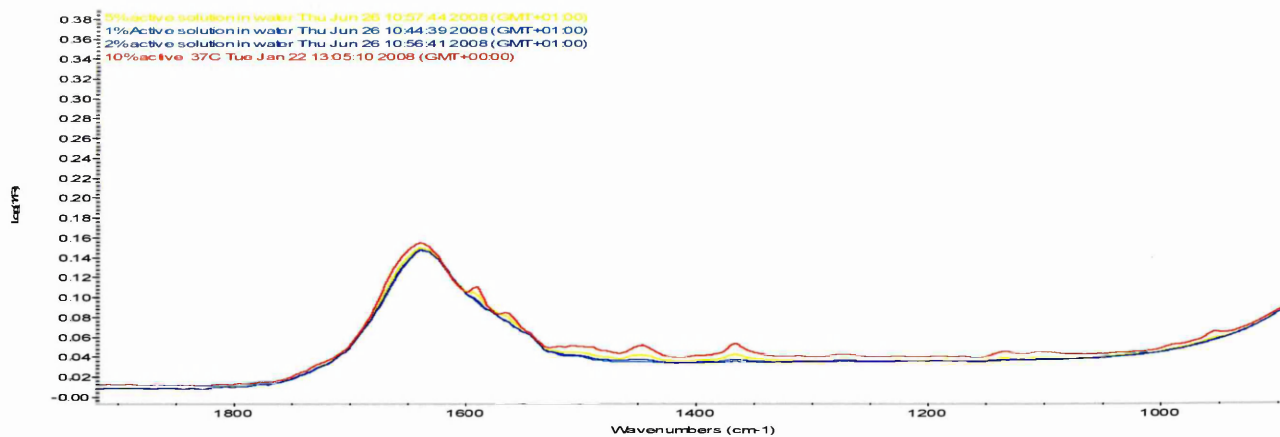
Increasing concentration of citric acid in solutions has an influence on the intensity and shape of the bands in regions  $1700\text{-}1500\text{ cm}^{-1}$   $\nu(\text{C}=\text{O})$  and  $1050\text{-}1400\text{ cm}^{-1}$   $\nu(\text{C}-\text{O})$ . The band at  $3600\text{-}3000\text{ cm}^{-1}$   $\nu(\text{O}-\text{H})$  were significantly reduced in more concentrated solutions and the shape of the band had changed. The carbonyl band is sensitive to hydrogen bonding, so in the aqueous solution it forms broad peak. The changes in this area can be correlated with water concentration and deprotonation of the acid. This is verified in the region  $1300\text{ cm}^{-1}$  with the appearance of the strong peak that could be assigned to the presence of the  $\text{COO}^-$  group.

## Aqueous solutions of active substance

a)



b)



c)

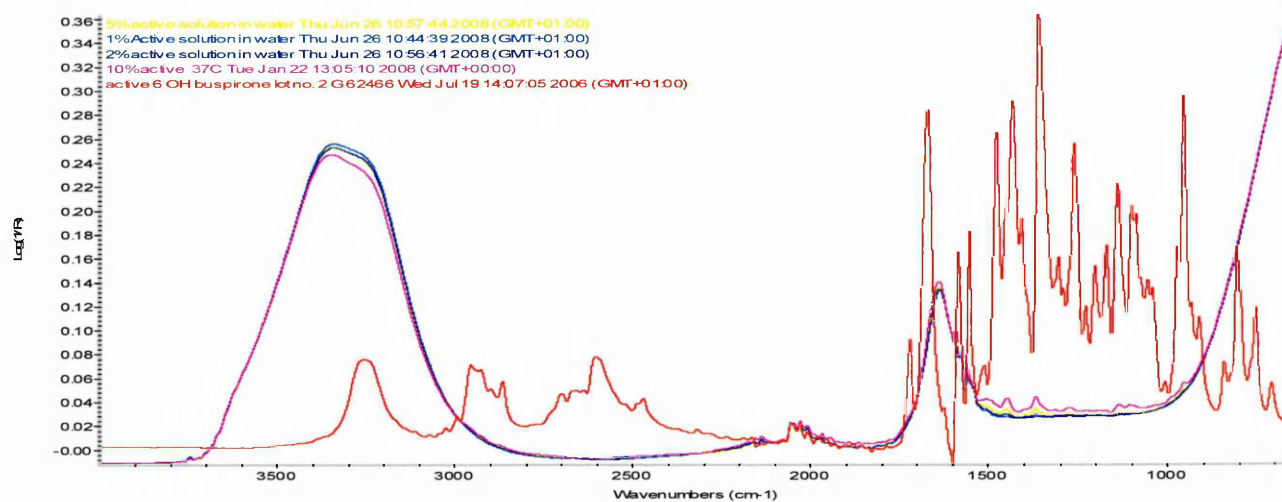


Fig 5-15. a) Active aqueous solutions spectra, b) Active substance spectra region 1500-1700  $\text{cm}^{-1}$  c) Comparison of active aqueous solutions spectra with solid drug spectrum.

Increasing concentration of API in a solution results in the increasing intensity of peaks in the region 1600-1500  $\text{cm}^{-1}$  due to ring vibrations and 1574-1541  $\text{cm}^{-1}$  pyridine ring breathing modes. There is a reduction of intensity in the region 3600-3000  $\text{cm}^{-1}$   $\nu(\text{OH})$  caused by increasing concentrations of API in the solutions. There is also a slight change in the band shape. It is evidence of the presence of weakly hydrogen bonded water in the system. Comparing API spectrum with that in solution the bands between 2700-2400  $\text{cm}^{-1}$  due to delocalized N...H bonding (the interaction of nitrogen with HCl) as expected is not present in solution spectrum [74, 154, 168]. During the production process the pH of 6-hydroksy buspirone solution is kept in the range pH 5-8 however there is no information published about the pKa value for this API.



### 5.3.2.2 Hydration experiments

#### 5.3.2.2.1 Formulation HPMC and active substance

The results of hydration experiments will be discussed based on the example of 80% HPMC 20% Active substance mixture.

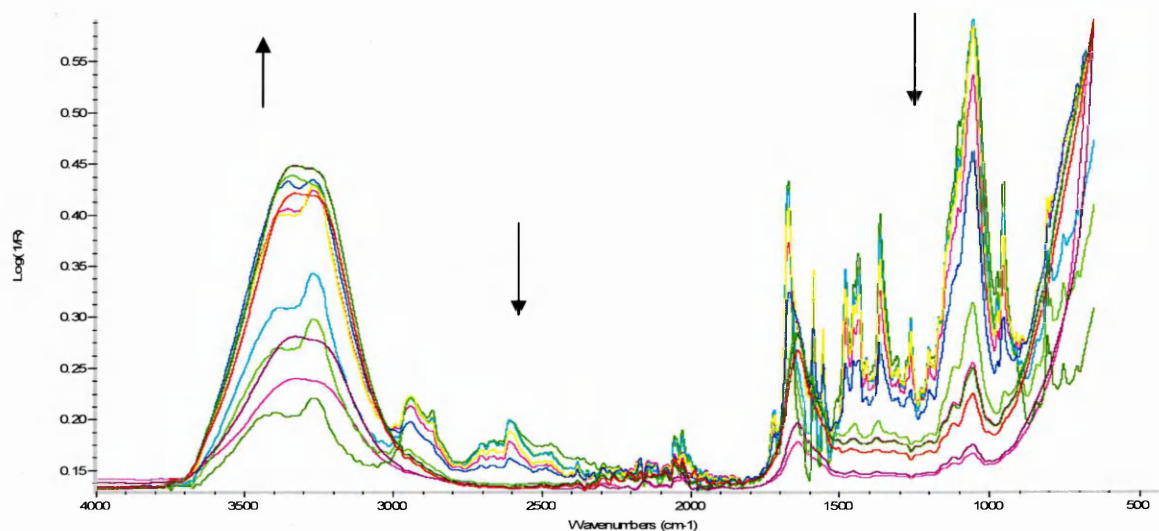


Fig 5-16 Selection of few first sample spectra collected from formulation 80/20HA during 12 h hydration experiment showing spectral changes from the solid mixture spectrum to the hydrated form (every 5 minutes).

Results obtained from hydration experiment binary mixture of HPMC and active substance (Fig 5-16) showed increased intensity of the band  $\nu(\text{O-H})$   $3006\text{--}3699\text{ cm}^{-1}$  associated with water up take and decreased band  $\nu(\text{C-O})$   $980\text{--}1160\text{ cm}^{-1}$  as a result of the polymer swelling process. Spectra collected from formulation of HPMC and active substance showed increasing impact of dissolution media in the sample with time. The formulations spectra showed a decreasing relatively strong absorbance band in the region  $1700\text{--}1650\text{ cm}^{-1}$  associated with  $\text{C=O}$  stretching mode and  $\text{C=C}$  skeletal benzene ring breathing modes in the region  $1600\text{--}1500\text{ cm}^{-1}$  [49, 50]. Also the  $2700\text{--}2400\text{ cm}^{-1}$  delocalized  $\text{N}\cdots\text{H}$  bonding is

no longer present in the hydrated sample. The increasing concentration of the dissolved active from the polymer matrix caused the reduction of the intensity of these bands. Also there are intense changes observed in the region  $3600\text{--}3000\text{ cm}^{-1}$  associated with the  $\nu(\text{OH})$  of water due to hydration process.

The obtained profiles shown in Fig 5-17 result from the integrated area of characteristic band representing each component:  $\sim 1100\text{ cm}^{-1}$  region  $\nu(\text{OH})$  for HPMC and the delocalized N...H complex band (region  $2400\text{--}2700\text{ cm}^{-1}$ ) for the active substance. After specifying the right and left side of the integrated band and the baseline the software application carries out the subtraction. Although the integration operates only in a narrow spectral region, the subtraction removes the entire spectrum of the compound.



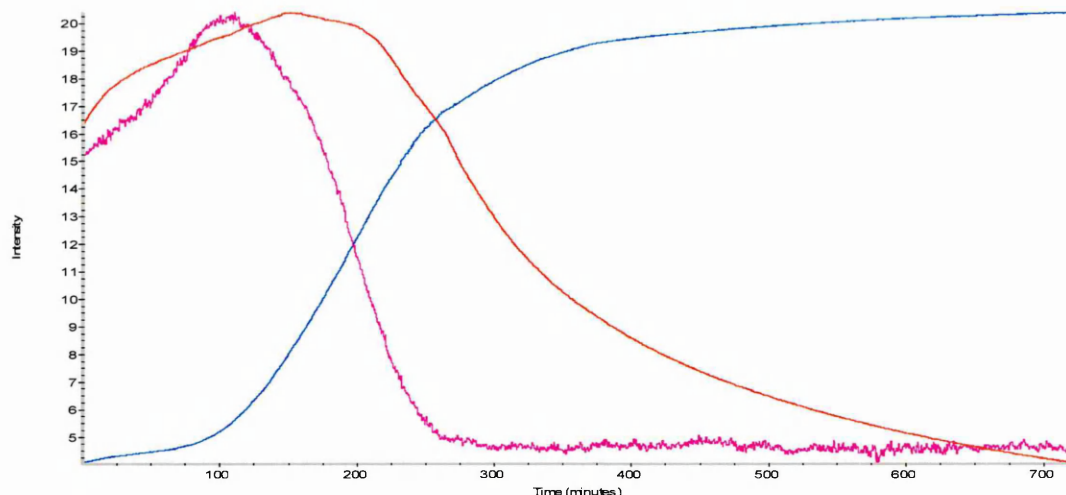


Fig 5-17. Profiles constructed from the characteristic integrated band areas of each component from the hydration experiment for the formulation 80% HPMC and 20% active substance; blue colour- water uptake, region  $3600\text{-}3000\text{ cm}^{-1}$ , red-HPMC region  $1160\text{-}996\text{ cm}^{-1}$ , pink-API region  $2600\text{-}2400\text{ cm}^{-1}$ .

In case of the active substance (Fig. 5-17) the profile decreased and achieved certain constant level. Dissolved active substance diffused out from the system matrix to the surrounding liquid reaching an equilibrium level. The initial increase of API and HPMC profile is associated with the presence of injected water which improves the contact between particles of the compressed powder with the ATR crystal. The rate of diffusion of the active substance over the whole experiment is faster than the relaxation time of the polymer indicating diffusion control. Linear profiles with reported in some cases induction time where sorption ratio is build gradually are quite characteristic for this particular category.

In order to obtain quantitative information the generated profiles were normalized and plotted against square root time.

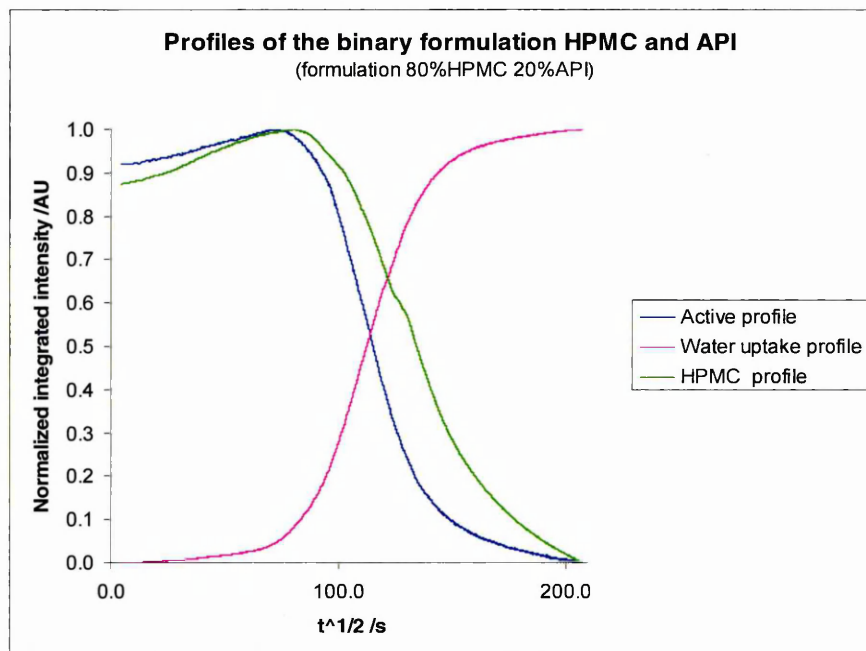


Fig 5-18. Normalized kinetic profiles of the hydrated sample formulation HA80/20

There are different approaches which one could use in order to analyze and discuss the diffusion rates. There are several studies published discussing the rate of solvent diffusion in the polymers, however the thickness of the sample is a required parameter to determine the diffusion coefficient [83, 169]. In this project the studied system suffers from the lack of information about the thickness of the sample as the hydration or hyphenation experiments are requiring the tablet not to be removed from the ATR crystal after its compaction and the thickness of the tablet can not be calculated from the compaction cell dimensions. Considering the limitations of the conducted experiments the measurements of the slope value and x intercept was proposed.

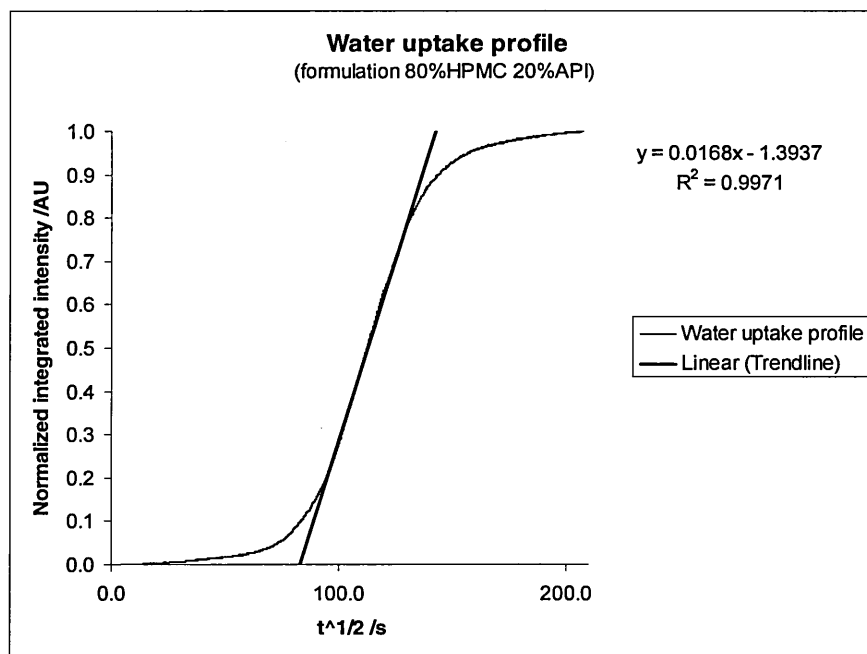


Fig5-19. The Water uptake profile of the formulation HA80/20

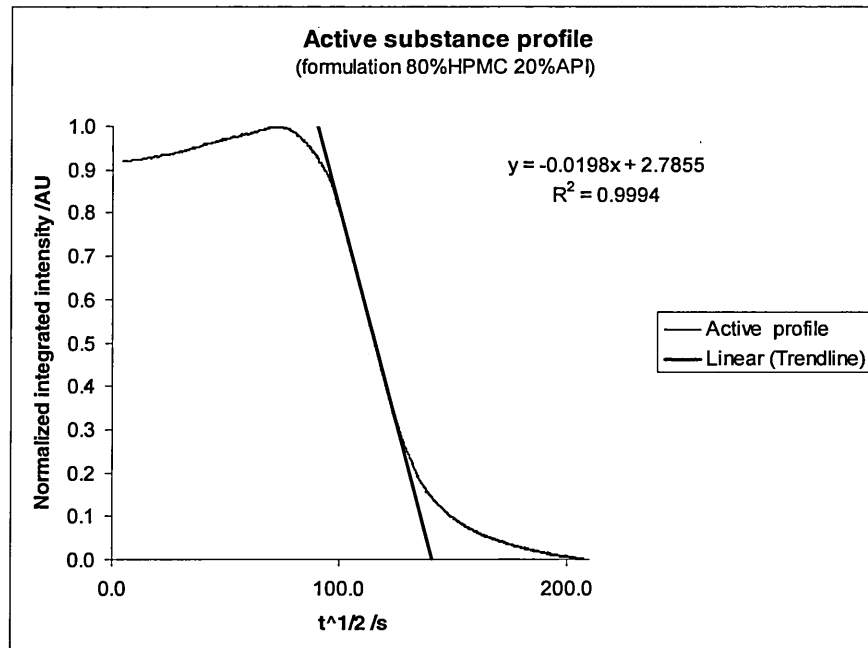


Fig5-20. The API profile of the formulation HA80/20

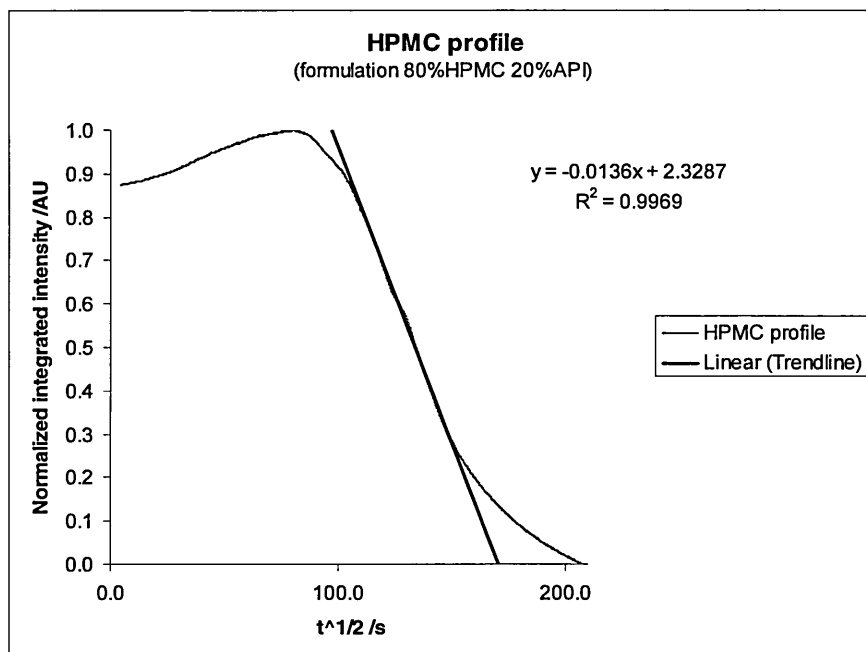


Fig. 5-21. The HPMC profile of the formulation HA80/20

Profiles quantitative data								
HPMC			Active substance			Water uptake		
Slope	Intercept [s]	R <sup>2</sup>	Slope	Intercept [s]	R <sup>2</sup>	Slope	Intercept [s]	R <sup>2</sup>
50% HPMC 50% active substance								
-0.0206	17015	0.994	-0.0144	13514	0.9951	0.0193	7437	0.9990
60% HPMC 40% active substance								
-0.0196	13719	0.9946	-0.0217	11109	0.9962	0.0198	6882	0.9994
70% HPMC 30% active substance								
-0.0178	26857	0.9962	-0.0263	16071	0.994	0.0171	6069	0.9992
80%HPMC 20% active substance								
-0.0136	29317	0.9369	-0.0198	19791	0.9994	0.0168	6881	0.9971
90% HPMC 10% active substance								
-0.0127	26802	0.9991	-0.0368	16538	0.9801	0.0138	5860	0.9974

Table 5-2 The slope, intercept and R<sup>2</sup> values for the analyzed binary formulation HPMC and active substance.

The analysis of the generated profiles for the binary formulation of HPMC and active substance (Fig 5-18-5-21) showed that with ingress of water into the tablet matrix the dissolved active substance diffuses out from the matrix faster whilst the polymer still continues the swelling process. The HPMC profiles showed the initial hydration of the polymer followed by the swelling process. There is a systematic change in the slope value for polymer which is increasing with the increasing concentration of HPMC in the sample. Water uptake slope values are decreasing with the increasing concentration of the HPMC in the sample, which confirms the suggested diffusion control process in the analyzed system. The API appears to be independent of concentration.

#### 5.3.2.2.2 Formulation HPMC and citric acid

The results of hydration experiments will be discussed based on the example of 50% HPMC 50% citric acid mixture.

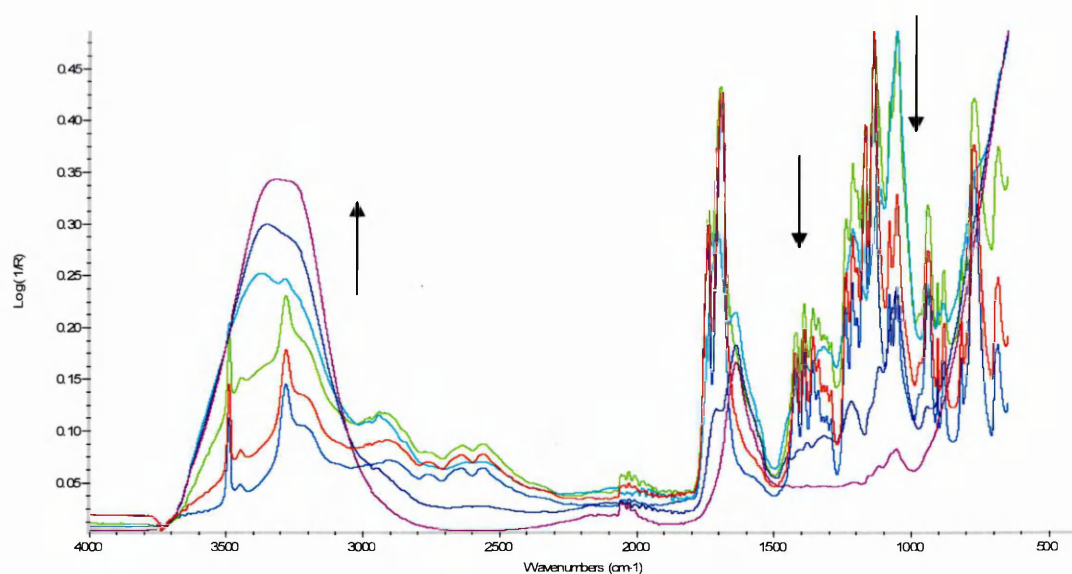
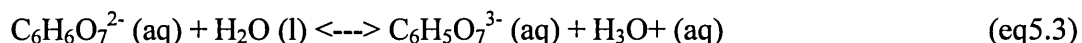
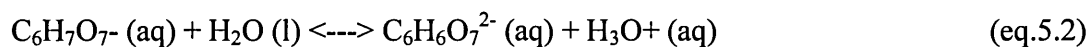
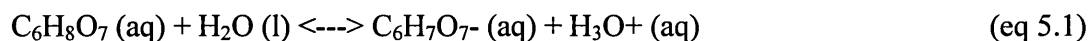


Fig 5-37. Selection of few first sample spectra collected from formulation 50/50HC during 12 h hydration experiment showing spectral changes from the solid mixture spectrum to the hydrated form (every 2 minutes).

.Results obtained from the hydration experiment with the binary mixture of HPMC and citric acid (Fig 5-37) showed increased intensity of the band  $\nu(\text{O-H})$  3006-3699  $\text{cm}^{-1}$  associated with water up take and a decreased intensity band of the  $\nu(\text{C-O})$  980-1160  $\text{cm}^{-1}$  as a result of the polymer swelling process. Spectra collected from this formulation showed an increasing impact of the dissolution media upon the sample with time. The citric acid in the sample showed changes in the intensity and shape of the decreasing bands in the regions 1700-1500  $\text{cm}^{-1}$   $\nu(\text{C=O})$  and 1050-1400  $\text{cm}^{-1}$   $\nu(\text{C-O})$ . The carbonyl band is sensitive to hydrogen bonding  $\sim 1715 \text{ cm}^{-1}$ , and there is evidence of the formation of the broad peak ( $\sim 1375 \text{ cm}^{-1}$ ) as result of citric acid reaction with dissolution media (eq5.1-5.3).

Equilibrium equations for the citric acid in the aqueous solution



The changes in this area are correlated with water concentration and deprotonation of the acid.

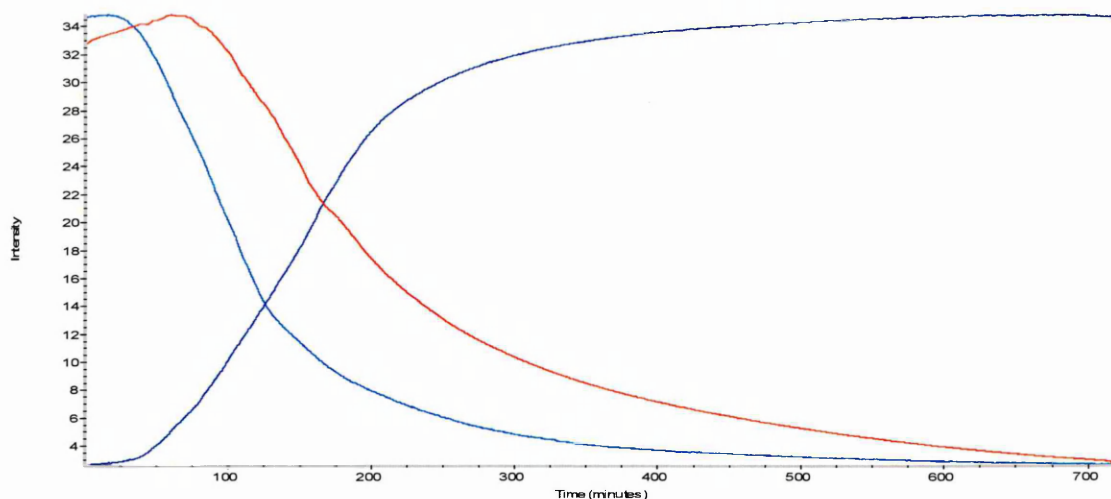


Fig 5-38. The profile constructed from the characteristic integrated band areas of each components obtained from the formulation of HPMC and citric acid; dark blue colour-water uptake, region  $3600\text{--}3000\text{ cm}^{-1}$ , red-HPMC region  $1160\text{--}996\text{ cm}^{-1}$ , blue-citric acid region  $\sim 950\text{ cm}^{-1}$ .

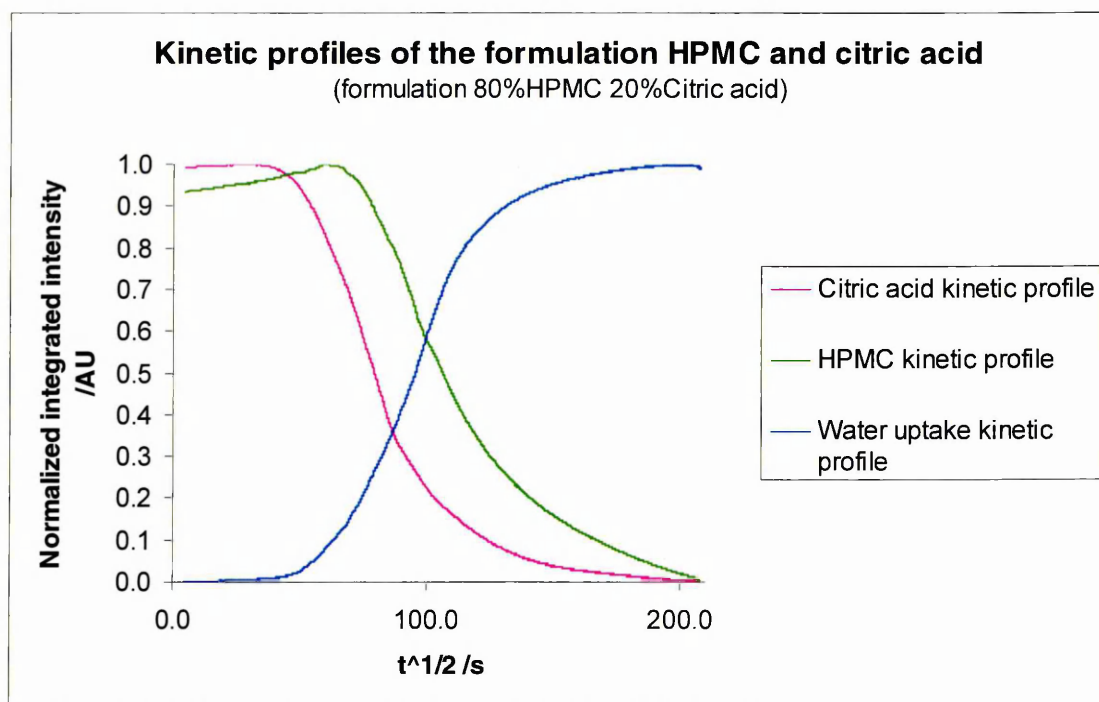


Fig. 5-39 Normalized profiles for formulation HC80/20.

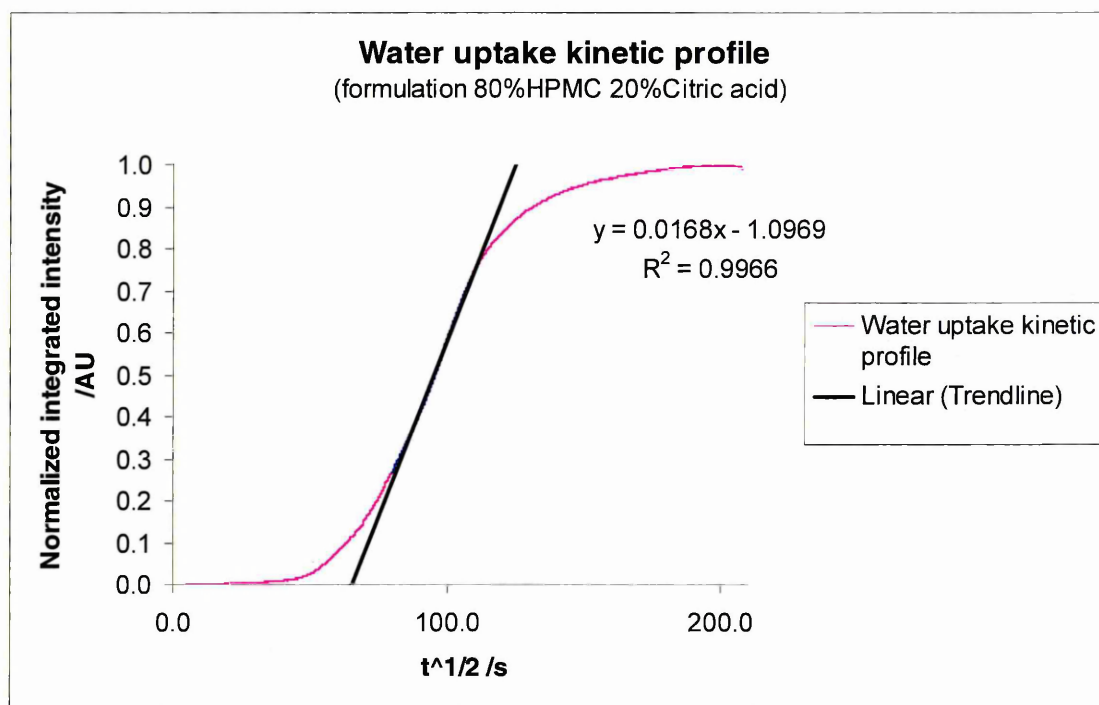


Fig. 5-40 Normalized profiles for water uptake.

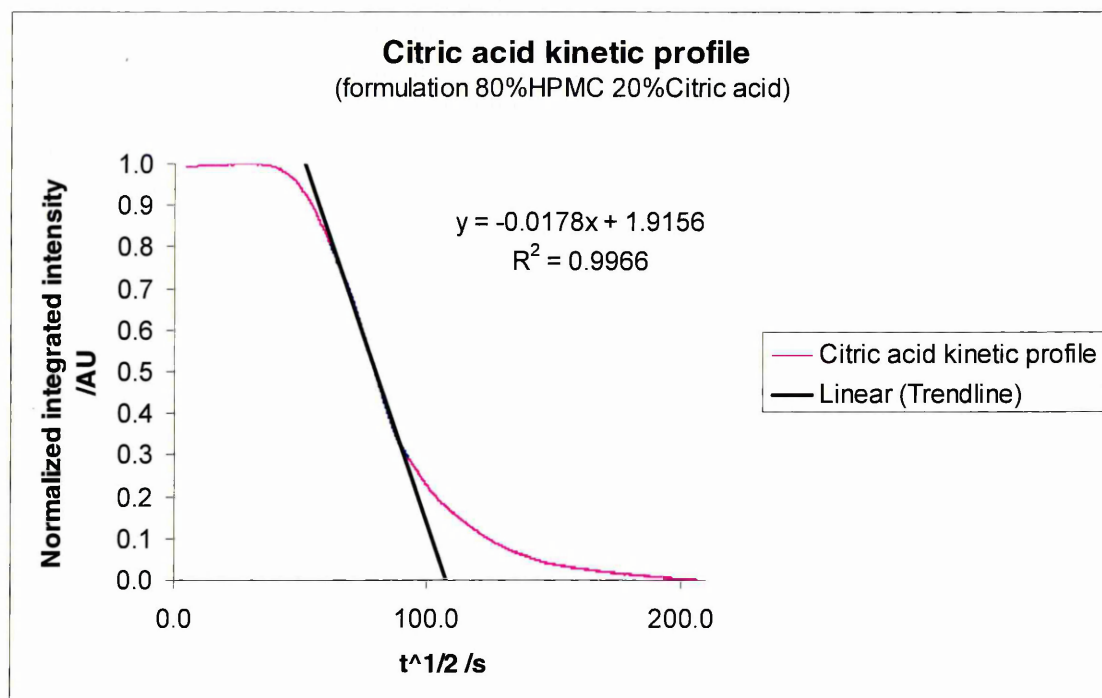


Fig. 5-41 Normalized profiles for citric acid.



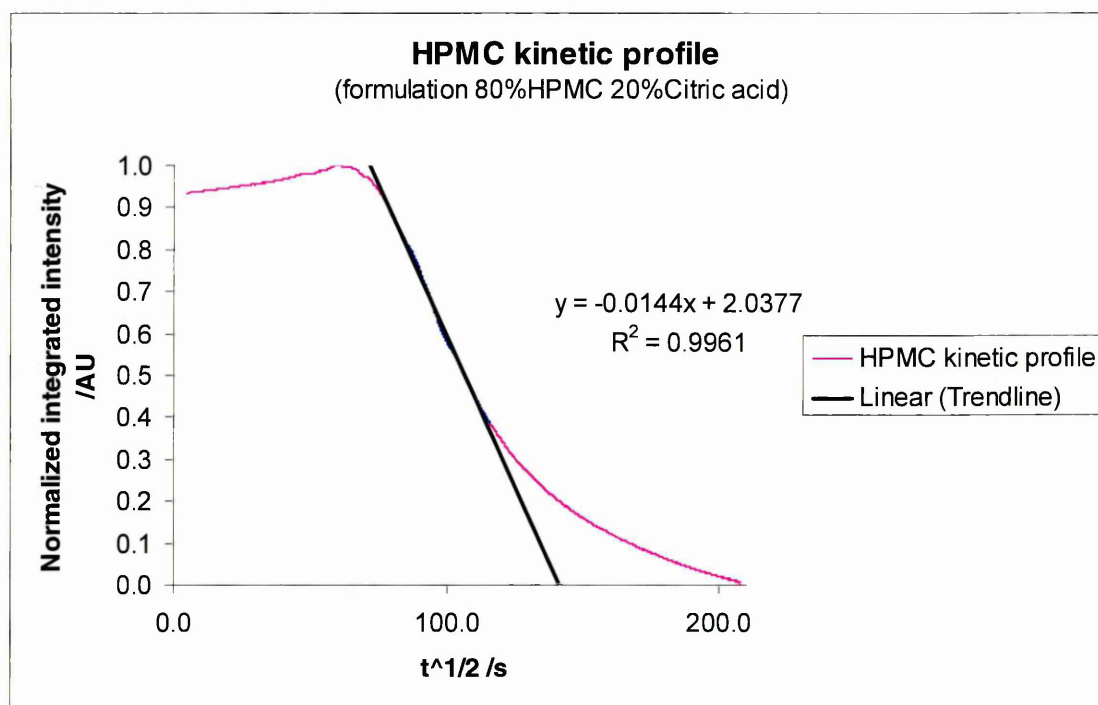


Fig. 5-42 Normalized profiles for HPMC.

Profiles quantitative data								
HPMC			Citric acid			Water uptake		
Slope	Intercept	R <sup>2</sup>	Slope	Intercept	R <sup>2</sup>	Slope	Intercept	R <sup>2</sup>
<b>50% HPMC 50% citric acid</b>								
- 0.0206	7388	0.9914	- 0.0313	5147	0.9966	0.0195	1532	0.9927
<b>80% HPMC 20% citric acid</b>								
- 0.0144	20023	0.9961	- 0.0178	11580	0.9966	0.0168	4263	0.9966
<b>90%HPMC 10% citric acid</b>								
- 0.0142	26202	0.9963	- 0.0204	18698	0.9965	0.0167	7683	0.992
<b>95% HPMC 5% citric acid</b>								
- 0.0139	26756	0.9923	- 0.0163	19701	0.998	0.015	8542	0.9979

Table 5-3 The slope, intercept and R<sup>2</sup> values for the analyzed binary formulation HPMC and citric acid.

Analysis of the generated profiles for the binary formulation of HPMC and citric acid (Fig. 5-38 to 5-42) showed that citric acid dissolves and diffuses out from the polymer matrix whilst the HPMC still continues the swelling process. The HPMC profiles showed the initial hydration of the polymer followed by the swelling process. There is a systematic change in the slope value (Table 5-3) for polymer which is increasing with the increasing concentration of HPMC in the sample as well as the water uptake profile showed decreasing slope values with increasing concentration of HPMC in the sample. The citric acid appears to be independent of concentration.

The kinetic profile of citric acid decreases and achieves certain constant level. Dissolved acid diffused out from the system matrix to the surrounded liquid reaching an equilibrium level. The rate of diffusion of the acid is higher than the relaxation time of the polymer which suggests the diffusion control process.

#### **5.3.2.3. Hyphenation experiments of API and HPMC**

The hyphenation experiments are discussed based on the mixture 80% HPMC 20% active substance and 60% HPMC and 40% of active substance in 0.1 N HCl and pH 6.8 phosphate buffer as a dissolution media.

### 5.3.2.3.1 Hyphenation experiments in the pH 6.8

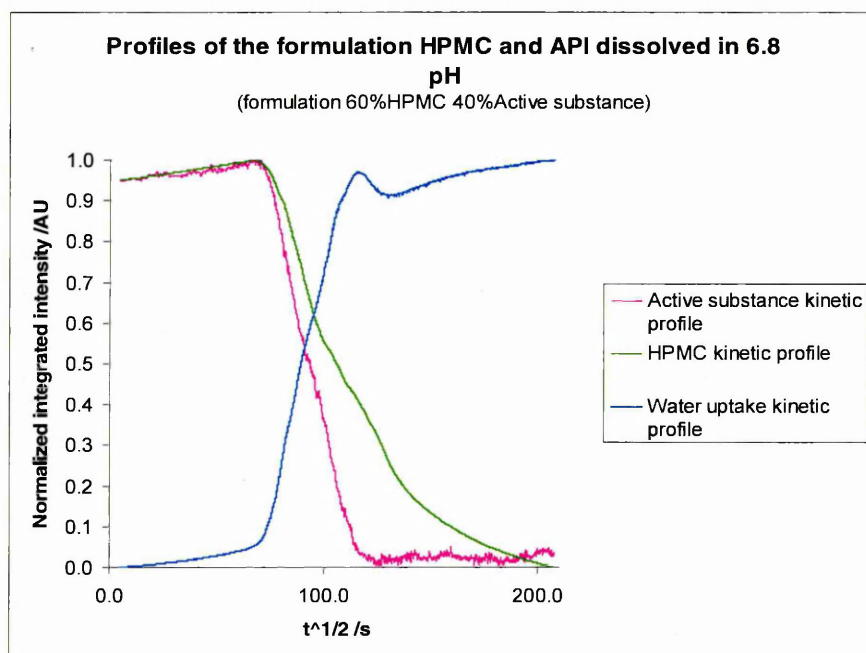


Fig. 5-43. The normalized kinetic profiles of the hyphenated samples from formulation HA 60/40

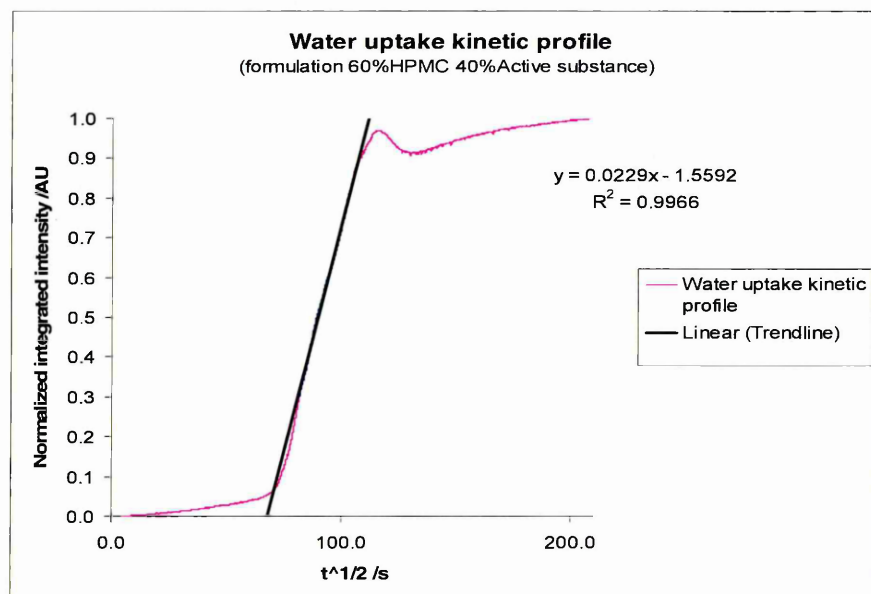


Fig. 5-44. The normalized kinetic profile of water uptake formulation HA 60/40

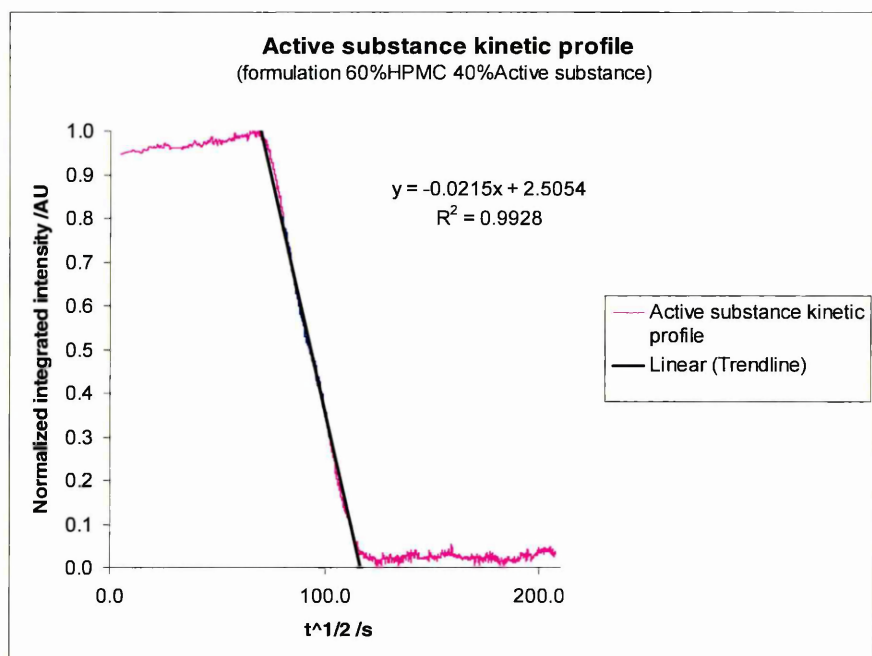


Fig. 5-45. The normalized kinetic profile of active substance formulation HA 60/40

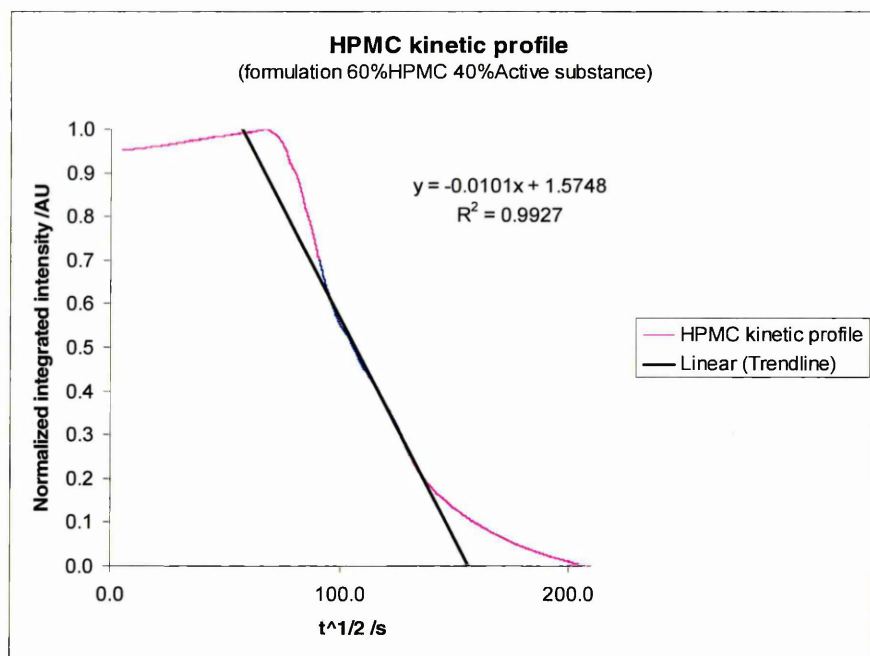


Fig. 5-46. The normalized kinetic profile of HPMC formulation HA 60/40

### 5.3.2.3.2 Hyphenation experiments in the 0.1N HCl

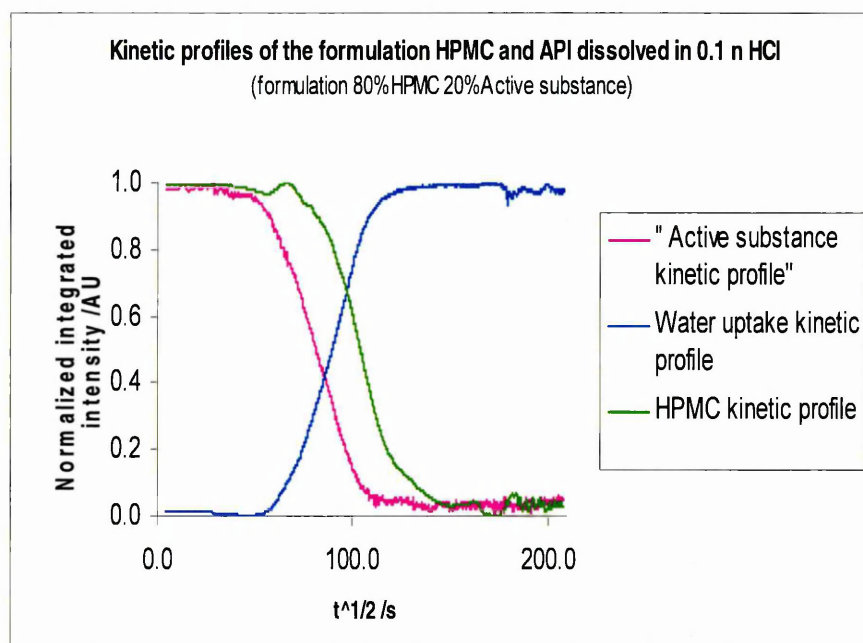


Fig. 5-47. The normalized kinetic profiles of formulation HA 80/20

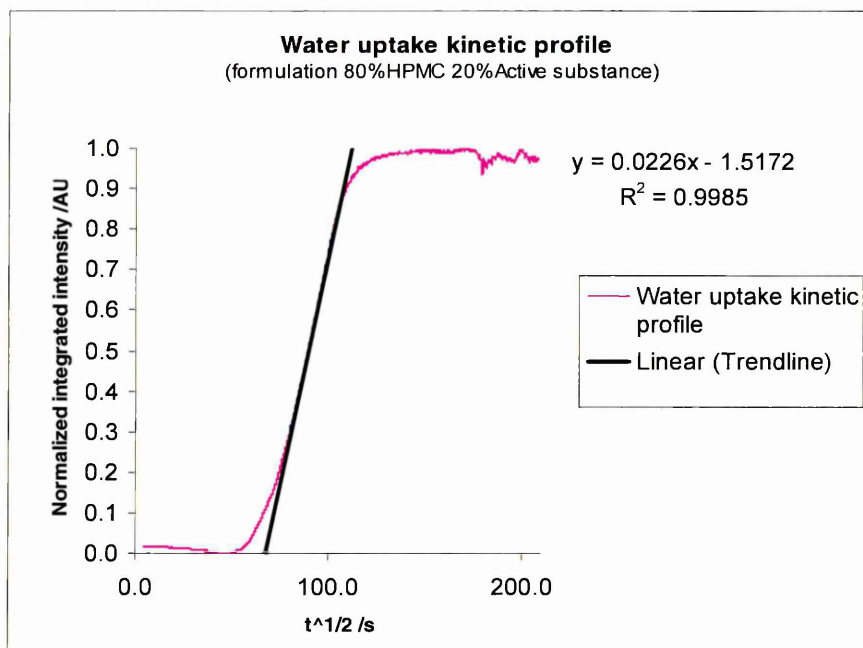


Fig. 5-48. The normalized kinetic profile of water uptake formulation HA 80/20

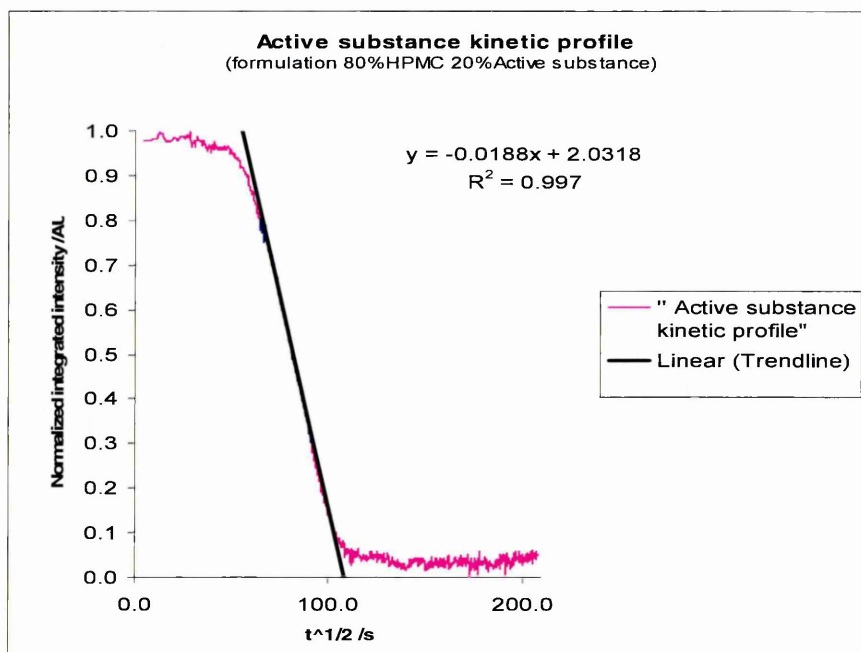


Fig. 5-49. The normalized kinetic profile of API formulation HA 80/20

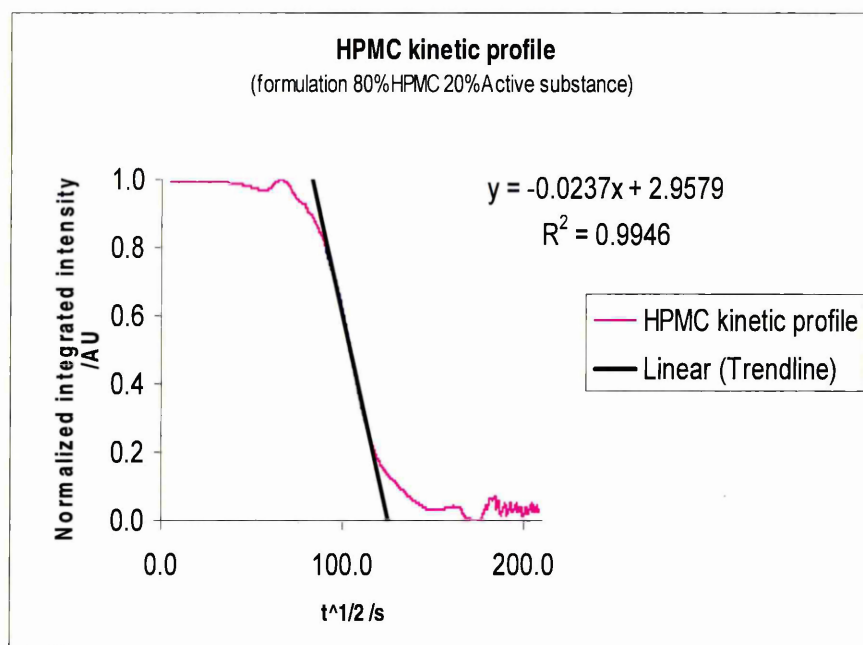


Fig. 5-50. The normalized kinetic profile of HPMC formulation HA 80/20

Kinetic profiles quantitative data								
HPMC			API			Water uptake		
Slope	Intercept	R <sup>2</sup>	Slope	Intercept	R <sup>2</sup>	Slope	Intercept	R <sup>2</sup>
<b>60% HPMC 40% API in 0.1 n HCl</b>								
-0.0225	14335	0.9995	-0.0187	8894	0.9904	0.0169	1408	0.9981
<b>80% HPMC 20% API in 0.1n HCl</b>								
-0.0237	15575	0.9946	-0.0188	11679	0.997	0.0226	4506	0.9985
<b>60%HPMC 40% API in 6.8 pH</b>								
-0.0101	24311	0.9927	-0.0215	13579	0.9928	0.0229	4635	0.9966
<b>80% HPMC 20% API in 6.8 pH</b>								
-0.0137	18053	0.9841	-0.0183	12823	0.9779	0.0149	2771	0.9991

Table 5-3 The slope, intercept and R<sup>2</sup> values for the analyzed binary formulation HPMC and citric acid.

The quantitative analysis (Table 5-3) of the kinetic profiles of the HPMC, API and water uptake in the binary formulation showed systematic changes within the slope values. Samples dissolved in 0.1 N HCl showed decreasing slope values for HPMC with increasing amount of HPMC in the sample, as we might expect considering the solubility of API in the acid. However the intercept values for API and HPMC are increasing. The intercept values give information about the time needed to observe the diffusion process occurring in the sample with a certain concentration. The water uptake profile values are increasing with the increasing concentration of HPMC in the sample. In the case of hyphenated experiments conducted in the pH 6.8 environment the slope values are decreasing with the increasing concentration of HPMC in the sample for all profiles. The intercept values are increasing in the case of HPMC and API. The obtained results showing the changes in the behaviour of the formulations depending on the dissolution media pH, what agrees with the results

obtained from dissolution testing. Also as observed the Figures 5-43 and 5-46 are suggesting swelling and further on dissolution process of HPMC.

Along with the analysis of the infrared results the output of the UV detector was considered to broaden the obtained information.

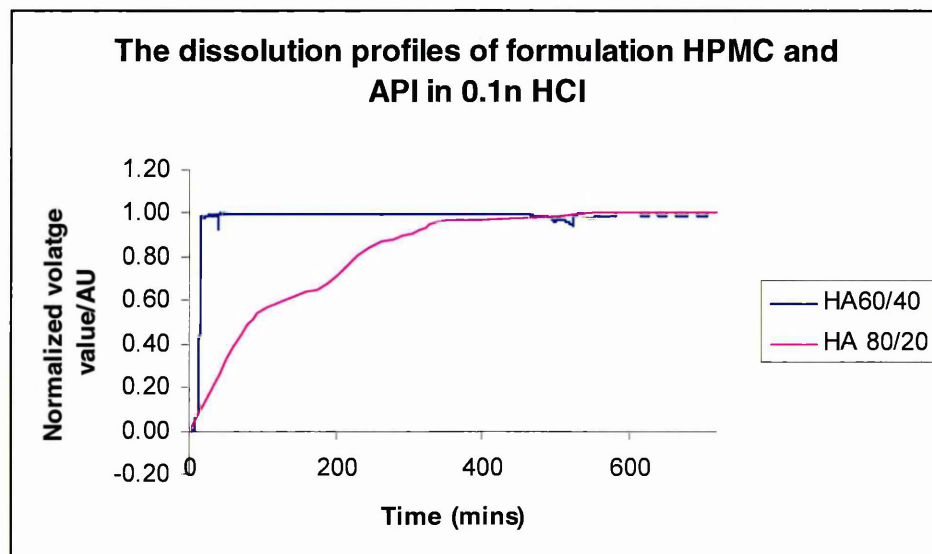


Fig 5-51. The output of UV reading for the formulation HA 80/20 and HA 60/40 during the dissolution testing in 0.1N HCl



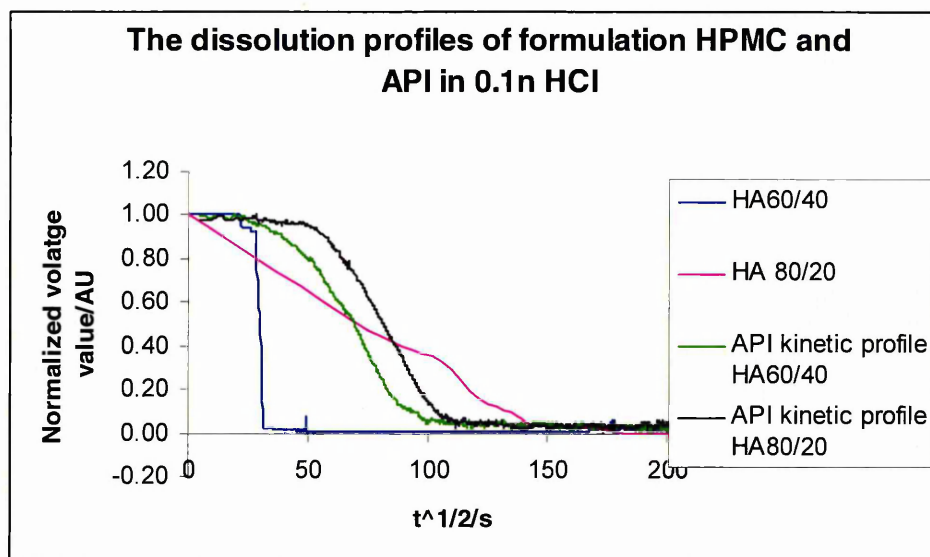


Fig 5-52. The normalized kinetic profiles for formulations HA 80/20 and HA 60/40 and the absorbance units (AU) from the UV with reduction as voltage value for dissolution media (1-H<sub>2</sub>O) dissolved in 0.1N HCl

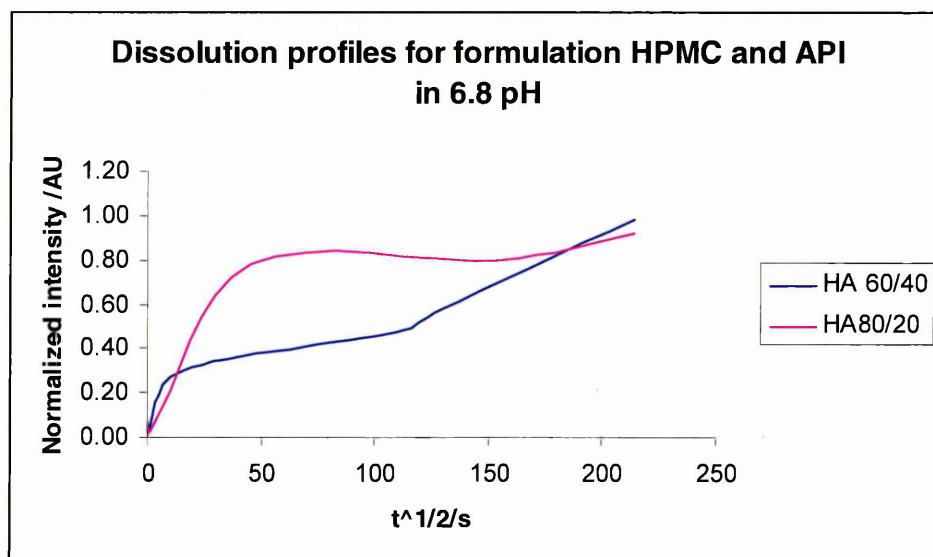


Fig 5-53. The output of UV reading for formulations HA 80/20 and HA 60/40 dissolved in pH 6.8.

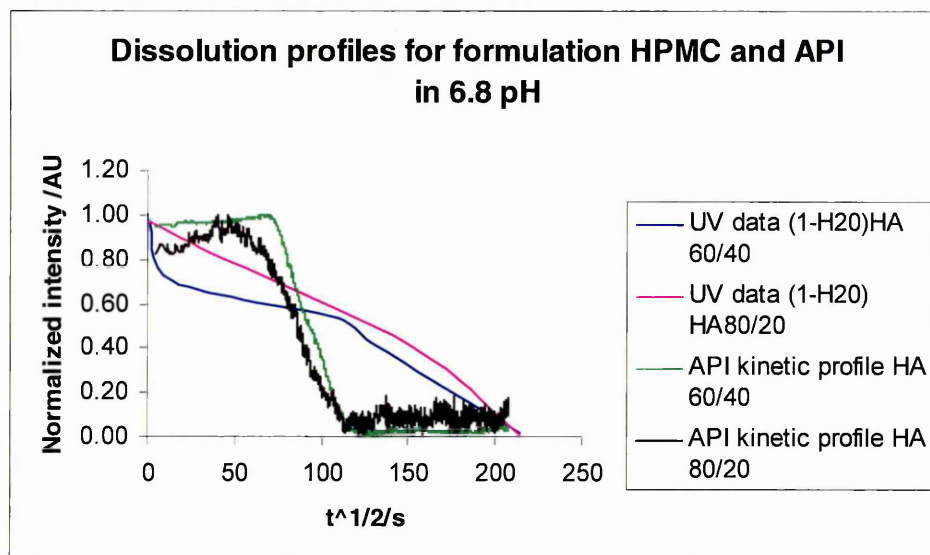


Fig 5-54. The normalized IR profiles for formulations HA 80/20 and HA 60/40 and output of the UV reading with the reduced values for dissolution media (1-H<sub>2</sub>O) dissolved in pH 6.8.

The profiles (Figs 5-51 to 5-54) obtained from UV detector showed significant differences when compared with the kinetic profiles obtained from the infrared spectroscopic analysis. The UV reading reflects the output from the top surface of the tablet, whereas the infrared spectra are collected from the bottom side of the tablet. The IR profiles showed a much faster ratio of drug dissolution than the UV kinetic profiles, as expected, since the PLS and NIR Imaging results obtained for solid tablets, showed the active substance had significant level of segregation on the top side of the tablet. In the case of hyphenated experiments this caused the differences in the UV measurements and the “dose dumping” effect. The UV profiles are very poor quality due to the low concentrations of the analyzed substances, irregular flow as the HPLC pump did not always deliver to the compaction cell as showed on the digital screen output and the non-conventional all the equipments set up.

### 5.3.3 Prediction of the possible components existing in the hyphenated samples using MCR data analysis

IR data obtained from binary mixtures hyphenation experiments were analysed using MCR-ALS method. Three different MCR applications (Tauler, Hanciewicz and PLS toolbox) were applied to allow an independent comparison of the calculated results. The function Fast Non Negative Least Squares (F-nnls) deciding when elements (x) are less than zero was found to be the most appropriate way to avoid the rotational ambiguity; the other used parameters are discussed in the section 5.2.6.

Validation of the method began with MCR analysis of three pure, dry component spectra of HPMC, active substance and citric acid. These spectra were collected using the FTIR-ATR instrument; the result achieved during MCR analysis was easily predicted.

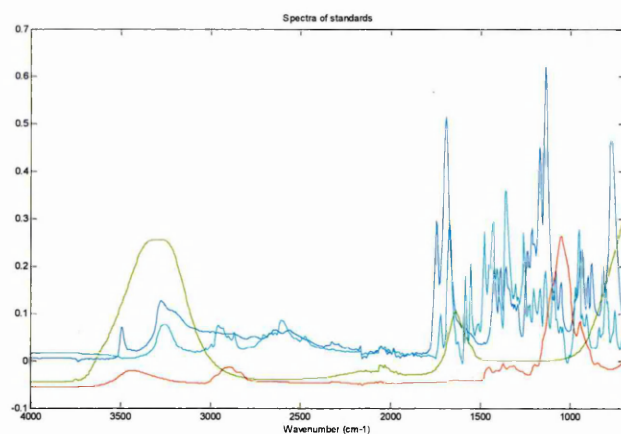


Fig 5-55. Standards coloured spectra of four components: red-HPMC, green-water, blue-active substance, dark blue-citric acid.

The next step was to build a new model; the data matrix contained twenty-one spectra of dry samples, each one from a different formulation. The presence of characteristic bands from each component in a particular spectrum allows the determination of pure compounds from the mixed matrix data. Moreover concentration profiles show predicted (average) values for dry samples used in an investigated matrix.

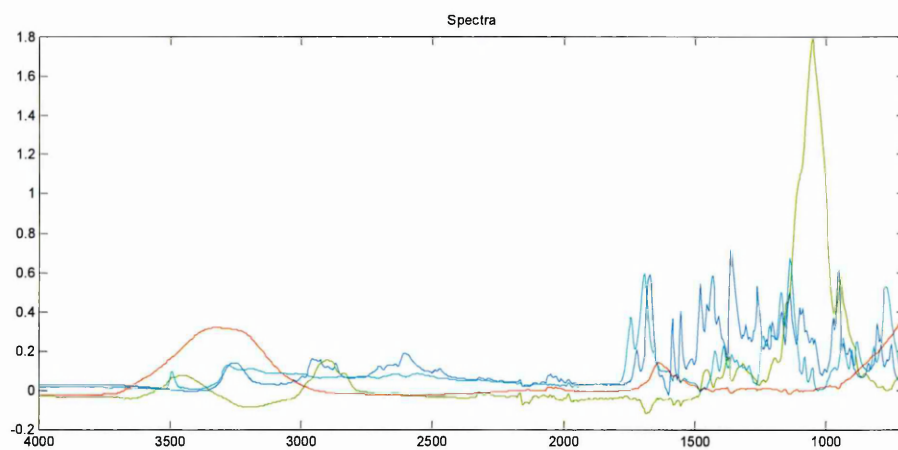


Fig. 5-56. Spectra of mixed matrix contained four excipients spectra marked with different colours: red-water, green – HPMC, blue- citric acid, dark blue – active substance.

The obtained data were compared with the real values and shown for every substance separately on Fig 5-58 to 5-63

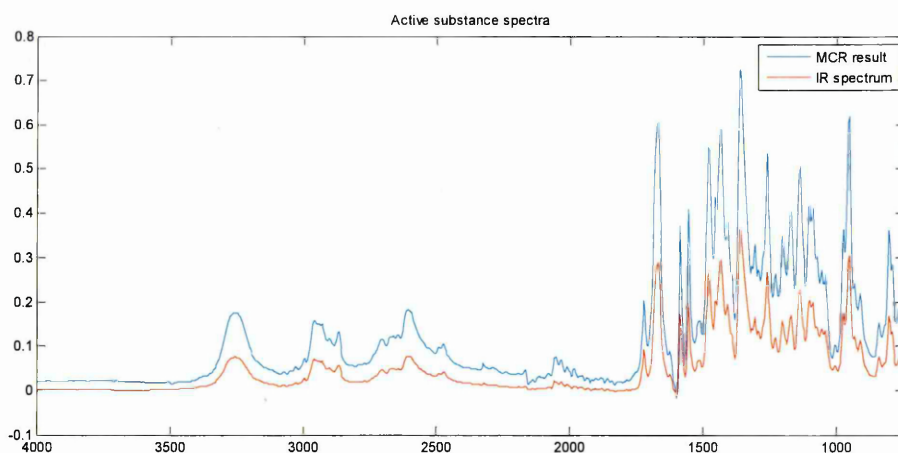


Fig. 5.57. Comparison of drug spectra, blue colour- MCR prediction, red colour-infrared spectrum.

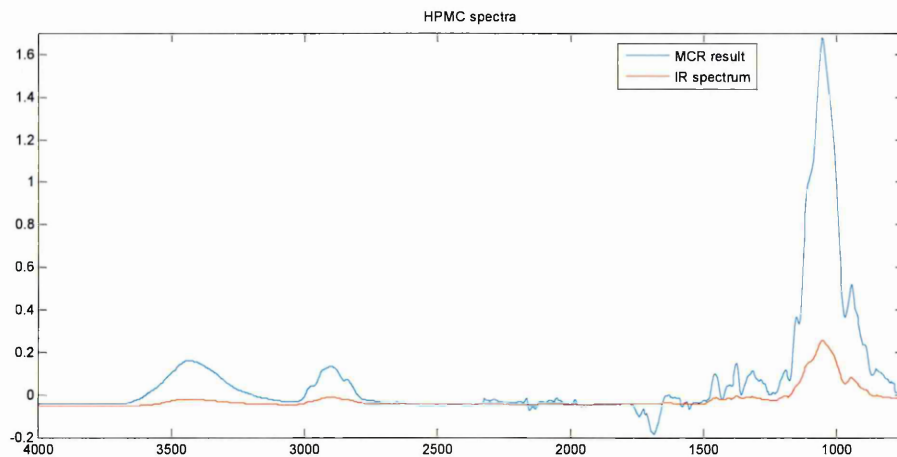


Fig. 5.58. Comparison of HPMC spectra, blue colour- MCR prediction, red colour-infrared spectrum.

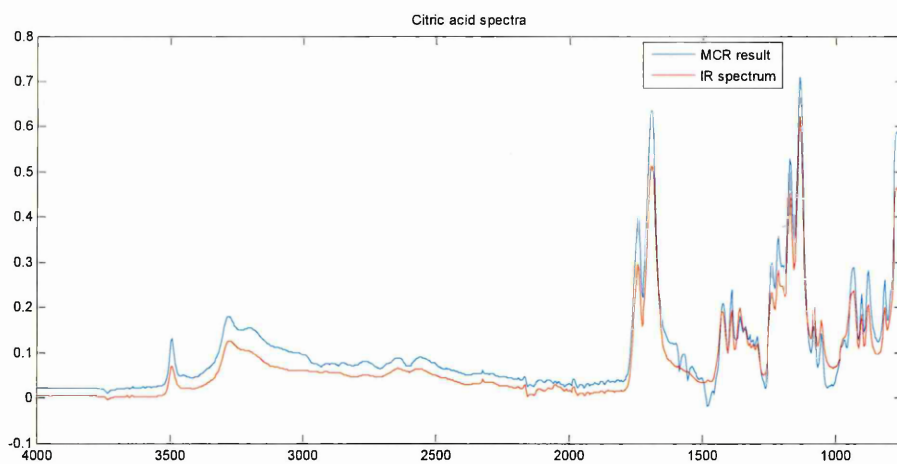


Fig. 5.59. Comparison of citric acid spectra, blue colour- MCR prediction, red colour-infrared spectrum.

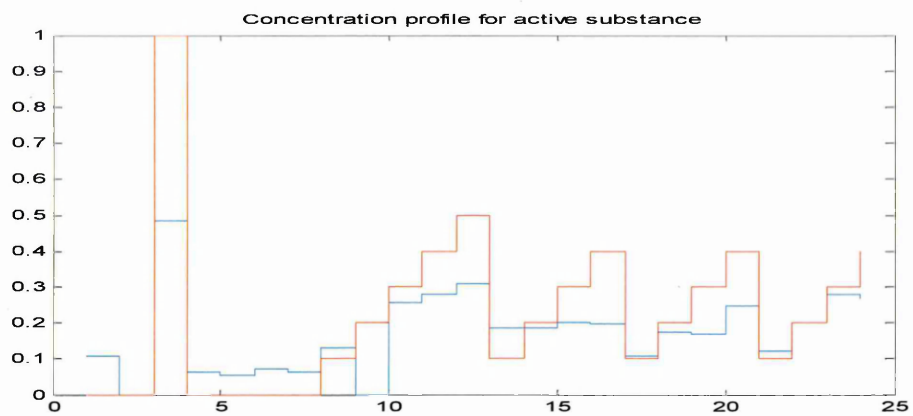


Fig 5-60. Concentration profiles of active substance, red colour - true values, blue colour - values predicted in MCR analysis.

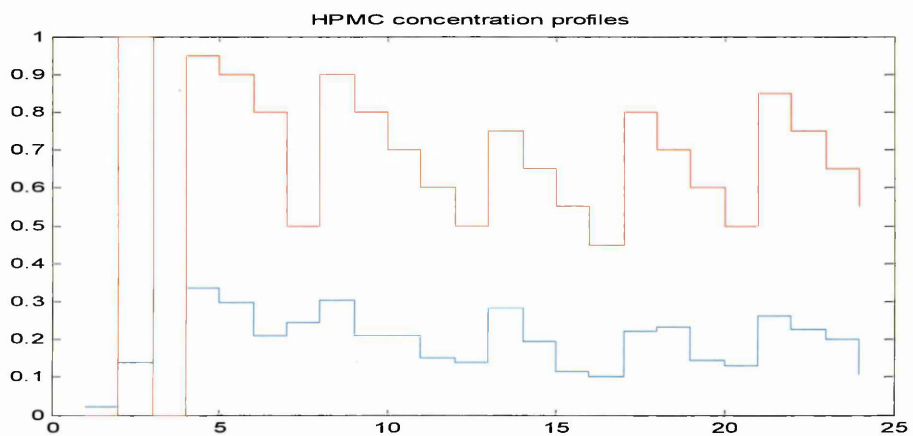


Fig 5-61. Concentration profiles of HPMC, red colour - true values, blue colour - values predicted in MCR analysis.

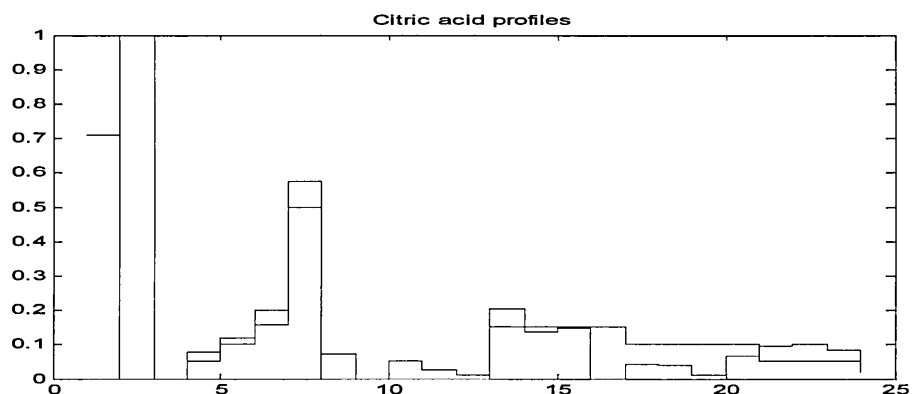


Fig 5-64. Concentration profiles of citric acid, red colour - true values, blue colour -values predicted in MCR analysis.

The output from the analysed data set (Fig 5-58 – Fig 5-64) provided spectra of dry excipients used in the formulations and also the concentration profiles which were compared to the real values used to prepare the mixtures. The predicted spectra showed high level of similarity to the real infrared spectra, and also the concentration values showed high resemblance to the accurate ones. The slightly larger intensity of the predicted spectra and values for concentrations are the effect of measurement noise and errors. The analysis of the validation model of the pure components and the binary systems solid dosage form spectra was conducted in the three applications simultaneously. All the methods; Hancewicz, Tauler and PLS Toolbox, provided similar results from the data set. Building the models from pure component spectra and validating the method was the critical step for the MCR analysis of the hydrated and hyphenated samples.

Unfortunately at first spectra and concentration profiles of binary mixtures from hydration results obtained as MCR result didn't show valuable information (Fig 5-65, 5-66). For



instance mostly on the component spectrum (from analysed binary or tertiary mixtures) bands coming out from the other compounds (included in a certain mixture) were significantly visible. Running analysis in three applications simultaneously didn't bring expected solution. Although almost from each analysed sample results received from Hancewicz and PLS Toolbox were very similar to each other.

The formulation HPMC and active substance HA50/50

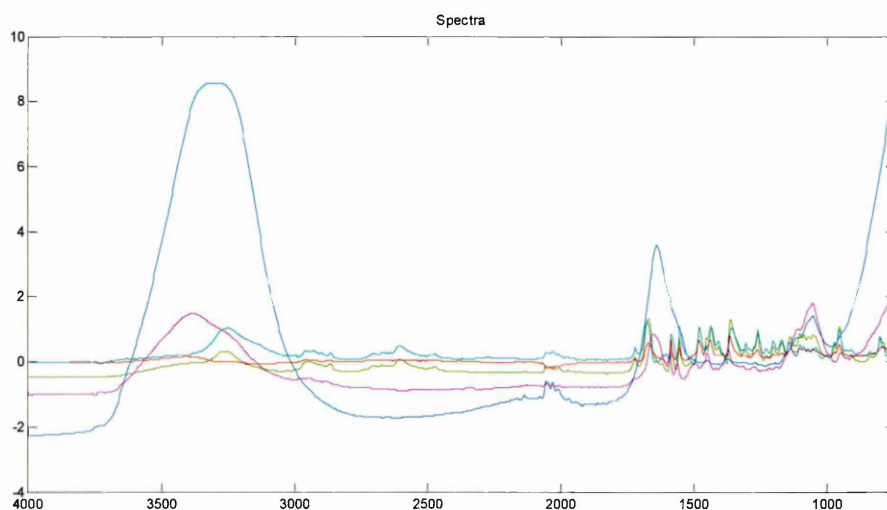


Fig 5.65 The MCR predicted spectra of formulation HA 50/50

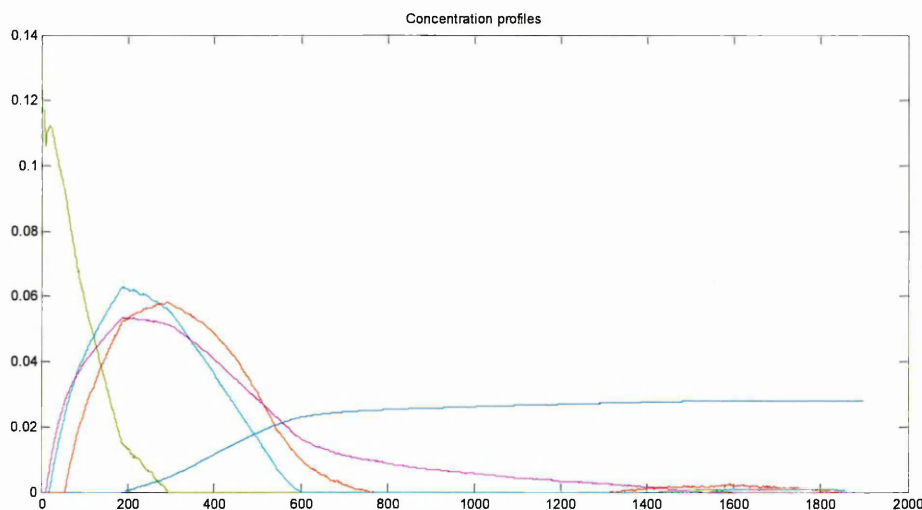
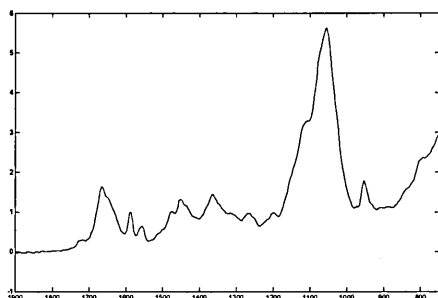


Fig 5-66. The predicted concentration profiles from the formulations HA 50/50, dark blue-water uptake, green-hydrated API, blue- API, red – HPMC, purple-hydrated HPMC.

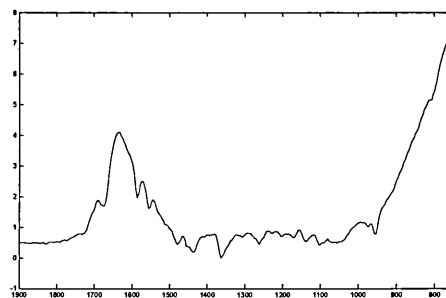
The difficulties with avoidance of rotational ambiguity and also the significant influence of dissolution media on the spectra of the samples caused the difficulties in getting any useful information from the data set.

The next step in the extended MCR analysis took the approach of narrowing the spectral window which is a method used sometimes in the chemometrics data analysis.

The example data is from the formulation of 60% HPMC and 40% active substance

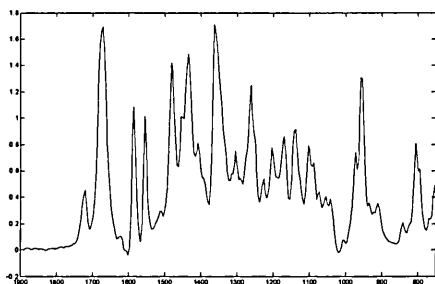


a)

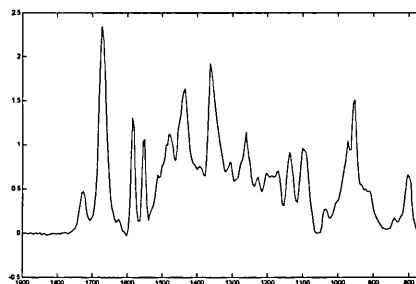


b)

Fig 5.67 The predicted MCR spectra for the hydrated sample HA 60/40 a) the spectrum of hydrated HPMC, b) spectrum of water

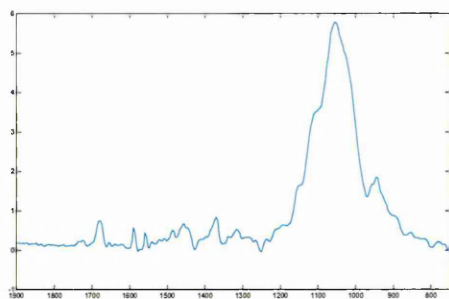


a)

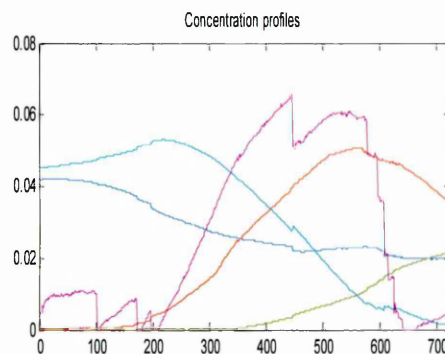


b)

Fig 5.68 The predicted MCR spectra for the hydrated sample HA 60/40 a) the spectrum of solid API, b) spectrum of hydrated API



a)



b)

Fig 5.69 The predicted MCR spectra for the hydrated sample HA 60/40 a) the spectrum of solid HPMC, b) concentration profiles; green-water uptake, light blue-HPMC, dark blue-API, purple- hydrated API, red-hydrated HPMC.

The generated results (Fig 5-66-Fig 5.68), showed the predicted results for the analyzed sample. The solid substances spectra show high level similarity to the pure components spectra collected on the ATR. Also one could recognize the spectra of hydrated API and HPMC. It is possible to recognize the concentration profiles as well however the hydrated species present in the sample show quite noisy and irregular profiles and one could have difficulties to justify the obtained results. The narrowing spectral window in the range from  $2000\text{-}900\text{ cm}^{-1}$  improved the obtained results however to could achieve more informative data the further reduction of the spectral range would need to be applied.

## **5.4 Conclusions**

The dissolution of the binary system gave an indication about the behaviour of the formulation in the different dissolution media. The percentage reaching almost 100% of the dissolved drug was observed in the case of the dissolution of the sample in 0.1 N HCl, the experiments in the distilled water seemed to provide a high amount of dissolved drug as well in the system. As expected the slowest dissolution was observed in the case of pH 6.8 phosphate buffer were after 12 h the amount of dissolved powder in the residue gel was still found, these observation confirm the pH dependence of the analyzed system.

The analysis of the hydration experiments data showed faster dissolution and diffusion of the active substance and citric acid in distilled water when compared to the HPMC kinetic profile, which clearly showed the swelling process in the perturbed polymeric system by the dissolution media whilst the other excipients in the discussed binary systems reached equilibrium already. These results were also observed in the case of the hyphenated samples. These findings suggested the diffusion control as a possible dominant process of the drug release in the discussed binary formulations. However the hyphenation experiment confirmed also the pH-dependence already observed in the case of dissolution data of the discussed systems.

The hyphenated samples data provided the information about behaviour of API and HPMC in a different dissolution media.

Finally the MCR data analysis was successfully validated and applied to the solid samples spectra data matrix. The application provided the comparable spectral and concentration data with that collected on the FTIR equipment. The predicted spectra and concentration

profiles proved the further possibility of using this application in order to analyse the hydrated and hyphenated samples of the binary and tertiary mixtures.

## **6. Investigations of tertiary formulations in the solid state.**

The important stage of the formulation method development is addition of new excipients to the formulation. The additional substances in the formulation may improve the compressibility, hardness, drug release etc. of the tablets but simultaneously the manufacturing process of the solid dosage form using the direct compression method becomes more challenging. Considering that compression process has a number of stages like rearrangement of the particles in the compacted powder upon the applied force to minimize the presence of free spaces, deformation of the powder and finally the possible bonding of the compressed substances; the formulation excipients should show similar densities, particle size/distribution and morphologies to minimize the possible segregation within the samples[132, 152, 170].

The physicochemical properties of the mixed powders together may increase the hardness of the tablet compared to the tablets made from pure excipients. Also the loading of the active substance in the formulation is one of the important factors in complex mixtures. The low concentration of active substance (up to 10% in the formulations) requires the particle size distribution of the powder giving the theoretical coefficients of variation less or equal to 1% to consider the mixture as homogeneous. The higher percentage of active substance in the formulation showed fewer difficulties with the API uniformity[132].

This chapter discusses the tertiary formulation tablet compaction process and the possible interactions between the mixed powders.

## **6.1 Aims:**

- To manufacture the reproducible tablets *in situ* on the ATR crystal from tertiary formulations and investigate possible interactions of the components of the mixtures
- To build the PLS model and predict the concentration values for the excipients of analyzed formulations
- To conduct the analysis of the components distribution in the tablets



## **6.2 Materials and methods:**

### **6.2.1 Materials**

Materials used in this Chapter 2.

### **6.2.2 Preparation of the mixtures**

Formulations were prepared according to proposed concentration values [%] (Table6-1).

#### **Tertiary formulation**

HPMC	Active	Cit Ac	HPMC	Active	Cit Ac	HPMC	Active	Cit Ac
85	10	5	80	10	10	75	10	15
75	20	5	70	20	10	65	20	15
65	30	5	60	30	10	55	30	15
55	40	5	50	40	10	45	40	15

Table6-1. Concentrations [%] of tertiary formulations.

The tertiary formulations were prepared by the method described in Section 3.2.2.2.

The active substance was ground and passed through the sieve a 106 microns to match the particle size of API with the other excipients.

### **6.2.3 Compaction process**

The compression of the tablets followed the procedure described in Section 3.2.4.2 and the parameters for the mixtures with particle size less than 106 microns detailed in Section

3.2.4.3

### **6.2.4 PLS analysis**

The predicted values of excipients concentration of the formulations were obtained as a result of the data analysis described in Section 3.2.5.

### 6.2.5 NIR Imaging

Distribution of the components and image data analysis was conducted according to parameters listed in Section 3.2.6.

The RGB analysis was continued in the Matlab R2007a and Octav software.

Using the information provided by components concentration from different tablets a RGB image was constructed. The components in a RGB image are divided by colours, where red corresponds to API, green to Citric Acid and blue to HPMC. Areas in the tablet where a component concentration is higher than other components will be visible when the three colour are combined. A low concentration will approximate the colour to black while a higher to their respective red, green or blue. For comparison reasons the components concentration are scaled so that each component gets equal chance to be represented in the RGB image. The values are scaled into the range [0.0 1.0] using equation (eq.1) where  $\min p$  is the minimum obtained value from component  $p$  and  $\max p$  the maximum.

$$RGB(i, p) = \frac{values(i, p) - \min p}{\max p - \min p} \quad (\text{eq.1})$$

where  $i = 1, \dots$ , pixels and  $p$  is the component number

As an example one could consider the concentration of component one (API) to be the highest and component two (Citric Acid) higher than component three (HPMC). In this case  $RGB(i, 1) > RGB(i, 2) > RGB(i, 3)$  which results in a color closer to red, or pure red in case  $RGB(i, 1) = 1.0$  and  $RGB(i, 2) = RGB(i, 3) = 0.0$ .

In case we have  $RGB(i, 2) > RGB(i, 1) > RGB(i, 3)$  then the final color will be closer to green, or pure green in case  $RGB(i, 2) = 1.0$  and  $RGB(i, 1) = RGB(i, 3) = 0.0$  [171, 172].

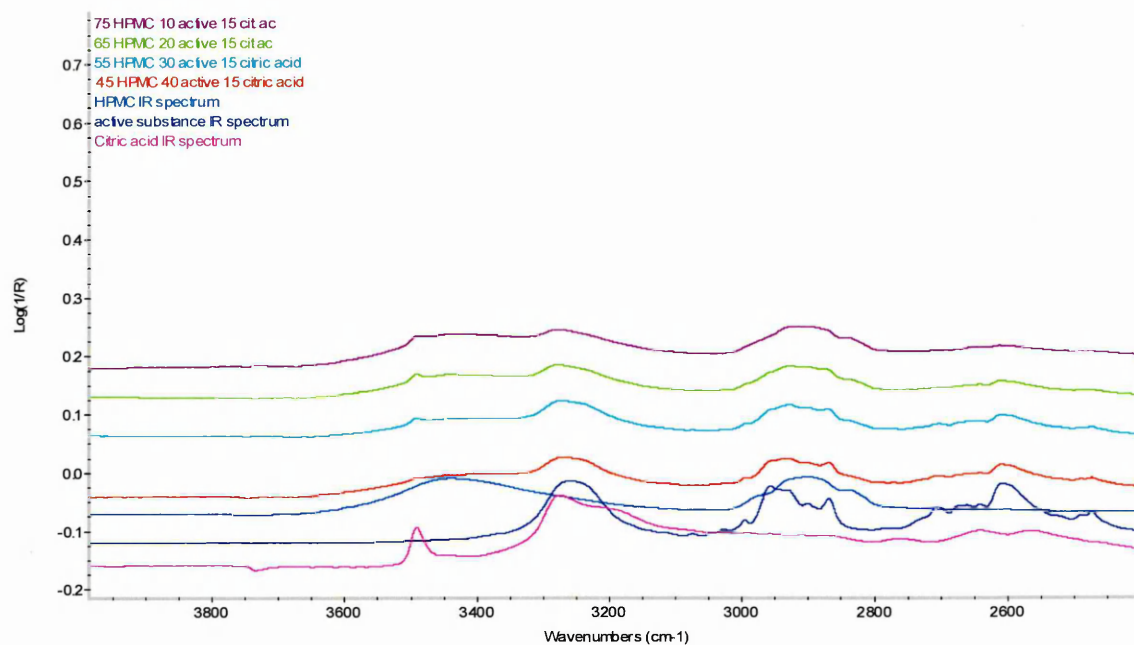
## **6.3 Results and discussion**

### **6.3.1 Investigations of possible interactions of the powders in the compacted tablet**

During the analysis of infrared spectra which provides the information on a molecular level the possible changes within the formulation excipients and active substance may be observed. The common interactions would involve the van der Waals force, hydrogen bonding or electron withdrawal by the neighbouring substituent, but also in a more complex structures it is more likely to find a new species in the mixed powders [69, 70, 154].

In this study spectra from the tertiary tablets were analyzed to investigate if any solid state interactions appeared or new polymorphic species emerged within the dry mixtures.

a)



b)

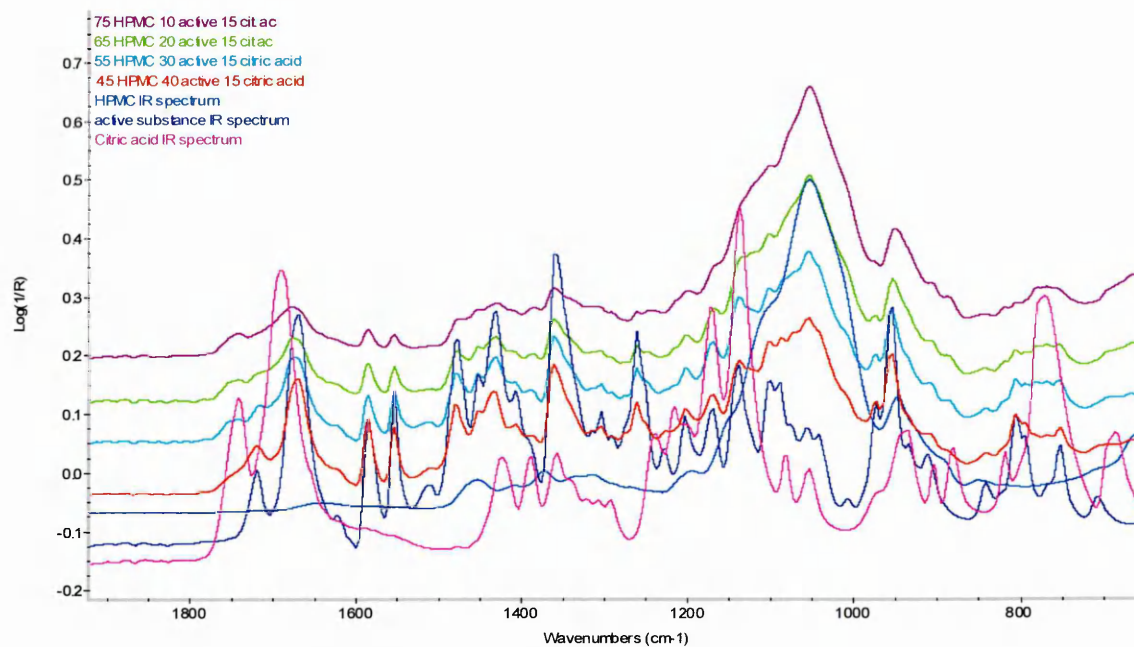
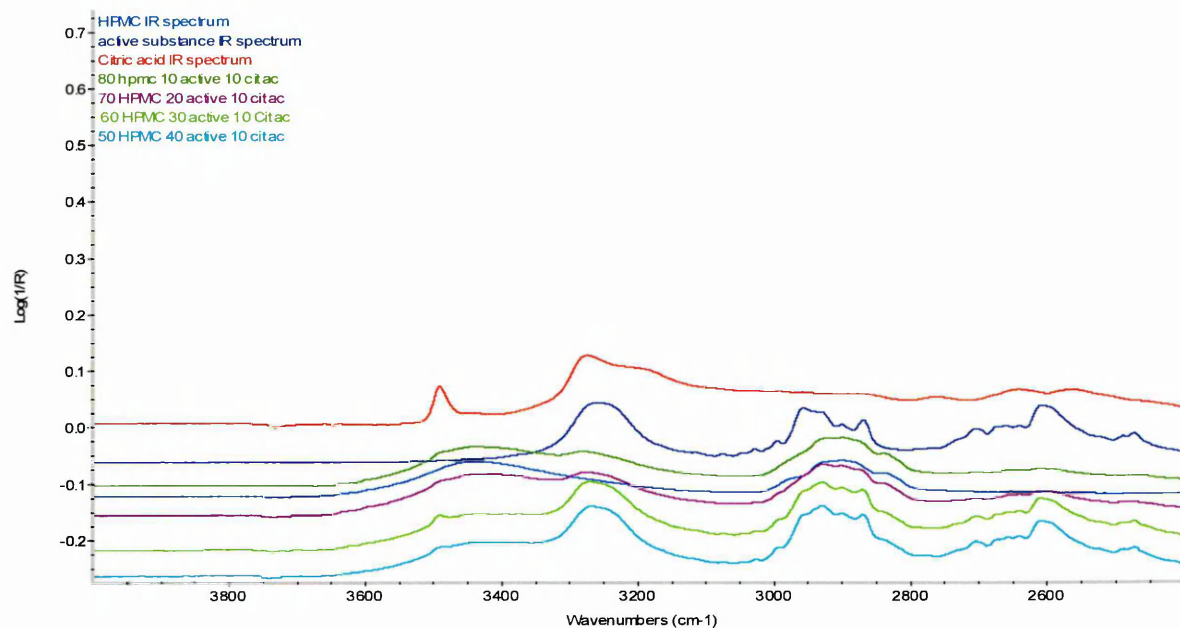


Fig. 6-1a),b). Infrared spectra of pure polymer, formulations of HPMC, active substance and 15% constant concentration value of citric acid, pure citric acid and active substance.

a)



b)

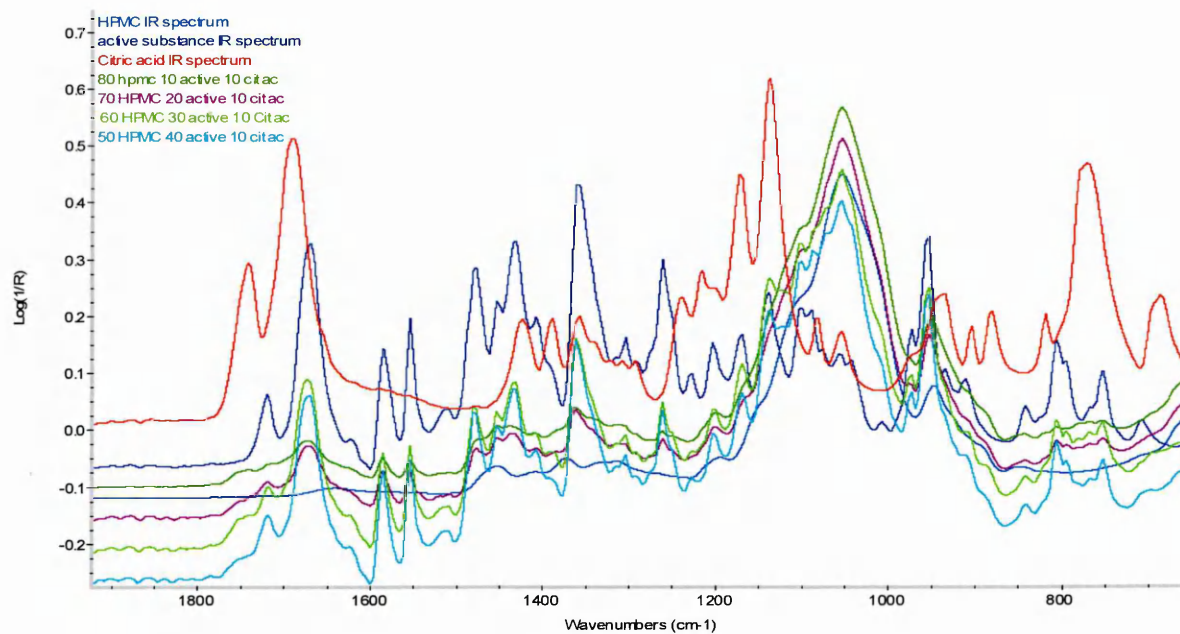
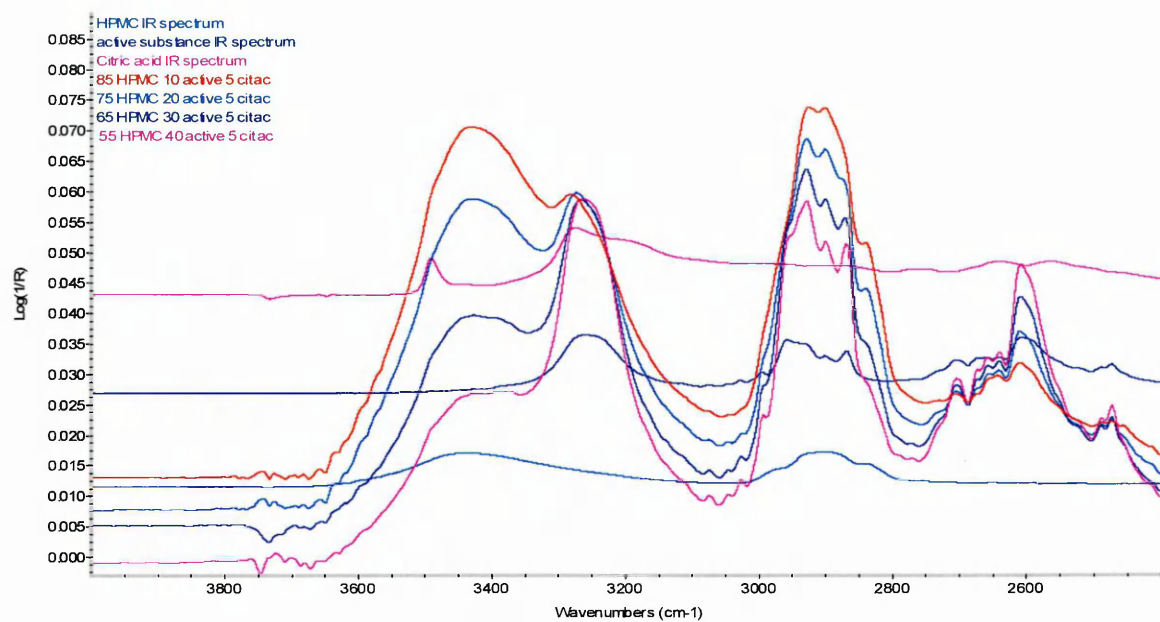


Fig. 6-2 a), b). Infrared spectra of pure polymer, formulations of HPMC, active substance and 10% constant concentration value of citric acid, pure citric acid and active substance.

a)



b)

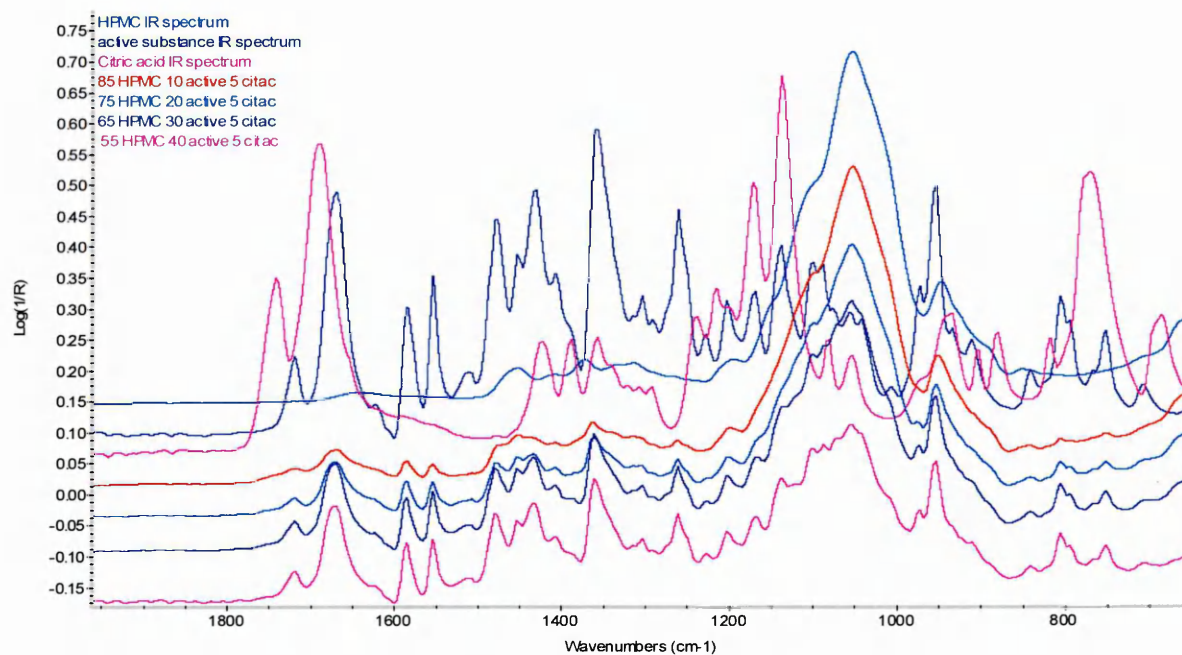


Fig 6-3a), b). Infrared spectra of pure polymer, formulations of HPMC, active substance and 5% constant concentration value of citric acid, pure citric acid and active substance.

The tertiary formulation spectra (Figs 6-1 to 6-3) showed decreasing intensity of the strong characteristic band at  $\sim 1100\text{ cm}^{-1}$   $\nu(\text{CO})$  associated with the presence of HPMC in the samples with increasing concentrations of citric acid and API. The shape of the bands in spectra of mixtures are changing proportionally to the increasing amount of API and citric acid in the sample. In the region  $\sim 3570\text{-}3200\text{ cm}^{-1}$  the shape of  $\nu(\text{OH})$  is slightly modified by the presence of  $\nu(\text{OH})$  band associated with citric acid where non bonded hydroxyl group forms narrow sub-maximum peak  $\sim 3500\text{ cm}^{-1}$  as well as OH group involved in hydrogen bonding stretching absorption at lower wavenumber within the discussed region. Increasing intensity of the API and citric acid bands proportionally to its concentration in the formulation is also observed in mixtures spectra at  $\sim 1750\text{-}1680\text{ cm}^{-1}$  region associated with the characteristic carbonyl group ( $\text{C}=\text{O}$  stretching frequency), and with presence of  $\sim 1175\text{-}1045\text{ cm}^{-1}$  strong absorption  $\nu(\text{CO})$  and  $\sim 955\text{-}890\text{ cm}^{-1}$  region associated with OH deformation vibration of carboxyl group [31, 32].

The relatively strong absorbance band in the region  $1700\text{-}1650\text{ cm}^{-1}$  is also associated with  $\text{C}=\text{O}$  stretching mode and  $\text{C}=\text{C}$  skeletal benzene ring breathing modes in the region  $1600\text{-}1500\text{ cm}^{-1}$  [49, 50].

There is no evidence for shifts in the positions of bands which suggest that the powders were admixed and compacted with no chemical interactions taking place between the excipients.

### 6.3.2 PLS data analysis

The concentration values of the excipients in the analyzed tablets were predicted using the PLS data analysis on the previously collected sample spectra from the tertiary formulations. The samples selected for PLS data analysis were divided into two sets: the calibration set which consisted of 47 samples and the prediction set which consisted of 25 samples. Preprocessing of all the data was conducted and included path length correction and mean-centering.

#### Tertiary formulations of HPMC, active substance and citric acid

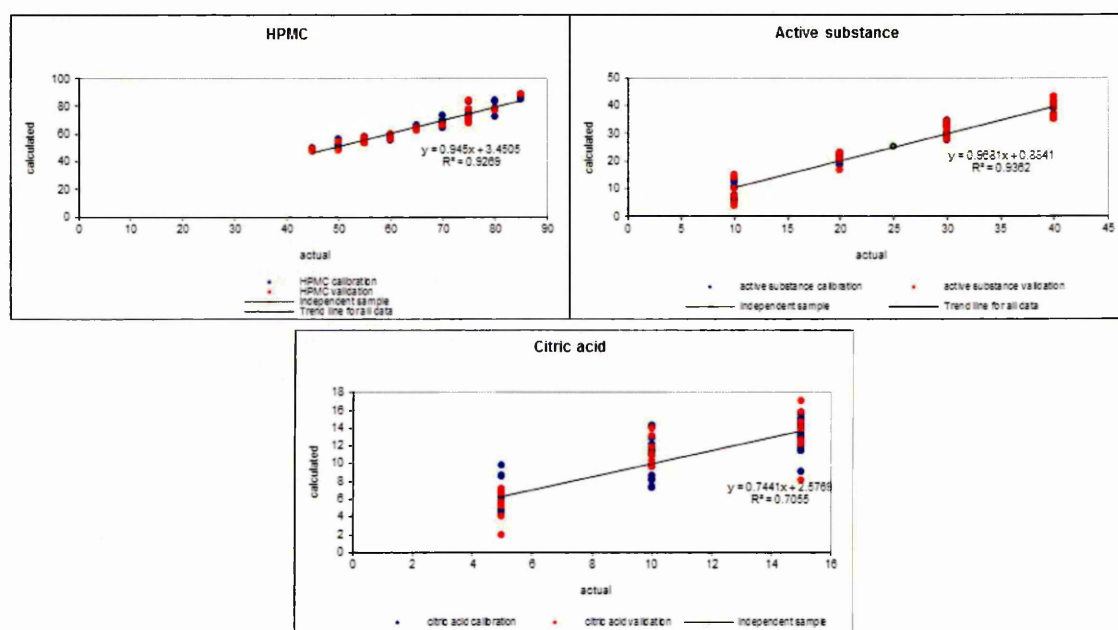


Fig. 6-4. Output of the PLS analysis showing the predicted versus calculated values for various tertiary mixtures of formulations HPMC, active substance and citric acid.



Mean and standard deviation for three components used in samples

actual citric acid [%]	mean citric acid [%]	st dev citric acid	actual API [%}	mean API [%}	st dev API	actual HPMC [%]	mean HPMC [%]	st dev HPMC
15	12.53	3.58	10	11.64	3.30	75	75.38	6.69
15	14.26	1.31	20	21.31	0.67	65	64.20	1.11
15	13.03	0.98	30	31.36	2.78	55	55.61	1.65
15	13.54	1.55	40	37.91	2.03	45	48.59	0.87
10	10.45	1.52	10	10.92	3.29	80	78.68	4.19
10	11.25	2.62	20	21.02	1.67	70	67.86	3.29
10	10.79	2.48	30	31.75	2.60	60	57.28	1.68
10	10.30	1.85	40	37.95	2.84	50	51.87	3.04
5	6.49	0.80	10	6.04	2.32	85	87.13	1.61
5	5.93	0.71	20	20.94	2.14	75	72.86	2.55
5	5.17	1.75	30	30.85	1.34	65	64.51	1.36
5	6.21	2.80	40	39.31	2.86	55	54.57	0.47

Table 6-2 Comparison of the mean and standard deviation calculated concentration with the actual concentration for the samples.

The plots (Fig6-4) are showing the predicted concentration versus the actual one. The data fitted into the PLS linear model obtaining values of  $R^2$  coefficient  $> 0.9$  for HPMC and slightly better for active substance, low value for citric acid  $\sim 0.71$ . However as the collected spectra shows a bit of the variability in the intensity values for the bands those differences in the data as well as possible measurement error will influence the final  $R^2$  coefficient value.

The predicted concentration values are showing variability compared to the actual concentration numbers. The mean and standard deviation values (Table 6-2)

are confirming slightly bigger variability between samples containing 15% of Citric acid compare to the samples with the 5% of the organic acid in the formulation.

The results suggest higher level of heterogeneity of the tablets in the formulation HPMC, API and 15% of citric acid comparing with the mixtures made from the formulation with the constant concentration of citric acid 5%.

Considering the lower level of reproducibility showed by the analyzed samples from the formulation consisting from HPMC, API and 15% of Citric acid compare to the tablets made from formulation containing constant concentration of citric acid 5% one could assume that the tablets may show different structural properties including possible segregation of the compounds and different compact compressibility, which may have affect on the drug dissolution from such a matrices.

For all the tertiary mixtures the Press plot showed that 6 factors are required to describe variance in the data. Choosing less number of factors didn't improve the analysis.

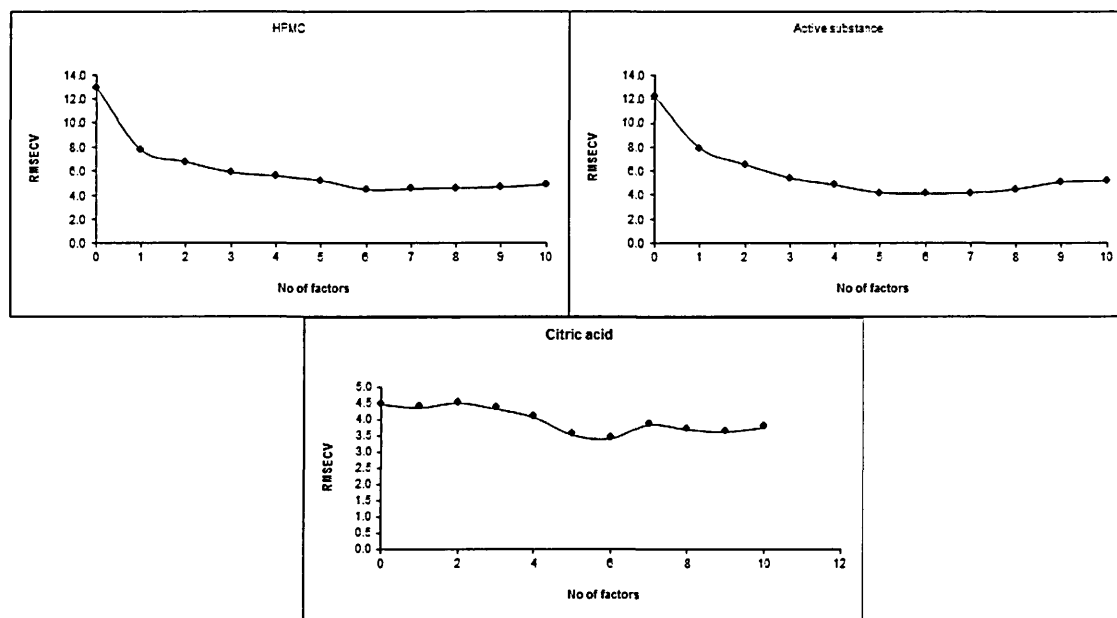


Fig 6-5 Press plots showing the number of factors required for PLS analysis of the tertiary formulations HPMC, active substance and citric acid.

The PLS analysis provides predicted spectra of pure components which can be compared with the IR spectra collected from pure standard substances (Fig 6-6).

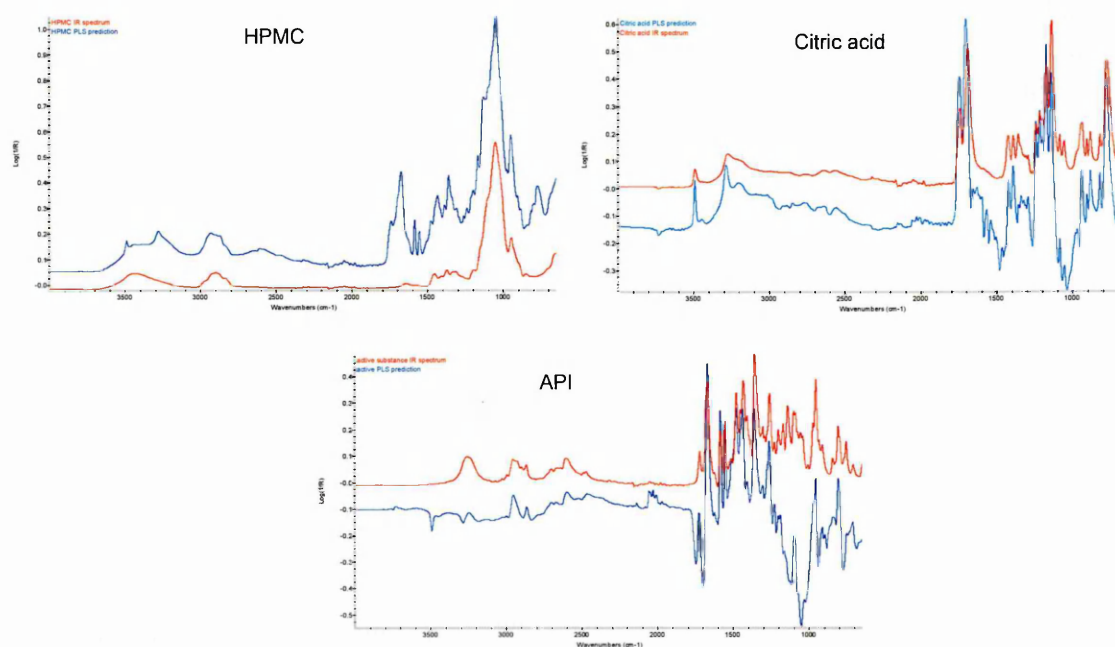


Fig. 6-7 Predicted pure component spectra from PLS analysis compared with the IR spectra of pure substances: red colour -IR spectra, blue colour-the predicted PLS spectra.

The predicted spectra in case of HPMC (blue colour) showed increased intensity values compared with the real IR spectra, whilst in the case of PLS prediction the active substance and citric acid spectra showed lower intensity values. The presence of any noise and the wide variety of the bands intensity according to used variety of different concentrations is affecting the final intensity of the estimated spectra. Analyzing the position and shape of the particular bands, characteristic for the substances one could recognize the presence of HPMC in the analyzed samples as well as citric acid. Citric acid predicted spectrum shows strong presence of characteristic bands for this organic acid however the negative peak

associated with presence of the polymer in the sample in the region of  $1100\text{cm}^{-1}$ , which suggests co-linearity of the component concentrations.

The API predicted spectrum contains the negative peaks associated with the presence of citric acid and HPMC in the sample. In fact one could have difficulties to recognize the presence of API in the sample based only on the information from the predicted spectra. There are no band shifts present in the predicted spectra.

The principal components spectra (Fig 6-8) indicated the presence of characteristic bands for citric acid and HPMC. Although the PC's spectra show a big resemblance to those two substances, there is very small amount bands associated with the active substance. The PC3 shows the spectrum similar to the tablet spectrum collected after the compaction process.

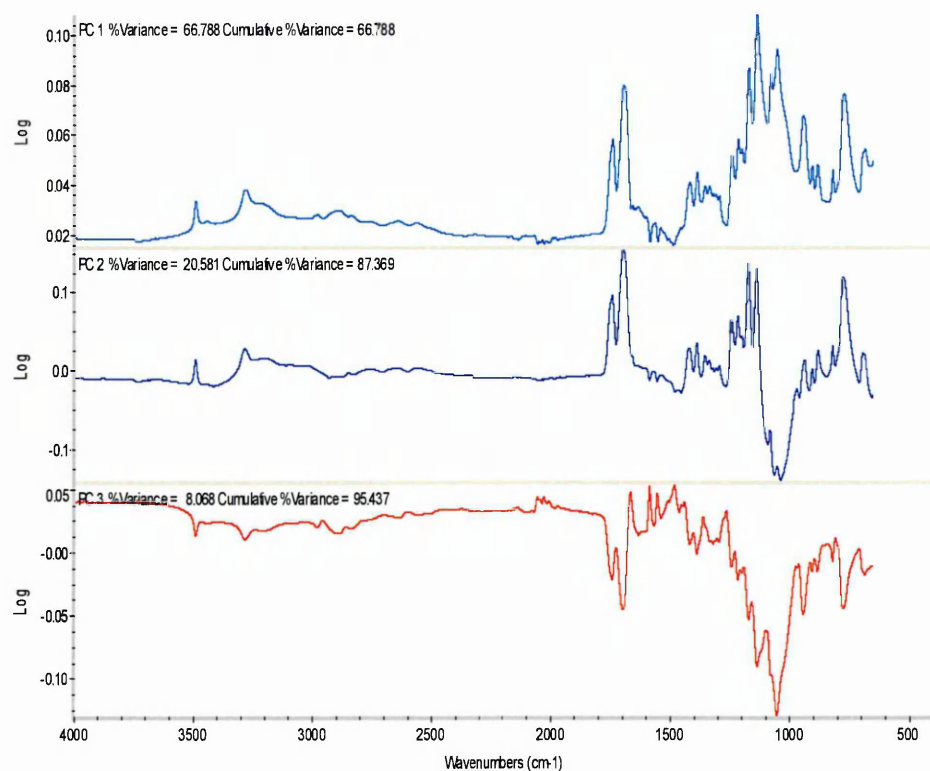


Fig. 6-8 Principal components predicted by the PLS analysis of HPMC and citric acid formulations.

### 6.3.3 NIR Imaging

The complex systems consisting on three or more excipients are requiring the more advanced methods to analyze the components distribution within the tablet matrix. It becomes more critical to justify the level of heterogeneity in the analyzed system as the presence of any possible substance's clusters or aggregates will dramatically influence the dissolution profiles of the tested formulation.

The analyzed tertiary formulation results were applied to the further RGB analysis in order to achieve the information about content uniformity of the samples[84, 98].

#### 6.3.3.1 The tertiary formulations of HPMC, active substance and citric acid

The image results are discussed on the examples of chosen formulations.

Results show a set of six images from both sides of tablets prepared using blended powders. Samples were prepared as outlined in Chapter3.

#### **Formulation 45% HPMC 40% active substance 15% citric acid**

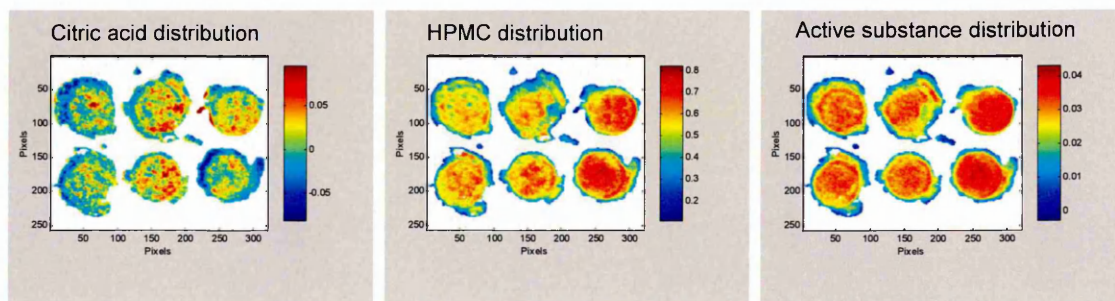


Fig 6-9. NIR images from top side of tablets and prepared by blending mixture

HAC45/40/15 of HPMC, active substance and citric acid and using torque 90 [cN.m] applied pressure.

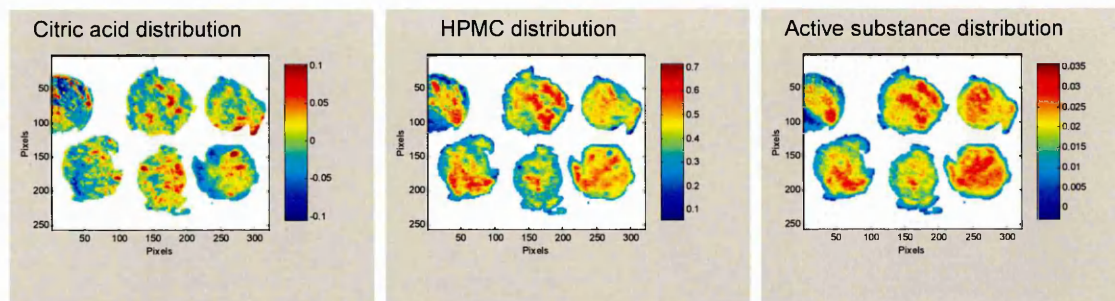


Fig 6-10. NIR images from bottom side of tablets prepared by blending mixture HAC45/40/15 of HPMC, active substance and citric acid and using torque 90 [cN.m] applied pressure.

### Formulation 65% HPMC 20% active substance 15% citric acid

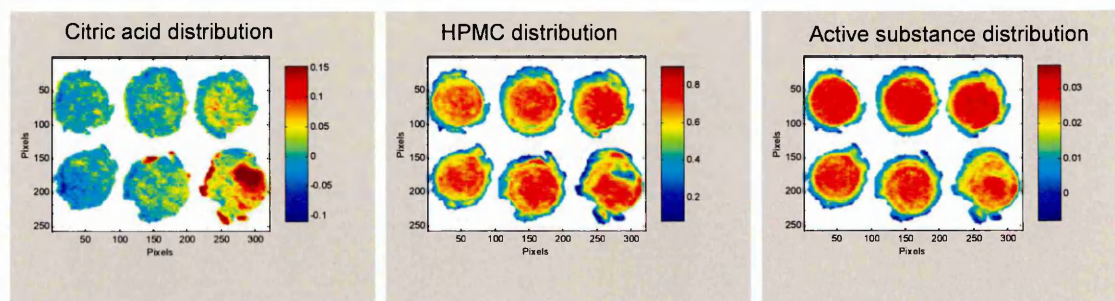


Fig. 6-11. NIR images from top side of tablets prepared by blending mixture HAC65/20/15 of HPMC, active substance and citric acid and using torque 90 [cN.m] applied pressure.

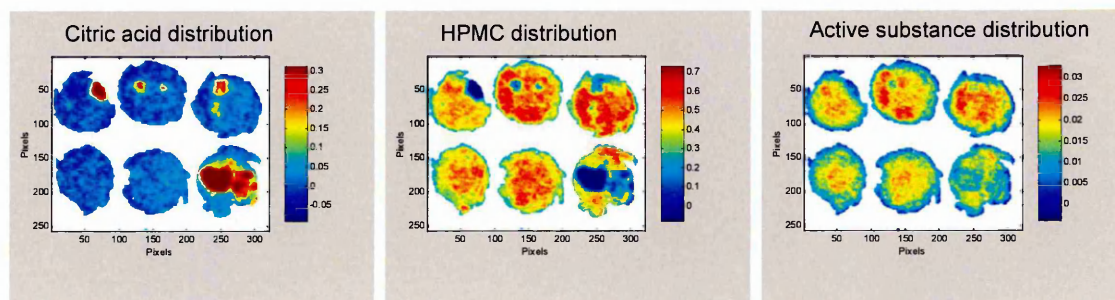


Fig. 6-12. NIR images from bottom side of tablets prepared by blending mixture HAC65/20/15 of HPMC, active substance and citric acid and using torque 90 [cN.m] applied pressure.



### Formulation 50% HPMC 40% active substance 10% citric acid

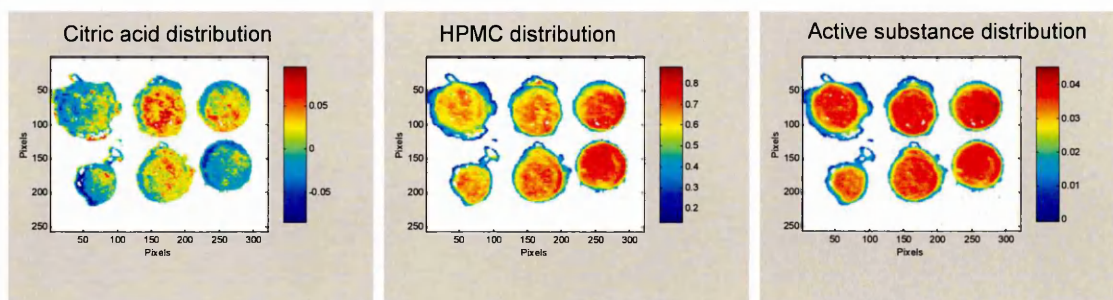


Fig. 6-13. NIR images from top side of tablets prepared by blending mixture HAC50/40/10 of HPMC, active substance and citric acid and using torque 90 [cN.m] applied pressure.

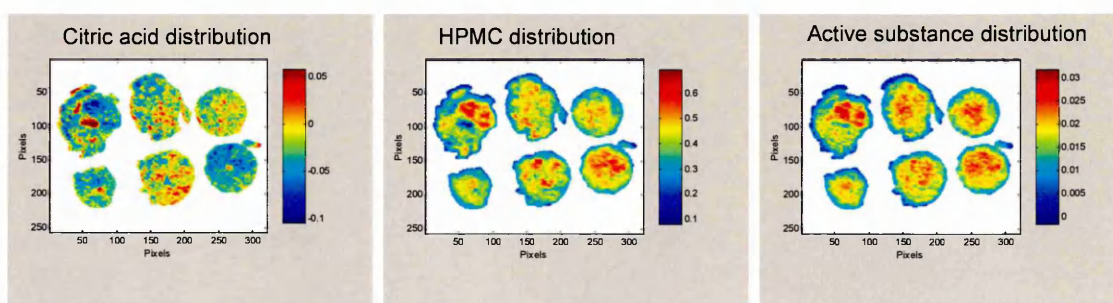


Fig. 6-14. NIR images from bottom side of tablets prepared by blending mixture HAC50/40/10 of HPMC, active substance and citric acid and using torque 90 [cN.m] applied pressure.

### Formulation 70% HPMC 20% active substance 10% citric acid

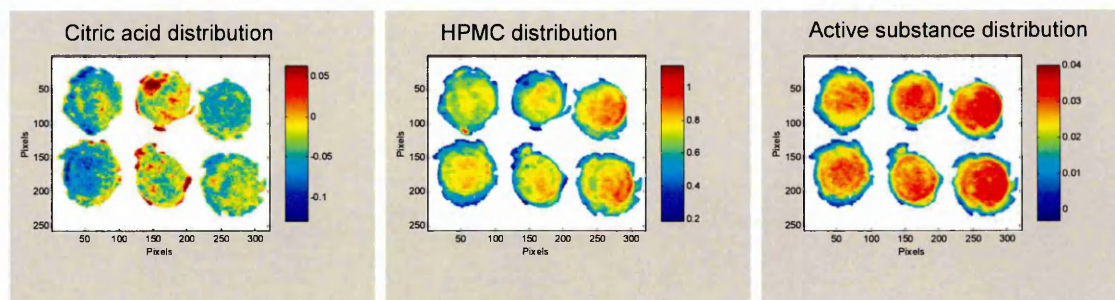


Fig. 6-15. NIR images from top side of tablets prepared by blending mixture HAC70/20/10 of HPMC, active substance and citric acid and using torque 90 [cN.m] applied pressure.

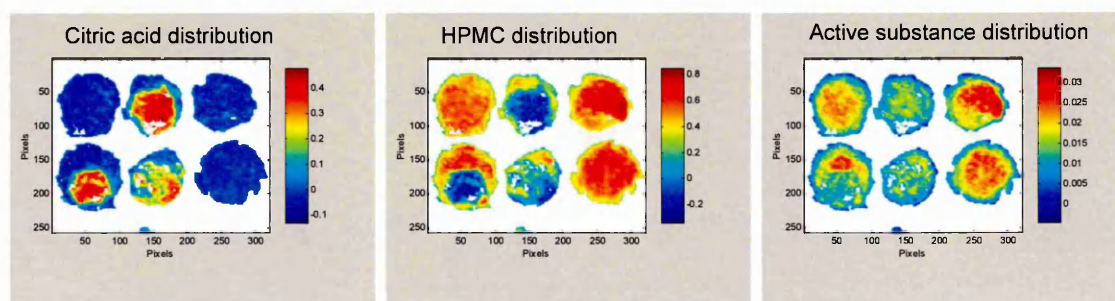


Fig. 6-16. NIR images from bottom side of tablets prepared by blending mixture HAC70/20/10 of HPMC, active substance and citric acid and using torque 90 [cN.m] applied pressure.



### Formulation 55% HPMC 40% active substance 5% citric acid

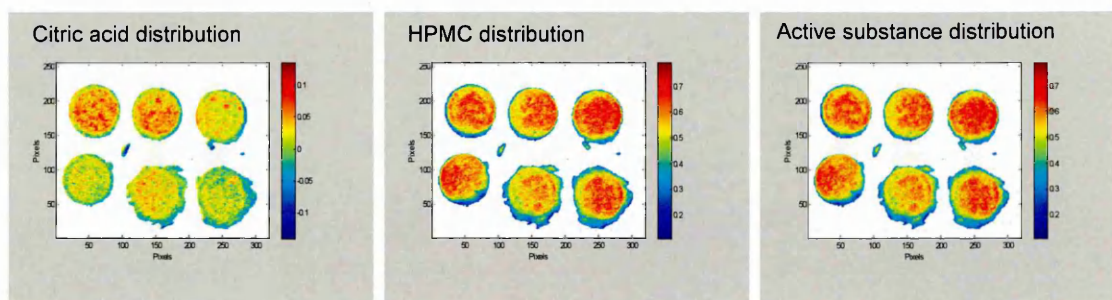


Fig 6-17. NIR images from top side of tablets prepared by blending mixture HAC55/40/5 of HPMC, active substance and citric acid and using torque 90 [cN.m] applied pressure.

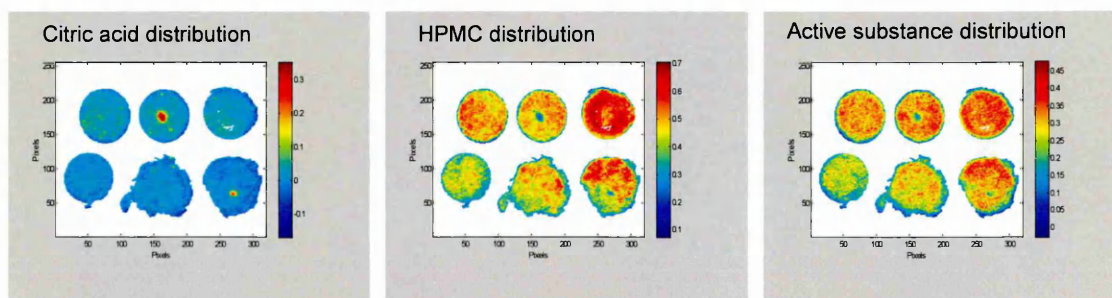


Fig 6-18. NIR images from bottom side of tablets prepared by blending mixture HAC55/40/5 of HPMC, active substance and citric acid and using torque 90 [cN.m] applied pressure.

### Formulation 75%HPMC 20%Active substance 5% Citric acid

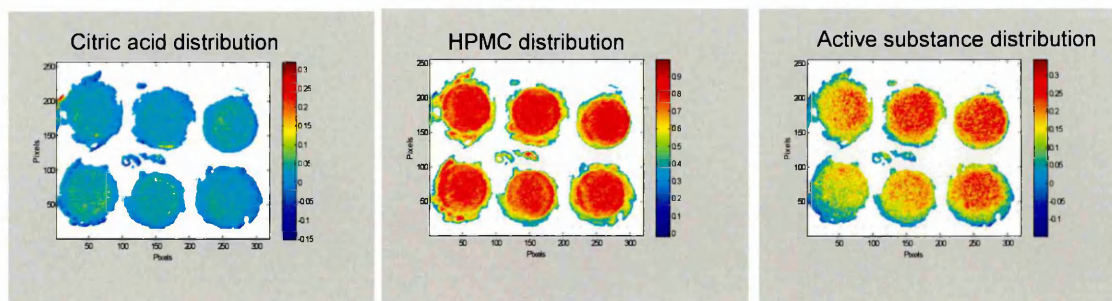


Fig 6-19. NIR images from top side of tablets prepared by blending mixture HAC75/20/5 of HPMC, active substance and citric acid and using torque 90 [cN.m] applied pressure.

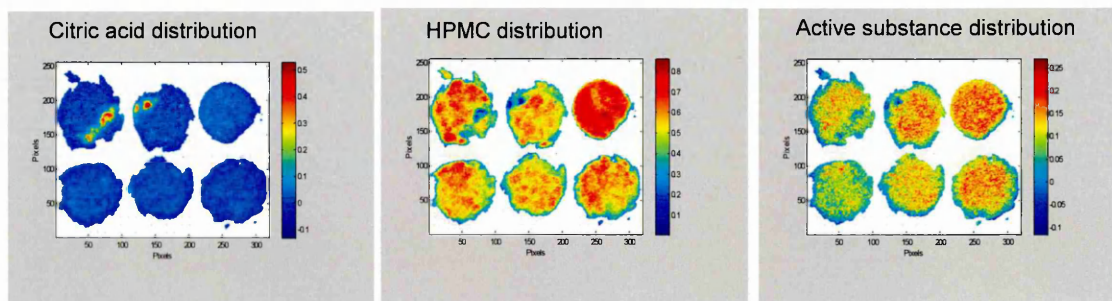


Fig 6-20. NIR images from bottom side of tablets prepared by blending mixture HAC75/20/5 of HPMC, active substance and citric acid and using torque 90 [cN.m] applied pressure.

The generated NIR images of the formulations of HPMC, API and Citric acid (Fig 6-9 to 6-20) showed the distribution of the three excipients present in the analysed tablets. These chemical maps of the samples provided the information about the level of intensity of the particular component on the tablet surface. The red colour is associated with strong intensity value and therefore high concentration value of the component, whilst dark blue colour is an indication of the low concentration of the substance in the particular region of the sample. There is a significant difference in the distribution of the components observed

between the samples images collected from the top and bottom side of the tablets containing different concentration values of HPMC and API. The tablet images from the top surface show more uniform distribution of HPMC and active substance. However the citric acid aggregates can be found on the images of the bottom side of the tablets. The presence of aggregates/proper clusters of the acid is increasing on the tablet surface with decreasing concentration of active substance and increasing amount of HPMC within the formulation. In the case of formulation 75%HPMC20%active substance and 5% citric acid (Fig 6-20) the citric acid showed very low intensity values. The heterogeneous distribution of the citric acid was confirmed as well by the PLS analysis. Also the tablets from the top side images have recognizable regular shape whilst the bottom side of the tablet is deformed by the relaxation of the polymer during the tablet manufacturing process. The further analysis of the samples confirms observed in the binary system the general trend of segregation of the compacted powders within the tablet; the distributed HPMC and API is observed along on the top side of the tablets showing high intensity values, whilst on the bottom side all the ingredients are present. Also the roughness of the sample surface has an influence on the quality of the generated images, smoother sample surface the top side of the tablet gives a better quality image than the bottom side.

Although from the collected images one could discuss about the distribution of the components particles it is impossible to relate the components intensity values to the concentration of the particular ingredient within the set of 6 tablets from the same concentration of the component and within different formulations and actually determine the uniformity of the tablet surface. The intensity values for the components show different scale for each of them (colorbar) as they are adjust according to the maximum and minimum values of the pure standard material absorption.

The outcome of the normalized NIR images analysis with the scale (0,1) for the components intensity values didn't bring the expected results as the maxima for Citric acid and API are relatively low to compare with the HPMC intensity max value.

The possible improvement of the data analysis could be obtained by performing the RGB analysis which would enable to show all the excipients of the tablet on the one image and give information about the homogeneity of the tablets.

#### 6.3.3.2 The RGB results of tertiary formulation of HPMC, active substance and citric acid bottom side

The analysis was applied to the data collected from the bottom side of the tablets so the results could be compared to the FTIR data recorded from the same surface of the tablet.

The colors associated with the substances: red-API, green-Citric acid, blue-HPMC.

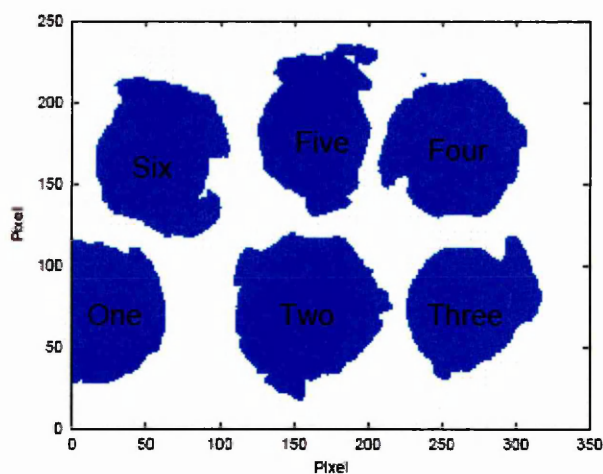


Fig. 6-21. Tablets general snapshot describing the number order given to the samples for performed RGB analysis.

**45%HPMC 40%Active 15%Citric acid**

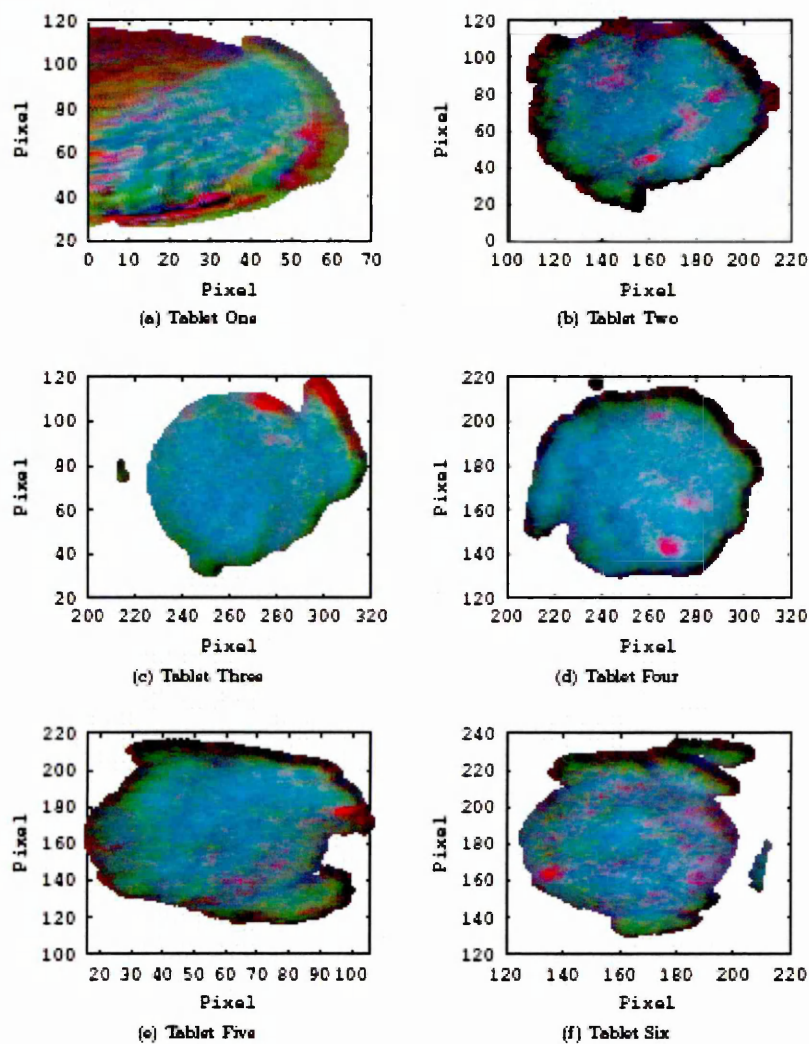


Fig. 6-22 The RGB analysis of the tablets from the formulation 45% HPMC 40% active substance 15% Citric acid bottom side; order of the tablets according to the Fig 6-21.



**65% HPMC 20% Active substance 15% Citric acid**

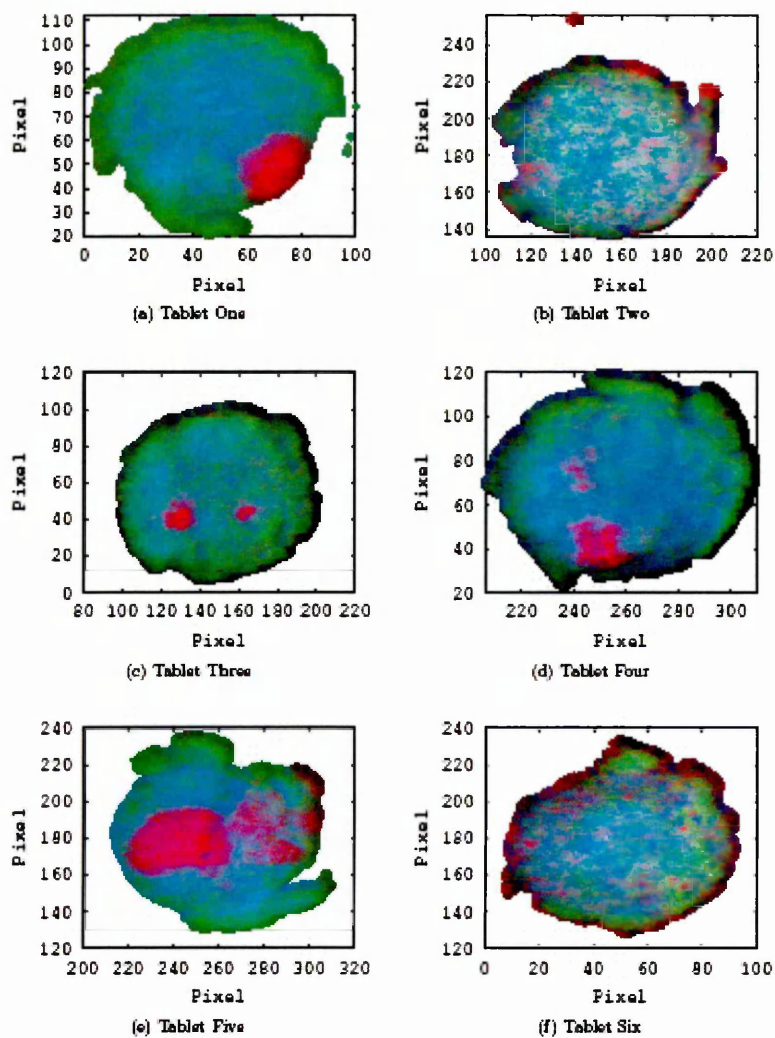


Fig. 6-23 The RGB analysis of the tablets from the formulation 65% HPMC 20% active substance 15% Citric acid bottom side; order of the tablets according to the Fig 6-21.

**50% HPMC 40% Active substance 10% Citric acid**

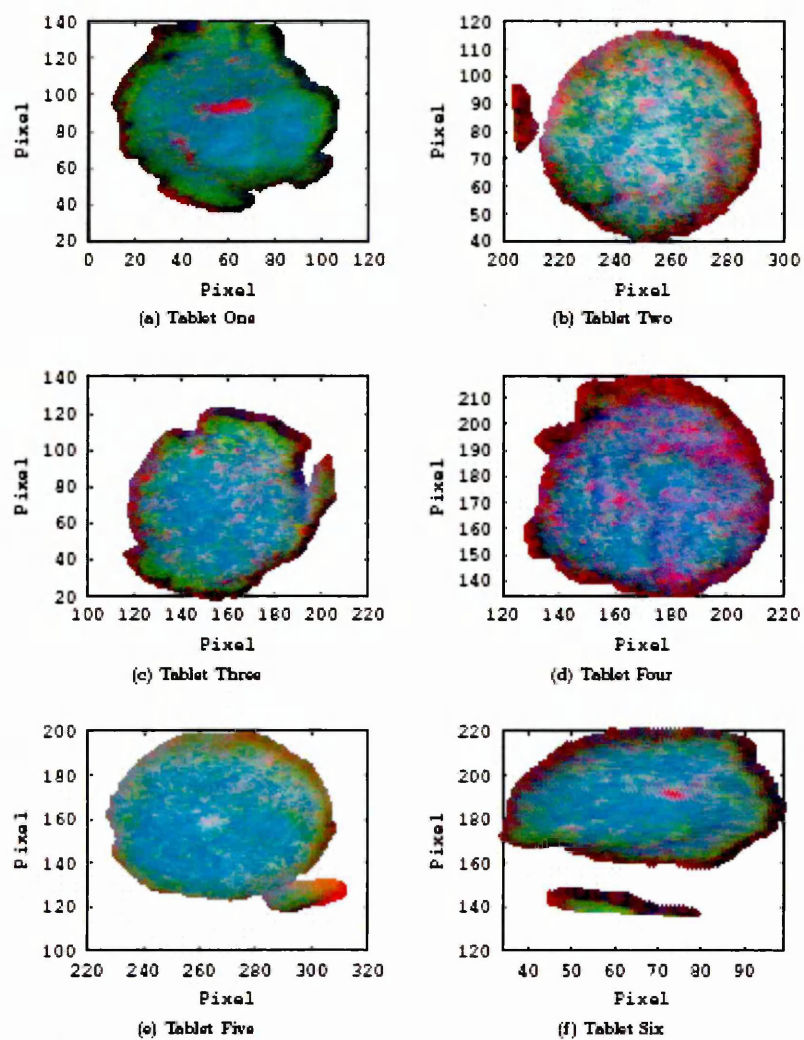


Fig. 6-24 The RGB analysis of the tablets from the formulation 50% HPMC 40% active substance 10% Citric acid bottom side; order of the tablets according to the Fig 6-21.

**70% HPMC 20% Active substance 10% Citric acid**

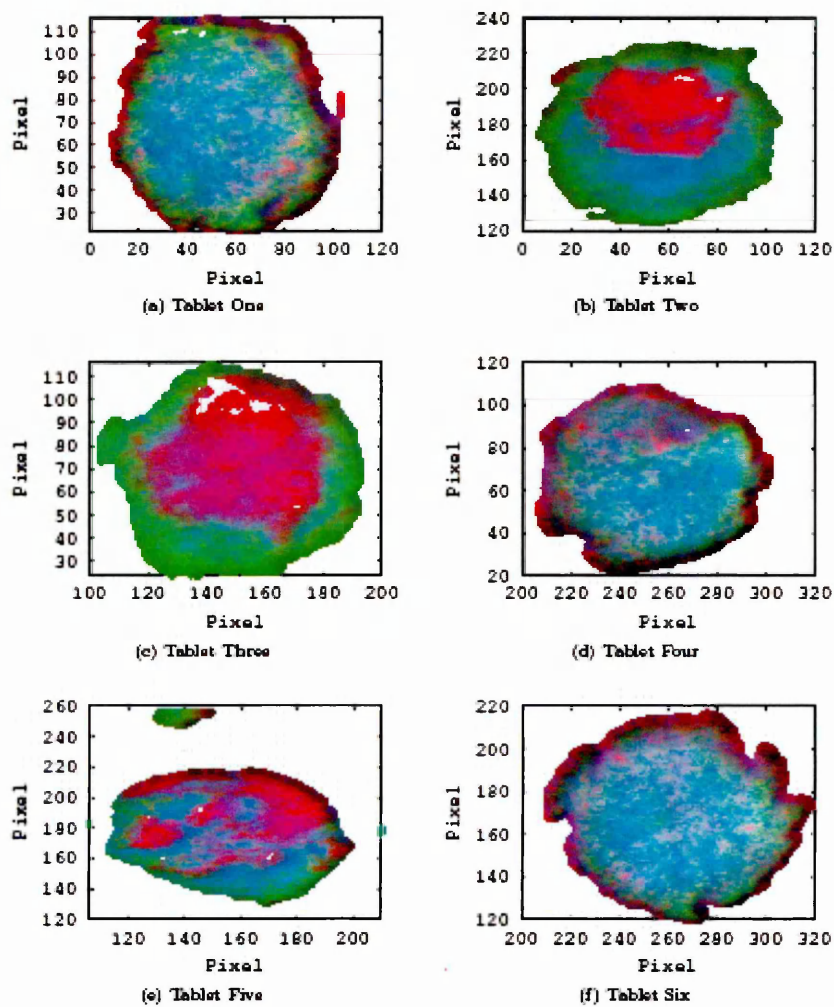


Fig. 6-25 The RGB analysis of the tablets from the formulation 70% HPMC 20% active substance 10% Citric acid bottom side; order of the tablets according to the Fig 6-21.



**55% HPMC 40% Active substance 5% Citric acid**

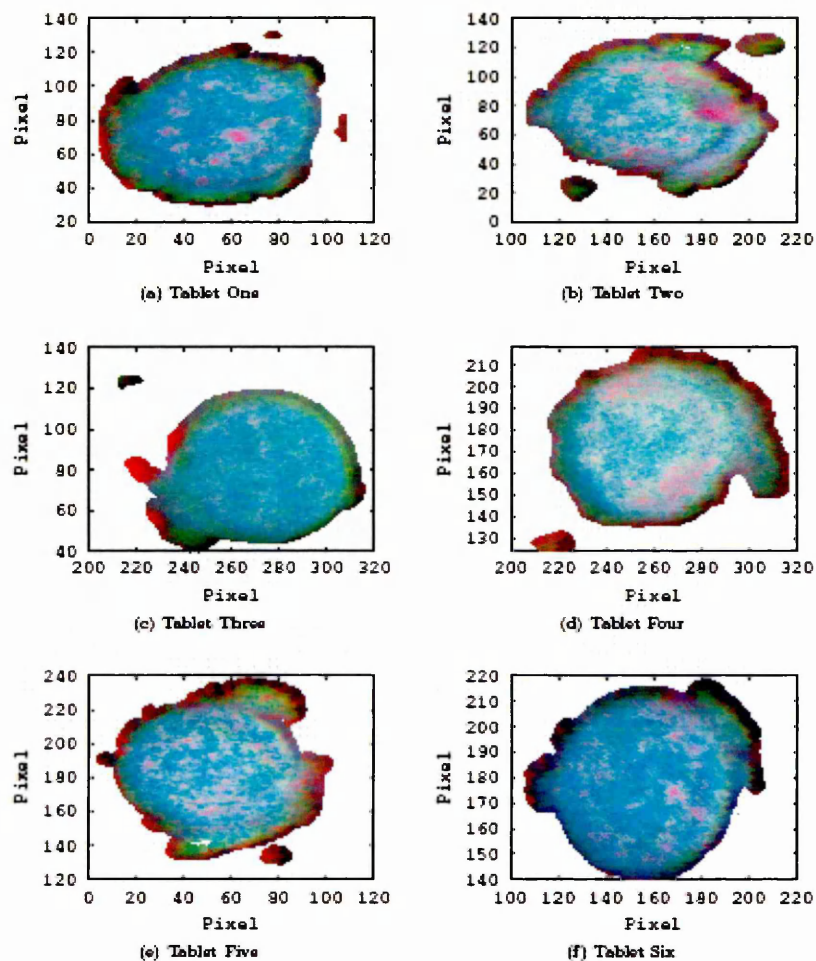


Fig. 6-26 The RGB analysis of the tablets from the formulation 55% HPMC 40% active substance 5% Citric acid bottom side; order of the tablets according to the Fig 6-21.

**75% HPMC 20% Active substance 5% Citric acid**

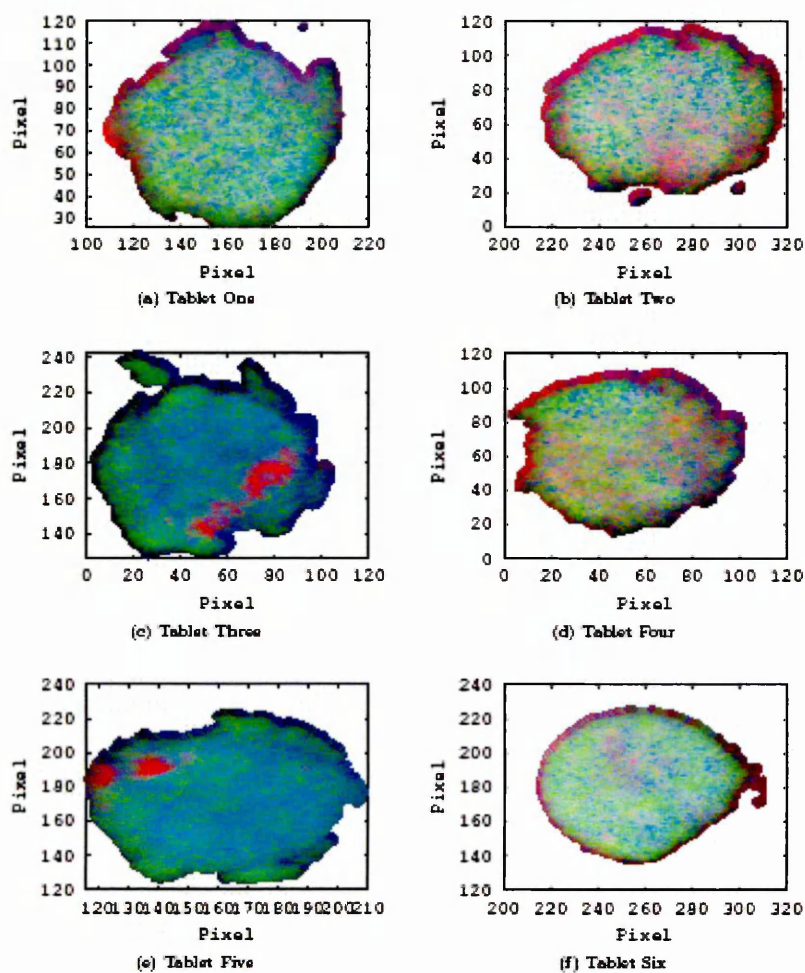


Fig. 6-27 The RGB analysis of the tablets from the formulation 75% HPMC 20% active substance 5% Citric acid bottom side; order of the tablets according to the Fig 6-21.

The RGB output analysis (Figs 6-22 to 6-27) showed the distribution of the three components on the tablets surface [173, 174]. The maximum values of the intensity of the particular components are associated with the dark red, green and blue color, the low values intensity are showed as light red, blue, green respectively. The analysis of the generated images showed increasing heterogeneity of the samples with the increasing amount of HPMC in the formulation. Also increased amount of aggregates/ high concentration clusters of citric acid but also an API is visible on the surface of the tablets with the concentration of the API equal to 20% which one could have a difficulties to justify just based on the analysis of the previous images. The higher level of content uniformity is observed within the set of 6 tablets with the constant concentration of citric acid 5% for both 20% and 40% of active substance (Figs 6-21 to 22). The significant variability is visible in the case of formulation with constant concentration of 15% and 10% of citric acid. The formulation containing 15% of citric acid showed the significant amount of HPMC-blue colour on the tablet surface along with the presence of citric acid-green color whilst in the case of another formulation (10% of citric acid) the influence of API and citric acid is much more visible, the surfaces are heterogeneous within the same data sets. This data are confirming the observations based on the PLS data analysis. One could assume that the compressibility of the powders as well as their physical and chemical properties causing segregation of the components and the differences in the compacted structure of the tablet.

The RGB analysis confirmed increased level of heterogeneity in the tertiary system compare to the binary formulations. The possible improvement of the tertiary systems could be achieved by using the particle size analyzer to confirm particle size of components during the preparation of the formulation to minimize the particle size differences between API, citric acid and HPMC.

## **6.4 Conclusions**

The solid dosage forms tertiary systems data analysis provided information about physico-chemical properties of the prepared formulations. The FTIR analysis of the compacted mixtures showed the presence of the characteristic bands for the analyzed substances however no changes in a position of the bands were observed. There is no indication of the hydrogen bonding between the mixed excipients in the spectra. The spectrum of the mixed substances showed overlapping peaks of the characterized excipients what confirms the need of developing more advanced data analysis in the case of future hydration and hyphenation experiments.

The conducted PLS data analysis showed variability in the reproducibility of the samples in the case of Citric acid and these results were also compatible with the chemical imaging data. The HPMC and active substance obtained results from PLS showed higher level of variance in the tablets compared to the binary systems. Chemical maps of the HPMC distribution confirmed the more heterogeneous surface with increasing concentration of this component in comparison with API distribution. The most uniform formulation are the mixtures containing the constant concentration of the citric acid equal 5%, which was also confirmed by the PLS data analysis.

The images of the top side of the tablets showed the general tendency of active substance to segregation on that part of the tablet as all analyzed samples indicated higher intensity for the API particles than on the bottom side.

## **7. Investigations of the tertiary formulations in a dissolution media.**

Drug dissolution of the more complex systems involves many interactions of polymer matrix, drug substances and added excipients. There are several mathematical models used to describe the drug dissolution process from the swellable matrices. However every system depending on the physico-chemical properties of the components shows different dissolution process characteristic. The chemical reactions, hydration of the sample, protonation/deprotonation, the emergence of new species, possible hydrogen bonding and solvation have influence on the final drug release result.

Standard dissolution testing provides the final values of the dissolved drug in the experiment and it also shows the percentage of the released substance in a certain amount of time. However this technique is not able to provide any information about the formulation on the molecular level [151, 153].

In this chapter the solid tablets from the tertiary formulation compacted on the diamond ATR were introduced to the dissolution media and the possible interactions are within the samples discussed.

## **7.1 Aims:**

- To investigate the drug release from tertiary formulation in a different pH media
- To monitor the hydration and hyphenation experiments and develop information about the formulation behaviour in static and dynamic conditions
- To apply the MCR data analysis on the hydrated and hyphenated samples data and investigate the possible changes within the analyzed systems.

## **7.2 Materials and methods:**

### **7.2.1 Materials**

Materials used in this chapter are listed in Appendix A

### **7.2.2 The analyzed formulation [%]**

HPMC	Active	Cit Ac	HPMC	Active	Cit Ac
85	10	5	75	10	15
75	20	5	65	20	15
65	30	5	55	30	15
55	40	5	45	40	15

Table7-1. Concentrations of tertiary formulations

The tertiary formulations were prepared by the method described in Section 3.2.2.2.

The active substance was passed through the sieve to match a particle size of API with the other excipients.

### **7.2.3 Dissolution testing**

The dissolution experiments procedure is discussed in Chapter 5, section 5.2.3.

### **7.2.4 Hydration and Hyphenation experiments**

The hydration and hyphenation experiments method is discussed in Chapter 5, section 5.2.5.

### **7.2.5 MCR data analysis**

The parameters used for the MCR data analysis are described in Chapter 5 section 5.2.6.

## **7.3 Results and discussion**

### 7.3.1 Hydration experiments

The results of hydration experiments will be discussed based on the example of 65% HPMC 20% Active substance 15% citric acid mixture.

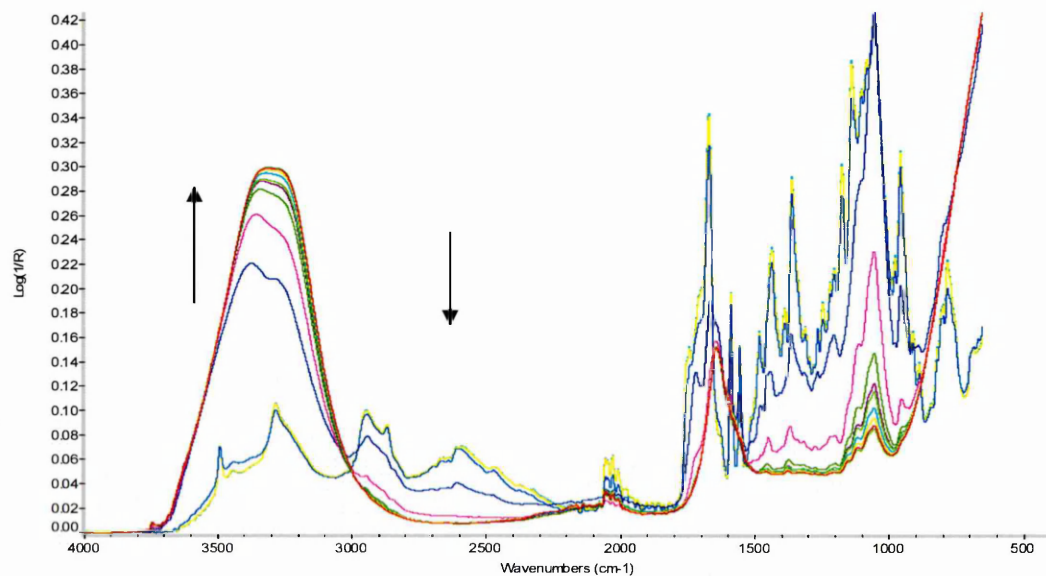


Fig 7-1 Spectra from the hydrated sample HAC 65/20/15 collected during 12 h experiment

Results obtained from hydration experiment tertiary formulation of HPMC and active substance and citric acid (Fig. 7-1) showed increased intensity of the band  $\nu(\text{O-H})$  3006-3699  $\text{cm}^{-1}$  associated with water up take and decreased band  $\nu(\text{C-O})$  980-1160  $\text{cm}^{-1}$  as a result of the polymer swelling process. Spectra collected from this formulation showed increasing impact of dissolution media in the sample with time. The formulations spectra showed a decreasing relatively strong absorbance band of API in the region 1700-1650  $\text{cm}^{-1}$  associated with  $\text{C=O}$  stretching mode and  $\text{C=C}$  skeletal benzene ring breathing modes in the region 1600-1500  $\text{cm}^{-1}$  [49, 50]. Also the 2700-2400  $\text{cm}^{-1}$  delocalized  $\text{N}\dots\text{H}$  bonding is



no longer present in the fully hydrated sample. The increasing concentration of the dissolved active from the polymer matrix caused the reduction of the intensity of these bands. The citric acid in the sample showed changes in the intensity and shape of the decreasing bands in the regions  $1700\text{--}1500\text{ cm}^{-1}$   $\nu(\text{C}=\text{O})$  and  $1050\text{--}1400\text{ cm}^{-1}$   $\nu(\text{C}-\text{O})$ .

In order to obtain quantitative information the generated profiles were normalized and plotted against square root time.

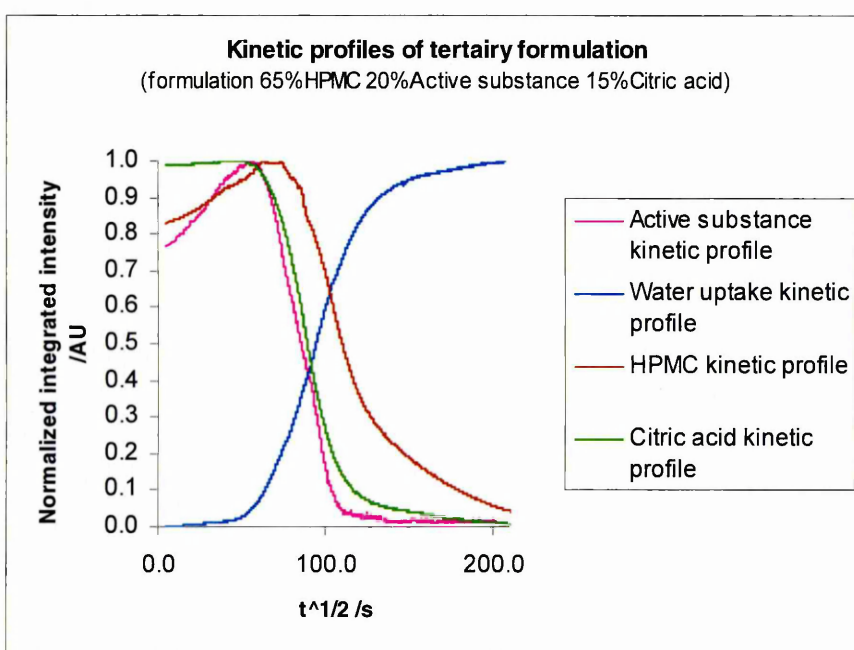


Fig 7-2. Normalized kinetic profiles of the hydrated sample formulation HAC65/20/15

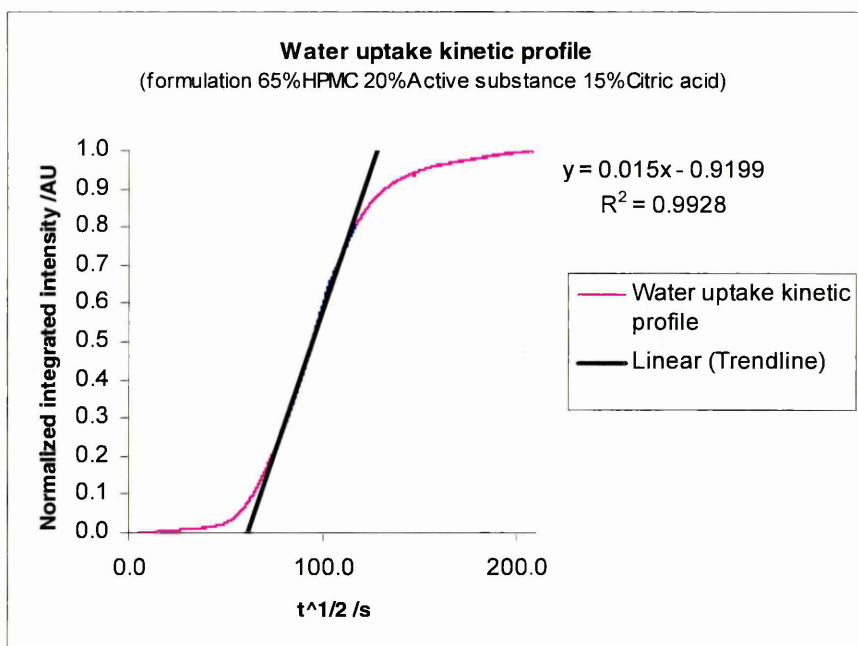


Fig 7-3. Normalized profiles of the water uptake

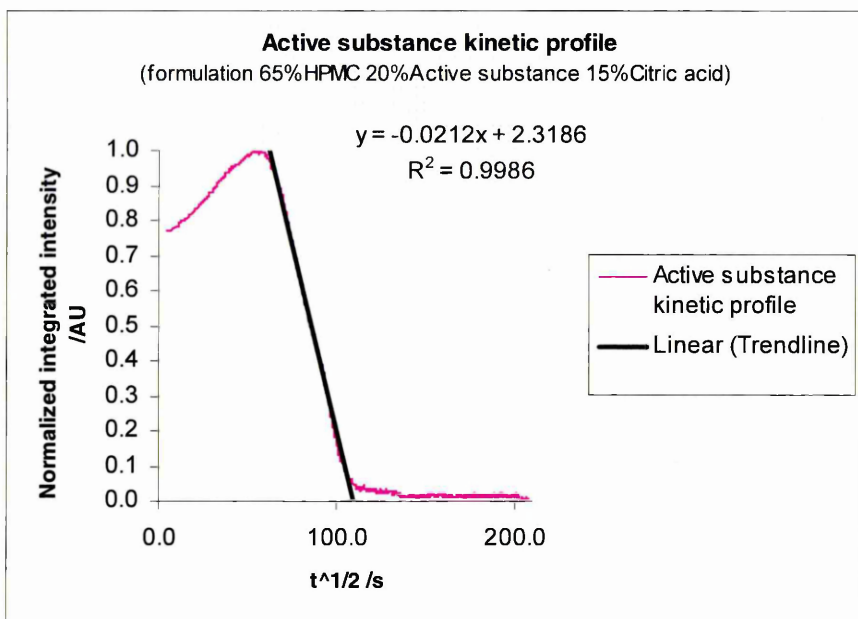


Fig 7-4. Normalized profiles of the API

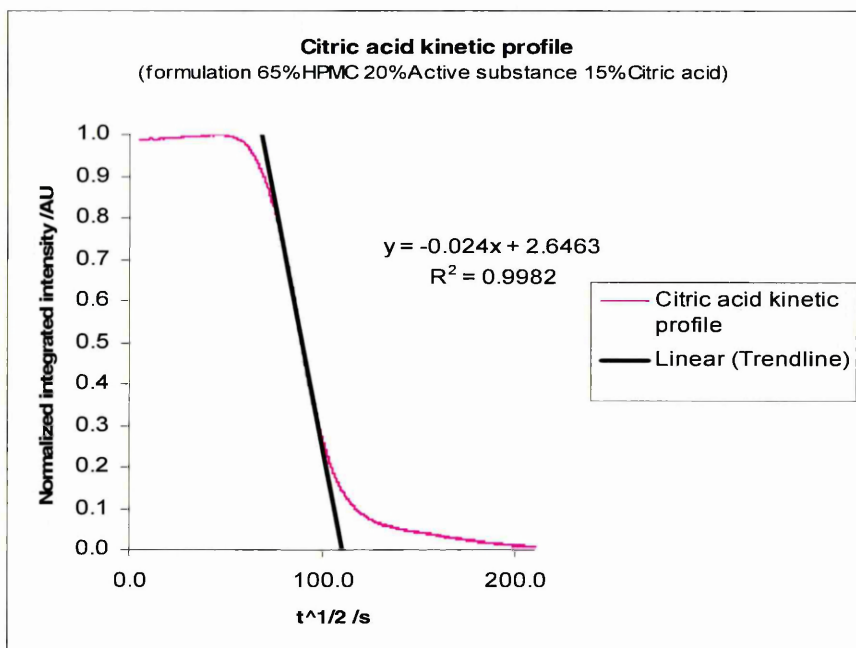


Fig 7-5. Normalized profiles of the citric acid

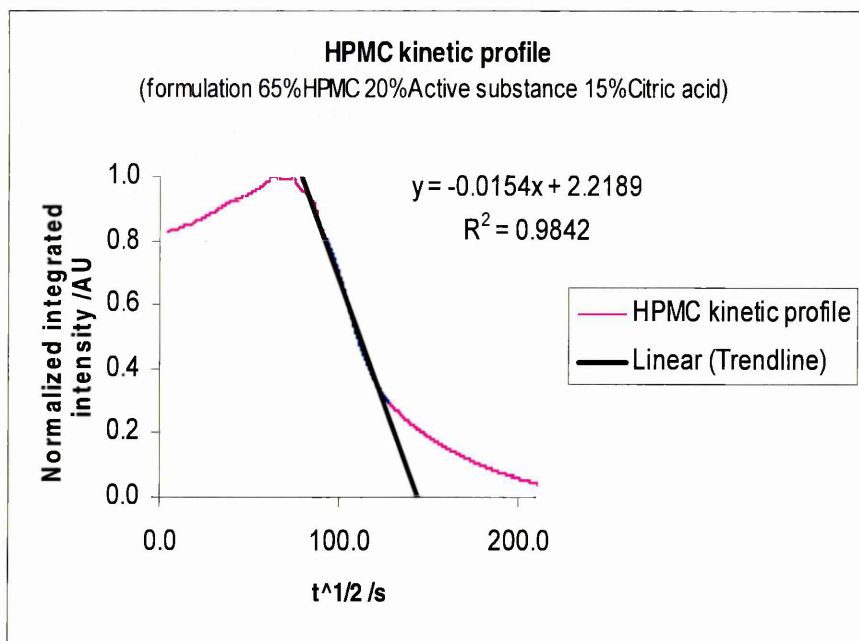


Fig 7-6. Normalized profiles of the HPMC

The analysis of the generated profiles for the tertiary formulation (Fig 7-2-7-6) showed that with ingress of water into the tablet matrix the dissolved active substance diffuses out from

the matrix faster whilst the polymer still continues the swelling process. The citric acid dissolves and diffuses out slower from the polymer matrix than API, however the citric acid profile shows the rapid diffusion rates as expected considering the results from NIR Imaging which showed the aggregates of the citric acid and heterogeneous distribution of that component. The HPMC profiles showed the initial hydration of the polymer up to 180 min and then followed by the swelling process.

The slope is the vertical distance divided by the horizontal distance between any two data points on the line, this represents the rate of change along the regression line.

There is a systematic change in the slope value (Table 7-2) for polymer and API, which increases with increasing concentration of HPMC in the sample. Water uptake slope values mainly decrease with increasing concentration of HPMC in the sample, which confirms the suggested diffusion control process in the analyzed system. Citric acid appears to be independent of concentration. There is similar tendency between the HPMC and water uptake profiles compared to the binary formulations observed in Chapter 5. For both binary and tertiary systems the water uptake profile slope value decreases with increasing concentration of HPMC in the sample. However citric acid and API appears to be independent from the HPMC concentration for both systems.

Kinetic profiles quantitative data					
Formulation		Water uptake	Citric acid	API	HPMC
HAC 45/40/15	Slope	0.0164	-0.0197	-0.0218	-0.0236
	Intercept[s]	3931	13608	14648	20449
	R <sup>2</sup>	0.9965	0.9954	0.9959	0.9872
HAC 55/30/15	Slope	0.0176	-0.0201	-0.0212	-0.0202
	Intercept[s]	3445	12444	11960	19081
	R <sup>2</sup>	0.999	0.9971	0.9986	0.9979
HAC 65/20/15	Slope	0.015	-0.024	-0.0212	-0.0154
	Intercept[s]	3760	12157	11960	20759
	R <sup>2</sup>	0.9928	0.9982	0.9986	0.9842
HAC 75/10/15	Slope	0.0143	-0.0178	-0.019	-0.0145
	Intercept[s]	3912	15411	13940	25840
	R <sup>2</sup>	0.9946	0.9968	0.9924	0.9907

Table 7-2 The slope, intercept and R<sup>2</sup> values for the analyzed binary formulation HPMC, citric acid and active substance

### 7.3.2 Effect of different pH dissolution media on the drug release from tertiary formulations.

The dissolution experiments for formulation HPMC, active substance and constant concentration of citric acid 5% were conducted in distilled water, pH 6.8 phosphate buffer and 0.1 N HCl; pH 1.5.

The formulation HPMC, active substance and constant concentration of citric acid 5% was chosen for dissolution and hyphenation experiments since the data collected from the solid dosage form (PLS data analysis and NIR Imaging) suggested the lowest level of heterogeneity compared to the other tertiary systems.

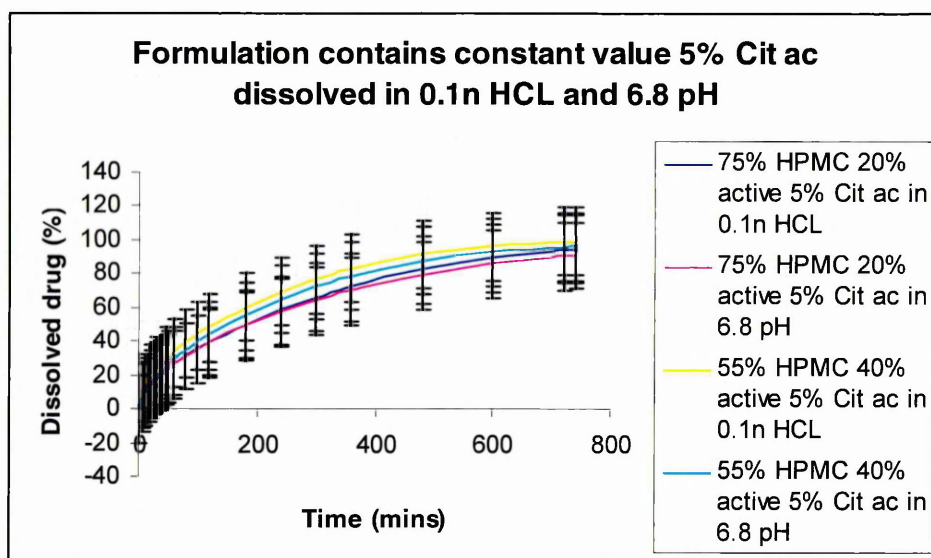


Fig. 7-8 Mean dissolution profiles for formulations of HPMC, citric acid and active substance, the 200 mg tablets were placed in pH 6.8 phosphate buffer and 0.1N HCl as the dissolution media.

The dissolution profiles of tertiary mixtures (Fig 7-8) showed a significant difference between the samples with the drug loading 40% and 20% tested in pH 6.8 and 0.1N HCl. Quicker release and higher percentage of dissolved API was observed in the case of the samples with the API concentration 40%. The addition of citric acid to the formulation improved the dissolution of the samples dissolved in pH 6.8 when compared to its absence (Fig 5-5). The percentage of the dissolved drug is similar to that dissolved in 0.1 N HCl. The obtained results clearly show the pH dependence of the samples. As one could expect the citric acid in the polymer matrix builds up the so called “microenvironmental pH” which allows for drug release independently of the pH of surrounding media. In the result both samples with drug concentration 40% dissolved with similar drug percentage.

#### 7.3.3 Hyphenation experiments

The hyphenation experiments are discussed based on the mixture 55% HPMC 40% active substance and 5% of citric acid.

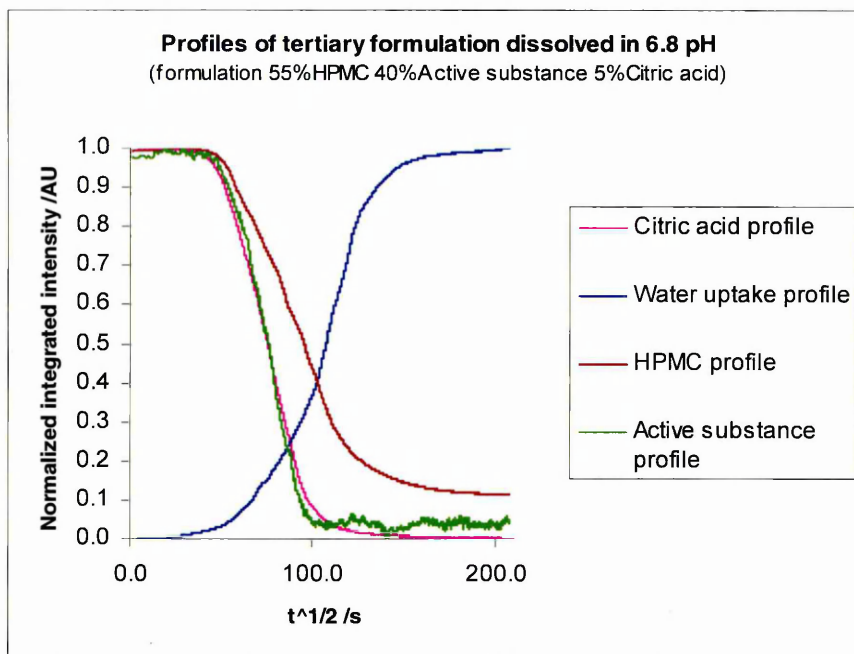


Fig 7-9. Normalized profiles of the formulation HPMC, API and citric acid.

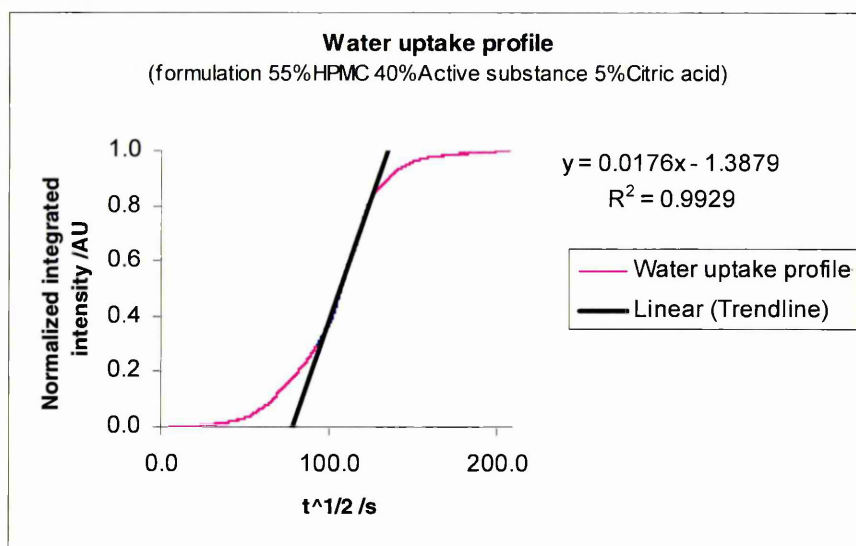


Fig 7-10. Normalized profiles of water uptake.



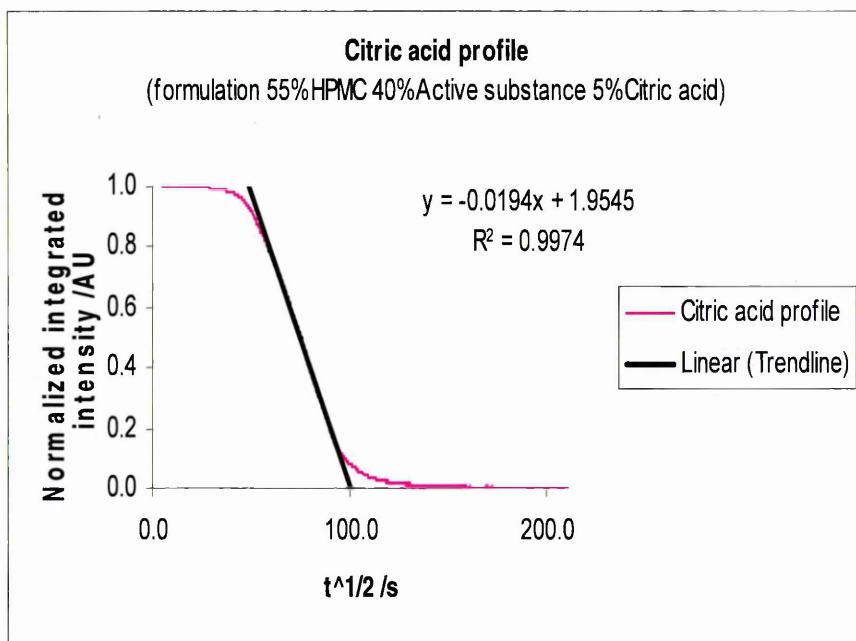


Fig 7-11. Normalized profiles of Citric acid.

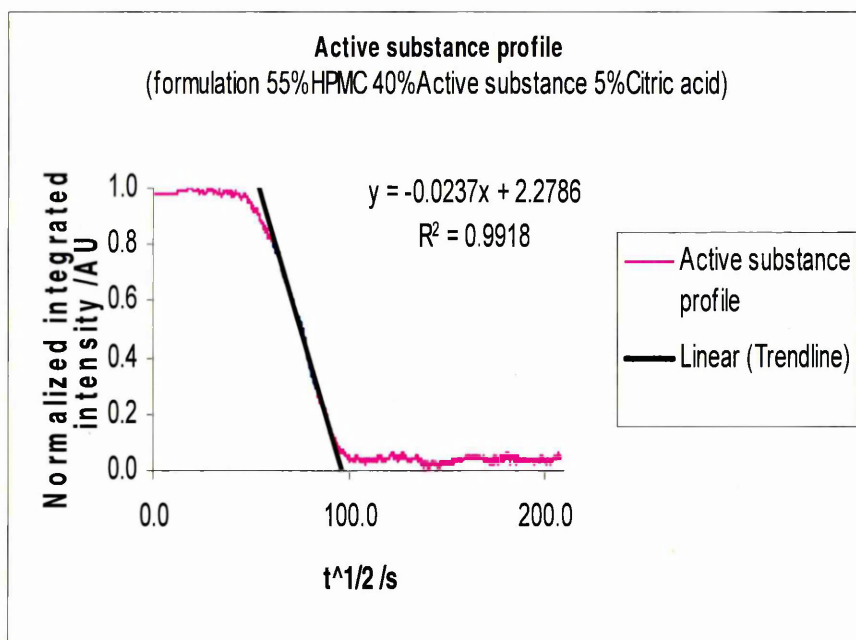


Fig 7-12. Normalized profiles of API.

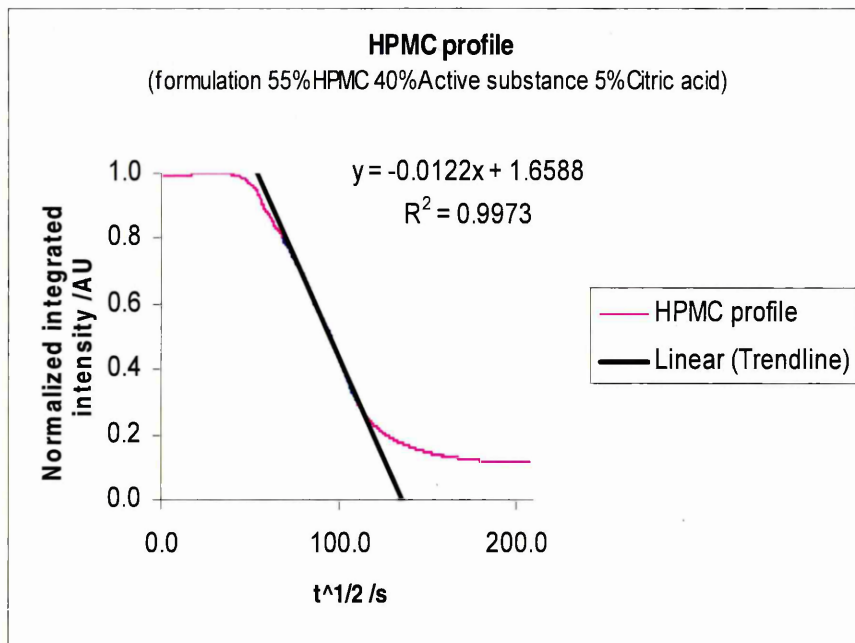


Fig 7-13. Normalized profiles of HPMC

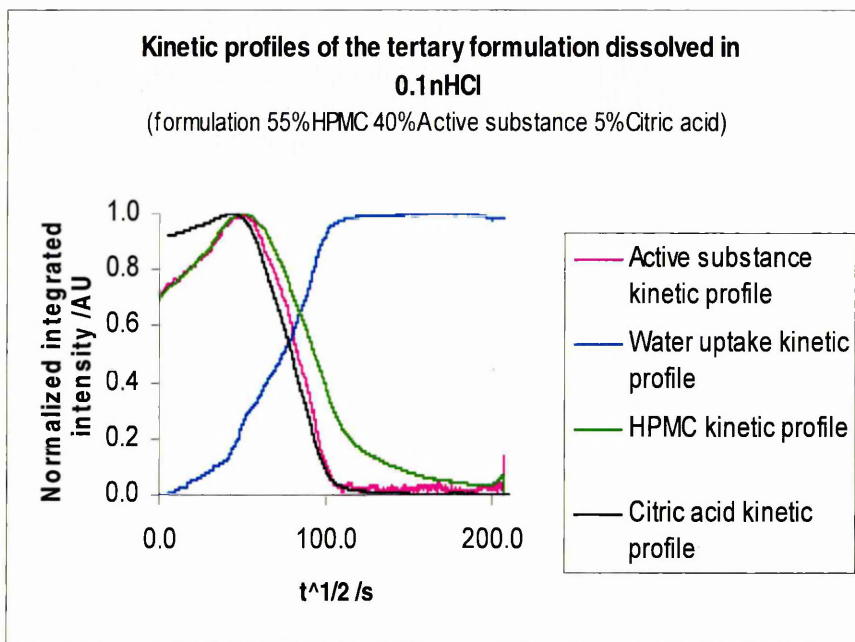


Fig 7-14. Normalized profiles of formulation HPMC, API, citric acid.

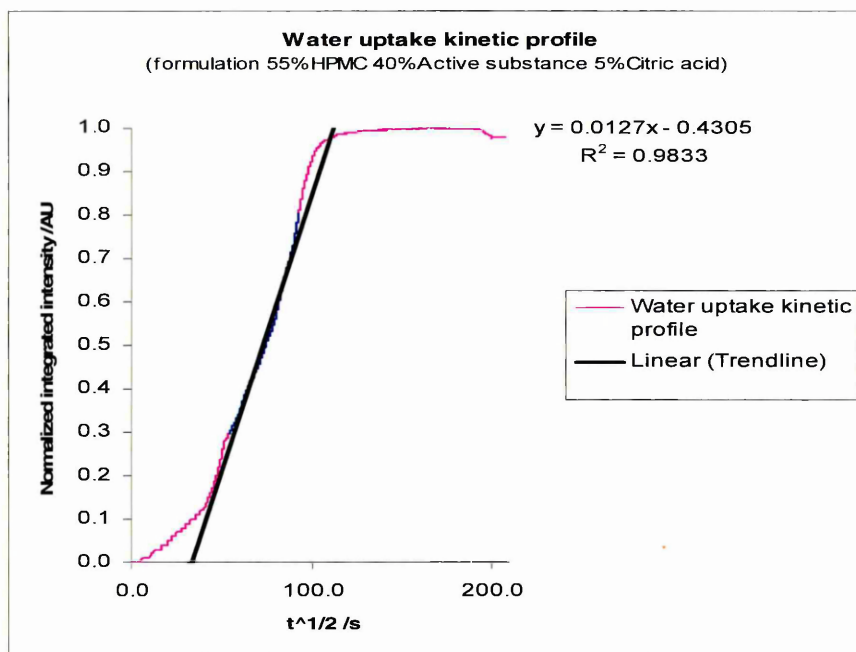


Fig 7-15. Normalized profiles of HPMC.

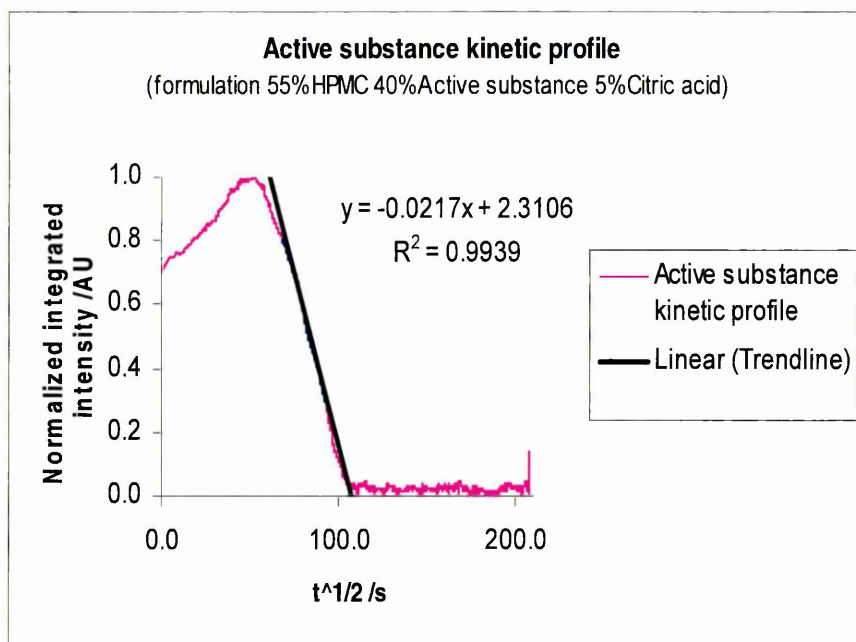


Fig 7-16. Normalized profiles of API.

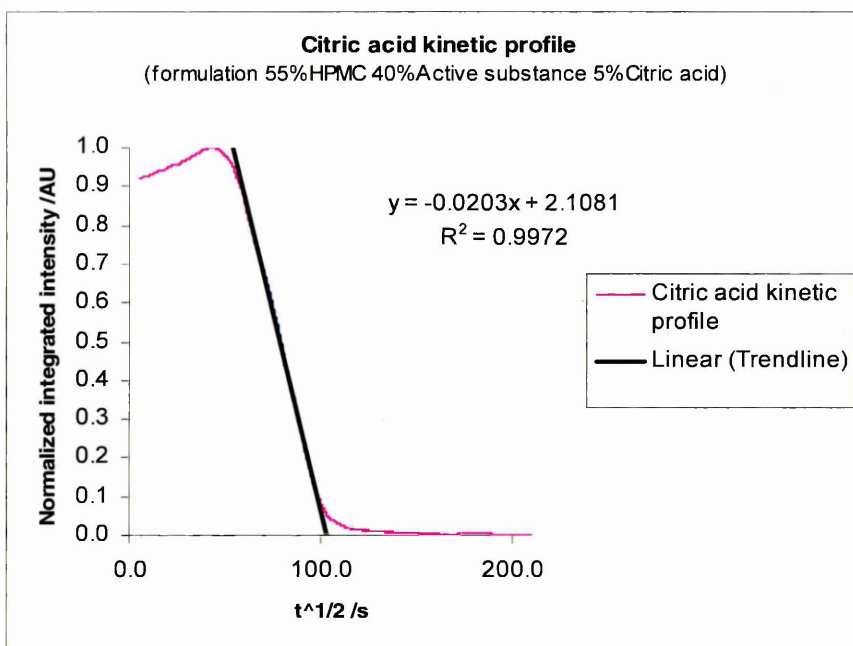


Fig 7-17. Normalized profiles of Citric acid.

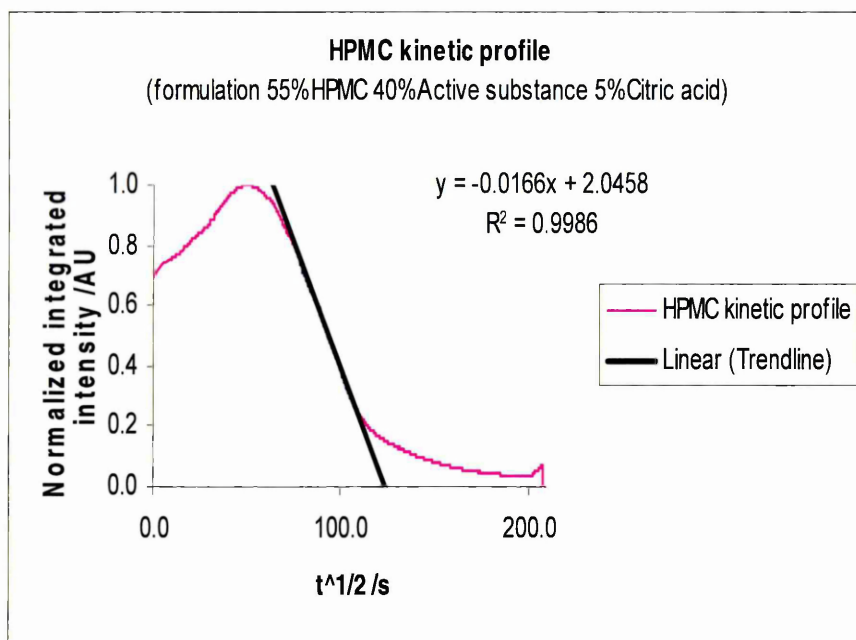


Fig 7-15. Normalized profiles of HPMC.

Kinetic profiles quantitative data					
Formulation		Water uptake	Citric acid	API	HPMC
HAC 55/40/5 in 0.1 N HCl	Slope	0.0127	-0.0203	-0.0217	-0.0166
	Intercept[s]	1148	10783	11336	15188
	R <sup>2</sup>	0.9965	0.9954	0.9959	0.9872
HAC 75/20/5 In 0.1 N HCl	Slope	0.0133	-0.0201	-0.0185	-0.015
	Intercept[s]	2125	1427	15556	25658
	R <sup>2</sup>	0.999	0.9971	0.9986	0.9979
HAC 55/40/5 in pH 6.8	Slope	0.0176	-0.0194	-0.0237	-0.0122
	Intercept[s]	5778	10149	9243	18486
	R <sup>2</sup>	0.9928	0.9982	0.9986	0.9842
HAC 75/20/5 In pH 6.8	Slope	0.0141	-0.0159	-0.0113	-0.0145
	Intercept[s]	2540	12805	23400	25840
	R <sup>2</sup>	0.9946	0.9968	0.9924	0.9907

Table 7-3 The slope, intercept and R<sup>2</sup> values for the analyzed binary formulation HPMC, citric acid and active substance

The analysis of the generated profiles for the tertiary formulations (Fig 7-9 to 7-15) showed that with ingress of water into the tablet matrix the dissolved active substance diffuses out from the matrix whilst the polymer still continues the swelling process. The citric acid dissolves and diffuses out from the polymer matrix and API, in the case of 0.1N HCl dissolution media. The HPMC profiles showed the initial hydration of the polymer followed by the swelling process as indicated by an initial increase in integrated intensity followed by its decrease.

The quantitative analysis (Table 7-3) of the kinetic profiles of the HPMC, API, citric acid and water uptake in the tertiary formulations showed systematic changes within the slope values. Samples dissolved in 0.1N HCl showed increasing slope values for HPMC and water uptake, with an increasing amount of HPMC in the sample, as we might expect considering acid dissolution media.

In the case of hyphenated experiments conducted in the pH 6.8 environment the slope values increases with increasing concentration of HPMC in the sample for API and citric acid profiles. The water uptake profile slope value decreases with increasing concentration of HPMC in the sample.

The intercept values increase in the case of citric acid, HPMC and API for the samples dissolved in pH 6.8, as HPMC concentration is increased and for API and HPMC from samples dissolved in 0.1N HCl. The obtained results show the onset of the changes in the behaviour of the formulations depending on the dissolution media pH, which agrees with the results obtained from dissolution testing.

Comparing the hyphenation experiments of the binary and tertiary system; in the case of samples dissolved in 0.1 N HCl the API and HPMC slope values decreases with increasing concentration of HPMC, in the case of pH 6.8 this trend is observed for HPMC profile slope values, no regular tendency is present in the case of API.

Along with the analysis of the infrared results the output of the UV detector was considered to broaden the information obtained.

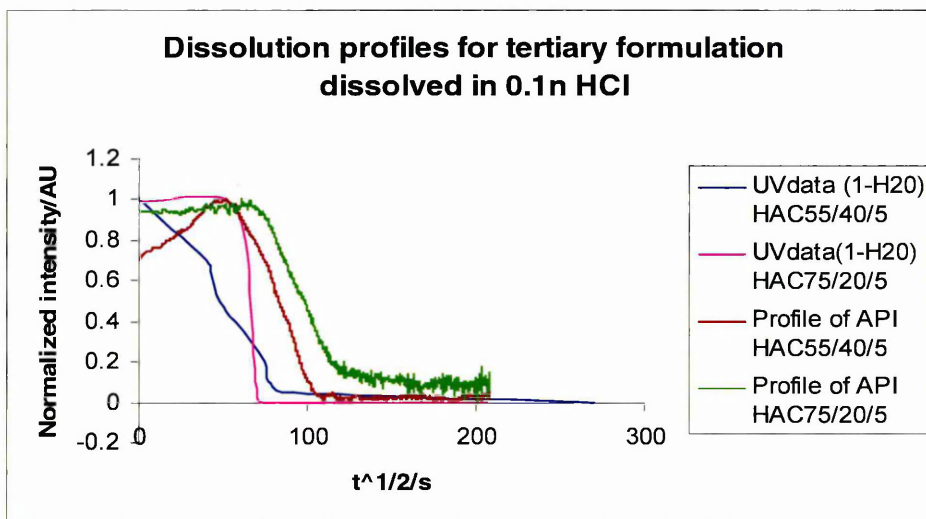


Fig.7-16. The normalized kinetic profiles of formulation HAC 55/40/5 and HAC 75/20/5 and output of the UV reading with the reduced values for dissolution media (1-H<sub>2</sub>O) dissolved in 0.1 N HCl

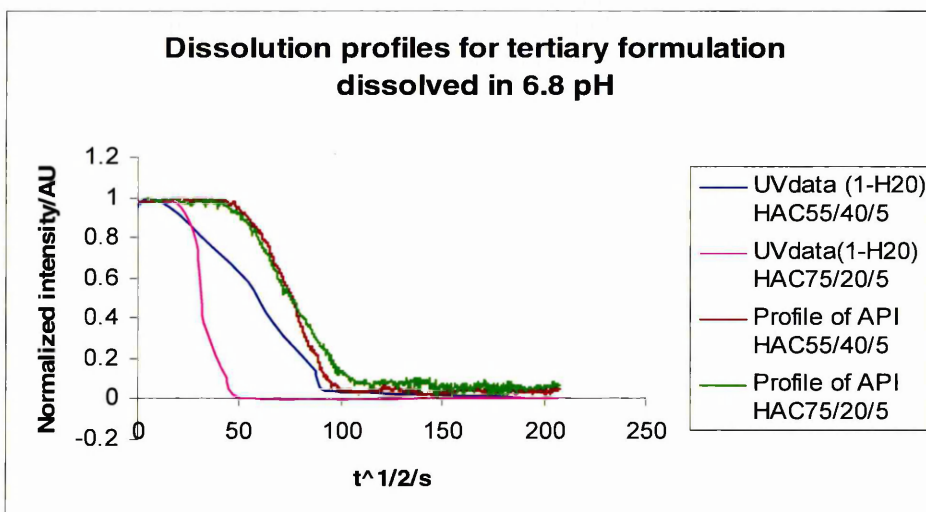


Fig.7-17. The normalized kinetic profiles of formulation HAC 55/40/5 and HAC 75/20/5 and output of the UV reading with the reduced values for dissolution media (1-H<sub>2</sub>O) dissolved in pH 6.8

The profiles (Fig 7-16 to 7-17) obtained from UV detector showed significant differences when compared with the kinetic profiles obtained from the infrared spectroscopic analysis. The UV profiles are similar to those of the binary systems since they showed much faster rate of drug dissolution than the respective profiles generated from infrared data. This is anticipated considering the PLS and NIR Imaging results obtained for solid tablets. The active substance showed the level of segregation on the top side of the tablet, which in the case of hyphenated experiments causes the differences in the UV measurements. The UV output shows the active substance dissolved quickly in a very short period of time and presumably the first measurements of UV detector are connected with the active substance segregated on the top side of the tablet.

The UV profiles are very poor quality due to the low concentrations of the analyzed substances, irregular flow as the HPLC pump and non-conventional equipments set up.



### 7.3.3 MCR data analysis

The results of the tertiary formulation hyphenation experiments will be discussed on the example of the sample HAC 55/40/5 in pH 6.8

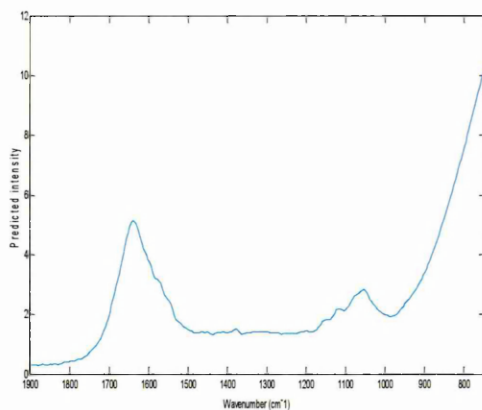


Fig 7-18 Predicted spectrum of water

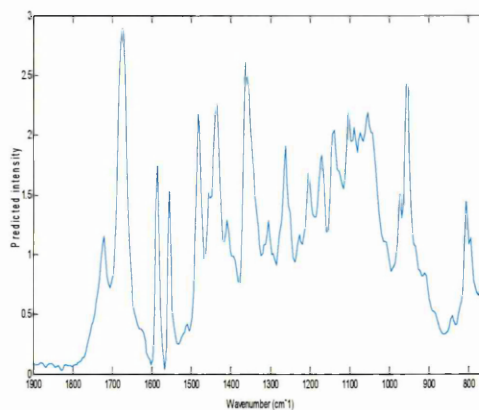


Fig 7-19 Predicted spectrum of API

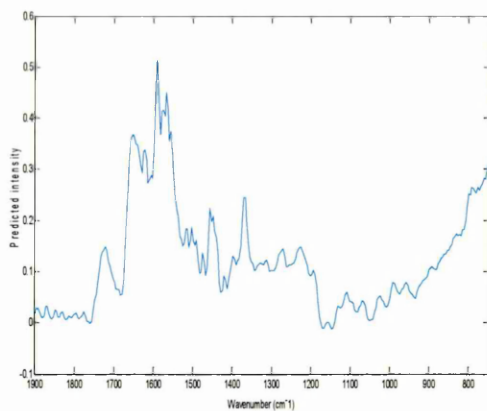


Fig 7-19 Predicted spectrum of hydrated  
citric acid

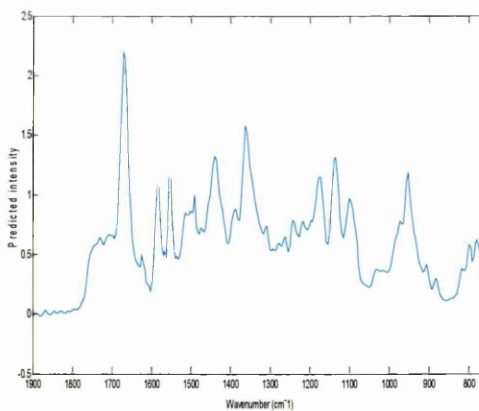


Fig 7-20 Predicted spectrum of hydrated API

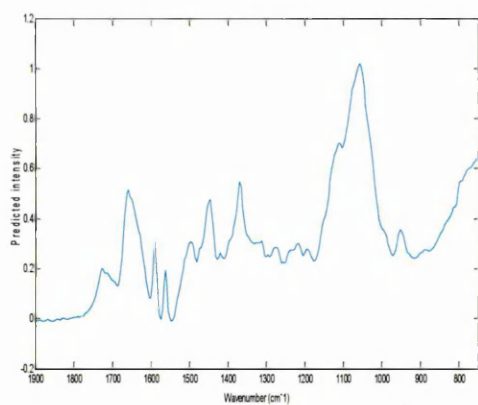


Fig 7-21 Predicted spectrum of hydrated HPMC

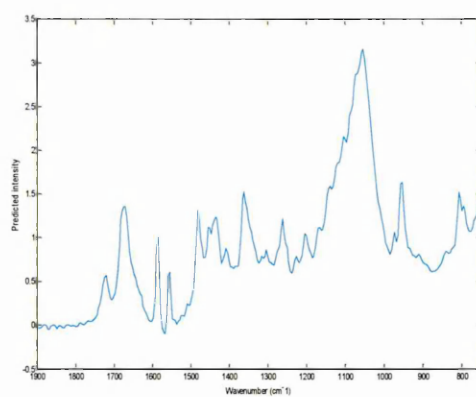


Fig 7-22 Predicted spectrum of HPMC

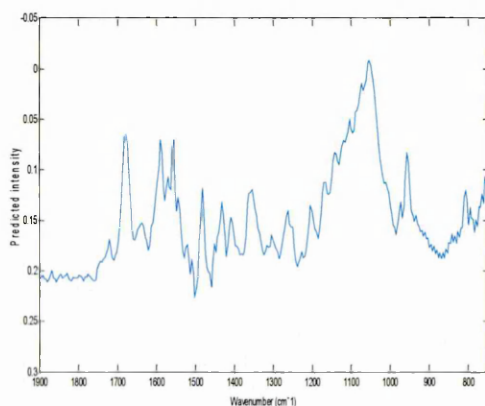


Fig 7-23 Predicted spectrum of solid API.

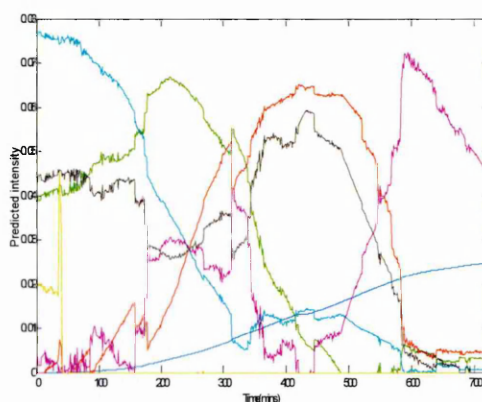


Fig 7-24 Predicted

concentration profiles;

green colour – water uptake, grey-API,

blue-HPMC, light green – citric acid,

red-hydrated API, dark blue-hydrated

HPMC, puple-hydrated citric acid

The generated results (Figs 7-18 to 7-24), showed the predicted spectral results (the axis X intensity values versus the wavenumber axis Y) and concentration profiles (the axis X intensity values versus the time (mins) axis Y the analyzed sample). Analyzing the generated spectra one could easily recognize the spectrum of water and solid API.

However, the rest of the spectra contain bands coming from other excipients of the formulation. In addition Fig 7-19 showed the negative spectrum which has band associated with all components in the formulation.

The MCR analysis is supposed to predict, based on the data matrix, the possible components of the mixture.

In the case of this formulation, the prediction should show the presence of solid excipients, water and hydrated forms of excipients. However the analysed data set didn't show expected results as the spectral information was very noisy and contained a mixture of bands characteristic for excipients.

The narrowing spectral window in the range from 2000-900  $\text{cm}^{-1}$  improved the data analysis however to achieve more informative data and avoid the rotational ambiguity the further reduction of the spectral range would need to be applied.

## **7.4 Conclusions**

The dissolution experiments performed on the tertiary system provided information about the behaviour of the formulation in the different dissolution media. Almost 100% of the dissolved drug was observed in the case of the dissolution of the samples in 0.1N HCl or pH 6.8. As expected the impact of citric acid on the dissolution results was observed and confirmed the pH dependence of the analyzed system.

The analysis of the hydration experiments data showed the dissolution and diffusion of the active substance and citric acid, whilst the HPMC kinetic profile showed the continuous swelling process of the perturbed polymeric system by the dissolution media. These results were also observed in the case of the hyphenated samples. These findings suggested the diffusion control as a possible dominant process of the drug release in the formulations. However the hyphenation experiment confirmed also the pH-dependence already observed in the case of dissolution data of the discussed systems.

The hyphenated samples data provided the information about behaviour of API, citric acid and HPMC in a different dissolution media.

Finally the MCR data analysis was applied to the hyphenated samples spectra data matrix. The predicted spectra and concentration profiles proved the further need of development of data analysis as the obtained results were not very good quality in order to compare the hydrated and hyphenated samples of tertiary mixtures. However, the heterogeneity of the compacted samples may be the underlying problem due to the poor results.

## **8. Conclusions:**

The optimization of the parameters for a reproducible manufacturing process of the formulation was conducted testing the effect of different mixing procedures, (manual shaking, tumble blending and grinding) and variability of particle size on the uniformity of the formulations determined by the FTIR-ATR with PLS data analysis and NIR Imaging. The binary formulations of HPMC and Citric acid showed that the samples without matching particle size and mixing procedure had a high degree of heterogeneity. The presence of component aggregates on the surfaces of the analyzed samples determined by NIR imaging, PLS data analysis and also Infrared spectra. It was observed that the particle size had a significant impact on experimental data in terms of reproducibility and heterogeneity of the samples.

The optimal tablet reproducibility and homogeneity of components has been achieved by controlling the particle size of the substances used for mixture preparation. The samples were compacted *in situ* on the ATR crystal in a compaction cell which proved to be a successful tool in a small scale tablet manufacturing process. The variation in the intensity of FTIR-ATR spectra, PLS analysis and NIR imaging confirmed homogeneity of the binary formulation and higher level of heterogeneity in the case of tertiary formulations.

The dissolution of the tertiary system gave an indication about the behaviour of the formulations in the different dissolution media. The percentage reaching almost 100% of the dissolved drug was observed in the case of the dissolution of the samples in 0.1 N HCl and pH 6.8 respectively. As expected the impact of citric acid on the dissolution results was observed what confirmed the pH dependence of the analyzed system.

The analysis of the hydration experiments data showed the faster dissolution and diffusion of the active substance and citric acid in both systems compare to the HPMC kinetic profile

which clearly showed the continues swelling process whilst the other excipients reached equilibrium already. These results were also observed in the case of the hyphenated samples.

The diffusion control is a possible dominant process of the drug release in the analyzed formulations. Also the hyphenation experiments confirmed the pH dependence already observed in the case of the dissolution data of the discussed systems.

Finally the MCR data analysis was applied to the solid sample spectra and hyphenated samples spectra data matrix. The predicted spectra and concentration profiles from the hydrated and hyphenated experiments proved the further need of development of data analysis.

## **8.2 Further work**

The studies of drug controlled release from hydrophilic matrices were limited to the binary and tertiary mixtures. Further development of the formulation would require adding more excipients to build new compositions and investigate the behaviour of the multi-component tablets. However, hydration and hyphenation experiments of the binary and tertiary mixtures could be still challenging if we could reconsider few significant factors having impact on the further development of the project.

#### 8.2.1 Reconstruction of the compaction cell

Originally, the compaction cell was made from brass, as this material was supposed to be ideal for drugs which are salts chemically, and it could ensure a lack of reactivity of the compound with the compaction cell. However, if during the experiment the medium used for dissolution of the sample was 0.1 n HCl, after several experiments, the built up of the passivation layer in the water channels was visible. In a result a breakage of this layer leads to the corrosion of the internal channels in the compaction cell and surroundings of the sample.

For further static hydration and hyphenation experiments, it would be necessary to make the compaction cell from Teflon, as this material is resistant to pH changes, and could prevent from any possible leakages of the medium in the sample die/ screw area from the compaction cell during the experiment. Another advantage of a new compaction cell (Fig8-1) would be a presence of another connection on the top of the cell with the water channels in order to minimize the amount of time needed to fill the cell with the required medium.

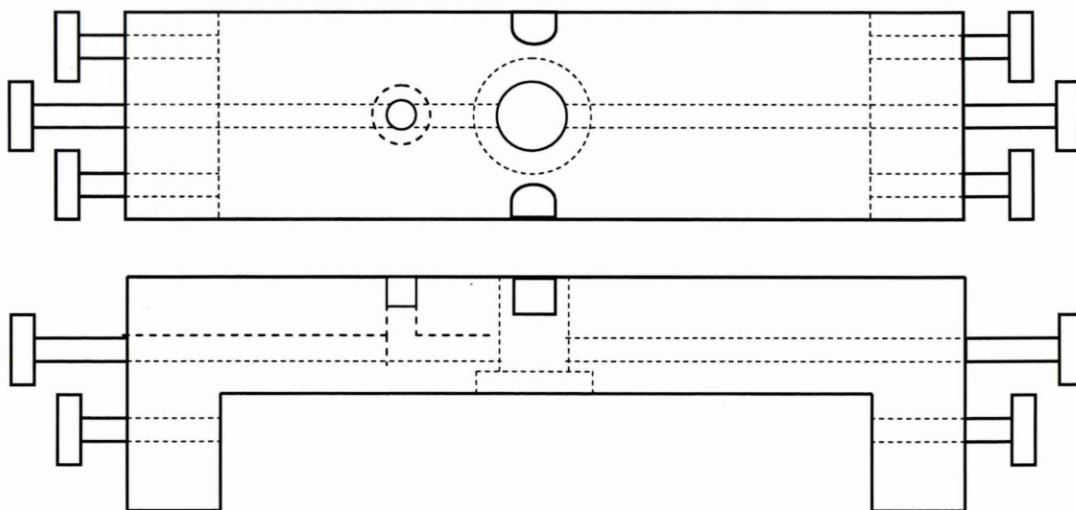


Fig 8-1. The design of the compaction cell.

### 8.2.2 ATR-FTIR Imaging as a main technique of further investigation.

The FTIR-ATR application used to conduct the hydration and hyphenation experiments achieved spectral information about the analysed systems on a molecular level.

However spectroscopic imaging techniques can provide more detailed data about the investigated samples. In the last few years, Kazarian's group reported about the possible applications of FTIR Imaging for pharmaceutical and biomaterial samples [168, 175-177] and also some work on monitoring of polymer dissolution using FTIR Imaging was carried out by Ribar [178]. The examples of investigations carried on pharmaceutical samples involved drug release and tablet dissolution [147, 148, 168, 175, 179], water sorption in pharmaceutical substances under controlled humidity [175] and quite a lot of work done on polymers diffusion or dissolution in solvents. ATR-FTIR Imaging is a powerful tool that could improve the results of the experiment, giving additional spatial information from the samples. In comparison with normal transmission FTIR microscopy (resolution 40-50 micrometers) such an imaging system is able to achieve a very high spatial resolution down



to few micrometers as well as the acquisition of the images and data analysis is much faster than in case of FTIR microscopy where measurement of the reasonable area of the sample and further data analysis of obtained map of the surface will take hours [168, 176].

### 8.2.3 Future experiments

Further work should involve further optimization of the particle size of the excipients using particle size analyzer and in the next stage the hydration and hyphenation experiments on binary and tertiary mixtures using FTIR Imaging technique.

Kazarian's group published results of hydration experiments conducted in a compaction cell on binary mixture HPMC and drug. However the experiment was lacking the continuous dynamic conditions as the liquid (distilled water) was provided by a syringe, the investigated tablets covered only half surface of the ATR crystal what makes an additional requirement of very high level homogeneity of the tablet to could approve the spectroscopic results. The data were calculated for the whole amount of the sample [148].

The innovative approach of this project would involve using the dynamic conditions in the experiment ( HPLC pump) what could ensured the constant flow of the liquid, changing pH of dissolution media from 1.5 (0,01 N HCl) to 6.8 phosphate buffer could give more understanding of the behaviour of the investigated formulation. The samples would be compacted directly in situ on the ATR crystal and cover the surface of the internal reflectance element. The data collected from the investigated tablet would be further analysed and the obtained information about the spatial distribution of excipients in contact with dissolution media could provide an important basis for understanding of the mechanism of drug release in analysed system and building a mathematical model for the optimisation of controlled drug delivery. Further on the research could continue on

mixtures with addition of other excipients like lubricant i.e magnesium stearate, filler i.e. avicel to develop and optimise the controlled release formulation.

## References:

1. Robert O. Williams III, M.A.S., Vorapann Mahaguna, *Method to recover a lipophilic drug from hydroxypropyl methylcellulose matrix tablets*. AAPS PharmSciTech, 2001. **2**: p. 1-9.
2. Hamid A. Merchant, H.M.S., Jaweria Tazeen, Rabia I. Yousuf, *Once-daily tablet formulation and in vitro release evaluation of cefpodoxime using hydroxypropyl methylcellulose: A technical note* AAPS PharmSciTech, 2006. **7**: p. E1-E6.
3. Giorgio Pifferi, P.R., *The safety of pharmaceutical excipients*. Il Farmaco, 2003. **58**: p. 541-550.
4. J.J. Escudero, C.F., M.R. Jiménez-Castellanos, *Compaction properties, drug release kinetics and fronts movement studies from matrices combining mixtures of swellable and inert polymers. II. Effect of HPMC with different degrees of methoxy/hydroxypropyl substitution*. International Journal of Pharmaceutics, 2009. **in press**: p. 1-9.
5. M. L. Vueba; L. A. E. Batista de Carvalho; F. Veiga; J. J. Sousa; Maria, E.P., *Role of Cellulose Ether Polymers on Ibuprofen Release from Matrix Tablets*. Drug Development and Industrial Pharmacy, 2005. **31**: p. 653 - 665.
6. Sara Richardson, L.G., *Characterisation of the substituent distribution in starch and cellulose derivatives*. Analytica Chimica Acta, 2003. **497**: p. 27 - 65.
7. T.Heinze, T.L., *Unconventional methods in cellulose functionalization*. Prog. Polym. Sci, 2001. **26**: p. 1689 -1762.
8. C.Clasen, W.M.K., *Determination of viscoelastic and rheo-optical material functions of water soluble cellulose derivatives*. Prog. Polym. Sci, 2001. **26**: p. 1839-1919.
9. Anna Viride, B.W., Thomas Andersson, Susanna Abrahamse'n-Alami, Anette Larsson, *Influence of substitution pattern on solution behavior of hydroxypropyl methylcellulose*. Biomacromolecules, 2009. **10**: p. 522-529.
10. Oscar E. Pe' rez, C.C.S.n., Juan M. Rodri'guez Patino, Ana M. R. Pilosof, *Thermodynamic and dynamic characteristics of hydroxypropylmethylcellulose adsorbed films at the air-water interface*. Biomacromolecules, 2006. **7**: p. 388-393.
11. G.K.Greminger, J., C.P.Strange, K.L.Krumel, J.L.Hudson, Jr, *Hydroxypropyl methylcellulose ethers and method of preparation*. US Patent no 3,839,319, 1974.
12. Company, D.C., *Using methocel cellulose ethers for controlled release of drugs in hydrophilic matrix systems*. 1984: p. 1 - 34.
13. J. Siepmann, N.A.P., *Modeling of drug release from delivery systems based on hydroxypropyl methylcellulose (HPMC)* Advanced Drug Delivery Reviews, 2001. **48**: p. 139 - 157.
14. N.A.Peppas, *Hydrogels in medicine and pharmacy*. Vol. I,II,III. 1985.
15. T. Loftsson, T. K. Guçmundsdttir, *The effect of water-soluble polymers on aqueous solubility of drugs*. International Journal of Pharmaceutics, 1996. **127**: p. 293-296.
16. Sarkar, N., *Kinetics of thermal gelation of methylcellulose and hydroxypropylmethylcellulose in aqueous solutions*. Carbohydrate Polymers, 1995. **26**: p. 195-203.
17. J. L. Ford , K.M., *Thermal analysis of gels and matrix tablets containing cellulose ethers*. Thermochemica Acta, 1995. **248**: p. 329-345.

18. Ford, J.L., *Thermal analysis of hydroxypropylmethylcellulose and methylcellulose: powders, gels and matrix tablets*. International Journal of Pharmaceutics, 1999. **179**: p. 209–228.
19. C.M. Rosell, J.A.R., C. Benedito de Barber, *Influence of hydrocolloids on dough rheology and bread quality*. Food Hydrocolloids, 2001. **15**: p. 75-81.
20. C. Wollenweber, A.V.M., R. Miller, R. Daniels, *Adsorption of hydroxypropyl methylcellulose at the liquid:liquid interface and the effect on emulsion stability*. Colloids and Surfaces, A: Physicochemical and Engineering Aspects, 2000. **172**: p. 91–101.
21. S. Mezdoura, G.C., M.J. Cashb, C. Michona, *Surface rheological properties of hydroxypropyl cellulose at air–water interface*. Food Hydrocolloids, 2007. **21**: p. 776–781.
22. B. Person, S.N., L. Sundeliif, *On the characterization principles of some technically important water-soluble nonionic cellulose derivatives. Part II: Surface tension and interaction with a surfactant*. Carbohydrate Polymers, 1995. **29**: p. 119-127.
23. R. Villalobos, J.C., P. Hernandez, G. Gutierrez, A. Chiralt, *Gloss and transparency of hydroxypropyl methylcellulose films containing surfactants as affected by their microstructure*. Food Hydrocolloids, 2005. **19**: p. 53–61.
24. Escudero, J., Ferrero, C., Jiménez-Castellanos,, *Compaction properties, drug release kinetics and fronts movement studies from matrices combining mixtures of swellable and inert polymers: effect of HPMC of different viscosity grades*. Int. J. Pharm, 2008. **351**: p. 61–73.
25. VN.Le , P.L., A.Gayot , MP.Flament *Influence of granulation and compaction on the particle size of ibuprofen--development of a size analysis method*. Int J Pharm., 2006. **14**: p. 72-77.
26. Ford, J.L., M.H.Rubinstein, J.E.Hogan, *Formulation of sustained release promethazine hydrochloride tablets using hydroxypropylmethylcellulose matrices*. International Journal of Pharmaceutics, 1985c. **24**: p. 327.
27. Ford, J.L., M.H.Rubinstein, J.E.Hogan, *Dissolution of poorly water soluble drug, Indomethacin from Hydroxypropylmethylcellose controlled release tablets*. Journal of Pharmacy and Pharmacology, 1985b. **37**: p. 33.
28. M. V. Velasco, J.L.F., P. Rowe, Ali R. Rajabi-Siahboomi, *Influence of drug:hydroxypropylmethylcellulose ratio, drug and polymer particle size and compression force on the release of diclofenac sodium from HPMC tablets*. Journal of Controlled Release, 1999. **57**: p. 75–85.
29. A. Nokhodchi, M.H.R., J.L. Ford, *The effect of particle size and viscosity grade on the compaction properties of hydroxypropylmethylcellulose 2208*. International Journal of Pharmaceutics, 1995. **126**: p. 189-197.
30. Ford, J.L., M.H.Rubinstein, A. Changela, J.E.Hogan, *Influence of pH on the dissolution of Promethazine Hydrochloride from Hydroxypropylmethylcellulose controlled release tablets*., Journal of Pharmacy and Pharmacology, 1985a. **37**: p. 115.
31. A.D.Cross, R.A.J., *An Introductio to practical Infra-red spectroscopy*. 1969: Butterworths & CO Ltd.
32. Coates, J., *Interpretation of Infrared spectra, a practical approach*. Encyclopedia of Analytical Chemistry, 2000: p. 10815-10837.
33. Chi L. Li, L.G.M., James L. Ford and Matthew Roberts, *The use of hypromellose in oral drug delivery*. Journal of Pharmacy and Pharmacology, 2005. **57**: p. 533-546.

34. Eyjolfsson, R., *Hydroxypropyl methylcellulose mixtures: effects and kinetics of release of an insoluble drug*. Drug Development and Industrial Pharmacy, 1999. **25**(5): p. 667-669.
35. M. Sheikhzadeh, S.R., M. Taffish, S. Murad, *Solubility analysis of buspirone hydrochloride polymorphs: Measurements and prediction*. International Journal of Pharmaceutics 2007. **338**: p. 55-63.
36. S.Kiortsis, K.K., Th.Broussali, S. Malamataris, *Drug release from tableted wet granulations comprising cellulosic (HPMC or HPC) and hydrophobic component*. European Journal of Pharmaceutics and Biopharmaceutics, 2005. **59**: p. 73-83.
37. R. Bettini, P.L.C., P. Santi, G. Massimo, N.A. Peppas, P. Colombo, *Translocation of drug particles in HPMC matrix gel layer: effect of drug solubility and influence on release rate*. Journal of Controlled Release, 2001. **70**: p. 383 - 391.
38. A. Jayan, R.J.M., M. Walther, C.D. Melia, *Understanding of the mechanism of drug release in mixed HPMC/PEO matrices*. Pharm. Sci., 1999. **1**: p. 385.
39. M. Victoria Velasco, J.L.F., Philip Rowe, Ali R. Rajabi-Siahboomi, *Influence of drug:hydroxypropylmethylcellulose ratio, drug and polymer particle size and compression force on the release of diclofenac sodium from HPMC tablets*. Journal of Controlled Release, 1999. **57**: p. 75-85.
40. Samuel J. Bonacorsi Jr, R.C.B., George M. Luke, Jeffrey S. DePue, J. Kent Rinehart, Balu Balasubramanian, Lisa J. Christopher, Ramaswamy A. Iyer *Synthesis of the anxiolytic agent [14C] 6-hydroxy-buspirone for use in a human ADME study*. Journal of Labelled Compounds and Radiopharmaceuticals, 2007. **50**: p. 65-71.
41. Daniel J. Watson, E.D.D., Jeffrey S. DePue, Atul S. Kotnis, Simon Leung, and Brian C. O'Reilly, *Development of a Safe and Scalable Oxidation Process for the Preparation of 6-Hydroxybuspirone: Application of In-Line Monitoring for Process Ruggedness and Product Quality*. Organic process research and development, 2004. **8**: p. 616-623.
42. Randy C. Dockens, D.E.S., I. Edgar Fulmor, Michele Wehling, Mark E. Arnold, Robert Croop, , *Pharmacokinetics of a Newly Identified Active Metabolite of Buspirone After Administration of Buspirone Over Its Therapeutic Dose Range J*. Clin. Pharmacol., 2006. **46**: p. 1308-1312.
43. Randy C. Dockens, A.Q.T., Jianing Zeng, Robert Croop, *Pharmacokinetics of 6-hydroxybuspirone and its enantiomers administered individually or following buspirone administration in humans*. Biopharmaceutics & Drug Disposition, 2007. **28**: p. 393 - 402.
44. J.P. Yevich, R.F.M., Jianqing Li, F. Yocca, *R-6-hydroxy-buspirone*. US Patent no 2003/0055063 A1, 2003.
45. J.P. Yevich, R.F.M., Jianqing Li, F. Yocca, *S-6-hydroxy-buspirone*. US Patent no 6,821,976,B2, 2004.
46. *US Pharmacopeia* 2008.
47. M. Sheikhzadeh, S.R., A. Jutan, T. Manifar, *Quantitative and molecular analysis of buspirone hydrochloride polymorphs*. Journal of Pharmaceutical Sciences, 2006. **96**: p. 569-583.
48. M. Sheikhzadeh, S.M., S. Rohani *Response surface analysis of solution-mediated polymorphic transformation of buspirone hydrochloride*. Journal of Pharmaceutical and Biomedical Analysis 2007. **45**: p. 227-236.
49. Nizar Al-Zoubi, H.S.A., Yasser Bustanji, Khaled Aiedeh, Stavros Malamataris *Sustained-release of buspirone HCl by co spray-drying with aqueous polymeric*

- dispersions*. European Journal of Pharmaceutics and Biopharmaceutics 2008. **69**: p. 735-742.
50. M. Sheikhzadeh, S.R., A.Jutan, T.Manifar, K.Murthy, S.Horne, *Solid-state characterization of buspirone hydrochloride polymorphs*. Pharmaceutical Research, 2006. **23**(5): p. 1043-1050.
  51. A.H. Goldberg, A.A.S., *Anionic exchange polymer complexes of buspirone*. US Patent, 2001: p. US 6,268,368 B1
  52. Z. Plotkowiak, M.P.-B., *Kinetics of thermal decomposition of buspirone hydrochloride in solid state*. Acta Poloniae Pharmaceutica, 2000. **57**: p. 63-65.
  53. A Sakr, M.A., *Pharmacokinetics of buspirone extended-release tablets: a single-dose study*. J. Clin. Pharmacol. , 2001. **41**: p. 783-789.
  54. A.Sakr, M.A., *A comparative multidose pharmacokinetic study of buspirone extended-release tablets with a reference immediate-release product*. J. Clin. Pharmacol., 2001. **41**: p. 886-894.
  55. J.T. Apter, L.A.A., *Buspirone: future directions*. Journal of Clinical Pharmacology, 1999. **19**: p. 86-93.
  56. K.V.Harvey, R.B., *Augmentation with buspirone: a review*. Annals of Clinical Psychiatry, 1995. **7**: p. 143-147.
  57. E.H.Kerns, R.A.R., K.J.Volk, M.S.Lee, *Buspirone metabolite structure profile using a standard liquid chromatographic-mass spectrometric protocol*. Journal of chromatography, 1997. **698**: p. 133-145.
  58. H.Wong, R.C.D., L.Pajor, S.Yeola, J.E.Grace,Jr., A.D.Stark, R.A.Taub, F.D.Yocca, R.C.Zaczek, Yu-Wen.Li, *6-hydroxybuspirone is a major active metabolite of buspirone: assessment of pharmacokinetics and 5-hydroxytryptamine 1A receptor occupancy in rats*. Drug metabolism and disposition, 2007. **35**: p. 1387-1392.
  59. Mingshe Zhu, W.Z., Humberto Jimenez, Donglu Zhang, Suresh Yeola, Renke Dai, Nimish Vachharajani, James Mitroka, *Cytochrome P450 3A-mediated metabolism of buspirone in human liver microsomes*. Drug metabolism and disposition 2005. **33**: p. 500-507.
  60. J Ploen, J.A., M. Heschel, C. S. Leopold, *Citric acid as a pH-modifying additive in an extended release pellet formulation containing a weakly basic drug*. Drug Development and Industrial Pharmacy, 2009. **35**: p. 1210-1218.
  61. R. K. Janjikhel, C.M.A., *Dissolution of Ibuprofen Enantiomers from Coprecipitates and Suspensions Containing Chiral Excipients*. Pharmaceutical Development and Technology, 1999. **4**: p. 9-17.
  62. S. Siepe, W.H., H. Borchert , B. Lueckel, A. Kramer, A. Ries, R. Gurny, *Microenvironmental pH and microviscosity inside pH-controlled matrix tablets: An EPR imaging study*. Journal of Controlled Release, 2006. **112**: p. 72-78.
  63. Siepmann J, P.N., *Modeling of drug release from delivery systems based on hydroxypropyl methylcellulose (HPMC)*. Adv Drug Deliv Rev, 2001. **48**: p. 139-57.
  64. J. Siepmann, K.Podual., M. Sriwongjanya, N. A. Peppas, R. Bodmeier, *A New Model Describing the Swelling and Drug Release Kinetics from Hydroxypropyl Methylcellulose Tablets*. Journal of Pharmaceutical Sciences, 1999. **88**: p. 65-72.
  65. C. Ferrero, A.M.o.-R., M.R. Jime'nez-Castellanos, *Fronts movement as a useful tool for hydrophilic matrix release mechanism elucidation*. International Journal of Pharmaceutics, 2000. **202**: p. 21-28.
  66. Paolo Colombo, R.B., Nikolaos A. Peppas, *Observation of swelling process and diffusion front position during swelling in hydroxypropyl methyl cellulose (HPMC)*

- matrices containing a soluble drug*. Journal of Controlled Release, 1999. **61**: p. 83–91.
67. N.B.Colthup, L.H.D., S.E.Wiberley, *Introduction to infrared and raman spectroscopy*. 1990: Academic press, INC.
  68. M. Avram, *Infrared spectroscopy, Applications in Organic Chemistry*. 1966: John Wiley & Sons Ltd, .
  69. J.J.Koeing, *Spectroscopy of polymers*. 1992, Washington DC: American Chemical Society, .
  70. B.H.Stuart, *Infrared spectroscopy: Fundamentals and applications*. 2004: John Wiley & Sons, Ltd.
  71. C.N.Banwell, *Fundamentals of molecular spectroscopy*. 1972: McGraw-Hill book company.
  72. M.R.Holter, S.N., G.H.Suits, W.L.Wolfe,G.J.Zissis, *Fundamentals of Infrared Technology*. 1962: The Macmillan company,New York.
  73. CITRA, P.H.A.M.J., *Orientational order determination by Internal Reflection Infrared Spectroscopy*. Elsevier Science Ltd, 1996. **66**: p. 227-253.
  74. P.R.Griffiths, *Chemical infrared Fourier transform spectroscopy*. 1975: John Wiley & Sons Ltd, .
  75. B.C.Smith, *Fundamentals of Fourier transform infrared spectroscopy* 1996: CRC Press.
  76. D.I.Bower, W.F.M., *The vibrational spectroscopy of polymers*. 1989: Cambridge University Press.
  77. S.Wartewig, R.H.H.N., *Pharmaceutical applications of Mid-IR and Raman spectroscopy*. Advanced Drug Delivery Reviews, 2005. **57**: p. 1144-1170.
  78. A. Tuchbreiter, J.M., J. Zimmermann, P. Walter, R. Mulhaupt, , , *High-Throughput Evaluation of Olefin Copolymer Composition by means of Attenuated Total Reflection Fourier Transform Infrared Spectroscopy* J. Comb. Chem. , 2001: p. 598-603.
  79. F.M.Mirabella, J., *Internal Reflection Spectroscopy*. 1992: Marcel Dekker, Inc.
  80. N.J.Harrick, *Internal reflection spectroscopy*. 1985: John Wiley & Sons Ltd., 13 - 63.
  81. A.R.Hind, S.K.B., A.Mckinnon, *At the solid /liquid interface: FTIR/ATR- the tool of choice*. Advances in Colloid and interface science 2001. **93**: p. 94-114.
  82. R.H. A. Ras, R.A.S., C. T. Johnston, *Relation between s-Polarized and p-Polarized Internal Reflection Spectra: Application for the Spectral Resolution of Perpendicular Vibrational Modes* J. Phys. Chem. , 2007. **111**: p. 8787-8791.
  83. Y. A. Elabd, M.G.B., T. A. Barbari, *Time-Resolved Fourier Transform Infrared/Attenuated Total Reflection Spectroscopy for the Measurement of Molecular Diffusion in Polymers*. J. POLYM. SCI., 2003. **41**: p. 2794-2807.
  84. A. E. Dowrey , G.M.S., C. Marcott,, *Industrial Applications of Near- and Mid-IR Imaging*. American Pharmaceutical Review, 2006: p. 1-5.
  85. E. N. Lewis, J.S., E. Lee, *Near-infrared Chemical Imaging and the PAT Initiative*. SPECTROSCOPY, 2004.
  86. R C. Lyon, D.S.L., E. Neil Lewis, E Lee, Lawrence X. Yu, Everett H. Jefferson, Ajaz S. Hussain, *Near-Infrared Spectral Imaging for quality assurance of pharmaceutical products: Analysis of tablets to assess powder blend homogeneity*. AAPS PharmSciTech, 2002. **3**: p. 1-15.

87. J. Dubois, E.N.L., *Advanced Troubleshooting Of Dissolution Failure* The Pharmaceutical Solutions Update, 2009: p. 38-45.
88. E. Neil Lewis, L.H.K., E Lee, *Near-Infrared Chemical Imaging. A valuable tool for the pharmaceutical industry*. G.I.T. Laboratory Journal, 2007. **1-2**: p. 26-28.
89. Reich, G., *Near-infrared spectroscopy and imaging: Basic principles and pharmaceutical applications*. Advanced Drug Delivery Reviews, 2005. **57**: p. 1109–1143.
90. J. Dubois, J.-C.W., J.K.Warrack, J. Schoppelrei, E. N. Lewis, *NIR Chemical Imaging for counterfeit pharmaceutical products analysis*. SPECTROSCOPY, 2007: p. 1-6.
91. Spectral Dimensions NIR CHEMICAL IMAGING SYSTEMS, M.I., *Technical Information and Specifications*.
92. Spectral Dimensions NIR Chemical Imaging Systems, M.I., *10 reasons for using Near Infrared Chemical Imaging (NIRCI) for the analysis of solid or powdered samples*. Technical note MRK1305-02, 2009.
93. Spectral Dimensions NIR Chemical Imaging Systems, M.I., *ISys™ Chemical Imaging Software, Powerful Chemical Image Analysis for Spectroscopists*.
94. P.Gemperline, *Practical guide to chemometrics*. 2006: CRC Press.
95. D.L.Massart, B.G.M.V., S.N.Deming, Y.Michotte, L.Kaufman, *Chemometrics: a textbook*. 1988: Elsevier Science Publishers.
96. Corp, G.I., *PLSplus/IQ, Users guide, Add-on application*. 1991: Galactic Industries Corp.
97. M.J.Adams, *Chemometrics in analytical spectroscopy*. 1995: RSC
98. A S. EL-Hagrasy, H.R.M., F D'amico, R A. Lodder, J K. Drennen, *Near-Infrared spectroscopy and imaging for the monitoring of powder blend homogeneity*. Journal of pharmaceutical science,, 2001. **90**: p. 1298-1307.
99. N.Jovanovic', A.G., A. Bouchard, W. Jiskoot, *Near-Infrared Imaging for studying homogeneity of protein-sugar mixtures*. Pharmaceutical Research, 2006. **23**: p. 2002-2013.
100. C. Gendrin, Y.R., C. Spiegel, C. Collet, *Monitoring galenical process development by near infrared chemical imaging: One case study*. European Journal of Pharmaceutics and Biopharmaceutics, 2008. **68**: p. 828–837.
101. Y. Roggo, N.J., A. Edmond, P. Chalus, M. Ulmschneider, *Characterizing process effects on pharmaceutical solid forms using near-infrared spectroscopy and infrared imaging*. European Journal of Pharmaceutics and Biopharmaceutics, 2005. **61**: p. 100–110.
102. Y. Roggo, A.E., P. Chalus, M. Ulmschneider, *Infrared hyperspectral imaging for qualitative analysis of pharmaceutical solid forms*. Analytica Chimica Acta, 2005. **535**: p. 79–87.
103. F. Chau, Y.L., J. Gao, X. Shao, *Chemometrics from basics to wavelet transform*. 2004: John Wiley & Sons, Inc.
104. Spectral Dimensions NIR Chemical Imaging Systems, M.I., *Measuring blend uniformity in pharmaceutical tablets with NIR Chemical Imaging (NIR-CI)*. Application note, MRK779-01.
105. W. Li, A.W., L. Araba, D. Winstead, *Determination of water penetration and drug concentration profiles in HPMC-based matrix tablets by Near Infrared Chemical Imaging*. Journal of pharmaceutical sciences, 2010. **99**: p. 3081-3088.
106. Brereton, R.G., *Chemometrics, Data Analysis for the Laboratory and Chemical Plant*. 2003: John Wiley & Sons Ltd.



107. Clarke, F., *Extracting process-related information from pharmaceutical dosage forms using near infrared microscopy*. Vibrational Spectroscopy, 2004. **34**: p. 25–35.
108. L.R. Hilden, C.J.P., S.I.F. Badawya, Emil M. Friedman, *NIR chemical imaging to guide/support BMS-561389 tablet formulation development*. International Journal of Pharmaceutics, 2008. **353**: p. 283–290.
109. H. MA, C.A.A., *Characterization of pharmaceutical powder blends by NIR Chemical Imaging*. Journal of Pharmaceutical Sciences,, 2008. **97**: p. 3305-3320.
110. M. B. Lopesa, J.W., *Investigation into classification/sourcing of suspect counterfeit Heptodin<sup>TM</sup> tablets by near infrared chemical imaging*. Analytica Chimica Acta, 2008. **633**: p. 149–155.
111. C. Gendrin, Y.R., Ch. Collet, *Content uniformity of pharmaceutical solid dosage forms by near infrared hyperspectral imaging: A feasibility study*. Talanta, 2007. **73**: p. 733–741.
112. B.J. Westenberger, C.D.E., A. S. Fussner, S.Jenney, R. E. Kolinski, T. G. Lipe, R. C. Lyon, and L.K.R. T. W. Moore, A. P. Smith, J. A. Spencer, K. D. Story, D. Y. Toler, A. M. Wokovich, L. F. Buhse, *Quality assessment of internet pharmaceutical products using traditional and non-traditional analytical techniques*. International Journal of Pharmaceutics, 2005. **306**: p. 56–70.
113. T. Furukawa, H.S., H. Shinzawa, I. Noda, S. Ochiai, *Evaluation of homogeneity of binary blends of poly(3-hydroxybutyrate) and poly(L-lactic acid) studied by Near Infrared Chemical Imaging (NIRCI)*. Analytical Sciences, 2007. **23**: p. 871-876.
114. R.B.Shah, M.A.T., M.A.Khan, *Process analytical technology: Chemometric analysis of Raman and Near-Infrared spectroscopic data for predicting physical properties of extended release matrix tablets*. Journal of pharmaceutical science,, 2006. **96**: p. 1356-1365.
115. José Manuel Amigo, C.R., *Direct quantification and distribution assessment of major and minor components in pharmaceutical tablets by NIR-chemical imaging*. European Journal of Pharmaceutical Sciences, 2009. **37**: p. 76-82.
116. T. Puchert, D.L., J.C. Menezes, G. Reich, *A multivariate approach for the statistical evaluation of near-infrared chemical 4 images using Symmetry Parameter Image Analysis (SPIA)*. European Journal of Pharmaceutics and Biopharmaceutics, 2011. **In press**.
117. C. Ravna, E.S., R. Bro, *Near-infrared chemical imaging (NIR-CI) on pharmaceutical solid dosage forms—Comparing common calibration approaches*. Journal of Pharmaceutical and Biomedical Analysis, 2008. **48**: p. 554–561.
118. Frederick W. Koehler IV, E.L., Linda H. Kidder, E. Neil Lewis, *Near infrared spectroscopy: the practical chemical imaging solution*. NIR SPECTROSCOPY, 2002. **14**: p. 12-17.
119. S. Sonja Sekulic, H.W.W., Daniel R. Brannegan, Elizabeth D. Stanley, Christine L. Evans, Steven T. Sciavolino, Perry A. Hailey, Paul K. Aldridge, *On-Line Monitoring of Powder Blend Homogeneity by Near-Infrared Spectroscopy*. Anal. Chem., 1996. **68**: p. 509-513.
120. Abdi, H., *Partial Least Squares Regression and Projection on Latent Structure Regression (PLS-Regression)*. Wiley Interdisciplinary Reviews: Computational Statistics, 2009: p. 1-23.
121. S.J Hasswell, A.D.W., *Chemometrics: the issues of measurement and modelling*. Analytica Chimica Acta, 1999. **400**: p. 399-412.

122. Michael Cauchi, C.B., Steve Setford, *Simultaneous Quantitative Determination of Cadmium, Lead, and Copper on Carbon-Ink Screen-Printed Electrodes by Differential Pulse Anodic Stripping Voltammetry and Partial Least Squares Regression*. *Electroanalysis*, 2008. **20**(23): p. 2571–2577.
123. R. D. Tobias, *An Introduction to Partial Least Squares Regression*. (SAS Institute Inc., Cary, NC): p. 1-7.
124. B.K.Lavine, *Chemometrics*. *Anal. Chem.*, 2000. **72**: p. 91-97.
125. H. Swierenga, A.P.d.W., R. J. van Wijk, L. M. C. Buydens *Strategy for constructing robust multivariate calibration models*. *Chemometrics and Intelligent Laboratory Systems*, 1999. **49**: p. 1-17.
126. De Maesschalck, R.D.J.-R., D.L. Massart *The Mahalanobis distance*. *Chemometrics and Intelligent Laboratory Systems*, 2000. **50**: p. 1-18.
127. R.C.Denny, *Visible and Ultraviolet spectroscopy*. 1987: John Wiley & Sons.
128. D.G.Watson, *Pharmaceutical analysis*. 1999: Churchill Livingstone.
129. M. N. Roshdy, R.L.S., J. B. Schwartz, *The effect of formulation composition and dissolution parameters on the gel strength of controlled release hydrogel tablets*. *Pharmaceutical Development and Technology*, 2001. **6**: p. 583–593.
130. R. Hanson, V.G., *Handbook of dissolution testing*. 2004: Dissolution technologies.
131. J.T.Carstensen, *Advanced pharmaceutical solids*. 2001, New York.
132. D. Chulia, M.D., Y. Pourcelot, *Powder technology and pharmaceutical process*, ed. Elsevier. 1994.
133. M.C. Bonferoni, S.R., F. Ferrari, M. Bertoni, G.K. Bolhuis, C. Caramella, *On the employment of l carrageenan in a matrix system III. Optimization of a l carrageenan-HPMC hydrophilic matrix*. *Journal of Controlled Release*, 1998. **51**: p. 231–239.
134. K. Kolter, D.F., *Structure and dry binding activity of different polymers, including kollidon VA 64*. *Drug Development and Industrial Pharmacy*, 2000. **26**: p. 1159–1165.
135. S. I. Farag Badawy, T.J.L., M. M. Menning, *Effect of drug substance particle size on the characteristics of granulation manufactured in a high-shear mixer*. *AAPS PharmSciTech*, 2000. **1**: p. 1-7.
136. I.J. Hardy, W.G.C., C.D. Melia, *Compression and compaction properties of plasticised high molecular weight hydroxypropylmethylcellulose (HPMC) as a hydrophilic matrix carrier*. *International Journal of Pharmaceutics*, 2006. **311**: p. 26–32.
137. Ch. Gustafsson, C.N., H. Lennholm, M. C. Bonferoni, C. M. Caramella, *Characteristics of hydroxypropyl methylcellulose influencing compactibility and prediction of particle and tablet properties by infrared spectroscopy*. *JOURNAL OF PHARMACEUTICAL SCIENCES*, 2003. **92**: p. 494-504.
138. Sh. A. Mitchell, T.D.R., T. P. Dasbach, *A compaction process to enhance dissolution of poorly water-soluble drugs using hydroxypropyl methylcellulose*. *International Journal of Pharmaceutics*, 2003. **250**: p. 3-11.
139. Ch. Gustafsson, M.C.B., C. Caramella, H. Lennholm, Ch. Nystroma, *Characterisation of particle properties and compaction behaviour of hydroxypropyl methylcellulose with different degrees of methoxy/hydroxypropyl substitution*. *European Journal of Pharmaceutical Sciences*, 1999. **9**: p. 171–184.
140. A. Nokhodchi, J.L.F., P. H. Rowe, M. H. Rubinstein, *The effects of compression rate and force on the compaction properties of different viscosity grades of*

- hydroxypropylmethylcellulose* 2208. *International Journal of Pharmaceutics*, 1996. **129**: p. 21-31.
141. Y. Huang, K.H.K., A. D. Moore, M. Hilliard-Lott, *Effects of manufacturing process variables on in vitro dissolution characteristics of extended-release tablets formulated with hydroxypropyl methylcellulose*. *Drug Development and Industrial Pharmacy*, 2003. **29**: p. 79–88.
  142. Yuh-Tyng Huang, T.-R.T., Chun-Jen Cheng, Thau-Ming Cham, *Formulation design of an HPMC-based sustained release tablet for pyridostigmine bromide as a highly hygroscopic model drug and its in vivo/in vitro dissolution properties*. *Drug Development and Industrial Pharmacy*, 2007. **33**: p. 1183–1191.
  143. S. Kiese, A.P., W. Friess, H. Mahler, *Shaken, not stirred: Mechanical stress testing of an IgG1 antibody*. *Journal of Pharmaceutical Sciences*, 2008. **97**: p. 4347-4366.
  144. B. Chaudhuri, A.M., F. J. Muzzio, M. S. Tomassone, *Cohesive effects in powder mixing in a tumbling blender*. *Powder Technology*, 2006. **165**: p. 105–114.
  145. M. E. Pina, F.V., *The Influence of diluent on the release of theophylline from hydrophilic matrix tablets*. *Drug Development and Industrial Pharmacy*, 2000. **26**: p. 1125–1128.
  146. H. Friedrich, A.N., R. Bodmeier, *Solid state and dissolution rate characterization of co-ground mixtures of nifedipine and hydrophilic carriers*. *Drug Development and Industrial Pharmacy*, 2005. **31**: p. 719–728.
  147. I. Weerd, K.I.A.C., S.G.Kazarian, *An innovative design of compaction cell for in situ Ft-IR imaging of tablet dissolution*. *Vibrational Spectroscopy*, 2004. **35**: p. 9-13.
  148. J. Weerd, S.G.K., *Combined approach of FTIR imaging and conventional dissolution tests applied to drug release*. *Journal of Controlled Release*, 2004. **98**: p. 295–305.
  149. Elkady, E.F., *Simultaneous spectrophotometric determination of diclofenac potassium and methocarbamol in binary mixture using chemometric techniques and artificial neural networks*. *Drug Testing and Analysis*, 2010.
  150. Y. Xie, Y.S., Y. Zhang, B. Zhao, *Near-infrared spectroscopy quantitative determination of Pefloxacin mesylate concentration in pharmaceuticals by using partial least squares and principal component regression multivariate calibration*. *Spectrochimica Acta Part A: Molecular and Biomolecular Spectroscopy*, 2010. **75**: p. 1535–1539.
  151. F. Fichtner, A.R., G. Alderborn *Particle size distribution and evolution in tablet structure during and after compaction*. *International Journal of Pharmaceutics*, 2005. **292**: p. 211-225.
  152. K. Kachrimanis, S.M., *Compact size and mechanical strength of pharmaceutical diluents*. *European Journal of Pharmaceutical Sciences*, 2005. **24**: p. 169-177.
  153. S.R. Byrn, W.X., A.W. Newmann, *Chemical reactivity in solid-state pharmaceuticals: formulation implications*. *Advanced Drug Delivery Reviews*, 2000. **48**: p. 115-136.
  154. R.T. Morrison, R.N.B., *Organic Chemistry*. 1987: Allyn and Bacon, Inc. USA.
  155. M. P. Tucker, Q.A.N., F. P. Eddy, K. L. Kadam, L. M. Gedvilas, J. D. Webb, *Fourier transform infrared quantitative analysis of sugars and lignin in pretreated softwood solid residues*. *Applied Biochemistry and Biotechnology*, 2001. **91-93**: p. 51-61.

156. J. Hirsch, L.T., M. Hollein, *FT-NIR analysis of wine*. Thermo Electron Application Note: 50813, 2004: p. 1-4.
157. A.D. Karande, C.V.L., P.W.S. Heng, *Calibration sampling paradox in near infrared spectroscopy: A case study of multi-component powder blend*. International Journal of Pharmaceutics, 2010. **395**: p. 91–97.
158. M. Dumarey, I.S., Y. Vander Heyden, *Prediction and interpretation of the antioxidant capacity of green tea from dissimilar chromatographic fingerprints*. Journal of Chromatography B, 2010. **878**: p. 2733–2740.
159. E Neil Lewis, J.E.C., F. Clarke, *A near infrared view of pharmaceutical formulation analysis*. NIR news, 2001. **12**: p. 16-18.
160. E. Neil Lewis, L.H.K., E Lee, *NIR chemical imaging—near infrared spectroscopy on steroids*. NIR News, 2005. **16**: p. 1-3.
161. E Neil Lewis, L.H.K., Eunah Lee, *NIR Chemical Imaging as a Process Analytical Tool*. Innovations in Pharmaceutical Technology, 2006. **17**.
162. David J. Wargo, J.K.D., *Near-infrared spectroscopic characterization of pharmaceutical powder blends*. Journal of Pharmaceutical and Biomedical Analysis, 1996. **14**: p. 1415-1423.
163. Harden, J.W., Glover D, Redding. Jr, Bruce K, *Method for increasing the active loading of compressible composition forms* US Patent 6,716,453 2004: p. 1-14.
164. J.J. Andrew, T.M.H., *Rapid analysis of Raman image data using two-way multivariate curve resolution*. Applied Spectroscopy, 1998. **52**: p. 797-807.
165. Mathworks, T., *The PLS toolbox manual*. Mathworks technical documentation, 2007: p. 1-56.
166. Takka S, S.A., Goldberg A., *Development and validation of an in vitro-in vivo correlation for buspirone hydrochloride extended release tablets*. J Control Release., 2003. **88**: p. 147-157.
167. C.Sammon, G.B., P.Timmins, C.D.Melia., *The application of attenuated total reflectance Fourier transform infrared spectroscopy to monitor the concentration and state of water in solutions of a thermally responsive cellulose ether during gelation*. Polymer, 2005. **47**.
168. S.G. Kazarian, K.L.A.C., *Applications of ATR-FTIR spectroscopic imaging to biomedical samples*. Biochimica et Biophysica Acta, 2006. **1758**: p. 858–867.
169. Vesely, D., *The rate of solvent diffusion in amorphous polymers*. Macromolecules, 1999. **138**: p. 215-223.
170. Jones, D., *Pharmaceutics-dosage form and design*. 2008: Pharmaceutical press USA.
171. E.Part-Enander, A.S., B. Melin, P. Isaksson, *The Matlab Handbook*. 1996: Addison Wesley Longman.
172. Mathworks, T., *Getting started with matlab 7*. 2007: The Mathworks, software technical documentation.
173. Spectral Dimensions NIR CHEMICAL IMAGING SYSTEMS, M.I., *Near Infrared Chemical Imaging to assess content uniformity*. technical note MRK889-01, 2007: p. 1-4.
174. Spectral Dimensions NIR CHEMICAL IMAGING SYSTEMS, M.I., *ISys: Figures and Graphs to Illustrate Blend Quality Results*. Technical note MRK976-01, 2007: p. 1-3.
175. K.L.A. Chan, S.G.K., *Macro FTIR imaging in transmission under a controlled environment*. Vibrational Spectroscopy, 2005.

176. Sergei G. Kazarian, K.L.A.C., Veronique Maquet, Aldo R. Boccaccini, *Characterisation of bioactive and resorbable polylactide/Bioglass® composites by FTIR spectroscopic imaging* Biomaterials, 2004. **25**: p. 3931-3938
177. Patrick Wray, K.L.A.C., James Kimber, Sergei G. Kazarian, *Compaction of pharmaceutical tablets with different polymer matrices studied by FTIR imaging and X-ray microtomography*. 2008. **97**: p. 4269 - 4277.
178. T. Ribar, J.L.K., R. Bhargava, *FTIR Imaging of Polymer Dissolution. 2. Solvent/Nonsolvent Mixtures*. Macromolecules, 2001. **34**: p. 8340-8346.
179. K.L.A. Chan, S.G.K., *Macro FTIR imaging in transmission under a controlled environment*. Vibrational Spectroscopy, 2005. **35**: p. 12-17.